Investigating the Unique features of Self-assembled Hen Egg White Lysozyme Nano-aggregates using Biophysical Approaches

A thesis submitted in partial fulfilment of the requirements for the Degree of Doctor of Philosophy

By

Ms. Tulsi Swain

Roll no 10610606

Department of Biosciences and Bioengineering

Indian Institute of Technology Guwahati

Guwahati-781039

Assam, India

August 2017

Indian Institute of Technology Guwahati

Department of Biosciences and Bioengineering

Declaration

I hereby declare that the thesis entitled "**Investigating the unique features of Self-assembled Hen Egg White Lysozyme Nano-aggregates using Biophysical approaches"** is the result of investigation carried out by me in the Department of Biosciences and Bioengineering, Indian Institute of Technology Guwahati, under the supervision of Prof. Rajaram Swaminathan. This work has not been submitted either in whole or in part to any other University/ Institution for any research degree.

IIT Guwahati **Tulsi Swain**

August 2017

Indian Institute of Technology Guwahati

Department of Biosciences and Bioengineering

Certificate

This is to certify that Tulsi Swain has prepared the thesis entitled **"Investigating the unique features of Self-assembled Hen Egg White Lysozyme Nano-aggregates using Biophysical approaches"** for the degree of Doctor of Philosophy. The work has been carried out under my supervision in the Department of Biosciences and Bioengineering, Indian Institute of Technology, Guwahati and in strict conformity with rules laid down for the purpose. It is the result of her investigation and has not been submitted either in whole or in part to any University/ Institution for any research degree.

IIT Guwahati (**Prof. Rajaram Swaminathan**)

August 2017 Supervisor

Table of Contents

Acknowledgments

In this whole journey, I have made many mistakes, embraced those mistakes and flaws, learnt from them and finally developed myself.

I would like to thank my *supervisor* Prof. R. Swaminathan for helping me grow personally as well as professionally. Today I could finish my PhD successfully and I could enrich myself with lots of research skills. In my first year when I had enrolled into the course, I didn't know how to prepare a buffer correctly, how to run a gel, how to give a presentation etc. and lot more. Thanks for investing in me ample amount of time and letting me learn the things naturally. I am grateful to you for your unconditional support during my Ph.D. Sir; you are irreplaceable in my life.

I would like to take this opportunity to thank my doctoral committee comprising of *Dr. Dipankar Bandyopadhyaya*, *Dr. B. Anand* and *Dr. Vikash Dubey*. Throughout these years, the scientific inputs by the committee in my research helped me in my growth and development. Thank you Bandyopadhyaya sir for giving me ideas to improve my presentation skills and your words "you hit a century" after my synopsis seminar still gives me goose bumps. Thank you Anand sir for asking me thought provoking questions which helped me to improvise my analytical thinking. Thank you Dubey sir for providing me ideas on how to trouble shoot for my experiments.

I am really grateful to *Prof. Pranab Goswami* for freely allowing me to use the DLS instrument from his lab. Sir, thanks for encouraging me by your words.

I am also indebted to *Dr. Rajan Sankarnarayanan*, Structural Biology laboratory in CCMB (Centre for cell and Molecular Biology) for helping me to carry out SAXS experiments and letting me use the SAXS facility.

I am thankful to *Yoganand*, *Himanshu* and *Siddarth* for helping me out in setting up the chromatography experiments. I am also thankful to *Sameer* for your immense help provided to me during the conference ICANN.

I am indebted to the NMR facility of Central Instruments facility (CIF) at IIT Guwahati for helping me to carry out fluorine NMR measurements. I am thankful to *Mr. Chandan* for giving me extra time slots to perform my experiments.

Acknowledgments

I would like to acknowledge *Prof. Atreya* from NMR research centre, IISC Bangalore for providing NMR facility for recording relaxation parameters which proved to be very useful in my research.

I never knew writing down the scientific results is tougher than performing experiments unless and until I wrote my thesis. However, I got to learn the intricacies of scientific writing from a workshop conducted by *Prof. R. Uppaluri* which was filled with lots of fun and knowledge.

I am thankful to IIT Guwahati for providing me an environment conducive for carrying out my research work. I got the opportunity to attend the lectures by some of the finest scientists and eminent personalities of the world through tech fest. During my stay at IIT, I got to learn Spanish with the help of exchange program students which I thoroughly enjoyed.

I am grateful to all my lab mates *Amrendra, Shruti, Zia, Saumya, Dilip, Anurag, Nayajyoti* and *Brahamnanda* for their cooperation. Thanks to each one of you for being there in different phases of my life and for lifting me up.

I really feel blessed to have *Tasneem Ali* as my friend who has always inspired me and let my spirits remain high. You know your words always help me to look forward into the future rather than cribbing about the past. You really remind me my worth.

I am thankful to my friend, *Darilang Mawrie* who was there throughout in this journey of mine. Dari, you always bring a comforting feeling when you are there around. *Sangita Bharati*, my friend who has really supported me, understood me in the crucial phase of my life. Please let me mention this, your thesis titled ‘on domestic violence’ says it all about you as a woman.

My *Bou* (grandmother), I love you a lot. The strength of character which is instilled within you has flowed into me.

The most difficult part which I faced during my PhD was the battle with my own inner demons which manifested in the form of fear and anxiety. I am grateful to my ever supporting family who has patiently helped me to deal with my limitations. I really feel proud to have you both, mommy and papa, as my parents who always want to see their daughter not only successful but useful to the people. Mommy, I have seen all the sacrifices you have made in your life to raise your daughters. I feel really blessed to have my super talented and

intelligent sisters, *Tapu* and *chandru* with me. You both by your actions have taught me to always break the stereotype and the taboos of the society.

'*Sensei*', (means mentor in Japanese) I just want to say that I have remained undefeated by any form of obstacles I faced. Thanks for all the encouragement which helped to make me believe in myself and thereby helping me unleash my hidden potential. Because of you, I have remained true to myself without bothering about petty criticisms. I take the determination today sensei (*Dr. Daisaku Ikeda*) that I will make you proud of me and will help to remove the misery from the society through my work.

My deep gratitude goes to my comrades in faith. All of your prayers and selfless support has empowered me.

I would like to request to all those who will ever read my thesis. Please raise your voice, or be the voice for those who do not have any voice, against any kind of oppression which you face. Don't be silent spectators or bystanders when you see any form of injustice, nepotism or discrimination in society or at your place of work. I salute those neutral observers or I would rather call them 'spineless' who choose to remain dumb. As a result, the oppressor becomes stronger and the oppressed section becomes weaker.

"Listen to the whispers of your inner voice rather than the noise of external cacophony.
Don't let your dreams get crushed."

Tulsi Swain

Indian Institute of Technology Guwahati

Introduction

HEWL (Hen egg white lysozyme) as protein is readily available and represents an excellent experimental system to study protein aggregation, being highly homologous to human lysozyme in structure. It is a wonderful system to study self-assembly of higher order structures.

Hen lysozyme is one of the proteins which falls into the category of non-disease related amyloidogenic proteins. Protein misfolding resulting in amyloidosis leads to onset of various pathogenic diseases. Researchers in the past have put lots of efforts to develop potential novel therapies to remove or block the progression of amyloid deposits[1] **(Hawkins et al., 2003)**. Lots of evidence exist which prove the phenomenon of protein aggregation and amyloidosis to be related but different processes in terms of the toxic species involved in causing diseases[2] **(Serrano et al., 2006)**.

Many reviews have been published which have described in detail the characteristics of fibril formation by different proteins belonging to lysozyme family[3] **(Nilsson et al., 2007, Swaminathan et al., 2011)**. The striking similarity between hen lysozyme and human lysozyme[4] in terms of sequence identity and structure similarity[5] makes lysozyme as the most well studied protein with respect to protein aggregation **(De Felice et al., 2006, Ventura et al., 2005)**. The theoretically generated protein aggregation profiles, which predict the aggregation propensity, for hen lysozyme and human lysozyme have been reported to be highly similar. Various experimental demonstrations have shown different conditions which induce fibril formation[6] in human lysozyme[7] such as high temperature, ethanol, low pH and so on **(Dobson et al., 2001, Fonatana et al., 2006).**

Depending on the conditions, protein aggregation may lead to formation of ordered aggregates or amyloid fibrils and sometimes may favour the formation of disordered amorphous aggregates[8] **(Fink et al., 1998).** As per the basic model of aggregation, it has been proposed that large hydrophobic patches present on the surface of partially folded intermediates are the key factors for intermolecular interactions which lead to aggregation. There are certain important elements such as amino acid sequence of the protein, pH, temperature, ionic strength, presence of denaturants; fraction and stability of partially folded intermediates that determine the propensity of aggregation **(Wetzel et al., 1993, Fink et al., 1995)**. Even locally unfolded states of a globular protein have been shown to initiate

aggregation. As a result of conformational change in the native state, protein molecules can self-assemble, triggering amyloid formation[9] **(Dobson et al., 2009)**.

Lysozyme is a small globular protein composed of 129 amino acids. It is α-helical rich protein and has 4 disulfide bridges (C6-C127, C30-C115, C64-C180, and C76-C94).The isoelectric point[10] of HEWL is 11.3 **(Sasse et al., 1965)**. Nephropathy and hepatomegaly have been identified as the most common clinical features of systemic amyloidosis caused by deposition of human lysozyme amyloid fibrils[11] **(Skinner et al., 1997)**. Hydrophobicity of side chains, charge and propensity to form β-sheet structures are the crucial factors which have an influential role in protein aggregation[12] **(Dobson et al., 2006)**.

HEWL is a well-studied model system which forms amyloid *in vitro* and has been widely used in research due to its low cost and well characterized structure. Amyloid formation is a rather complex protein self-assembly process. Oligomer aggregates formed in amyloid pathway are referred to as amorphous aggregates, globulomers, prefibrillar aggregates etc. In order to know the therapeutic significance of the aggregation species, structural characterization of oligomers is important. Previously experiments carried out by our lab have shown that HEWL monomers self-associated on exposure to alkaline pH even in micromolar concentrations to form soluble oligomers[13] (**Homchaudhuri et al., 2006**). It was one of the significant findings which opened the pathway for further research in lysozyme aggregation. Various biophysical techniques have been employed in order to decipher the underlying mechanism behind HEWL aggregation pathway at alkaline pH 12.2.

Previous studies on aggregation pathway of human lysozyme focussed on detailed structural characterization of oligomeric species formed during the process[14] **(Fonatana et al., 2009)**. However, recently the focus has shifted from deciphering the aggregation mechanism involved in amyloid formation to fabrication of novel bio nanomaterials from amyloid fibrils. Researchers have effectively fabricated noble metal nanoparticle chains by using self-assembled amyloid fibrils of HEWL as biotemplates, thus exploiting the biological self-assembly phenomenon of amyloid fibrils[15] **(Gao et al., 2016)**.

It has been proposed that lysozyme aggregation[16] proceeds by Isodesmic mechanism that is aggregates grow by the addition of monomers. Isodesmic polymerization[17] occurs when the strength of non-covalent interactions between monomers is unaffected by the length of the chain[18]. There is no requirement of any critical monomer concentration for polymerization[19] to occur **(Tom et al., 2009, Udgaonkar et al., 2010, Frieden, 2007**, **Arata, 1999)**.

HEWL nanoparticles can be synthesized by controlling the monomer concentration in micro-nanomolar range during its aggregation at pH12.2 as it aggregates by an isodesmic polymerization mechanism[20] **(Ravi et al., 2014)**.

HEWL as protein is readily available and represents an excellent experimental system to study protein aggregation, being highly homologous to human lysozyme in structure, although only 40% identical in its sequence. It is a wonderful system to study self-assembly of higher order structures.

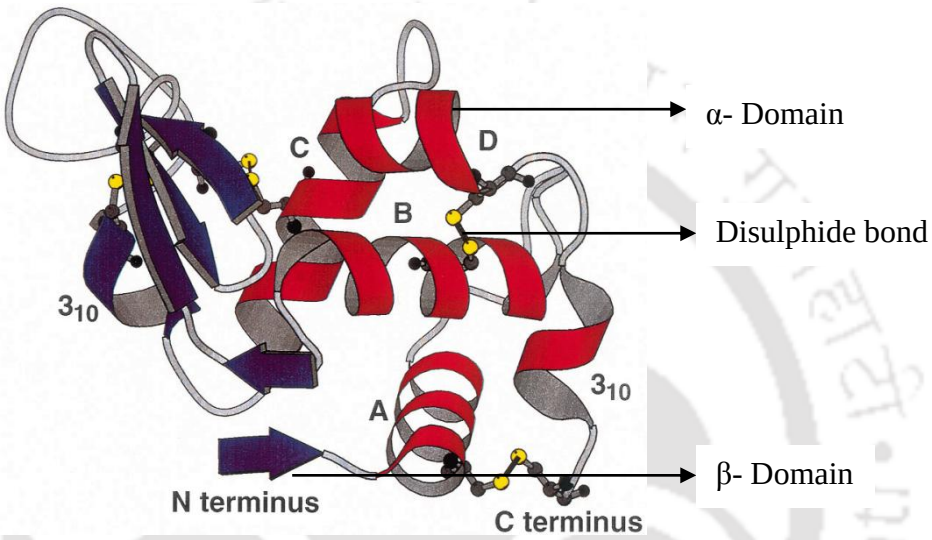

Figure: Structure of Hen egg white lysozyme

Similarity between Hen egg white lysozyme and Human lysozyme

Figure: SuperPose output for 5LVK (**Human Lysozyme**) chain A and 2LYZ (**Hen egg white Lysozyme**) chain A.

SuperPose is an online server used to superpose two or more protein structures. It aligns the protein structures by matching the secondary structure elements followed by 3-D alignment of protein backbone Cα atoms. At least two PDB files are given as input coordinate files. The program generates RMSD (Root mean square deviation of atomic positions) as the output from superimposition of input structures. Usually, the similarity in structures is measured by the RMSD of the Cα atomic coordinates.

This server can be used to assess how well the submitted structures match with each other. Almost 76.9 % similarity and 60 % identity has been found by superposition of human lysozyme and hen egg white lysozyme PDB files. The output is generated after sequence alignment of both the proteins.

Different mechanism of protein aggregation

In general, different mechanisms[21] have been reported for protein aggregation **(Arakawa et al., 2009)** which can be grouped into 5 categories: 1) Association of *native protein monomer* due to its self-complementary nature in order to form reversible small oligomers 2) Association of *conformationally altered monomer* due to partial unfolding in response to external stress which results in formation of higher order irreversible oligomers 3) Aggregation of *covalently modified monomers* 4) *Nucleation controlled* aggregation process in which there is the formation of a critical nucleus by addition of monomers which acts as seed for formation of larger aggregates 5) Binding of native monomer to a *surface* involving either hydrophobic or electrostatic interactions results in a change in conformation and thus induces aggregation.

Isodesmic mechanism of polymerization

Many neurodegenerative diseases are the consequence of aggregation of various proteins/peptide systems which involves amyloid formation. Aggregation and polymerization, both the terms can be used to describe amyloid formation. Both are same but aggregation implies a nonspecific process while polymerization implies a defined process. Polymerization from structured monomers can be of two types:

1) Isodesmic polymerization (linear)
2) Nucleation-elongation polymerization

Isodesmic polymerization occurs when the strength of non-covalent interactions between monomers is unaffected by the length of the chain. There is no requirement of any critical monomer concentration for polymerization to occur.

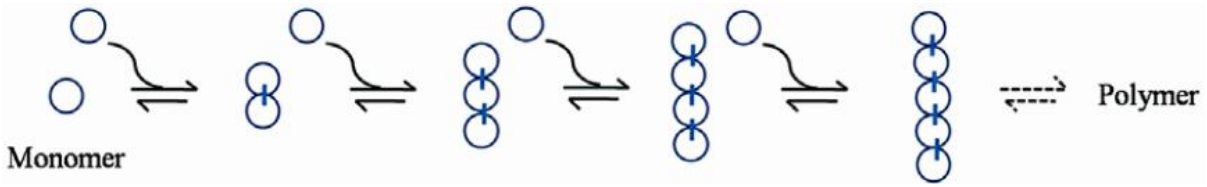

Figure: Graphical representation of the mechanism by which a monomer can polymerize into supramolecular polymer i.e. Isodesmic supramolecular polymerization (**Kumar et al., 2010**).

Introduction to protein nanoparticles

Nanomaterials derived from proteins, especially protein nanoparticles are biodegradable, non-antigenic, and metabolizable which can also be easily tailored for surface modification and covalent attachment of drugs and ligands[22] **(Babaei et al., 2008)**.

Molecular self-assembly can serve as an approach for preparing functional nanostructures. It is characterized by specific association of molecules dictated by non-covalent interactions. It was proposed that protein design could be used to fabricate devices through a '*bottom up*' approach, in which proteins are used as monomeric building blocks for the fabrication of higher order structures via self-assembly. Peptides and proteins are particularly attractive as building blocks because much is known about their folding and stability as well as about rules governing protein–protein interactions[23] **(Schneider et al., 2004)**. Protein nanoparticles (PNPs) which are formed through self-assembly of protein monomers have been used in many applications including diagnostic three-dimensional probes, MRI contrast reagents, semiconductor devices, template for hybrid materials etc. They have unique characteristics such as small size, high Surface-to-volume ratio, size uniformity, stable structure, and nontoxicity. Constructing artificial nanostructures by self-assembly has been a major challenge. Synthesis of Lysozyme nanoparticles[24] has already been reported by self-assembly but the method of fabrication used was heat gelation which could degrade the protein and the size of nanoparticles obtained was > 100 nm **(Shao et al., 2007)**.

Natural protein capsules are constructed by self-assembling the protein subunits into nano-cages. Apoferritin, viral capsids, DNA binding protein, small heat shock protein are some of the examples of protein cages. Their utilization as nanocarriers for drug delivery system and

cancer imaging probe[25] has been examined by taking advantages of their native hollow structure **(Kimura et al., 2010)**.

Biological nanocarriers available in nature

Protein cages are perfect examples of nanocarriers built from natural materials by a process of self-assembly. One of the characteristic features of protein cage structures is their size uniformity, i.e. they exhibit an extremely homogeneous size distribution. Protein cages can be chemically or biologically engineered in many ways, such that they can be used for drug delivery applications. **Iron storage protein ferritin** is one of the examples which have been used as a delivery vehicle for the MRI contrast agent Gadolinium.

Another extensively studied biological cage structure is the **small heat shock protein**. They have been studied for the encapsulation and release of the antitumor agent doxorubicin. Recently, the use of small heat shock proteins as a vehicle for the targeted delivery of imaging agents, for the diagnosis of atherosclerosis, has been reported.

Viral based nanocarriers[26] consist of several protein molecules which have the advantages of biocompatibility, easy functionalization and uniform size distribution. Cowpea chlorotic mottle virus (CCMV), viral nanocarriers has been utilized for encapsulation of DNA, gold nanoparticles, incorporation of quantum dots (QDs) and light absorbing inorganic molecules.

Preparation methods for the synthesis of protein nanoparticles (PNPs)

Procedures are established for the preparation of PNPs but current techniques available have certain limitations such as heterogeneous size distribution of NPs, loss of biological activity, potential biological risks due to the use of toxic cross-linkers. Unfortunately, suitable methods are not available for tuning the size of nanoparticles. Hence, new methods need to be developed for preparation of nanoparticles with controllable size and narrow size distribution.

Protein nanoparticles	Techniques used for synthesis	Average diameter of NPs	Limitations
Recombinant human gelatin NPs[28]	Desolvation	50-230 nm	Use of cross linkers may be toxic
Insulin[29]	Electrospray drying	80-110 nm	Complex set up Loss of biological activity
Lysozyme[30]	Supercritical fluids technology	0.1-5 µm	Complex set up Large particle size Lysozyme activity is affected
Albumin NPs	Emulsification		Need of organic solvent
Bovine Serum Albumin[31]	Desolvation	100, 400 & 800 nm	Use of cross linkers which may be toxic
Human Serum Albumin[32]	Desolvation	>300 nm	Use of cross linker may limit the biodegradability

Importance of *Self-assembly* mechanism in nanoworld

A broad range of nanoparticles have been synthesized previously by self-assembly but here we have restricted our focus to protein nanoparticles and nanostructures. Self-assembly is one of the methods for constructing nanoparticles with wide range of functionalities.

Self-assembly[33] can be broadly described as the organization of the building blocks into various ordered nanostructures or macroscopic structures either spontaneously by direct specific interactions or indirectly by using external fields or templates (**Liz-Marzan et al., 2010**). The process of self-assembly can be controlled by modulating the characteristics of particles so as to influence the interactions occurring between them.

Protein aggregates as protein nanoparticles

One of the methods to achieve the formation of monodisperse nanoparticles by disaggregating the protein crystals includes supercritical fluid[34] technology (**Castor, 2005**). Researchers have shown a significant reduction in size range to 1.5-6.5 µm from 50-600 µm particles while generating lysozyme nanoparticles by Superfluids technology. The Superfluids protein nanoparticles technology has a minimal impact on biological activity of the proteins.

Moreover, no changes have been reported on structural integrity of the proteins after application of this technology. However, the cumbersome apparatus to generate the protein nanoparticles is one of the major limitations of this method.

Amyloid fibrils and supramolecular nanostructures as functional biomaterials

The transition from native globular structure into supramolecular assemblies has been thoroughly studied previously which is a result of self-assembly of polypeptide molecules into amyloid fibrils. As previously thought to be toxic misfolded products of protein aggregation amyloid fibrils are now recognized as novel nanoscale biomaterials[35] **(Knowles et al., 2007)**.

Table: Applications of protein amyloids (Amyloids with beneficial biological activities).

Amyloids	*Constructs*	*Applications*
Hen Egg White Lysozyme amyloid fibrils[36]	Self-assembled macroscopic thin films (Highly stable and rigid)	Self-assembled protein scaffold control the alignment of fluorophores
Amyloid fibrils of analogs of Gonadotropin releasing hormone[37]	Amyloid fibrils in the form of gels of long-acting gonadotropin analogs	Depot for controlled release of biologically active peptide drugs
Sup35p-NM variant[38]	Self-assembled amyloid protein fibers covalently linked to gold nanoparticles	Conducting metal nanowires constructed on the template of protein fibers
Silk-moth chorion amyloid fibrils[39]	Self-assembled amyloid fibrils of chorion like peptides	Protect the oocyte and developing embryo of silkmoth

One of the major challenges involved in characterization of HEWL nanoparticles is the determination of structure of the intermediates involved in the aggregation pathway as the system is polydisperse involving lots of heterogeneity. On providing conditions necessary for unfolding of the protein such as denaturants, change in pH, temperature the phenomenon of self-assembly initiates with the buried hydrophobic regions of the protein being exposed to aqueous environment. The outcome of interactions between the exposed hydrophobic parts results in oligomerization of protein monomer units. Moreover, when the experimental conditions are near pI (isoelectric point) of the protein, aggregation of the protein leads to

formation of amorphous aggregates. Intermolecular associations via hydrophobic-hydrophobic interactions are believed to be the main driving force behind the self-assembly mechanism. Positive charges build up on the surface of the oligomers when transferred to pH 7.0. Intermolecular associations of monomers strengthened by disulfide linkage (S-S) renders the protein conformation to be further stable against any electrostatic repulsion faced by the oligomeric units when transferred from pH 12.2 to pH 7.0. Detailed characterization of a complex self-assembling system presents an enormous challenge due to the heterogeneous nature oligomeric species which are the main constituents of the system. Their inherent instability and transient nature adds to the complexity of the self-assembled macromolecular system.

Chromatographic techniques based on charge separation (Ion exchange chromatography) and molecular size and shape (Size exclusion chromatography) have been used to achieve the separation of differently populated species of HEWL aggregates. IEC (Ion exchange chromatography) proved to be extremely useful to separate different states of HEWL aggregates on the basis of charge. Several strategies have been used to track the conformational transition of HEWL aggregates. The sensitivity of fluorescence emission spectra of ANS to changes in hydrophobicity of microenvironment have been used to extract information for aggregates transferred to pH 7.0. The goal of ANS studies was to ascertain the stability of HEWL aggregates, formed in pH 12.2, after transfer to neutral pH. To evaluate the polydispersity of nanosized HEWL aggregates; DLS was used as a characterization technique. DLS was shown to accurately analyze the size distribution of monomeric HEWL and polydisperse HEWL oligomers. The different analytical methods which have been used to investigate the system under study were useful in providing critical information. Measurements were carried out separately on monomeric entity and oligomeric species to carry out a comparative study. TEM was used as imaging method to reveal the morphology of protein nanoparticles. Biophysical technique such as SAXS has been used to extract structural parameters of self-assembled HEWL aggregates. We report the characterization of HEWL protein with respect to tryptophan environment in native and aggregate state in different pH conditions. Various conjugation strategies have been optimized and adopted by us to link the fluorescent dyes to HEWL aggregates.

Proposed model for isodesmic aggregation of HEWL at pH 12.2

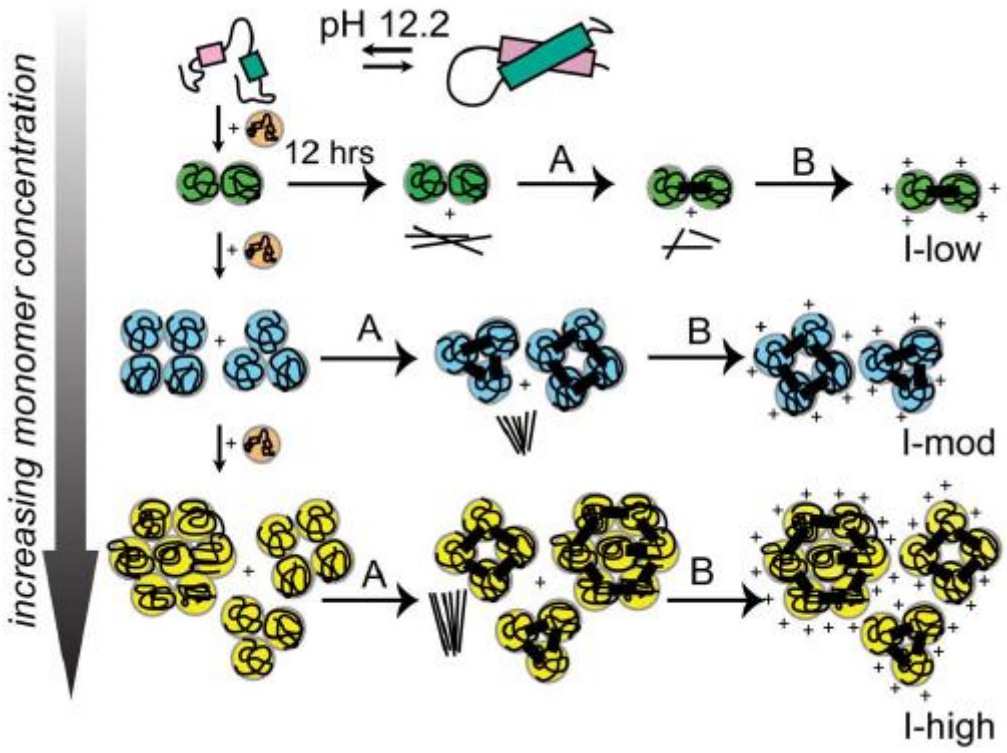

Figure: Exposure to pH 12.2 causes formation of partially unfolded HEWL monomers which triggers aggregation. As monomer concentration increases, growing oligomers form larger aggregates (small vertical arrows pointing down). Horizontal arrows reveal how by manipulating the monomer concentration to low (~0.3 µM), moderate (3-10 µM) and high (120 µM), equilibrium aggregation intermediates or protein nanoparticles of increasing average size were obtained. **Step A:** highlights formation of intermolecular disulfide bonds (thick bars) after 100 hours in pH 12.2. **Step B:** yields stable polycationic HEWL nanostructures after dilution into 100 mM pH 7.0 sodium phosphate buffer after 134 hours in pH 12.2**.** Thin line clusters indicate amyloid fibrils formed on pathway (**Ravi et al., 2014**).

References

1. Hirschfield, G. M. & Hawkins, P. N. Amyloidosis: new strategies for treatment. *Int. J. Biochem. Cell Biol.* **35,** 1608–1613 (2003).

2. Rousseau, F., Schymkowitz, J. & Serrano, L. Protein aggregation and amyloidosis: confusion of the kinds? *Curr. Opin. Struct. Biol.* **16,** 118–126 (2006).

3. Trexler, A. J. & Nilsson, M. R. The formation of amyloid fibrils from proteins in the lysozyme family. *Curr. Protein Pept. Sci.* **8,** 537–557 (2007).

4. Vieira, M. N. N., Figueroa-Villar, J. D., Meirelles, M. N. L., Ferreira, S. T. & De Felice, F. G. Small molecule inhibitors of lysozyme amyloid aggregation. *Cell Biochem. Biophys.* **44,** 549–553 (2006).

5. de Groot, N. S., Pallarés, I., Avilés, F. X., Vendrell, J. & Ventura, S. Prediction of 'hot spots' of aggregation in disease-linked polypeptides. *BMC Struct. Biol.* **5,** 1–15 (2005).

6. Frare, E. *et al.* Identification of the Core Structure of Lysozyme Amyloid Fibrils by Proteolysis. *J. Mol. Biol.* **361,** 551–561 (2006).

7. Dobson, C. M. The structural basis of protein folding and its links with human disease. *Philos. Trans. R. Soc. Lond. B. Biol. Sci.* **356,** 133–45 (2001).

8. Fink, A. L. Protein aggregation: folding aggregates, inclusion bodies and amyloid. *Fold. Des.* **3,** 9–23 (1998).

9. Chiti, F. & Dobson, C. M. Amyloid formation by globular proteins under native conditions. *Nat. Chem. Biol.* **5,** 15–22 (2009).

10. Sophianopoulos, A. J. & Sasse, E. A. Isoelectric point of proteins by differential conductimetry. *J. Biol. Chem.* **240,** 1864–1866 (1965).

11. Falk, R. H., Comenzo, R. L. & Skinner, M. The Systemic Amyloidoses. *N. Engl. J. Med.* **337,** 898–909 (1997).

12. Chiti, F. & Dobson, C. M. Protein Misfolding, Functional Amyloid, and Human Disease. *Annu. Rev. Biochem.* **75,** 333–366 (2006).

13. Homchaudhuri, L., Kumar, S. & Swaminathan, R. Slow aggregation of lysozyme in alkaline pH monitored in real time employing the fluorescence anisotropy of covalently labelled dansyl probe. *FEBS Lett.* **580,** 2097–2101 (2006).

14. Frare, E. *et al.* Characterization of Oligomeric Species on the Aggregation Pathway of Human Lysozyme. *J. Mol. Biol.* **387,** 17–27 (2009).

15. Xu, Z., Li, L., Li, H. & Gao, F. Synthesis of Self-assembled Noble Metal Nanoparticle Chains Using Amyloid Fibrils of Lysozyme as Templates. *Nanomater. Nanotechnol.* **6,** 1–7 (2016).

16. Price, W. S., Tsuchiya, F. & Arata, Y. Lysozyme Aggregation and Solution Properties Studied Using PGSE NMR Diffusion Measurements. *J. Am. Chem. Soc.* **121,** 11503–11512 (1999).

17. Kumar S. & Udgaonkar, J. B. Mechanisms of amyloid fibril formation by proteins. *Curr. Sci.* **98,** 639–656 (2010).

18. Frieden, C. Protein aggregation processes: In search of the mechanism. *Protein Sci.* **16,** 2334–2344 (2007).

19. De Greef, T. F. A. *et al.* Supramolecular polymerization. *Chem. Rev.* **109,** 5687–5754 (2009).

20. Ravi, V. K., Swain, T., Chandra, N. & Swaminathan, R. On the characterization of intermediates in the isodesmic aggregation pathway of hen lysozyme at alkaline pH. *PLoS One* **9,** (2014).

21. Philo, J. S. & Arakawa, T. Mechanisms of protein aggregation. *Curr. Pharm. Biotechnol.* **10,** 348–51 (2009).

22. Jahanshahi, M. & Babaei, Z. Protein nanoparticle: A unique system as drug delivery vehicles. *African J. Biotechnol.* **7,** 4926–4934 (2008).

23. Rajagopal, K. & Schneider, J. P. Self-assembling peptides and proteins for nanotechnological applications. *Curr. Opin. Struct. Biol.* **14,** 480–486 (2004).

24. Pan, X., Yu, S., Yao, P. & Shao, Z. Self-assembly of β-casein and lysozyme. *J. Colloid Interface Sci.* **316,** 405–412 (2007).

25. Makino, A. & Kimura, S. Preparation of peptide- and protein-based molecular assemblies and their utilizations as nanocarriers for tumor imaging. *React. Funct. Polym.* **71,** 272–279 (2011).

26. Ma, Y., Nolte, R. J. M. & Cornelissen, J. J. L. M. Virus-based nanocarriers for drug delivery. *Adv. Drug Deliv. Rev.* **64,** 811–825 (2012).

27. Zhen, X., Wang, X., Xie, C., Wu, W. & Jiang, X. Cellular uptake, antitumor response and tumor penetration of cisplatin-loaded milk protein nanoparticles. *Biomaterials* **34,** 1372–1382 (2013).

28. Won, Y. W. & Kim, Y. H. Recombinant human gelatin nanoparticles as a protein drug carrier. *J. Control. Release* **127,** 154–161 (2008).

29. Gomez, A., Bingham, D., Juan, L. de & Tang, K. Production of protein nanoparticles by electrospray drying. *J. Aerosol Sci.* **29,** 561–574 (1998).

30. Rodrigues, M. A. *et al.* Anti-solvent effect in the production of lysozyme nanoparticles by supercritical fluid-assisted atomization processes. *J. Supercrit. Fluids* **48,** 253–260 (2009).

31. Jun, J. Y. *et al.* Preparation of size-controlled bovine serum albumin (BSA) nanoparticles by a modified desolvation method. *Food Chem.* **127,** 1892–1898 (2011).

32. Weber, C., Kreuter, J. & Langer, K. Desolvation process and surface characteristics of HSA-nanoparticles. *Int. J. Pharm.* **196,** 197–200 (2000).

33. Grzelczak, M., Vermant, J., Furst, E. M. & Liz-Marzán, L. M. Directed Self-Assembly of Nanoparticles. *ACS Nano* **4,** 3591–3605 (2010).

34. Castor, T. P. Protein nanoparticles. *NSTI-nanotech* **1,** 172–175 (2005).

35. Knowles, T. P. *et al.* Role of intermolecular forces in defining material properties of protein nanofibrils. *Science (80-.).* **318,** 1900–1903 (2007).

36. Knowles, T. P. J., Oppenheim, T. W., Buell, A. K., Chirgadze, D. Y. & Welland, M. E. Nanostructured films from hierarchical self-assembly of amyloidogenic proteins. *Nat. Nanotechnol.* **5,** 204–207 (2010).

37. Maji, S. K. *et al.* Amyloid as a depot for the formulation of long-acting drugs. *PLoS Biol.* **6,** 0240–0252 (2008).

38. Scheibel, T. *et al.* Conducting nanowires built by controlled self-assembly of amyloid fibers and selective metal deposition. *Proc. Natl. Acad. Sci. U. S. A.* **100,** 4527–4532 (2003).

39. Iconomidou, V. A., Vriend, G. & Hamodrakas, S. J. Amyloids protect the silkmoth oocyte and embryo. *FEBS Lett.* **479,** 141–145 (2000).

Chapter 2

Characterization of HEWL nanoparticles in terms of stability, size, activity and morphology

2.1 Estimation of stability of HEWL nanoparticles by steady state anisotropy of **Dansyl probe** conjugated to the protein

2.1.1 Introduction

Labeling biomolecules with fluorescent probes has been an attractive approach to study their applications in biological systems. Dansyl chloride is a widely used fluorescent probe for tagging the protein covalently via amine groups in the protein. Previously researchers have reported the use of dansyl chloride to carry out biophysical studies on proteins without hampering the biological activity or denaturation of proteins[1] (**Weber, 1952**). **Dansyl chloride (5-Dimethylaminonapthalene-1-Sulfonyl Chloride)** is an amine reactive fluorescent probe used to create bioconjugates with proteins, peptides, ligands and other biomolecules. Sulfonyl chlorides produce stable sulfonamide bonds on conjugation with proteins **[Figure 2.1.1]**. Non-fluorescent Dansyl chloride reacts with amines to form fluorescent Dansyl amides that exhibit large Stokes shift. It is an environment sensitive fluorescent probe. For the preparation of an optimal conjugate, it is very important to control the degree of labeling. The labeling reactions of amines with amine reactive probes are usually pH dependent. The ε–amino group of free lysine has a pKa of 10.5, so a slightly basic pH is required to make this amine group in non-protonated form. These probes target the terminal amines of proteins and ε-amino groups of lysine residues, in their non-protonated form. Therefore, a buffer in the pH range of 8.5 to 9.5 is used for optimal modification of lysine residues.

The question which we have addressed here refers to the stability of HEWL nanoparticles i.e. **how robust or intact the HEWL aggregates, formed in pH 12.2, remain after transfer to pH 7.0?** In order to monitor the stability of HEWL aggregates in pH 12.2 transferred to pH 7.0 in a time dependent way, steady state fluorescence anisotropy (r_{ss}) of dansyl probe was measured which gives an estimate of the size of the protein. This parameter yields information about the rotational correlation time (φ) of the fluorophore conjugated to the protein. In our case, r_{ss} represents an ensemble averaged measurement for the aggregate population. It gives a measure of the average size of the aggregates. In case of protein aggregation, the size of the overall diffusing protein species increases which in turn affects the overall tumbling rate of fluorophore conjugated protein. As a result φ also increases. Changes in size and integrity of dansyl labeled HEWL aggregates was monitored from r_{ss} of dansyl probe, after transfer to pH 7.0 in a time dependent way.

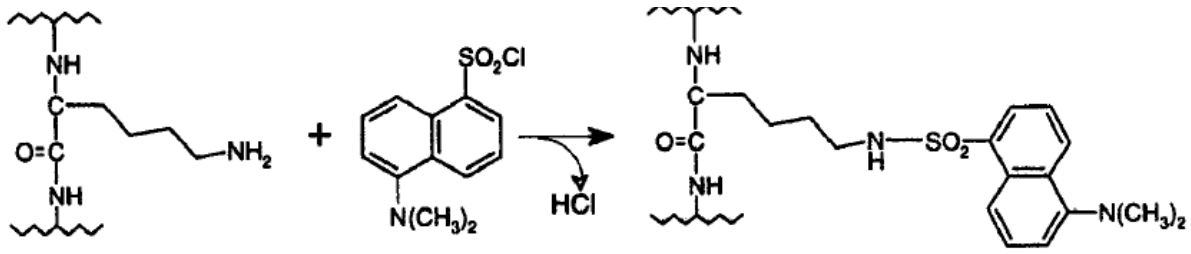

Figure 2.1.1: Reaction mechanism of Dansyl sulfonyl chloride with ε-amino of lysine residue[2] (**Levi et al., 2003**).

2.1.2 Materials and Methods

2.1.2.1 Materials

Hen egg white lysozyme- Cat no. L6876 (Sigma-Aldrich Chemicals Pvt. Ltd. India, Dansyl chloride – Cat no. D23 (Invitrogen, USA), DMF– Cat no. 4551 (Sigma-Aldrich Pvt. Ltd. India) & PD-10 pre-packed columns - Cat no.GE17-0851-01(Sephadex™ G-25M, GE Healthcare) were procured from sources as indicated in parenthesis.

2.1.2.2 Covalent Labeling of HEWL with dansyl chloride

For labeling reaction, 3 mM HEWL solution was prepared in 1 mL of 0.1 M $NaHCO_3$ buffer, pH 9.0 (chilled buffer stored at 4˚C). The reaction was carried out in alkaline conditions so as to make sure that ε–amino group of lysine residues and N-terminal residues of the protein remain in unprotonated form. This unprotonated form of the amine group is reactive towards dansyl and thus allows the dansylation to occur. Anhydrous DMF was used as solvent to dissolve the dye. Stock solution of 75 mM of dye was prepared by dissolving 2 mg of Dansyl chloride in 100 µL of DMF. In order to initiate the conjugation reaction, 50 µL of 75 mM reactive dye was added drop wise to 1 mL of 3 mM lysozyme solution which is kept under stirring. Subsequently, the reaction mixture was incubated at 4˚C for 3 hours with continuous stirring. 1.5 mL of 0.1 M $NaHCO_3$ buffer was further added to the reaction mixture to make up the volume to 2.6 ml. Protein modification reactions were performed at pH 9.0, Sodium Bicarbonate buffer in order to ensure optimal conjugation. For efficient dye conjugation to HEWL, reaction was carried out at 4˚Celsius. Unlabeled fluorophores or free dye was separated from the protein labeled with fluorophores by means of PD-10 gel filtration column. It should be noted that the column was equilibrated with 50 mM sodium phosphate buffer, pH 7.0 prior to loading the sample onto the column. The degree of labeling was

determined by measuring the protein and dye concentration in the labeled fractions. HEWL and Dansyl concentrations were estimated by measuring absorbance at 280 nm (ε_{HEWL} = 37, 970 $M^{-1}cm^{-1}$) and at 339 nm (ε_{Dansyl} = 3370 $M^{-1}cm^{-1}$) respectively. Labeled fraction with molar ratio of dye to protein as 1.4 was used further for the experiments. If protein/dye labeling ratio is 1.4, then this would contain 1.0 µM of HEWL of which 70 % of HEWL is likely to be labeled.

2.1.2.3 Sample preparation

Samples were prepared by mixing the labeled and unlabeled protein to achieve the desired concentration of protein for incubation.

a) **HEWL under aggregation condition (pH 12.2):** 120 µM HEWL with 1 µM dansyl-conjugated HEWL sample was incubated in pH 12.2. Without any further dilution the sample was used for r_{ss} measurements at different incubation time points.
b) **HEWL in native state (pH 7.0):** Similarly, 40 µM HEWL with 1 µM dansyl-conjugated HEWL was incubated in pH 7.0 and it was used as such for r_{ss} measurements at different incubation time points.
c) **HEWL nanoparticles (Transferred to pH 7.0):** In case of transferred samples, samples were incubated in pH 12.2 at two different concentrations (120 µM and 40 µM HEWL with 5 µM dansyl). Both the samples were diluted 10 fold when transferred to pH 7.0 at different time points. After different transfer points the samples were allowed to remain in pH 7.0. Steady state anisotropy measurements were taken at different incubation times in pH 7.0.

All the samples were incubated at room temperature (25˚C). Steady state anisotropy measurements were carried out at 298 K.

2.1.2.4 Steady state fluorescence anisotropy measurements

Fluorescence measurements were performed on Fluoromax-3 spectrofluorometer (Jobin-Yvon Horiba Inc., USA). G-factor correction and dark counts subtraction was performed before r_{ss} measurements. For dansyl-HEWL conjugates, excitation was done at 370 nm and emission at 444 nm. For HEWL sample incubated in pH 7.0 and pH 12.2, slit width for excitation was set at 1 nm and for emission slit width was set at 5 nm. In case of transferred samples, excitation and emission slit widths were set at 1 nm and 8 nm respectively.

2.1.3 Results and Discussion

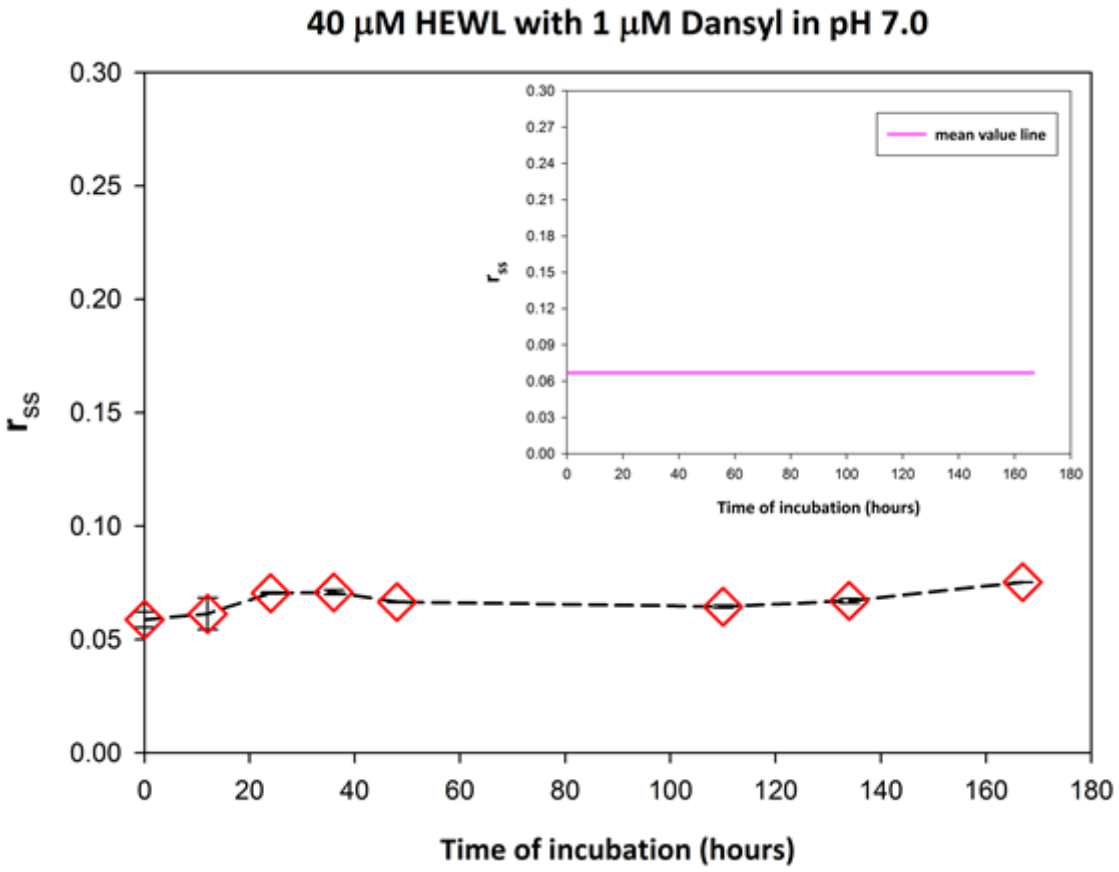

Figure 2.1.3.1: Steady state fluorescence anisotropy for 40 µM HEWL covalently tagged with dansyl probe incubated in pH 7.0 (native state). Steady state measurements were made with excitation at 370 nm and emission at 444 nm. Excitation and emission slit widths were set as 1 nm and 5 nm respectively. **Inset:** Plot of Mean value line for r_{ss} for 40 µM HEWL covalently tagged with dansyl probe incubated in pH 7.0. Mean line corresponds to a value of 0.066 i.e. arithmetic mean of r_{ss} values.

Steady state fluorescence anisotropy is one of the key techniques which is used to detect oligomers or protein aggregates in solution formed in aggregation pathway. Fluorescence anisotropy measurements are used to determine the tumbling rate of the fluorescent species in solution. As this tumbling rate is a function of the molecular size, r_{ss} is a parameter which gives an idea about the size of the rotating fluorescent probe. Most of the fluorophores rotate very fast in non-viscous aqueous solutions and exhibit their correlation time in picoseconds scale. Although r_{ss} represents an average value and doesn't take into account any heterogeneity of the species but is nevertheless useful in tracking the changes in overall size of the oligomers. We are interested in looking the average properties of the heterogeneous aggregates. At pH 7.0, it was observed that for HEWL covalently labeled with dansyl under native state, r_{ss} attained a value of ~ 0.06. Such a low value of r_{ss} also hints at the unhindered

rotation of the dansyl probe attached to a monomeric HEWL. This value remains unchanged with a time range of over 180 hours. Thus, incubation of the sample at pH 7.0 up to 7 days resulted in no significant change in r_{ss} value **[Figure 2.1.3.1]**. This indicates the absence of any self-association or aggregation of dansyl HEWL conjugate under these conditions. In other words, the overall structure of the native protein remains intact at pH 7.0 over an incubation period of 7 days.

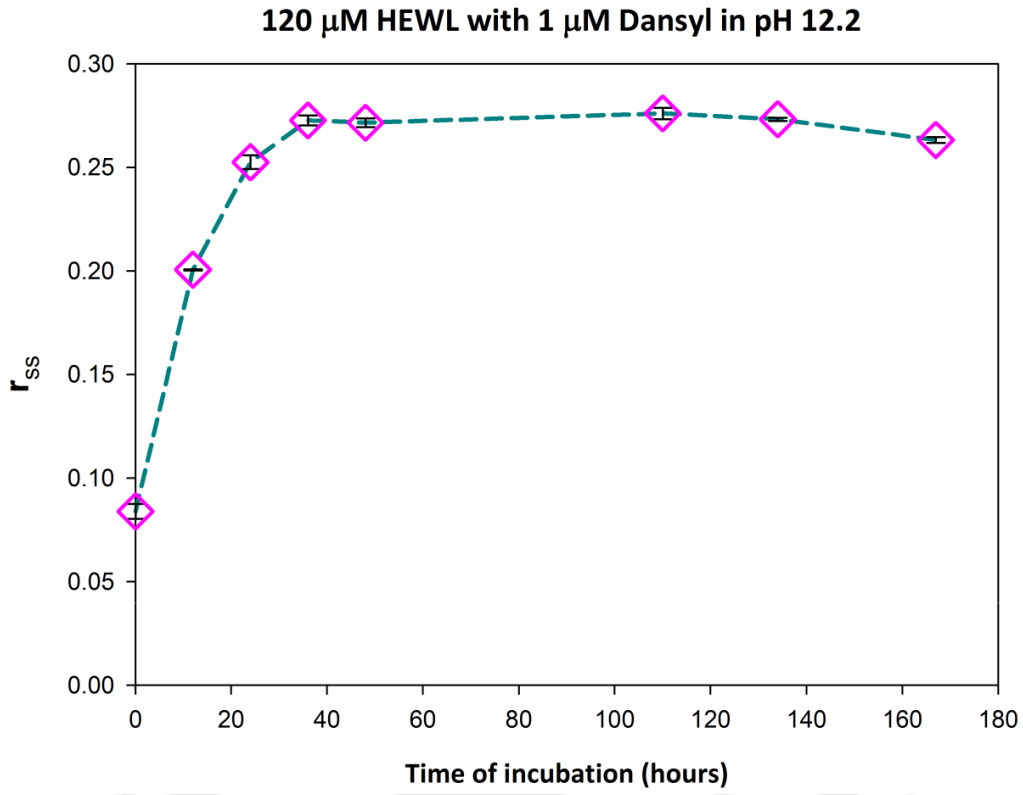

Figure 2.1.3.2: Fluorescence steady state anisotropy of 120 µM HEWL protein covalently labeled with dansyl sulfonyl chloride probe incubated in pH 12.2. Measurements were made with excitation at 370 nm and emission at 444 nm. Excitation and emission slit widths were set as 1 nm and 5 nm respectively.

Fluorescence lifetime of dansyl chloride does not change with time; moreover its mean life time also remains invariant with time[3] (**Homchaudhuri et al., 2006**). The lifetime of the dansyl probe also doesn't vary with change in pH[4]. The parameter r_{ss} is dependent on both rotational correlation time as well as fluorescence life time of the fluorescent probe. If the fluorescence life time (τ) of the probe remains constant then r_{ss} will be only be influenced by rotation correlation time (θ). Large protein molecules tagged to fluorescent dye will have slower Brownian rotational motion leading to an increase in r_{ss}. Henceforth, r_{ss} will give the correct picture of the molecular size of the diffusing species.

Steady state anisotropy is defined by **Perrin equation:**

$$r = \frac{r}{1+(\tau/\theta)} \quad \text{.....} \quad (1)$$

Here, r is the measured anisotropy and r_0 is the fundamental anisotropy. The above equation is for a single exponential decay. Steady state anisotropy is also given by an average of the anisotropy decay, r (t), over the intensity decay, I (t):

$$r = \frac{\int_0^\infty I(t)\, r(t) dt}{\int_0^\infty I(t) dt} \quad \text{.....} \quad (2)$$

Steady state anisotropy is given by the equation:

$$r = \frac{I_\parallel - I_\perp}{I_\parallel + 2I_\perp} = \frac{I_\parallel - I_\perp}{I_T} \quad \text{.....} \quad (3)$$

$I_\parallel$ is that component of the observed intensity which is parallel to the direction of polarized excitation light. When the intensity is perpendicular to the electric vector of excitation light, it is called $I_\perp$. I_T is the total fluorescence intensity.

Calculation of r_{ss} from measurements: r_{ss} is determined from the measured intensity ratio by including the instrument G factor. In order to determine the actual intensity ratio ($I_\parallel/I_\perp$), G factor is measured using horizontally polarized excitation:

$$G = \frac{S_V}{S_H} = \frac{I_{HV}}{I_{HH}} \quad \text{.....} \quad (4)$$

S_V and S_H are the sensitivities of the detection system for vertically and horizontally polarized light respectively. I_{HV} refers to horizontally polarized excitation and vertically polarized emission (first subscript represents excitation and second subscript is for emission polarizer). For example, G factor was calculated from ratio of measured I_{HV}/I_{HH}:

$$\frac{I_{HV}}{I_{HH}} = \frac{127672}{191988} = 0.665 = G$$

After determining G-factor, $I_{\parallel}/I_{\perp}$ can be calculated from the eqn:

$$\frac{I_{VV}}{I_{VH}} = G\,\frac{I_{\parallel}}{I_{\perp}} \quad \ldots\ldots\ldots\ldots\ldots\ldots\ldots\ldots \quad (5)$$

The ratio of I_{VV}/I_{VH} was obtained from measurements. When the G factor is known, $I_{\parallel}/I_{\perp}$ is calculated from equation no. 5.

$$\frac{I_{VV}}{I_{VH}} = 0.7806$$

$$\frac{I_{\parallel}}{I_{\perp}} = 0.7806 / 0.665 = 1.1738$$

Now, anisotropy can be calculated from the ratio of $I_{\parallel}/I_{\perp}$:

$$r = \frac{I_{\parallel}/I_{\perp} - 1}{I_{\parallel}/I_{\perp} + 2} = (1.1738 - 1) / (1.1738+2) = 0.055$$

Anisotropy can also be calculated from the equation:

$$r = \frac{I_{VV} - G\,I_{VH}}{I_{VV} + 2GI_{VH}} \quad \ldots\ldots\ldots\ldots\ldots\ldots\ldots \quad (6)$$

The presence or growth of aggregates was characterized by an increase in r_{ss} value from 0.08 to 0.2 after 12 hours of incubation in pH 12.2 as depicted from the **[Figure 2.1.3.2]**. This data is consistent with that reported by **Homchaudhuri et al.** for deciphering aggregation of HEWL by steady state anisotropy at pH 12.2. Here, the saturation of r_{ss} after 24 hours is clearly revealed from the plot. The initial increase in r_{ss} value upon exposure to alkaline pH clearly indicates a decrease in rotational diffusion of the dansyl conjugated HEWL. This is due to the growth of aggregates or formation of higher order oligomers and thus an increase in size of the lysozyme-dansyl conjugate. Thus, an increase in r_{ss} reflects the increase in molecular volume of the aggregates. The plateau observed in r_{ss} plot after 24 hours of incubation in pH 12.2 confirms that aggregates remain intact and stable for a time span of more than a week.

We have demonstrated the synthesis of HEWL nanoparticles with unique morphologies and architecture. It allows the flexibility of synthesis of size controlled protein nanoparticles by exploiting the monomer concentration. The size of HEWL aggregates in pH 12.2 may also be tailored to produce large or differently sized aggregates by manipulating the monomer concentration[5] **(Ravi et al., 2014)** and the incubation period in pH 12.2. It is very important to know whether the nanoparticles formed by HEWL aggregates are loosely bonded network or they form a compact structure. The question which arises here is whether HEWL nanoparticles formed by the self-association of HEWL monomers and oligomers will be able to withstand any kind of electrostatic repulsions upon transfer to pH 7.0.

In order to ensure that the synthesized nanoparticles are available for potential biological applications, they need to be stable enough. The assembly of the protein aggregates in pH 12.2 is a hydrophobically driven process. Upon transfer to pH 7.0 and when these complexes encounter coulombic repulsions due to the presence of excessive positive charges, it may lead to weakening of the nanoparticles assembly. There should be some other force more dominant than hydrophobic or non-covalent weaker forces to stabilize the nanoparticles.

So far, use of steady state anisotropy has proved to be the best approach to study the HEWL oligomers by means of measuring the rotational motion of dansyl probe covalently tagged to HEWL[4] (**Kumar et al., 2008**).

To analyze how stable or intact the preformed aggregates in pH 12.2 remain after transfer to neutral pH, r_{ss} measurements were carried out in a time dependent way after transfer to pH 7.0. Due to the positive charges developed on the surface of the nanoparticles, coulombic repulsions faced by the aggregates when transferred to pH 7.0 may destabilize the assembly.

In order to test the robustness of aggregates, r_{ss} measurements were performed with 2 different concentrations of dansyl labeled aggregates (40 µM and 120 µM HEWL aggregates). 120 µM HEWL aggregates transferred to pH 7.0 display a higher magnitude of r_{ss} compared to 40 µM transferred samples as shown in **Figure [2.1.3.3 & 2.1.3.4]**. This is consistent with the fact that aggregates with high concentration of monomer [M] will have higher molecular volume.

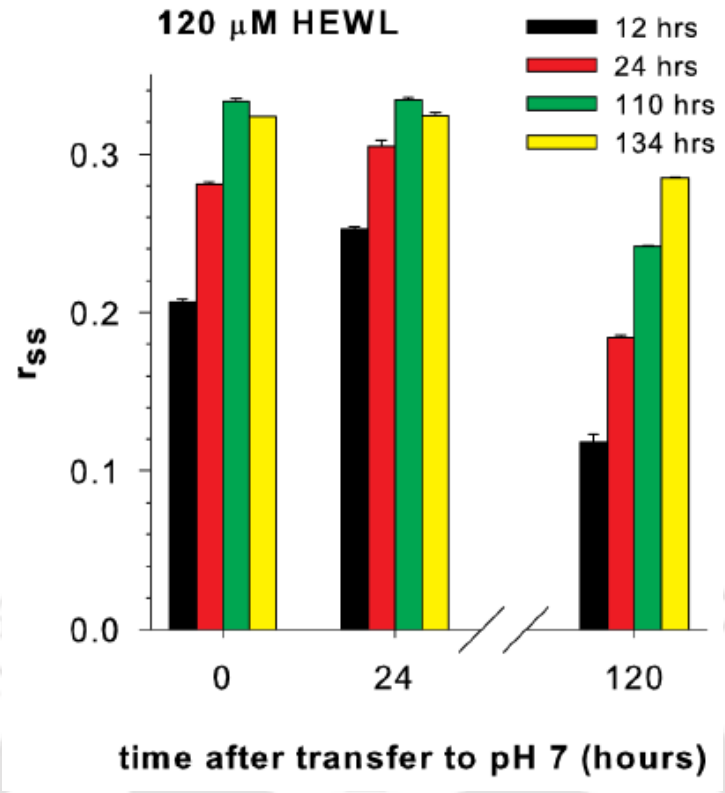

Figure 2.1.3.3: Changes in r_{ss} of Dansyl probe to assess the robustness of polycationic 120 µM HEWL aggregates transferred to pH 7.0. Aggregates were transferred to 100 mM sodium phosphate buffer, pH 7.0 from pH 12.2 with 10 fold dilution and at different time points: 12, 24, 110 & 134 hours.

Larger aggregates (120 µM) transferred early (12, 24 and 110 hours) get destabilized more easily than smaller aggregates upon transfer to neutral pH, due to columbic repulsions as depicted from the **[Figure 2.1.3.3]**.

40 µM aggregates are more robust as compared to 120 µM aggregates due smaller size leading to less repulsion in aggregates.(Concentration here refers to the monomer concentration [M] at which the aggregation was initiated). In case of early hours transferred samples i.e. 12 and 24 hours of incubation, r_{ss} values indicated a disruption of aggregates at later times of incubation period. Thus, it can be inferred that early hours transferred aggregates do not retain their robustness and eventually fall apart.

For 120 µM aggregates, when transferred to pH 7.0 at later times (110 and 134 hours), r_{ss} of dansyl probe does not show any rise or dip. The r_{ss} values remain stable even after 5 days of incubation, suggesting the intactness and robustness of size and shape of late hour transferred aggregates.

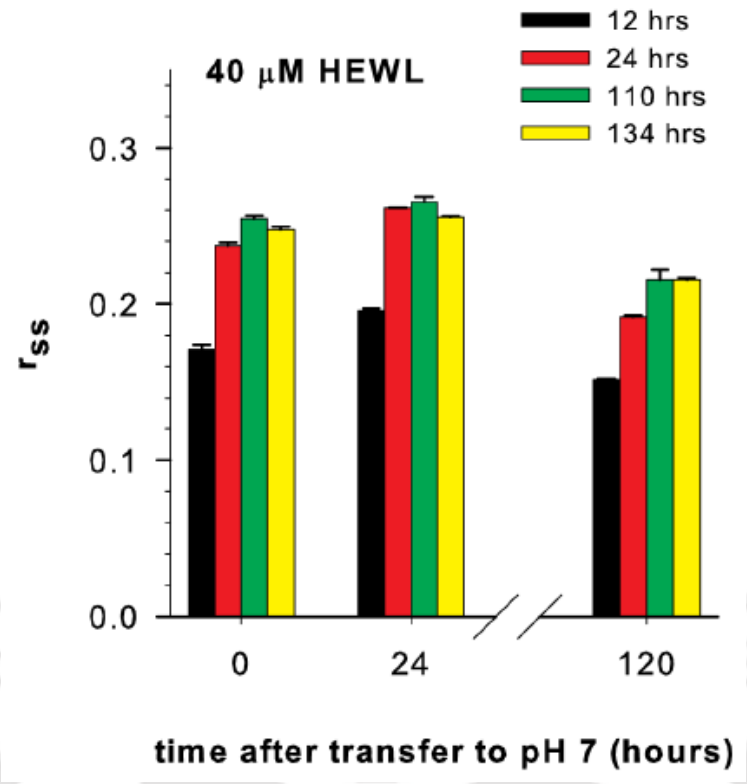

Figure 2.1.3.4: Changes in r_{ss} for dansyl conjugated 40 μM HEWL aggregates. The aggregates incubated in pH 12.2 were transferred with 10 fold dilution to pH 7.0 at different time points: 12, 24, 110 & 134 hours.

The scenario is different in case of 40 μM aggregates as these smaller aggregates apparently seem to be more intact in comparison to 120 μM aggregates. It is very clear from the **[Figure 2.1.3.4]** that even in early hours transferred samples (12 & 24 hours of incubation in pH 12.2); there is eventually less drop in r_{ss} value as compared to 120 μM aggregates. Henceforth, it can be interpreted that the integrity and robustness of 40 μM or smaller aggregates after transfer to pH 7.0 is comparably better than larger aggregates due to less electrostatic repulsions. The evidence provided in the present study suggests that the polycationic HEWL nanostructures seem to be stable in pH 7.0, when transferred after 5 days (134 hours) of incubation in pH 12.2. The underlying reason for this stability can be attributed to formation of intermolecular disulfide bonds which plays a critical role in strengthening of these nanoparticles. Even previously the significant role played by disulfide bonds in assembly of HEWL aggregates has been demonstrated[4] (**Kumar et al., 2008**).

Additionally, the study carried out by Kumar et al. has shown the effect of DTT, a disulfide reducing agent on the growth kinetics of aggregation. The major conclusion from the work reported was presence of DTT, is critical in the initial stages of aggregation in order to arrest the growth of HEWL aggregates. DTT acts as a potential inhibitor of aggregation in HEWL in alkaline pH by preventing the formation of aberrant disulfide bonds. The results have demonstrated the critical role of intermolecular disulfide bonds in the assembly and stability of the aggregates. Furthermore, significance of intermolecular disulfide bonds in the growth of HEWL aggregates has been demonstrated by our lab (**Ravi et al., 2014**). Blocking the free thiol groups with iodoacetamide in HEWL in pH 12.2, resulted in less compact, small sized aggregates due to the absence of inter disulfide bonds. Single molecule force spectroscopy measurements revealed that formation of incorrect disulfide bonds is a necessity in retaining the assembly together and in strengthening the hydrophobic interactions among monomers in the aggregates.

The inference which can be drawn from the r_{ss} data obtained for transferred samples is that longer incubation time in pH 12.2 allows the aggregates to be more compact and interlinked by higher no. of intermolecular disulfide bonds. Incubation up to 110 hours in pH 12.2 makes the polycationic nanoparticles toughened by intermolecular disulfide bonds. This causes the nanoparticles to remain intact upon transfer to pH 7.0 against any kind of strong electrostatic repulsions. Whereas, incubation in pH 12.2 for very shorter time period (12 & 24 hours), due to the lower population of these intermolecular disulfide crosslinking, leads to disassembly of the nanoparticles. Thus, these nanoparticles fail to keep themselves intact and fall apart upon incubation for longer times in pH 7.0 after transfer. This is evident from **[Figure 2.1.3.3]**.

2.1.4 Conclusion

In summary, our result demonstrates that steady state fluorescence anisotropy measurements provide us a good approach to monitor the stability of HEWL nanoparticles in pH 7.0. The behaviour of protein nanoparticles in pH 7.0 was studied by means of steady state anisotropy.

This study focussed on whether the polycationic HEWL nanoparticles retain their structure or disintegrate after transfer to pH 7.0 from pH 12.2. Intermolecular disulfide bonds between the oligomers formed at longer times of incubation in pH 12.2 have been proposed as the main force for holding the assembly together. These covalent bonds enable the nanoparticles to withstand any kind of electrostatic repulsion faced by them in pH 7.0.

2.2 DLS (**Dynamic light scattering studies**) of HEWL aggregates in a time dependent way

2.2.1 Introduction

DLS technique has the advantage that it can measure sizes of the order of magnitude of nanometer range. It is a hydrodynamic methodology available to measure the size of proteins in solution in terms of translational diffusion coefficient D (cm^2 s^{-1}).In addition, estimates of the molar mass of globular proteins can be obtained by assuming the molecules involved to be of spherical shape. When the monochromatic laser light is directed into the protein sample, the intensity scattered by the molecules in motion is recorded using a photodetector system. The intensity of the scattered light is measured at a fixed scattering angle, 90^o.

The Brownian motion of molecules leading to a collision with surrounding molecules in dynamic motion gives rise to fluctuations in the intensity of scattered light and from these fluctuations; normalized intensity autocorrelation function G (τ), as a function of delay time, can be derived. The term 'τ' refers to the delay time (milliseconds or microseconds). The decay of the correlation function, G (τ) in turn gives information on diffusion properties of the molecules in solution. The intensity fluctuations depend on the diffusivity of the protein molecules. Larger particles move slowly leading to slower intensity fluctuations. The major drawback of this technique is its sensitivity to even a small amount of large particles.

For globular proteins, DLS measurements allow estimation of molecular weight which is calculated using an empirical mass vs. size calibration curve. DLS will give only estimates of the molecular weight of macromolecules rather than an absolute value. A calibration curve of molecular weight vs. hydrodynamic size is used which assumes different models such as globular proteins, linear polysaccharides, dendrimers and branched polymers.

For spherical particles (globular proteins or spheroidal protein assemblies), single exponential decay occurs which can be represented by the equation:

$$G(\tau) - 1 = e^{-Dk2\tau} \quad \ldots\ldots\ldots\ldots \quad (1)$$

The above equation is valid for monodisperse population of macromolecules. D is the diffusion coefficient and k is the Bragg wave vector which is defined by

$$q = (4\pi n / \lambda) \sin(\theta/2) \quad \ldots\ldots\ldots\ldots \quad (2)$$

In the above equation, q is the scattering vector; λ is the wavelength of the incident light, n is the refractive index of the medium and θ is the scattering angle.

For multi modal distribution, auto correlation function is represented by an integral of normalized decay rates rather than a single exponential equation[6].

Autocorrelation coefficient is measured as:

$$G(\tau) = \int_0^\infty I(t)I(t+\tau)dt \quad \text{..... (3)}$$

Normalization of autocorrelation coefficients causes 1 as lower limit for G (∞) and 2 as upper limit for G (0).The correlation curves generated by the digital correlator give a picture regarding the size of the diffusing protein.

R_H, hydrodynamic radius is calculated from the measured diffusion coefficient by applying the Stokes- Einstein equation:

$$R_H = k_B T / 6\pi\eta D \quad \text{..... (4)}$$

T = Temperature, k_B = Boltzmann constant[1] and η is the dispersant viscosity.

D is the diffusion coefficient of macromolecules, a parameter form which the dimensions of a macromolecule as well as its molecular weight can be determined.

Intensity particle size distribution is transformed to mass or volume distribution by Mie theory. In case of intensity distribution, the region within each peak is proportional to the relative scattering intensity of each group of particles.

2.2.1.1 Characterization of aggregates by DLS

Aggregates due to their higher Mw will scatter strongly the laser light as compared to the monomer. DLS is a very fast technique for detection of aggregates and also very useful in the evaluation of polydispersity of the sample[7]. Several studies have shown that DLS can be used as a valuable tool to determine the aggregation state of particles but one of the important challenges which still exist in measuring the particle size of aggregates is the presence of very large aggregates which can dominate the scattering signal and lead to a biased result.

[1] **Boltzmann's constant** = 1.381 x 10^{-23} J/K

In the case of DLS measurements, the presence of aggregates greatly influences as well as contributes to a large amount of signal in the data. Based on DLS study, **Filipe et al.** have detected the masking effect of smaller aggregates by larger aggregates in polydisperse samples[8].

Mean hydrodynamic radii of the particle and polydispersity of the population are the two parameters which can be derived from the diffusion coefficient. Light scattering measurements for a polydisperse solution will give only an average diffusion coefficient. Moreover, the total scattered time correlation function of the solution is a result of superposition of the correlation functions of each of the individual species present in the solution[9].

High polydispersity index indicates a large variability in the particle size. For highly poly disperse samples containing groups of different particle sizes with multimodal solutions, Z-average is not suitable to describe the distribution results.

For characterization of HEWL aggregates, which fall in the nanometer size range, DLS is one of the important tools used by us for analysis of very heterogeneous protein aggregates.

The self-aggregation behaviour of HEWL at pH 12.2 was analyzed by DLS in a time dependent way. Hence, the question which has been given a reasonable importance in our study is **a) Can we track the changes in size and polydispersity as HEWL undergoes aggregation?**

We have put emphasis on DLS technique as a non-invasive characterization technique in order to observe the diffusion pattern and the growth behaviour of aggregates. Quantitative characterization of HEWL aggregates in a time dependent way is an important step to understand the relationship between incubation period of aggregates in alkaline pH and the increase in hydrodynamic size of aggregates.

Here we have attempted to resolve the growth kinetics of multiple oligomeric species, by DLS, which are in equilibrium with each other.

2.2.1.2 Review of literature

Hill et al. have studied in detail the kinetics of fibril formation by HEWL under acidic conditions by DLS[10]. Hydrodynamic radii of intermediate aggregates were estimated from DLS measurements. Moreover, the particle size distributions obtained gave a picture about the growth of aggregates of HEWL at pH 2.0 over an incubation period of 4 days. They have demonstrated the change in diffusion pattern and growth behaviour of aggregates as they grow in size with incubation time. A detailed analysis of the kinetics of nucleation of aggregates has been derived from particle size distributions.

Similar studies carried out by **Li et al.** have shown the use of DLS as a technique to characterize the protein clusters of radius of about 100 nm. Widths of the cluster size distribution, volume fraction and aggregate size have been derived for lysozyme protein from DLS data[11].

2.2.2 Materials and methods

2.2.2.1 Preparation of HEWL aggregates for DLS measurements

HEWL stock was prepared in milliQ water by the use of commercially available lysozyme. The stock solution was diluted to a concentration of 120 μM in sodium phosphate buffer pH 7.0 for the preparation of monomer sample. Prior to DLS measurements, the sample was filtered in order to avoid any preassembled aggregates.

For inducing aggregation, HEWL stock in milliQ water was diluted to 120 μM in 50 mM sodium phosphate buffer, pH 12.2. Protein concentration of the stock was determined by using absorbance at 280 nm (ε = 37, 970 M^{-1} cm^{-1}).HEWL monomer concentration was kept as 120 μM and was prepared in 50 mM pH 7.0, Sodium phosphate buffer.

Sample preparation - All the samples (monomer as well as aggregates) were filtered through 0.22 μ filter before performing the DLS measurement. Samples were filtered through syringe filter in order to remove the large dust particles so that they do not interfere with the particles of interest.

Hen egg white lysozyme was purchased from Sigma–Aldrich Company Pvt. Ltd. (Cat no. L-6876).

2.2.2.2 Experimental parameters

All the measurements were performed multiple times for each sample i.e. 3 consecutive measurements with each measurement consisting of 11 sub-runs with 10 second duration, in order to ensure reproducibility of the data. Thermal equilibration for the samples was performed for 120 seconds by means of inbuilt temperature control for cuvettes. All the measurements were carried out at 25^{o}C. Autocorrelation functions were collected, keeping the acquisition parameters same for each sample. Particle size distributions were then obtained from these autocorrelation functions using the algorithms provided by Zetasizer Nano S. The intensity correlation functions were collected at a measurement angle of 90°. Dynamic Light scattering studies were carried out using Malvern Nano Zetasizer apparatus (*Zetasizer Nano S, Malvern instruments*) equipped with a 3 mW He-Ne red light laser (λ = 633 nm).As from Eqn.2, the value of scattering vector (q) obtained is 18.7 x 10^{6} m^{-1} by using the appropriate values of parameters such as solvent refractive index (n = 1.33), the laser wavelength (λ = 633 nm) and scattering angle (θ = 90^{o}). All DLS measurements were performed under experimental conditions corresponding to a scattering vector of 18.7 μm^{-1}. For processing the data, Zetasizer software was used which is provided with Zetasizer Nano S instrument. In our case, data processing was performed with analysis mode for protein analysis. The parameters such as intensity size distribution, PDI and Z-average diameter were obtained from autocorrelation function by protein analysis mode. The software takes into account the cumulant fitted data to determine the quality of the data.

2.2.3 Results and Discussion

Z-average hydrodynamic radii of the HEWL oligomers were estimated by DLS in a time dependent way. The mean radius for the aggregates increases steeply for the initial 24 hours and then the increase becomes steadier over the due course of the time period of 18 days. The **[Figure 2.2.3 (a)]** displays an increase in Z-average radius for the aggregates corresponding to an increase in overall size of the aggregates. This is also reflected as an increase in scattering intensity for the aggregates with time. The increase in scattering signal for the aggregates coincides with the increasing trend as observed in mean hydrodynamic radii of the aggregate species.

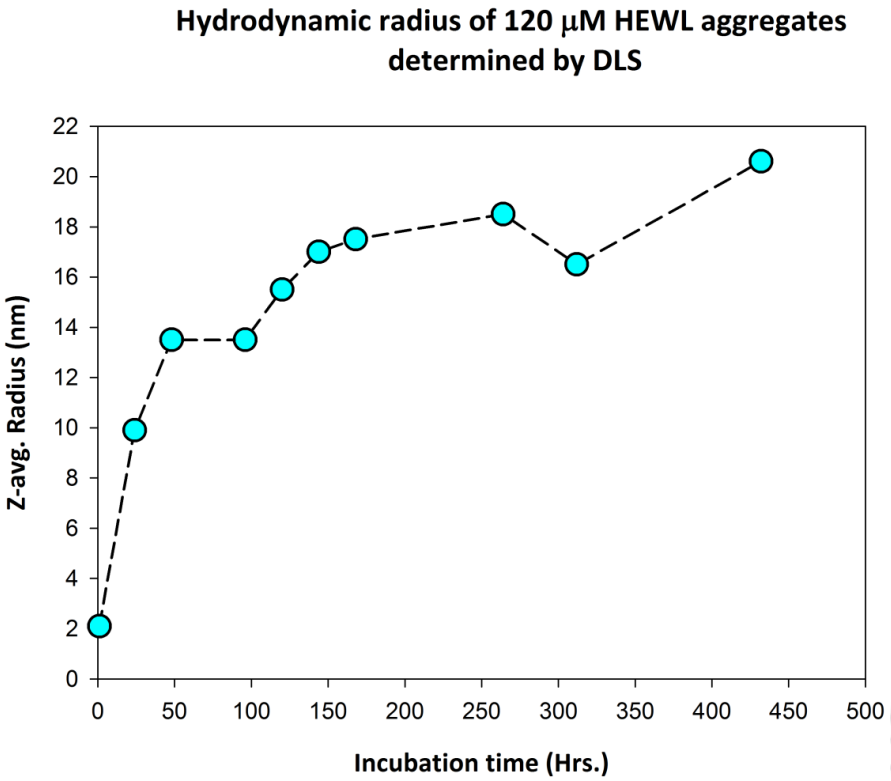

Figure 2.2.3 (a): Hydrodynamic radii of the particle size distributions obtained for 120 µM HEWL aggregates incubated in pH 12.2 from DLS measurements.

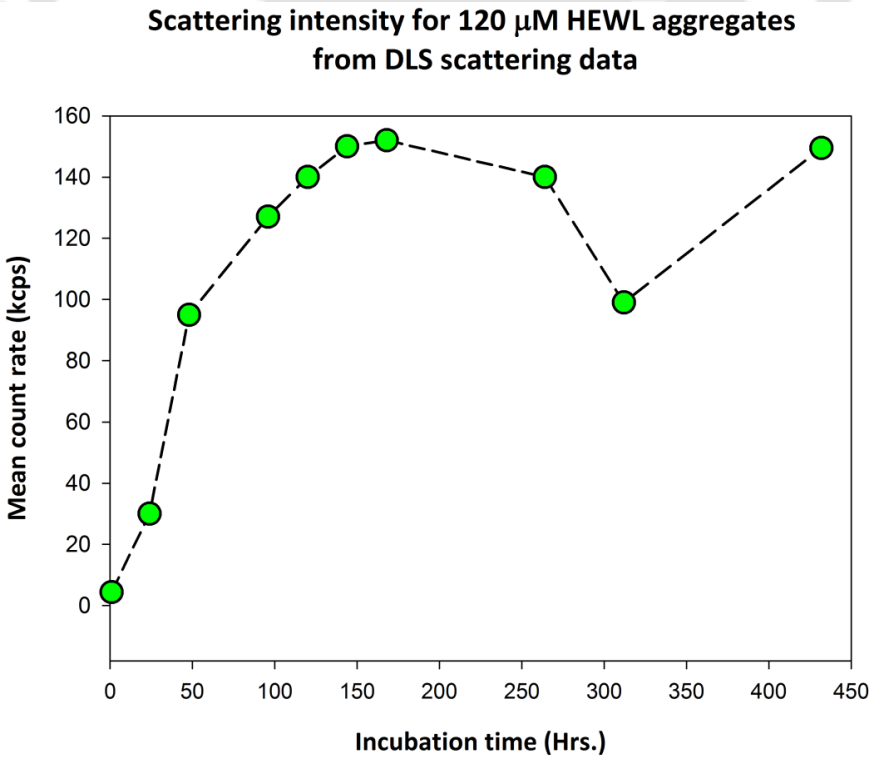

Figure 2.2.3 (b): Changes in scattering intensity in terms of mean count rate (kcps) on Y-axis versus incubation period (hours) on X-axis.

2.2.3.1 DLS size distribution results for **120 µM HEWL monomer**

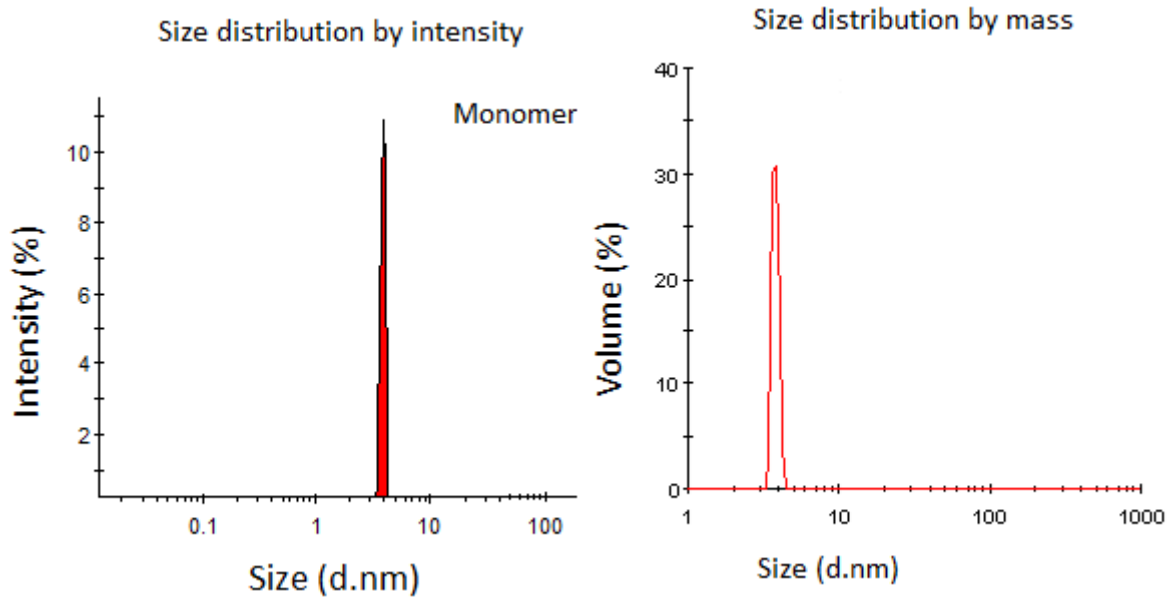

Figure 2.2.3.1: 120 µM HEWL monomer (freshly prepared) in 50 mM pH 7.0 Sodium phosphate buffer. Size distribution by volume plot is also shown in addition to intensity distribution plot for 120 µM HEWL monomer in pH 7.0 buffer.

Z-Average (d.nm)	3.88
% Pd (percent)	4.2
Mean CR[2] (kcps)	13
% Mass (d.nm)	100
Intercept	0.86
Peak polydispersity	Monodisperse
Estimated Mw (kDa)	15.3 ± 2

Table 2.2.3.1: Hydrodynamic parameters obtained from DLS measurements for 120 µM HEWL monomer.

Polydispersity: The peak polydispersity % is 4.2 which suggest that the peak is highly monodisperse. Sample contains one major population by volume.

Hydrodynamic radius: Hydrodynamic radius obtained for HEWL monomer is 1.94 nm which correlates well with the reported value in the literature for lysozyme[10].From the results obtained for HEWL monomer in pH 7.0, the relative narrow distribution is visible as compared to aggregates yielding an accurate Z-average diameter.

[2] Mean CR (kcps) – Derived count rate for intensity

2.2.3.2 DLS size distribution results for **120 µM HEWL aggregates** incubated for **1 hour** in pH 12.2

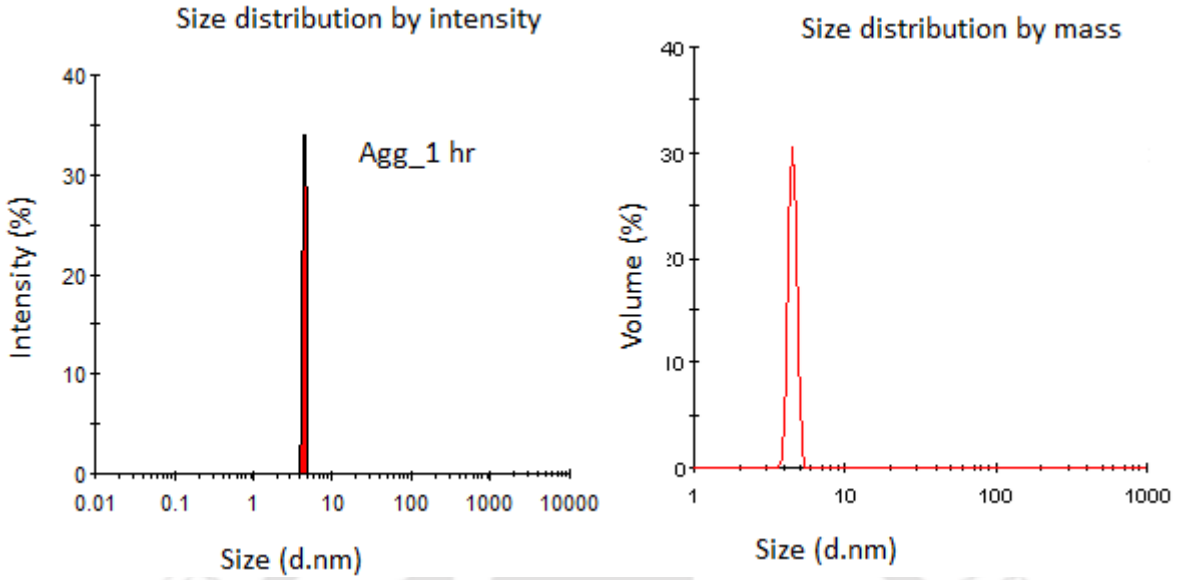

Figure 2.2.3.2: 120 µM HEWL aggregates in 50 mM pH 12.2 Sodium phosphate buffer (incubated for 1 Hr.). Size distribution by mass is also shown for 1 hour old HEWL aggregates.

Z-Average (d.nm)	4.52
% Pd (percent)	4.7
Mean CR (kcps)	4.2
% Mass (d.nm)	100
Intercept	0.76
Peak polydispersity	Monodisperse
Estimated Mw (kDa)	22.6 ± 1.1

Table 2.2.3.2: Hydrodynamic parameters obtained from DLS measurements for 1 hour old 120 µM HEWL aggregates.

Polydispersity: The peak polydispersity % is 4.7 which suggest that the peak is highly monodisperse. Sample contains one major population by volume.

Hydrodynamic radius: Hydrodynamic radius obtained for HEWL aggregates incubated for 1 hour is 2.26 nm which is slightly greater as compared to that of lysozyme monomer. This suggests that the protein molecules are unfolded when exposed to alkaline pH.

2.2.3.3 DLS size distribution results for **120 µM HEWL aggregates** incubated for **24 hours** in pH 12.2

Initially, PSD[3] showed a single narrow peak for 1-hour old aggregate. However, after a period of 24 hours, a second peak emerges which refers to large aggregate peak dominates the intensity size distribution. These results indicate the formation of another population of larger aggregates accompanied with smaller aggregates.

24 Hrs. old aggregates: In addition to the monomer peak, intensity distribution plot is showing additional peaks corresponding to aggregates of distinct sizes. Mass distribution plot **[Figure 2.2.3.3]** also revealed the presence of aggregates which are distinctly present in very low mass population.

Z-Average (d.nm)	19.8
PDI	0.43
Mean CR (kcps)	30.6
% Polydispersity	65.2
Intercept	0.91

Table 2.2.3.3: Hydrodynamic parameters obtained from DLS measurements for 1 day old 120 µM HEWL aggregates.

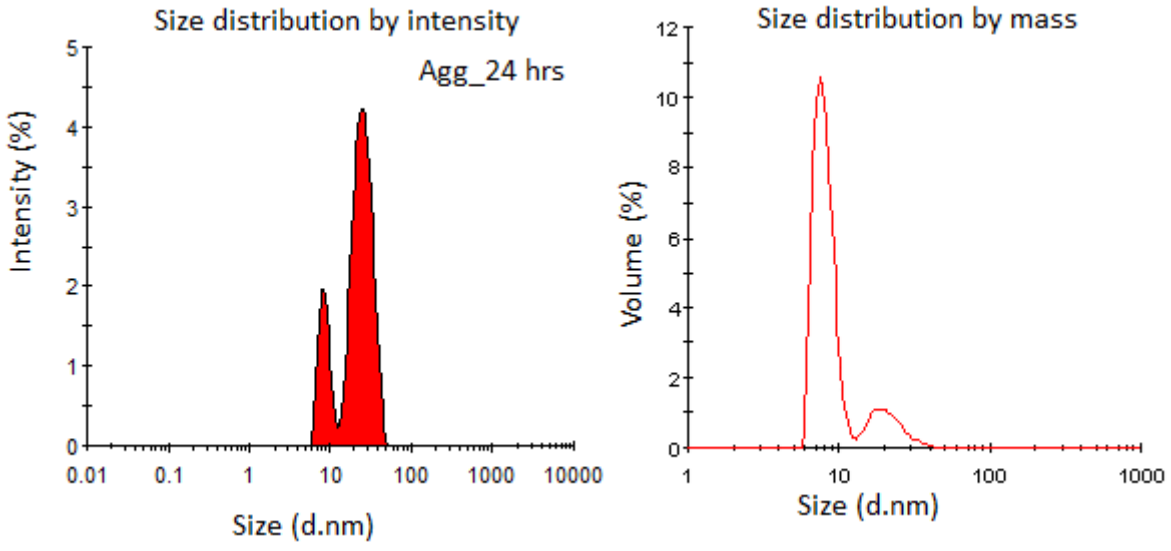

Figure 2.2.3.3: 120 µM HEWL aggregates in 50 mM pH 12.2 Sodium phosphate buffer (incubated for 24 Hours).Volume size distribution for 1-day old 120 µM HEWL aggregates in pH 12.2 buffer. The value for mass % denotes the mass composition for particles with different sizes in the distribution.

[3] **PSD** – Particle Size Distribution

Distribution results: The distribution is a multimodal distribution. In the case of 24 hours old aggregates, the particle size distribution is mostly composed of well resolved 2 major aggregate peaks with different hydrodynamic radii. One of the peaks is composed of aggregates of smaller hydrodynamic radii with 85 % of mass fraction dominating the whole population. The 2nd peak mostly comprises of aggregates with the larger size as the scattering intensity is 3.7 folds higher than that of the first peak but with a mass fraction ~ 15 %.

	Mode (nm)	% PD	% Intensity	% Mass	Peak Polydispersity
Peak 1	8.12	15.8	18	85	Monodisperse
Peak 2	24.6	26.7	67	15.1	Polydisperse

Polydispersity: Polydispersity index[4] is 0.43 which is greater than 0.3.It suggests that sample is highly polydisperse. The high value of polydispersity demonstrates a broad size range within the population indicating the presence of multiple species.

Hydrodynamic radius: The distribution results reveal that sample contains multiple peaks by volume. Hence, the Z-average value is skewed towards larger values. Hydrodynamic radius obtained for HEWL aggregates incubated for 24 Hrs. is 9.9 nm. Here, the distribution is separated into two well-resolved peaks. The 1st peak mainly constitutes of lower order oligomers or small aggregates with 18 % intensity and 85 % of mass fraction. The 2nd peak showed up with 3.7 folds higher intensity as compared to the first peak which is due to scattering by larger aggregates. Hence, the 2nd peak with higher polydispersity than the first peak mostly consists of higher order oligomers.

2.2.3.4 DLS size distribution results for **120 µM HEWL aggregates** incubated for **2 days** in pH 12.2

Z-Average (d.nm)	29.03
PDI	0.35
Mean CR (kcps)	95.4
% Polydispersity	58.9
Intercept	0.93

Table 2.2.3.4: Hydrodynamic parameters obtained from DLS measurements for 2 days old 120 µM HEWL aggregates.

[4] PDI – Polydispersity index

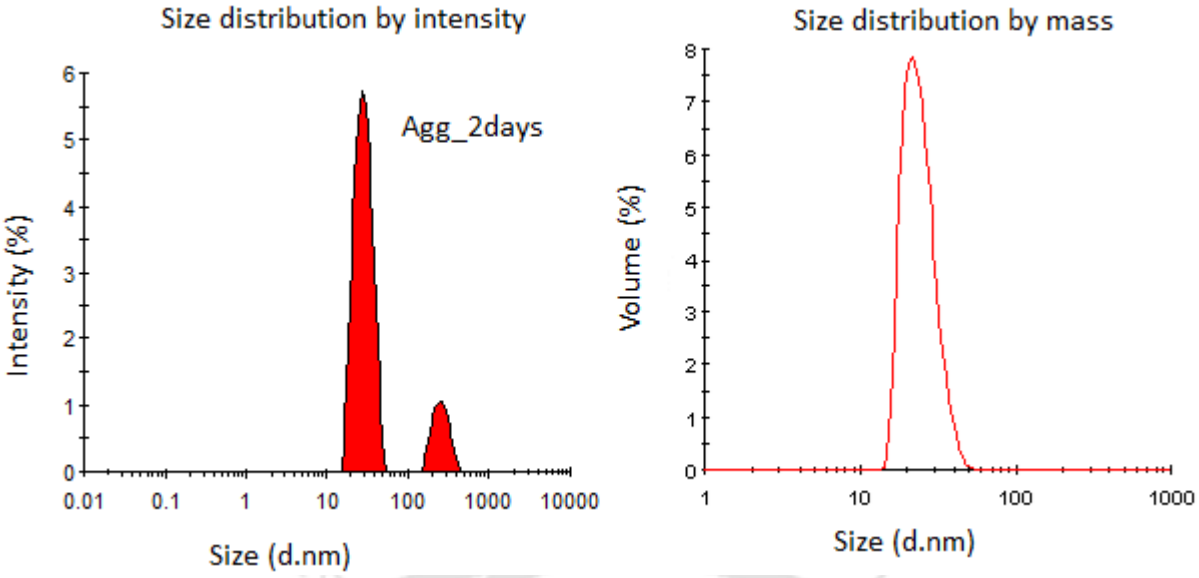

Figure 2.2.3.4: 120 µM HEWL aggregates in 50 mM pH 12.2 Sodium phosphate buffer (incubated for 2 days)

Distribution results: The distribution is a multimodal distribution.

	Mode (nm)	% PD	% Intensity	% Mass	Peak Polydispersity
Peak 1	27.0	24.8	85.3	99.9	Polydisperse
Peak 2	248.1	22.5	14.7	0.1	Polydisperse

It can be seen from the distribution plots that there is a gradual growth of aggregates and the aggregate peak becomes broader for 2 days old aggregates. The broad peak indicates the high polydispersity of the system. The aggregate peak, in fact, consists of multiple species such as small and large oligomers as well as monomers which are in equilibrium with each other. The second peak which appears with an intensity of 15 % corresponds to a mass fraction of 0.1 %. Thus, it can be inferred from this is that very large aggregates are also present but in extremely low fraction in the mass population.

However, one of the major limitations in DLS is the ability to resolve particles differing in their hydrodynamic radii by less than a factor of 2 or 3 **(Lorber et al., 2012)**. This can be one of the underlying reasons for the presence of only one broad peak in case of aggregates, in spite of the presence of small as well as large aggregates.

2.2.3.5 DLS size distribution results for **120 µM HEWL aggregates** incubated for **4 days** in pH 12.2

[Figure 2.2.3.5] displays the oligomeric state of HEWL aggregates after 4 days of incubation in pH 12.2. Biased result for Z-average diameter value in case of polydisperse samples is one of the disadvantages of DLS. As the larger particles will scatter more light as compared to the smaller ones, difficult of resolving differently sized population becomes prominent.

Z-Average (d.nm)	27.18
PDI	0.19
Mean CR (kcps)	127
% Polydispersity	43.4
Intercept	0.92

Table 2.2.3.5: Hydrodynamic parameters obtained from DLS measurements for 4 days old 120 µM HEWL aggregates.

Distribution results

	Mode (nm)	% PD	% Intensity	% Mass	Peak Polydispersity
Peak 1	28.3	26.5	100.0	100.0	Polydisperse

Mode: represents the highest peak in the distribution. In case if multiple peaks are present in the distribution, then mode is used to define the mid-point of different peaks.

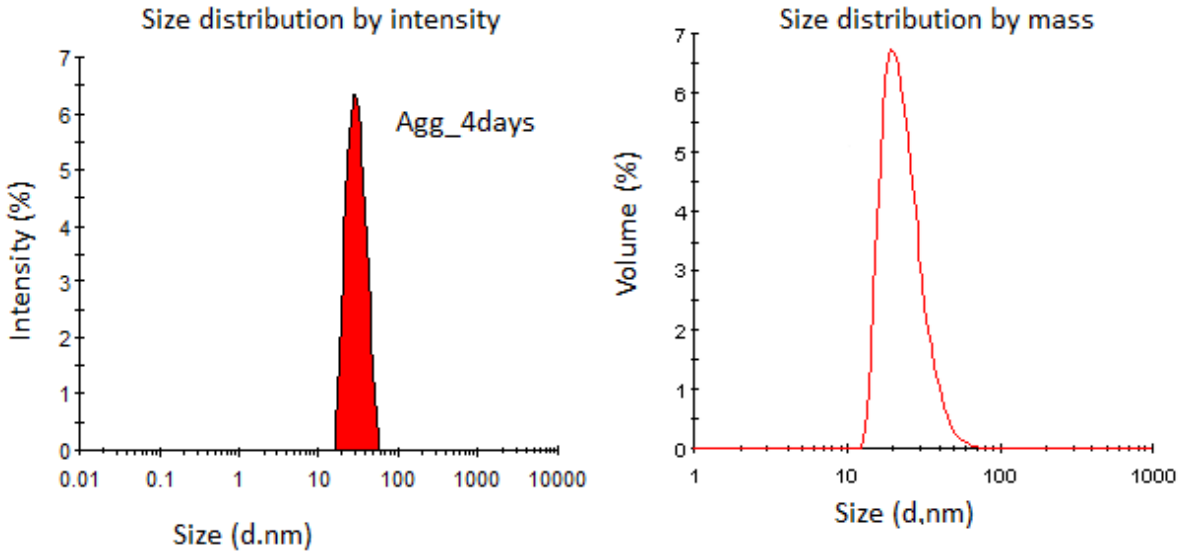

Figure 2.2.3.5: 120 µM HEWL aggregates in 50 mM pH 12.2 Sodium phosphate buffer (incubated for 4 days).

2.2.3.6 DLS size distribution results for **120 µM HEWL aggregates** incubated for **5 days** in pH 12.2

Z-Average (d.nm)	31.25
PDI	0.25
Mean CR (kcps)	138
% Polydispersity	50.4
Intercept	0.93

Table 2.2.3.6: Hydrodynamic parameters obtained from DLS measurements for 5 days old 120 µM HEWL aggregates.

Distribution results

	Mode (nm)	% PD	% Intensity	% Mass	Peak Polydispersity
Peak 1	39.08	48.9	98.3	100.0	Polydisperse

While particle size determination, drawbacks of DLS are revealed when there is the presence of very large particles in the distribution[12]. The dependency of sixth power of particle diameter on the scattered light intensity is a major hindrance in measurements. Even a very minute amount of large aggregates can obscure the presence of small aggregates or can produce an inaccurate result for size.

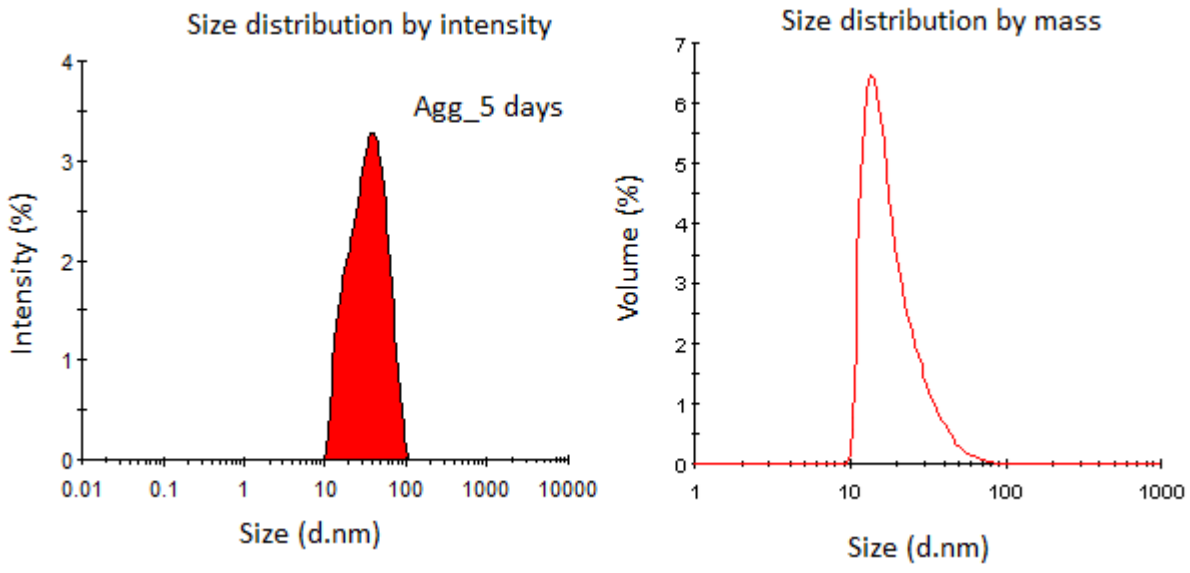

Figure 2.2.3.6: 120 µM HEWL aggregates in 50 mM pH 12.2 Sodium phosphate buffer (incubated for 5 days).

HEWL aggregates consist of mixture of larger aggregates, smaller aggregates and native population but **Figure [2.2.3.6]** shows only a single broad peak. This is due to the bias of

DLS measurements to larger particles. Hence, it is difficult to resolve different populations with sizes differences less than a factor of 3 in the distribution.

2.2.3.7 DLS size distribution results for **120 µM HEWL aggregates** incubated for **6 days** in pH 12.2

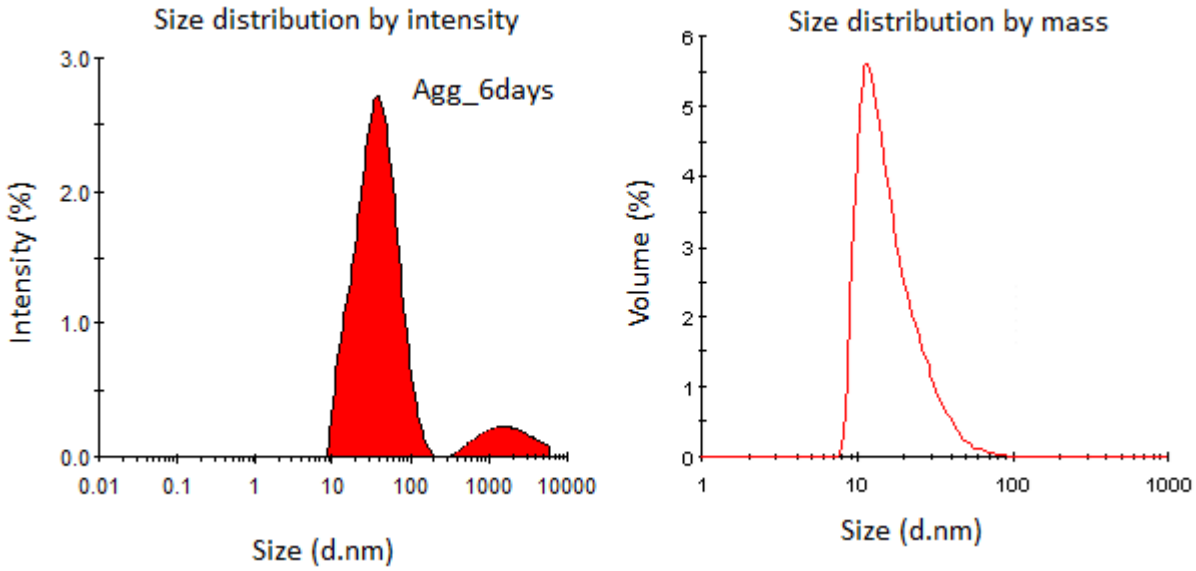

Figure 2.2.3.7: 120 µM HEWL aggregates in 50 mM pH 12.2 Sodium phosphate buffer (incubated for 6 days). Size distribution from DLS measurements obtained for 6-day old HEWL aggregates.

The contribution of large particles in polydisperse samples to the overall scattering is apparent from the distribution results. DLS data for HEWL aggregates incubated in pH 12.2 for 6 days shows: a) the main peak (peak 1) represents 90.4 % of the scattering intensity and an estimated 99.9 % fraction by weight. The % of peak polydispersity is 61.8 which represents a broad size distribution and reveals the presence of multiple species. The other peak (peak 2) is 9.6 % of the intensity but only 0.1 % by weight which is very insignificant.

Z-Average (d.nm)	33.76
PDI	0.35
Mean CR (kcps)	148.9
% Polydispersity	59.0
Intercept	0.92
Estimated Mw (kDa)	2510

Table 2.2.3.7: Hydrodynamic parameters obtained from DLS measurements for 6 days old 120 µM HEWL aggregates.

Distribution results

	Mode (nm)	% PD	% Intensity	% Mass	Peak Polydispersity
Peak 1	37.32	61.8	90.4	99.9	Polydisperse
Peak 2	1504	66.8	9.6	0.1	Polydisperse

2.2.3.8 DLS size distribution results for **120 µM HEWL aggregates** incubated for **7 days** in pH 12.2

Z-Average (d.nm)	34.66
PDI	0.36
Mean CR (kcps)	153.3
% Polydispersity	60.1
Intercept	0.93
Estimated Mw (kDa)	2670

Table 2.2.3.8: Hydrodynamic parameters obtained from DLS measurements for 7 days old 120 µM HEWL aggregates.

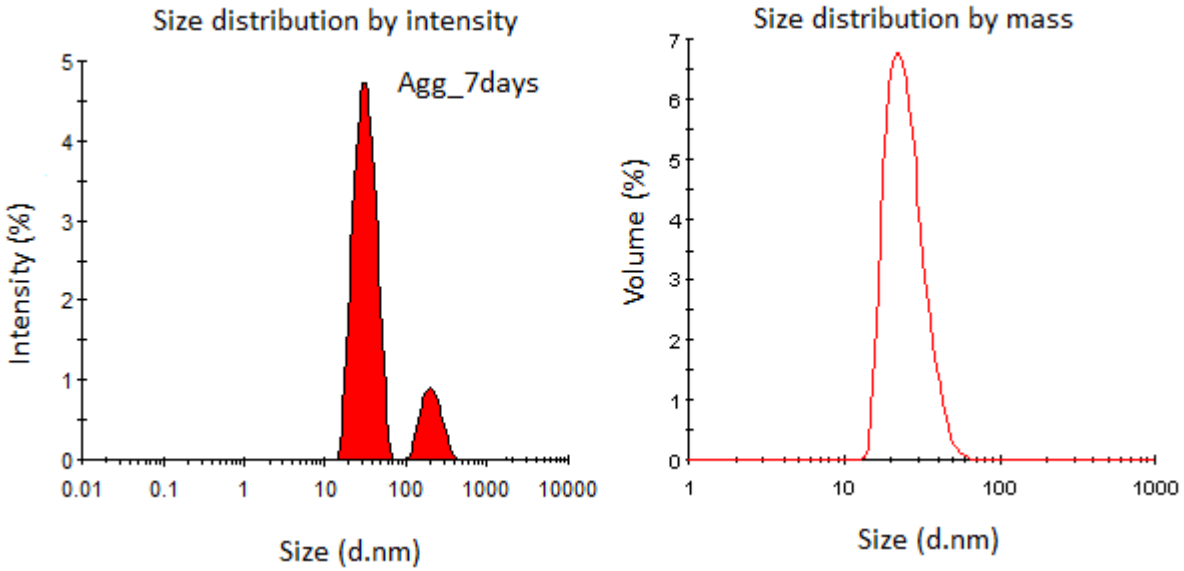

Figure 2.2.3.8: 120 µM HEWL aggregates in 50 mM pH 12.2 Sodium phosphate buffer (incubated for 7 days).

Distribution results

	Mode (nm)	% PD	% Intensity	% Mass	Peak Polydispersity
Peak 1	31.02	29.8	83.7	99.9	Polydisperse
Peak 2	196.9	27.5	14.7	0.1	Polydisperse

2.2.3.9 DLS size distribution results for **120 µM HEWL aggregates** incubated for **11 days** in pH 12.2

Z-Average (d.nm)	37.03
PDI	0.39
Mean CR (kcps)	140.6
% Polydispersity	62.7
Intercept	0.93
Estimated Mw (kDa)	3110

Table 2.2.3.9: Hydrodynamic parameters obtained from DLS measurements for 11 days old 120 µM HEWL aggregates.

Distribution results

	Mode (nm)	% PD	% Intensity	% Mass	Peak Polydispersity
Peak 1	39.08	42.9	83.5	99.9	Polydisperse
Peak 2	327.4	31.9	14.3	0.1	Polydisperse

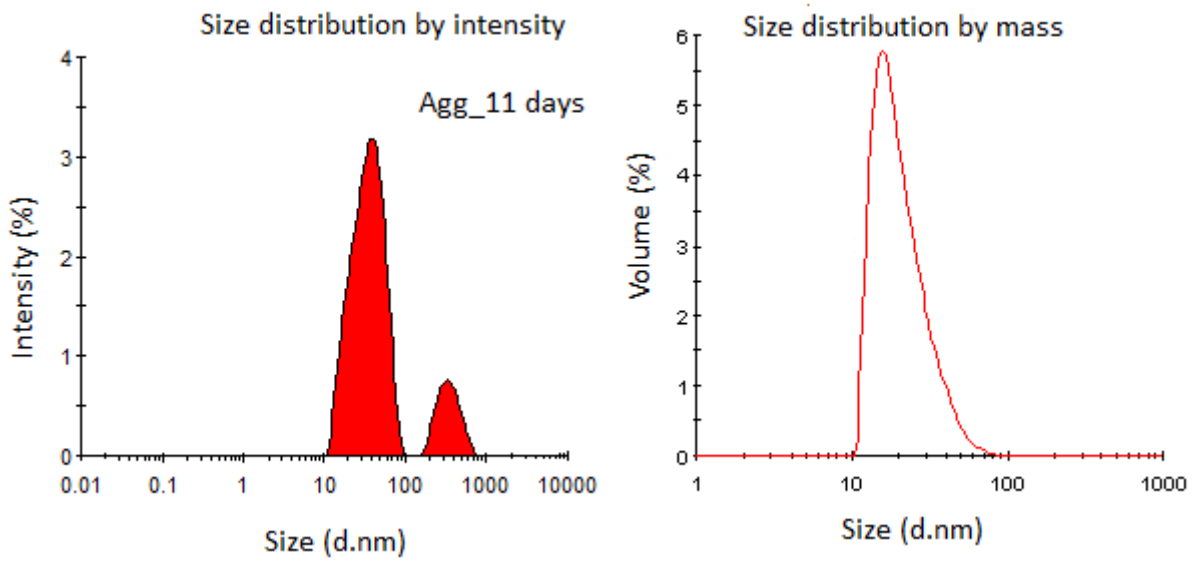

Figure 2.2.3.9: 120 µM HEWL aggregates in 50 mM pH 12.2 Sodium phosphate buffer (incubated for 11 days)

2.2.3.10 DLS size distribution results for **120 µM HEWL aggregates** incubated for **13 days** in pH 12.2

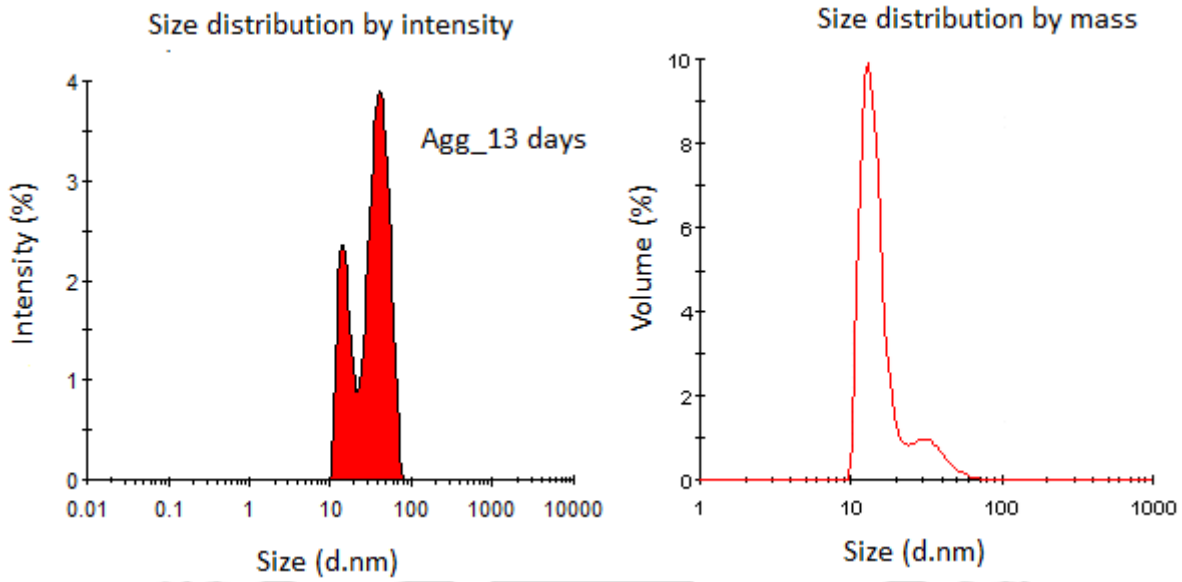

Figure 2.2.3.10: 120 µM HEWL aggregates in 50 mM pH 12.2 Sodium phosphate buffer (incubated for 13 days)

Presence of two distinct size aggregate populations is clearly confirmed from the intensity distribution plot **[Figure 2.2.3.10]**. It displays a peak with a shoulder which indicates the mixture of small aggregates with larger aggregates. The larger peak consists of population of aggregates of diameter of the order of 41 nm with polydispersity of 27.5 %. Additionally, the small shoulder peak consists of population of particle with diameter of 14.14 nm with polydispersity of 17.9 %.

Z-Average (d.nm)	32.93
PDI	0.38
Mean CR (kcps)	98
% Polydispersity	61.6
Intercept	0.94
Estimated Mw (kDa)	2360

Table 2.2.3.10: Hydrodynamic parameters obtained from DLS measurements for 13 days old 120 µM HEWL aggregates.

Distribution results

	Mode (nm)	% PD	% Intensity	% Mass	Peak Polydispersity
Peak 1	14.14	17.9	24.7	86.8	Polydisperse
Peak 2	40.93	27.5	63.1	13.2	Polydisperse

2.2.3.11 DLS size distribution results for **120 µM HEWL aggregates** incubated for **18 days** in pH 12.2

Z-Average (d.nm)	41.29
PDI	0.57
Mean CR (kcps)	149.5
% Polydispersity	75.7
Intercept	0.93
Estimated Mw (kDa)	4010

Table 2.2.3.11: Hydrodynamic parameters obtained from DLS measurements for 18 days old 120 µM HEWL aggregates.

Distribution results

	Mode (nm)	% PD	% Intensity	% Mass	Peak Polydispersity
Peak 1	9.8	12.8	5.7	71.0	Monodisperse
Peak 2	34.02	27.0	68.1	28.9	Polydisperse
Peak 3	9.98	19.8	26.2	0.1	Monodisperse

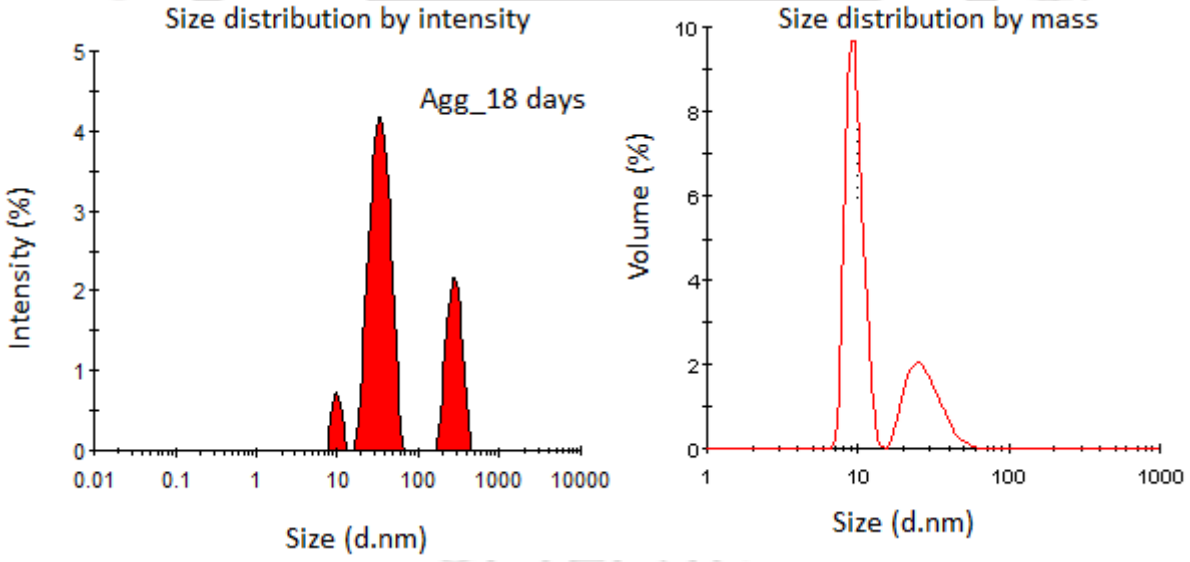

Figure 2.2.3.11: 120 µM HEWL aggregates in 50 mM pH 12.2 Sodium phosphate buffer (incubated for 18 days).

18 day old aggregates: Intensity size distribution plot shows 3 populations: 1st peak at 9.8 nm with just 5.7 % intensity but with a relative mass composition of 71 %, 2nd peak at 34.02 nm which is the group of larger size of particles which governs the distribution by intensity whereas by mass it is 28.9 % of the entire mass of the sample (lesser than peak 1) and 3rd peak is 26.2 % by intensity but only 0.1% by mass composition.

This denotes that the 3rd peak is insignificant by mass but due to larger size, it has significant contribution to the intensity scattering[11].

Translational diffusion coefficient of lysozyme computed from HYDROPRO software is 1.104E-06 cm^2/s. For HEWL monomer, translational diffusion coefficient was calculated from Stokes-Einstein equation by using the hydrodynamic radius obtained by DLS measurements. $D = k_B.T/ 6\pi\eta r$ which is the Stokes-Einstein equation, where T = 298 K, η = 0.00091 Pa.s and r = 1.9 nm (hydrodynamic radius of monomer). D is calculated to be 1.263E-06 cm^2/s (experimental) for HEWL monomer.

2.2.3.12 Growth kinetics of HEWL aggregates in pH 12.2 monitored with DLS

Brownian motion driven dispersion of smaller and larger particles gives rise to intensity fluctuations. Very rapid intensity fluctuations are seen in case of smaller particles as compared to the larger ones. These intensity signals can be further used to compute time correlation function of the scattered intensity. The rate of decay of the correlation function provides information about the particle size. Small particles move faster and the correlation drops very fast. On the contrary, in case of slowly moving larger particles correlation persists for a longer time. In case of faster diffusing smaller aggregates (4 days old), the calculated correlation curve decomposes very fast to baseline as compared to slower diffusing bigger aggregates (18 days old).The graph **[Figure 2.2.3.12]** clearly shows that there is a total loss of correlation within 1000 µs for aggregates which are 4 days old in contrast to aggregates which are 18 days old where the diffusing particle needs more than 10000 µs before complete loss of correlation.

After an incubation period of 24 hours, aggregates emerge with slower decay rates in correlation functions. The increase in shifting of the decay curve towards the right with decreasing decay rate suggest that size, as well as a fraction of larger aggregates in the population, is increasing with time. This shift in the decay also indicates a highly polydisperse nature of the sample. It also indicates the appearance of aggregates with increasing hydrodynamic diameter which seemed to have a slower diffusion after 24 hours of incubation of HEWL in pH 12.2. Henceforth, it can be concluded that larger aggregates start appearing within the population with slower decay time as revealed from the correlation curve.

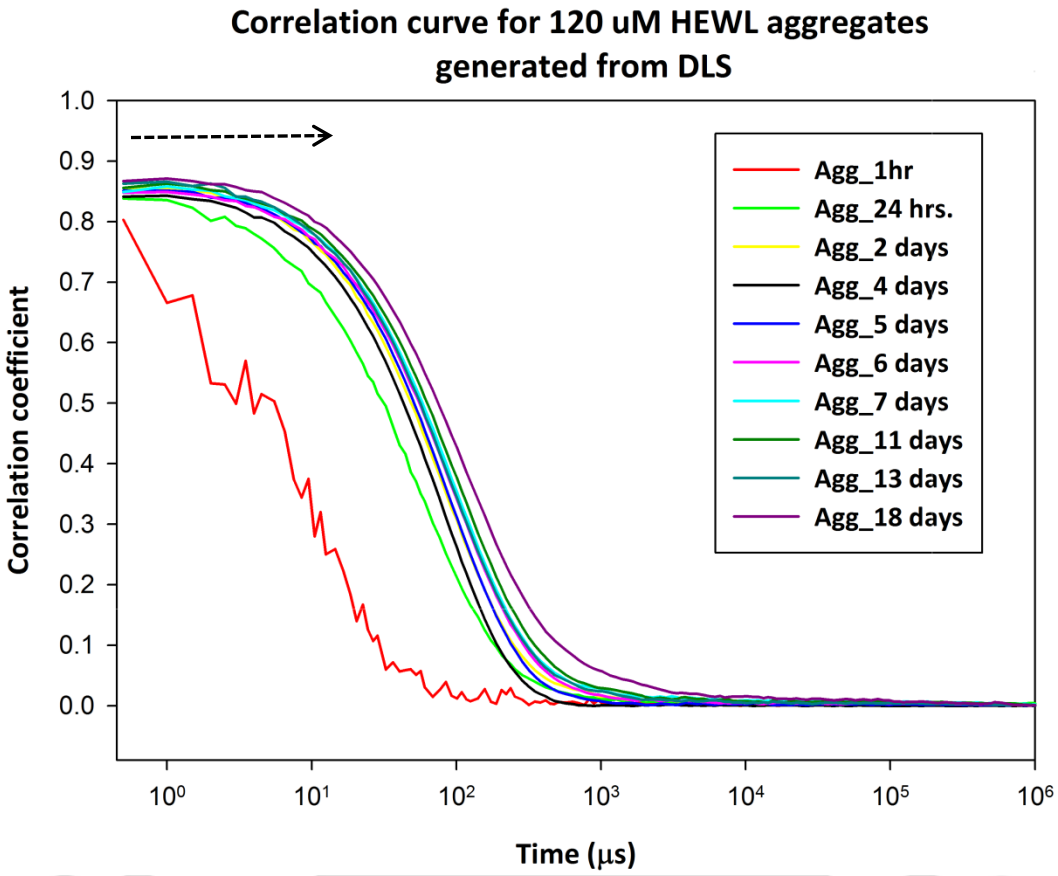

Figure 2.2.3.12: Normalized intensity autocorrelation function as a function of delay time. X-axis represents delay time, **τ** in **μs** and Y-axis represents correlation function as **g (τ)**.Plot shows the evolution of autocorrelation functions from light scattered by HEWL aggregates incubated in pH 12.2 for different time periods.

2.2.4 Conclusion and Perspectives

DLS was used to obtain the size distribution, polydispersity, Z- average hydrodynamic radius and average molecular weight of the aggregates. Particle size distributions were obtained for aggregates in a time dependent way. Size distribution data were computed as function of intensity, volume, and mass for polydisperse samples.

There was a clear distinction between the hydrodynamic radii of the monomer (Lysozyme in native state); protein monomer accompanied by oligomers and large HEWL aggregates. In this study, we have used DLS to monitor the changes in hydrodynamic radii and molecular weight as the aggregation proceeds.

- As the oligomerization proceeds, the scattering intensity, as well as hydrodynamic radii, increases for aggregates incubated in pH 12.2 at a concentration of 120 µM (same as monomer concentration) but the scattering intensity remains stationary in the case of monomer. Light scattered from protein monomer is insignificant as compared to the protein aggregates formed at the same concentration.
- Monomodal distribution was obtained for HEWL in native state (pH 7.0). Hydrodynamic radius obtained for HEWL monomer is 1.94 nm which correlates well with the reported value in the literature for lysozyme[11].
- A huge jump in the hydrodynamic radii is noticed in case of 24 hours incubated sample as compared to 1 hr. incubated sample in pH 12.2. This is depicted from the value of Z-average radii (r.nm) which accelerates from 2.26 nm to 9.9 nm. In aggregating condition, the particle radius increases up to 20 nm for 18 day old aggregates which is almost 10 times larger than the original monomer size. For aggregated samples, broadening was observed in the distribution as compared to a very narrow distribution of the HEWL monomer.
- According to Stokes-Einstein relationship for diffusion coefficient, large particles with higher molecular volume will diffuse slowly as compared to smaller particles. As the aggregation proceeds, the mean hydrodynamic particle size and molecular volume of the aggregates increase in a time dependent way which is clearly visible from the correlation curve.

References

1. Weber, G. Polarization of the fluorescence of macromolecules. 2. Fluorescent conjugates of ovalbumin and bovine serum albumin. *Biochem. J.* **51,** 155–167 (1952).

2. Levi, V. & González Flecha, F. L. Labeling of Proteins with Fluorescent Probes. *Biochem. Mol. Biol. Educ.* **31,** 333–336 (2003).

3. Homchaudhuri, L., Kumar, S. & Swaminathan, R. Slow aggregation of lysozyme in alkaline pH monitored in real time employing the fluorescence anisotropy of covalently labelled dansyl probe. *FEBS Lett.* **580,** 2097–2101 (2006).

4. Kumar, S., Ravi, V. K. & Swaminathan, R. How do surfactants and DTT affect the size, dynamics, activity and growth of soluble lysozyme aggregates? *Biochem. J.* **415,** 275–288 (2008).

5. Ravi, V. K., Swain, T., Chandra, N. & Swaminathan, R. On the characterization of intermediates in the isodesmic aggregation pathway of hen lysozyme at alkaline pH. *PLoS One* **9,** 1–12 (2014).

6. Lorber, B., Fischer, F., Bailly, M., Roy, H. & Kern, D. Protein analysis by dynamic light scattering: Methods and techniques for students. *Biochem. Mol. Biol. Educ.* **40,** 372–382 (2012).

7. Bishop, J. B., Martin, J. C. & Rosenblum, W. M. A light scattering method for qualitatively monitoring aggregation rates in macromolecular systems. *J. Cryst. Growth* **110,** 164–170 (1991).

8. Filipe, V., Hawe, A. & Jiskoot, W. Critical evaluation of nanoparticle tracking analysis (NTA) by NanoSight for the measurement of nanoparticles and protein aggregates. *Pharm. Res.* **27,** 796–810 (2010).

9. Berne, B. J. & Pecora, R. Laser Light Scattering from Liquids. *Annu. Rev. Phys. Chem.* **25,** 233–253 (1974).

10. Hill, S. E., Robinson, J., Matthews, G. & Muschol, M. Amyloid protofibrils of lysozyme nucleate and grow via oligomer fusion. *Biophys. J.* **96,** 3781–3790 (2009).

11. Li, Y., Lubchenko, V. & Vekilov, P. G. The use of dynamic light scattering and Brownian microscopy to characterize protein aggregation. *Rev. Sci. Instrum.* **82,** 0–8 (2011).

12. Amin, S., Barnett, G. V, Pathak, J. A., Roberts, C. J. & Sarangapani, P. S. Protein aggregation , particle formation , characterization & rheology. *Curr. Opin. Colloid Interface Sci.* **19,** 438–449 (2014).

13. Davies, R. C., Neuberger, A. & Wilson, B. M. The dependence of lysozyme activity on pH and ionic strength. *Biochim. Biophys. Acta* **178,** 294–503 (1969).

2.3 TEM imaging to probe the **morphology** of HEWL aggregates and HEWL nanoparticles

Morphological characterization of protein nanoparticles was done by TEM imaging.

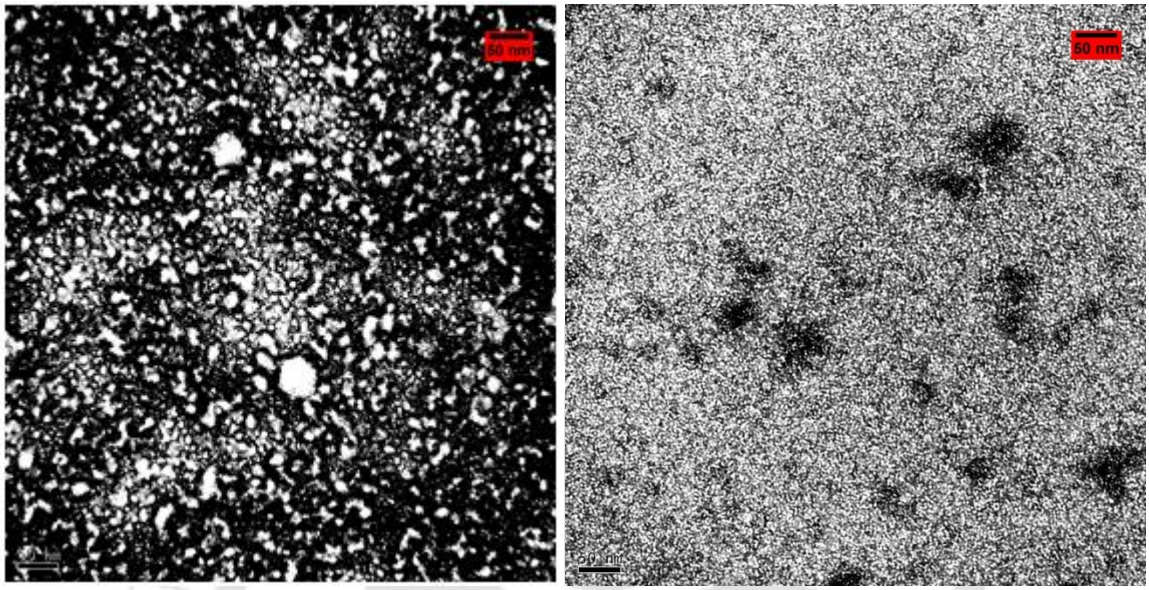

Figure 2.3.1: a) 120 µM HEWL aggregates incubated in pH 12.2 for 5 days b) 120 µM HEWL monomer in pH 7.0.

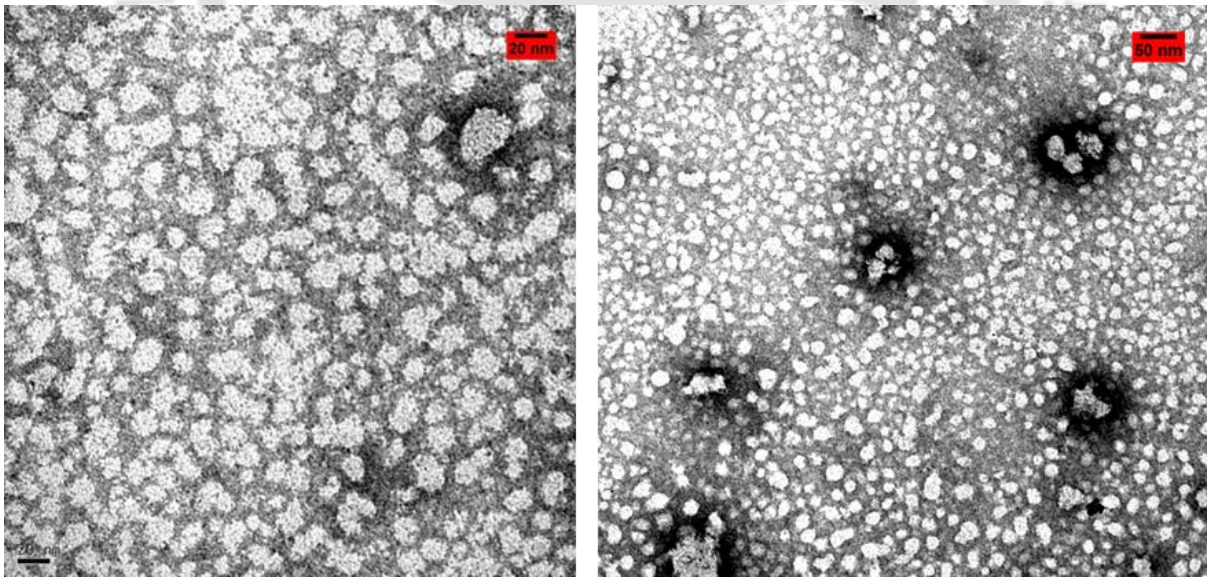

Figure 2.3.2: a) 120 µM HEWL aggregates incubated in pH 12.2 for 10 days and then transferred to pH 7.0 (20 nm resolution). b) 120 µM HEWL aggregates incubated in pH 12.2 for 10 days and then transferred to pH 7.0 (50 nm resolution).

Various analytical techniques have been successfully utilized to characterize the versatile HEWL protein nanoparticles. TEM imaging was done to view the changes in morphology of HEWL aggregates after transfer to pH 7.0.

2.3.1 Materials and Methods

1) **HEWL aggregates:** HEWL solutions were incubated at room temperature (25 ˚C) in 50 mM Sodium phosphate buffer pH 12.2 for 5 days. 5 µl of aggregates were placed on TEM copper grids.
2) **HEWL in native state:** 120 µM HEWL monomer solution was freshly prepared in 50 mM Sodium phosphate buffer pH 7. 5 µl of aggregates were placed on TEM copper grids.
3) **HEWL nanoparticles:** 120 µM HEWL aggregates incubated in pH 12.2 for 10 days and then transferred to pH 7.0 with 10 fold dilution. Accordingly, final concentration of the sample was 12 µM. The sample was allowed to stay in pH 7.0 for 2 days before TEM imaging.

Uranyl acetate [2% (w/v)] was used to accomplish the negative staining, samples were air dried and scanned in a high resolution ***JEOL transmission electron microscopy from JAPAN*** operating at an accelerating voltage of **200 kV**.

2.3.2 Results and Discussion

TEM is a high resolution technique which was used to probe the morphology of HEWL aggregates, HEWL in native state and HEWL nanoparticles. TEM images after acquisition were processed with freely available online software *Image J 1.49q*. Images were adjusted for brightness and contrast with the help of tool in the software. Particle size analysis was performed using the Particle size Analyzer r12, a plug in available for image J software.

TEM images confirmed the heterogeneous distribution of HEWL aggregates [**Figure 2.3.1 (a)**]. The polydisperse nature of the aggregates can be determined from the broad range of distribution obtained by particle size analysis. Particles obtained were of varied sizes ranging from 2 nm to 25 nm radii. Average particle calculated was 24 nm. Particles of circularity ranging from 0.313 to 1 were present in the population.

In case of HEWL in native state, TEM images revealed globular monomers of radii 1.9 - 2.8 nm [**Figure 2.3.1 (b)**]. This is consistent with the literature data reported for average size HEWL in native state. However, particles with radii of 4-5 nm were also found in the distribution. The sample was not completely monodisperse as HEWL is expected to form dimers in pH 7.0.

The distinct morphological change is clearly observed for protein nanoparticles [**Figure 2.3.2 (a) & (b)**]. Herein also, the polydisperse nature was exhibited by protein nanoparticles. Particles of radii ranging from 2 nm to 15 nm were present in the population as obtained by particle size analysis.

Particle size distributions derived from TEM images may not be completely reliable. For deriving the particle size distribution data, particles should be clearly separated. As in our case, there were overlapping particles in the image for aggregates due to high concentration of the sample. This could have led to inaccurate estimation of the particle sizes.

Due to the limitation of resources, imaging couldn't be performed in a time dependent way which resulted in limited data. Only for a single time point, the images were recorded for all the samples. In my thesis, I have used TEM images only for morphological characterization of monomer, aggregates and transferred samples.

2.4 Recoverable **enzymatic activity** of HEWL aggregates after transfer to pH 7.0

2.4.1 Introduction

Catalytic activity of lysozyme for bacterial cell walls of *Micrococcus lysodeikticus* is already well established in previous reports (**Davies et al., 1969**). The dependency of the activity of lysozyme towards bacterial cell suspensions on ionic strength and pH of the buffer has been demonstrated[13]. Lysozyme showed a remarkable high activity in the range of pH from 6.2 to 9.2 which is further dependent on the ionic strength of the medium.

In order to determine the amount of native population present in population of HEWL aggregates, catalytic activity is the best approach to determine the recoverable activity of HEWL aggregates after transfer to pH 7.0. The intriguing questions which we have addressed here: **a) what is the enzymatic activity profile of HEWL aggregates incubated in pH 12.2 transferred to pH 7.0 at different time points? b) What % of catalytic activity is retained for HEWL nanoparticles?**

Activity recovered for HEWL aggregates after transfer to neutral pH has been discussed. The catalytic activity which can be recovered for transferred samples tell us about the amount of monomeric protein present in the heterogeneous population of aggregates. Enzymatic activity of HEWL aggregates is proportional to the amount of native functional protein that can be reversibly recovered from the protein in non-native state. As enzymatic activity of HEWL aggregates is concentration independent and doesn't depend on the size of aggregates, we have reported here the results for only one concentration (120 µM) of transferred samples.

Previously, **Kumar et al.** have shown that formation of soluble HEWL aggregates in pH 12.2 abolishes activity. Although, 50 % activity was recovered from aggregates incubated for 2 hours in alkaline pH. However, authors have reported that for 24 hours old aggregates, there was complete loss of activity[4]. The decrease in activity is proportional to rise in aggregate population. The loss of HEWL activity in pH 12.2 reflects the depletion of native HEWL as irreversible folding of the protein occurs while the aggregation proceeds. Thus, formation of soluble irreversible HEWL aggregates at alkaline pH leads to loss of catalytic activity of the protein.

2.4.2 Materials and Methods

Hen egg white lysozyme (Cat no L-6876) and freeze-dried cells of *Micrococcus lysodeikticus* (A.T.C.C 4698) were purchased from Sigma-Aldrich Chemicals Pvt. Ltd., India.

HEWL in native state: 120 µM HEWL solution was prepared in 100 mM sodium phosphate buffer pH 7.0. The samples were incubated at 2 different temperatures i.e. one set at room temperature (20˚C – 22˚C) which fluctuated. In order to have a constant temperature, other set of samples were incubated at 28˚C in an incubator. For activity assay, the samples were diluted in assay buffer so that the concentration of the enzyme in final reaction mixture is 70 nM (1 µg/ ml).

HEWL nanoparticles: 120 µM HEWL aggregates incubated in 50 mM sodium phosphate buffer pH 12.2 were transferred to 100 mM sodium phosphate buffer pH 7.0 at different time points. The samples were transferred to pH 7.0 with 10 fold dilution such that the final concentration of the protein is 12 µM in the samples. After transfer to pH 7.0, samples were allowed to remain in pH 7.0 for 5 days (120 hours). Activity assay was carried out for the transferred samples at different transfer times as well as at different incubation period in pH 7.0 after transfer. The samples were incubated at 2 different temperatures. One set of samples were incubated at room temperature (20˚C to 22˚C). The other set of samples were incubated at 28˚C in an incubator. Activity assay was performed for both the sets of samples.

Stock solution of 2.34 mg/ml of Micrococcus Lysodeikticus was prepared in water as described[4] by **Kumar et al.** This solution was used as substrate for activity assays and was always freshly prepared for all the assay experiments. The substrate solution was further diluted to a concentration of 78 µg/ml in 50 mM sodium phosphate buffer, pH 7.0 (assay buffer). Thus, the final assay medium contains 78 µg/ml of substrate solution.

Inorder to carry out the activity assay, all the HEWL samples were diluted in assay buffer (Ionic strength of assay buffer is 0.05) in such a way that protein concentration was 70 nM in the assay medium. Enzyme kinetics experiments were carried out in Cary 100 double beam spectrophotometer. Enzyme activity of the HEWL samples was measured from the decrease in turbidity of the reaction mixture by monitoring the absorbance at 450 nm. The slope of bacteriolytic action was calculated for initial 30 seconds. The slope was plotted against incubation time. Experiments were performed in triplicates for each of the samples and the activity was reported as average of 3 independent measurements.

2.4.3 Results and Discussion

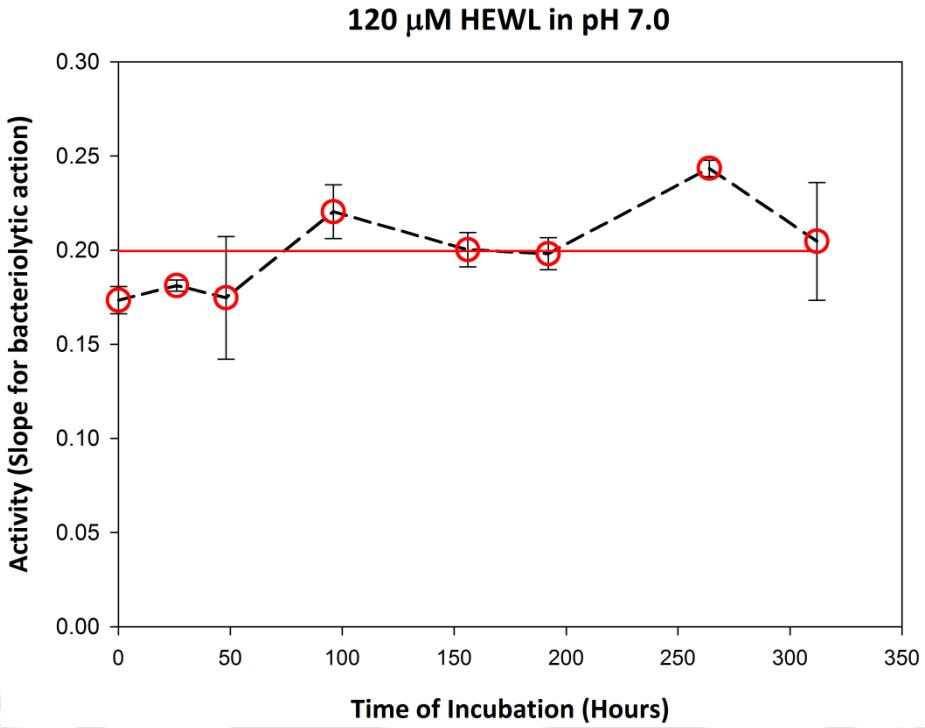

Figure 2.4.3.1: 120 µM HEWL incubated in 100 mM sodium phosphate buffer pH 7.0 at room temperature (20˚C – 22˚C). Initial rate of decrease (activity) was monitored by measuring absorbance 450 nm. Red solid line corresponds to mean value of the activity.

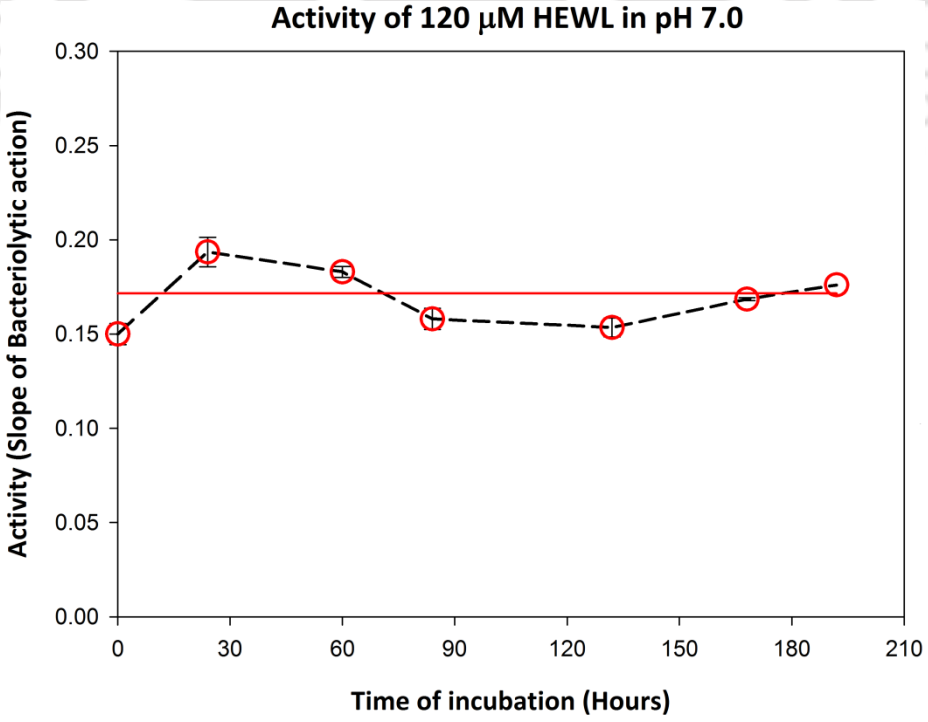

Figure 2.4.3.2: 120 µM HEWL incubated in 100 mM sodium phosphate buffer pH 7.0 at 28˚C. Red solid line corresponds to mean value of the activity.

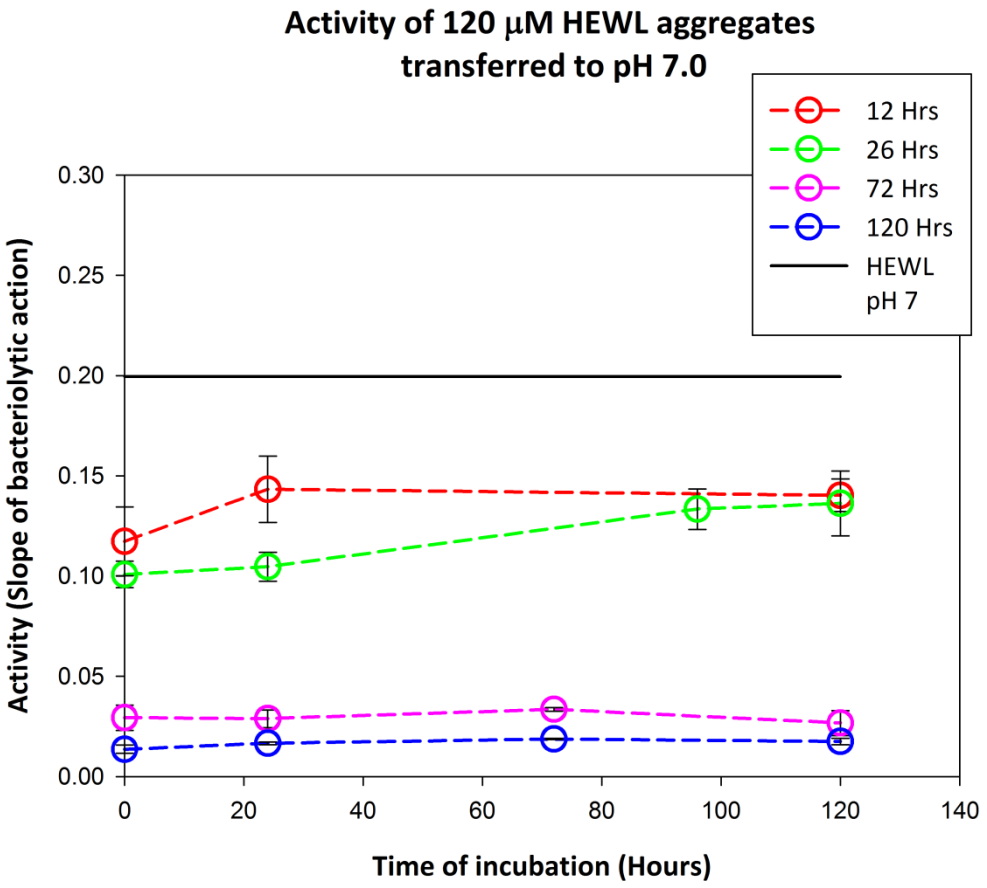

Figure 2.4.3.3: 120 µM HEWL aggregates were incubated in pH 12.2 and then transferred to 100 mM Sodium phosphate buffer pH 7.0 with 10 fold dilution. The transfer was carried out at different time points of incubation in pH 12.2: 12, 26, 72 & 120 hours. The samples were incubated at room temperature (20 °C - 22 °C). Activity assay was carried out for transferred samples in pH 7.0. Black solid line refers to the mean value for activity of 120 µM HEWL incubated in pH 7.0 at 20 °C-22 °C.

Previously, the depletion of activity of HEWL aggregates in pH 12.2 with time has been reported[4] by **Kumar et al**. Initially after 1 hour of incubation, almost 70 % activity could be recovered. This is proportional to the amount of native protein structure and function which can be recovered from the population of aggregates. However, gradually with increase in incubation time no amount of activity was recoverable after 24 hours. This decrease in activity clearly indicates the irreversible nature of HEWL aggregates. HEWL aggregates transferred after 72 hours and 120 hours displayed significantly less activity [**Figure 2.4.3.3**] in comparison to early hours transferred samples (12 & 26 hours). The aggregates transferred at early times retain significant amount of enzymatic activity whereas for late hours transferred samples there is complete loss of activity. This data is consistent with r_{ss} data for dansyl conjugated HEWL aggregates where early hours transferred samples fall apart due to the absence of intermolecular disulfide bonds.

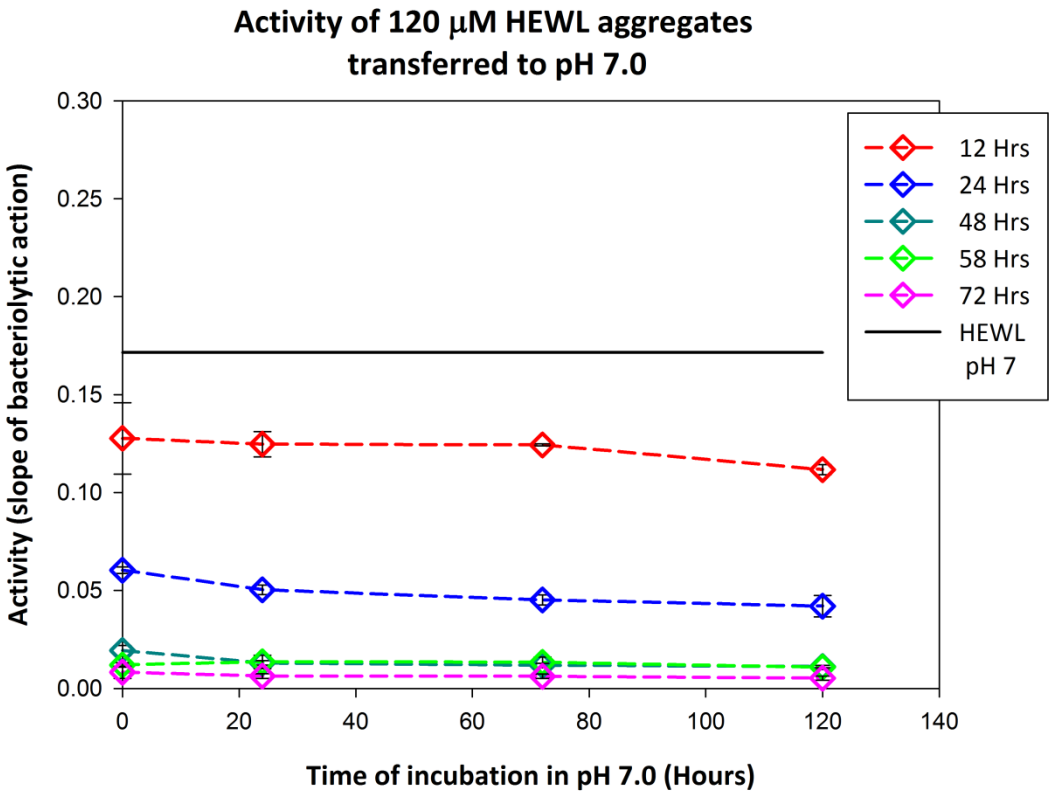

Figure 2.4.3.4: 120 µM HEWL aggregates were incubated in pH 12.2 and then transferred to 100 mM Sodium phosphate buffer pH 7.0 with 10 fold dilution. The transfer was carried out at different time points of incubation in pH 12.2: 12, 24, 48, 58 & 72 hours. The samples were incubated at room temperature (28 °C). Activity assay was carried out for transferred samples in pH 7.0. Black solid line refers to the mean value for activity of 120 µM HEWL incubated in pH 7.0 at 28 °C.

The absence of incorrect intermolecular –S-S- bonds at early times to fasten the aggregates together is the underlying reason for recovery of enzymatic activity in early hours transferred samples. Early hours transferred samples (12 hrs. and 24 hrs.) showed remarkable activity. In contrast to early hours transferred samples there was a significant drop in the activity for 72 hours transferred samples which reveal the formation of more stable and irreversible aggregates at later times [**Figure 2.4.3.4**]. Bacteriolytic activity of HEWL at concentration of 120 µM in pH 7.0 remains constant which indicates no loss of activity over an incubation period of 5 days [**Figure 2.4.3.1 & 2.4.3.2**]. A decrease of 20 % and 31 % in enzymatic activity was observed for early hours transferred samples (12 hours and 26 hours) respectively as compared to HEWL monomer. Hence, it can be said that samples transferred early to pH 7.0 recover substantial amount of enzymatic activity. Interestingly, 120 hours transfer samples showed almost 90 % loss in enzymatic activity [**Figure 2.4.3.3**]. Hence, at later times aggregates fail to retain their enzymatic activity.

Formation of intermolecular disulfide bonds at later time of incubation in pH 12.2 is responsible for holding the assembly together. These disulfide bonds keep the monomeric units together in oligomeric assemblies. The appearance of these inappropriate –S-S- bonds restricts the protein chain dynamics which is necessary for enzyme function. This results in loss of enzymatic activity. Incorrect –S-S- bonds may form when –SH groups in protein interior (shielded form solvent pH) come close enough.

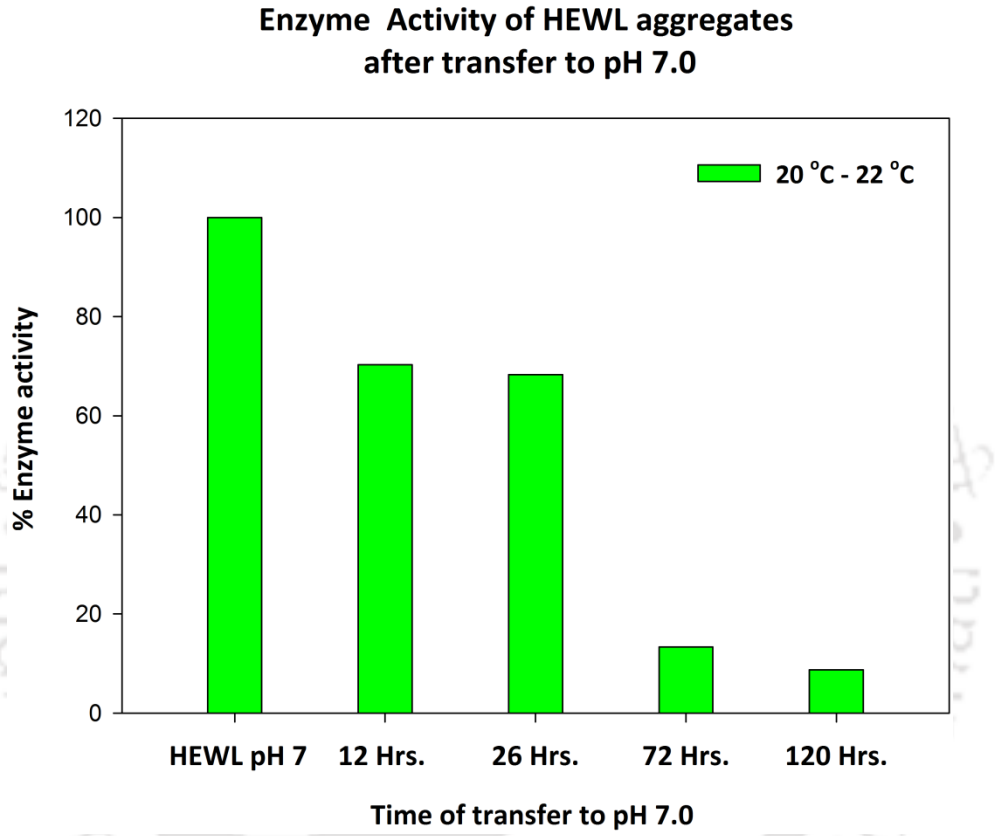

Figure 2.4.3.5: Percentage of HEWL activity recovered for HEWL aggregates after transfer to pH 7.0. The transfer was carried out after incubation at pH 12.2 for a) 12 hours b) 26 hours c) 72 hours & d) 120 hours. Activity for native 120 µM HEWL at pH 7.0 was normalized to 100 %. For all the transferred samples, % activity was calculated after 120 hours of incubation in pH 7.0 following the transfer.

Activity for 120 µM HEWL in pH 7.0 was normalised to 100 %. The percentage of enzyme activity of HEWL was calculated for transferred samples with reference to the native protein. In the above plot, activity was measured for transferred samples (12, 26, 72 & 120 hours transfer) incubated further for 120 hours in pH 7.0 after transfer. Remarkable amount of activity i.e. almost 70 % of activity was recovered for samples transferred at early times (12 & 26 hours). However, the activity dropped to ~ 13 % for 72 hours transferred samples [**Figure 2.4.3.5**]. In addition, insignificant amount of activity (9 %) was recoverable for aggregates transferred after 120 hours. Higher amount of activity could be recovered from

early hours transferred samples which suggests the presence of monomeric species in the population.

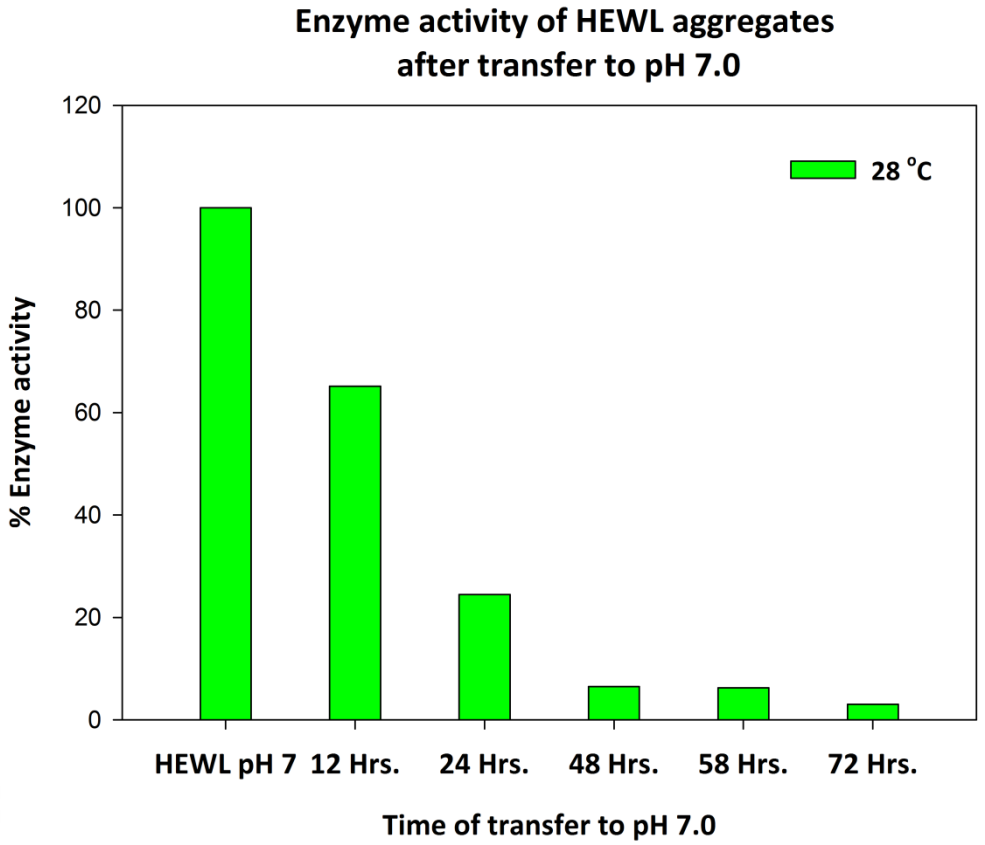

Figure 2.4.3.6: Percentage of HEWL activity recovered for HEWL aggregates after transfer to pH 7.0. The transfer was carried out after incubation at pH 12.2 for a) 12 hours b) 24 hours c) 48 hours d) 58 hours & e) 72 hours. Activity for native 120 µM HEWL at pH 7.0 was normalized to 100 %. For all the transferred samples, % activity was calculated after 120 hours of incubation in pH 7.0 following the transfer.

Almost 65 % of activity was observed for 12 hours transferred samples. 24 hours transferred samples retained about 24 % of activity. In contrast, significant amount of drop in activity which is about 6% was observed in case of 48 and 58 hours transferred samples [**Figure 2.4.3.6**]. Decrease in activity suggests the depletion of native population in transferred samples. Negligible activity was recoverable for 72 hours transferred samples.

The activity recovered from transferred samples, incubated for 120 hours in pH 7.0 after transfer, is expressed as % of activity[5] with respect to that of native lysozyme. The transferred samples and native lysozyme were incubated at the same temperature and the concentration was kept the same i.e. 120 µM for both so as to have comparable results.

[5] **Activity (%)** is the percent of lysozyme activity recovered.

Chapter 3

Exploring the hydrophobic interior of Self-assembled HEWL nanoaggregates using polarity sensitive extrinsic and intrinsic fluorescent probes

3.1 **Pyrene probe** as an index of microscopic polarity of the environment of HEWL nanoaggregates

3.1.1 Introduction

This chapter describes the use of pyrene dye in fluorescence studies of HEWL aggregates spontaneously formed by the mechanism of self-assembly[1]. Firstly, we have studied the behaviour of pyrene chromophore in different environments of aqueous solvents and organic solvents. Secondly, fluorescent properties of pyrene monomer are being used to characterize hydrophobic environment of protein oligomers. The transition from hydrophilic to hydrophobic environment can be easily probed by monitoring the fluorescence intensity of different bands in pyrene. The fluorescence intensity ratio of I_3/I_1 provides information about the microenvironment surrounding pyrene[2]. This represents a very important parameter which can be applied to characterize a hydrophobic oligomeric system. If the surface of the hydrophobic microdomains present in the aggregates is exposed to the aqueous environment, then pyrene molecules associate with the exposed hydrophobic patches. However, there is also the possibility of hydrophobic pockets being sufficiently buried in the aggregates so that it is inaccessible to the pyrene. The unique ability of pyrene to exhibit highly structured emission bands between 370 and 430 nm in response to the polarity of the solvent makes it a very useful probe to detect the microenvironment of a heterogeneous system. The structured profile of pyrene monomer exhibiting five characteristic peaks can be observed as vibronic structure in the spectroscopic data.

Hydrophobically driven self-assembly mechanism is the central theory behind the spontaneous aggregation of HEWL at pH 12.2.[3]At this high alkaline pH, HEWL monomer units associate by exposed hydrophobic surfaces to form oligomer units of few nanometres in diameter. One major finding that these oligomers are in fact protein nanoparticles of hydrodynamic radius of the order of ~ 19-20 nm in solution has already been reported by us. The flexibility in the synthesis of HEWL nanoparticles is that it allows controlling the design of different sized nanoparticles by varying the initial monomer concentration. During the initial stages of aggregation, intramolecular association lead to the formation of oligomeric assemblies. Later, aggregates turn into compact structures by intermolecular associations via disulphide bonds which make the overall structure a tightly held stable nanoparticle.

The information which can be retrieved from I_3/I_1, solvent polarity ratio, relates to polarity of direct environment of pyrene with a lower ratio corresponding to polar environment and higher ratio to non-polar environment.

Changes in fluorescence peak intensities of pyrene were monitored for pyrene in sodium phosphate buffer pH 7.0 in a time dependent way. Pyrene is a symmetrical aromatic fluorophore which falls into the category of polycyclic aromatic hydrocarbons (PAHs)[4].

Ham effect observed in pyrene was shown by **Durocher et al.** Ham effect is usually observed in aromatic hydrocarbons where certain vibronic bands are forbidden[5].This effect is pronounced for vibronically weak or forbidden transitions. Ham effect can be generally understood as intensification of 0-0 (first singlet-singlet transition), symmetry forbidden band in the electronic spectra of aromatic molecules in response to solvent effects. In contrast, a weaker Ham effect is observed for vibronically allowed bands. This phenomenon has been studied in detail in aromatic systems such as benzene, naphthalene, anthracene etc. Various authors have reported intensity enhancements of the forbidden vibronic bands of pyrene in relation to varying solvent polarity as a result of Ham effect which mainly arises due to interaction between solute and solvent molecules[6].

Nakajima et al. have utilized the intensity enhancement phenomena of pyrene to explore the microenvironments within the cavity of β-cyclodextrin. Investigations carried out by them reported a fluorescence enhancement in response to an increase in hydrophobicity of the pyrene environment due to the formation of inclusion complex between pyrene and cyclodextrin[2]. Reduction in intensity ratio of I_1/I_3 of the aromatic hydrocarbon provided information about the polarity of the environment in the cavity of β-cyclodextrin. Numerous studies by the same author have been attempted to elucidate the effects of solvent polarity, solvent dipoles, temperature and isomeric solvents on intensification of forbidden bands in fluorescence spectrum of pyrene[7]. Intensity enhancement of 0-0 forbidden band has been observed in aromatic solvents as compared to aliphatic non-polar solvents which can be assigned to the π- electron system. Temperature dependence of band intensifications has been shown to be directly related to the effects of solvent polarity. Comparative studies on ortho-, meta- and para- derivatives of dichlorobenzene emphasized on position of substituents in the aromatic system and solvent dipoles to have major effect on band intensifications.

In the study of micellar systems, pyrene fluorescence has been successfully employed to investigate the polarity of the environment in SDS micelles[8].The significant reduction in vibronic band intensities of forbidden bands especially 373 nm (0-0) band relative to the vibronically allowed 383 nm (0-2) band indicated the non-polar interior of the micelles. The sensitivity of the emission spectrum of the condensed aromatic hydrocarbon, pyrene, has been useful to probe the nature of micellar interior. The remarkable changes in the intensities

of solvent sensitive bands in comparison to solvent insensitive bands in the fluorescence spectra of pyrene have been attributed to the effects of solvent polarity[9].The increase in relative intensity of 0-0 band is proportional to the increase in order of polarity of the solvent. Pyrene monomer fluorescence has been widely used in the past to probe the micellar microenvironment of normal micelles as well as reverse micelles[10]. III/I vibronic band ratios have been used to study the aggregation behaviour of inverted and normal micelles by giving an estimate of cmc (critical micelle concentration) of micelles.

Pyrene chromophore has been used as a probe to characterize the hydrophobicity of HEWL nanoparticles in this part of thesis.

3.1.2 Materials and Method

All the HEWL samples were incubated at room temperature (25 °C). Samples were incubated with pyrene for 10 minutes before recording fluorescence intensity spectra. Final concentration of pyrene was kept as 2 µM in all the samples. For the transferred samples, the samples incubated in 50 mM Sodium phosphate buffer, pH 12.2 were transferred to 100 mM pH 7, Sodium phosphate buffer with 10 fold dilution after 144 Hrs. Pyrene spectra measurement was carried out for transferred samples at different time points starting from 0hr. till 244 Hrs. in pH 7.

3.1.2.1 Steady-state fluorescence measurements

Steady state fluorescence measurements were performed using 1 cm path length quartz cuvettes. Fluorescence intensity spectra were recorded 3 times independently and averaged to get the final average spectra in a Jobin-Yvon Fluoromax-3 spectrofluorometer. Background intensity from the buffer was subtracted from each respective sample inorder to deduct the contributions from Raman scattering of solvent water molecules. Excitation was performed at λex = 310 nm and intensity spectra were recorded from 325 nm to 450 nm with excitation slit width of 2 nm and emission slit width of 1 nm. The slit widths of the emission monochromator were kept narrow inorder to ensure that sharp I_3/I_1 peaks are obtained as broad slits may lead to poor resolution which could produce inaccurate I_3/I_1 results. While taking measurement, the concentration of protein was diluted from 120 µM to 12 µM in the cuvette. These experiments are much easier to perform because there is no requirement of any tedious labeling reaction and only simple incubation of the hydrophobic dye with the sample under observation is enough to probe the hydrophobicity.

3.1.2.2 Materials

Pyrene (Sigma Aldrich**,** Cat no. EU – 09617LR, Water for HPLC (Merck, Cat no. 617650), Methanol for HPLC (Merck, Cat no. 1730), 1-Butanol GR (Merck, Cat no. 17758), Acetonitrile (Sigma Aldrich, Cat no. 34998), Ethanol (Merck, Cat no. 1.00983), Dimethyl Formamide (Sigma Aldrich, Cat no. 4551), Chicken egg white lysozyme (Sigma Aldrich, Cat no. L6876).

3.1.2.3 Experimental conditions

Concentration dependent studies of the hydrophobic pyrene group in aqueous solution revealed the existence of pyrene in monomeric state at very low concentrations (< 0.01 mM).The concentration of pyrene was kept low in all the respective solvents in order to have a purely monomeric solution because as the concentration increases, emission from the excimer complex starts to dominate[11]. In a very low concentration regime, no evidence of pre association of pyrene molecules has been found in previous studies. Association of two pyrene molecules due to close proximity results in excimer emission with an additional loss of the fine structure usually seen in case of monomeric pyrene. Hence; the concentration of pyrene was kept as 2 µM in order to avoid complications due to excimer formation.

The concentration of protein nanoparticles was kept as 12 µM for recording pyrene spectra. Prior to measurements, different lower concentrations of nanoparticles were tried but due to low emission intensity, the fine structure of the peaks was indistinguishable. At very low concentration of protein such as 4 µM, ratio of the peaks I_3 and I_1 was immeasurable due to very noisy signal.

Calculations: The intensity peak ratio (peak III/peak I) was calculated for each sample by considering the fluorescence intensity at λem = 373 nm as peak I and intensity at λem = 383 nm as peak III.

3.1.3 Results and Discussion

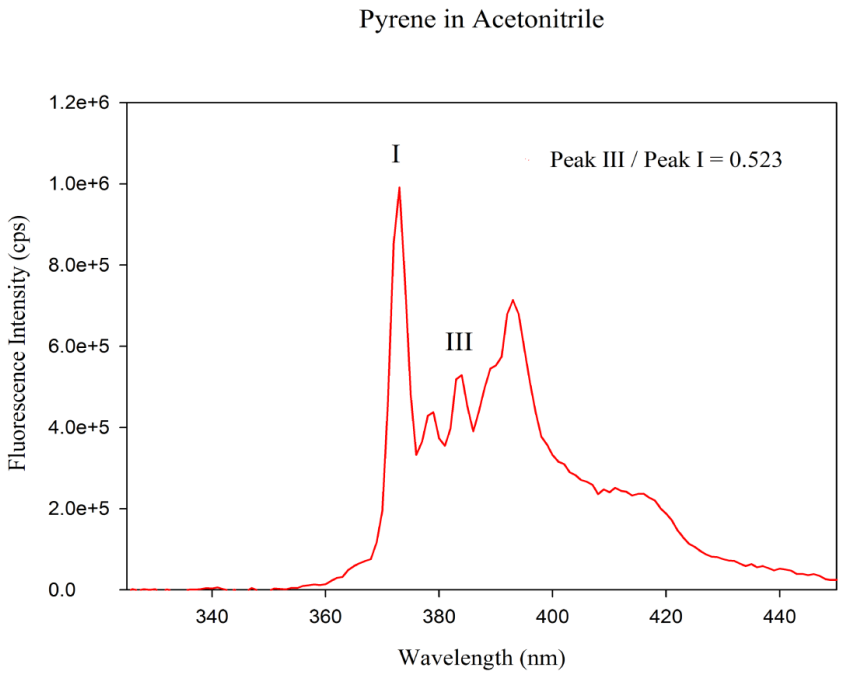

Figure 3.1.3.1 (a): Pyrene monomer fluorescence in Acetonitrile (Polar solvent). Peak I represents intensity at 373 nm and peak III represents intensity at 383 nm. In case of polar solvents I_3/I_1 =0.5 – 0.8.

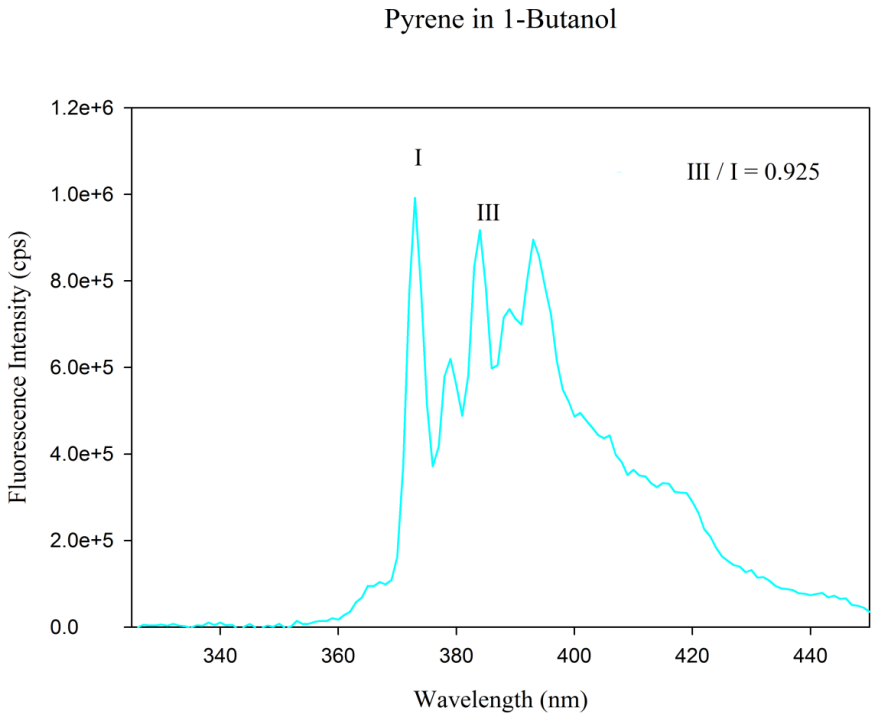

Figure 3.1.3.1 (b): Pyrene monomer fluorescence in 1-Butanol (non-polar solvent). In case of non-polar solvents I_3/I_1 = 0.8 – 1. Fluorescent intensity vibronic structures of pyrene show characteristic solvent dependence.

2 µM Pyrene in diff. solvents	Intensity Ratio Peak 3/Peak 1 (*Experimental*)	Intensity Ratio Peak 3/Peak 1 (*Reported*)
DMSO	0.493	0.5[16], 0.512[17]
Acetonitrile	0.523	0.54[16],0.56[17]
N,N-Dimethylformamide	0.539	0.552[17]
HPLC Water	0.565	
Water	0.62	0.63[16]
Methanol	0.72	0.75[16], 0.74[17]
Ethanol	0.8	
2-Propanol	0.879	0.917[17]
1-Butanol	0.925	0.98[16]

Table 3.1.3.1: Experimentally determined Py values along with literature values are summarized in various solvents of varying polarity.

Solvent polarity: Variation in the ratio of the fluorescence emission intensities of bands I and III of the vibronic spectra of pyrene depends on the solvent polarity scales. Fluorescence of pyrene in different solvents of varying polarity has been reported by us. The Py solvent polarity scale can be best described as the ratio of the emission intensities for bands III and I in the emission spectrum of polycyclic aromatic hydrocarbons (e.g. pyrene) which serves as a direct measure for the polarity of the solvent[17]. The experimentally determined III/I emission intensities ratios of pyrene in different solvents of varying polarity are in good correlation with the previously reported Py values. III/I values obtained ranged from 0.88 for the non-polar solvent, 2-propanol to 0.493 for dimethyl sulfoxide, which is a polar solvent.

Incubation Time(Hrs.)	144 Hrs. HEWL transferred sample in pH 7.0	2 µM Pyrene in pH 7	120 µM HEWL in pH 7
0	0.933	0.57	0.582
24	0.688	0.567	0.593
72	0.642	0.585	0.598
96	0.75	0.577	0.58
120	0.601	0.582	0.592
172	0.639	0.568	0.578
244	0.714	0.572	0.592

Table 3.1.3.2: Peak III/I ratio of Pyrene monomer fluorescence (Experimental data) for a) 120 µM HEWL aggregates transferred after 144 hours of incubation in pH 12.2 to pH 7.0 with 10 fold dilution, b) Pyrene in only buffer pH 7.0 (no protein) & c) 120 µM HEWL monomer incubated in pH 7.0.

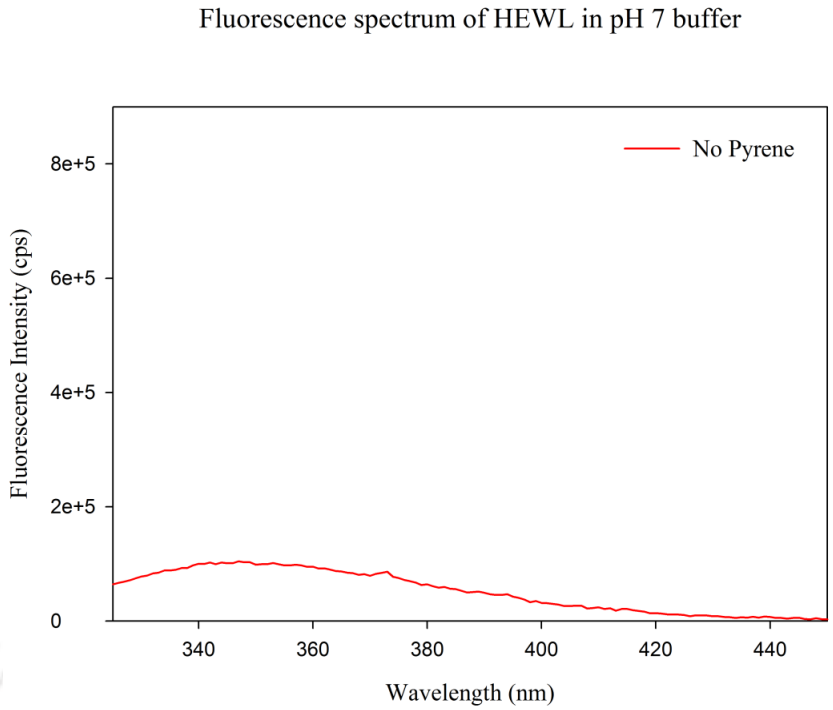

Figure 3.1.3.2 (a): Emission spectra of HEWL in pH 7 buffer in absence of pyrene. Excitation was performed at 310 nm with Ex slit / Em slit = 2 nm / 1 nm.

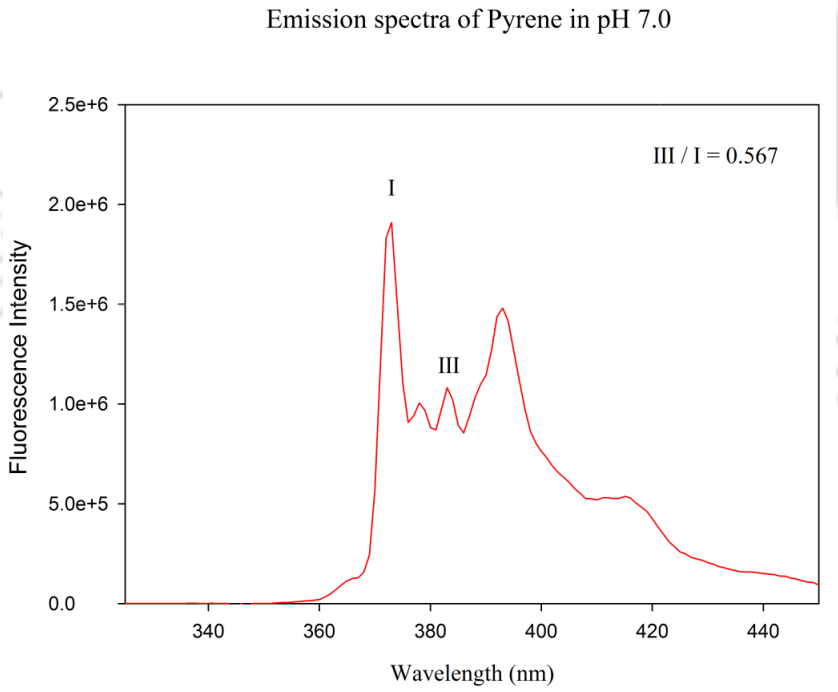

Figure 3.1.3.2 (b): Fluorescence emission spectra of Pyrene in 100 mM Sodium phosphate buffer, pH 7.0. Pyrene concentration is kept as 2 µM.

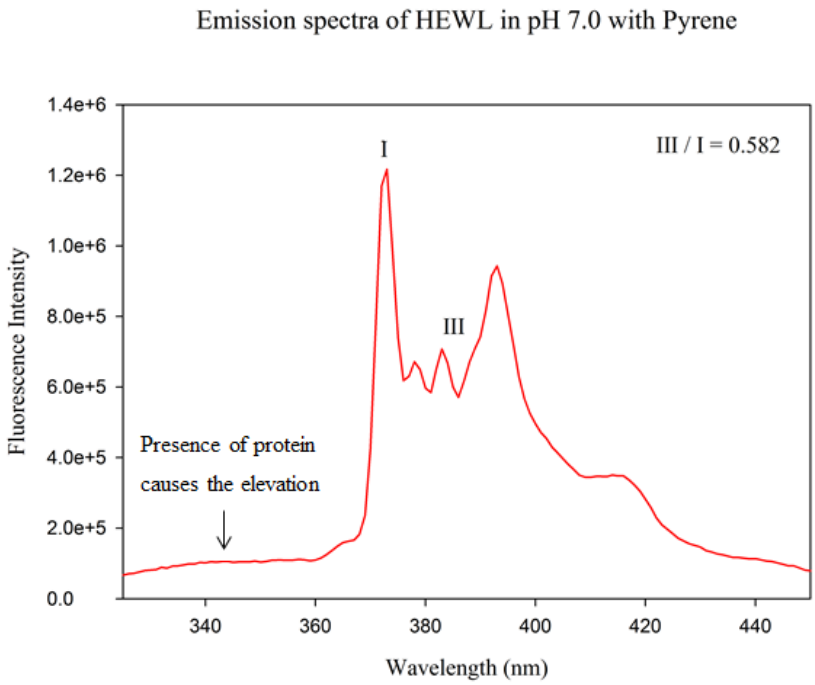

Figure 3.1.3.2 (c): Fluorescence emission spectra of pyrene incubated with 120 µM HEWL protein_0 Hr. Excitation was performed at 310 nm, Ex slit / Em slit – 2 nm / 1 nm. Concentrations of protein in the cuvette while recording the spectra was kept as 12 µM. Dilutions were performed in 100 mM pH 7.0 Sodium phosphate buffer.

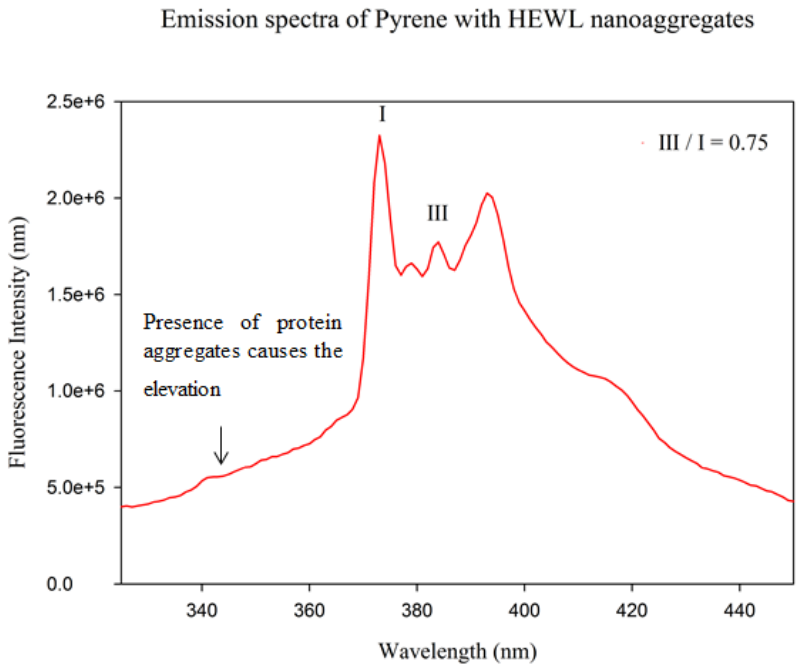

Figure 3.1.3.2 (d): Fluorescence emission spectra of pyrene with HEWL nanoparticles.120 µM HEWL protein sample was incubated in 50 mM Sodium phosphate buffer pH 12.2 for 144 hours to form HEWL aggregates. The formed aggregates were transferred to 100 mM Sodium phosphate buffer pH 7.0 with 10 fold dilution to form positively charged HEWL nanoparticles which were further allowed to remain in pH 7.0 for 96 hours before incubation with Pyrene. 2 µM Pyrene was incubated with HEWL nanoparticles for 10 minutes before recording the spectra.

3.1.4 Discussion

Exceptionally high sensitivity to solvent polarity, its symmetry and its unique photophysical fluorescent properties make pyrene advantageous in biological studies. Pyrene is a strongly hydrophobic fluorescent probe, with a characteristic emission spectrum exquisitely sensitive to its microenvironment. It exhibits monomer fluorescence emission peaks that reports about the polarity of the probe microenvironment. The fluorescence emission spectrum of pyrene is characterized by five major vibronic bands I, II, III, IV, V with well-defined peaks at ~ 375, 379, 385, 395 and 410 [12]. Peak III; corresponding to the third vibronic band with 0-2 transition, is sensitive to the polarity of the probe's microenvironment as a result of coupling of electronic and vibronic states. In comparison to the emission intensity of peak I (first vibronic band with 0-0 transition), the intensity of peak III is significantly enhanced in hydrophobic environments. In contrast, the intensity of peak I is significantly higher than that of peak III in polar environments. Hence, the ratio of the fluorescence emission intensities of peak I/III can be employed to detect polarity in the vicinity of the probe. Pyrene fluorescence was chosen as indicator of polarity for the protein nanoaggregates. Experiments performed by **Kalyanasundaram et al.** in 1976 have already shown the ratio of fluorescence intensities at 383 nm to 372 nm to be inversely dependent on polarity of the pyrene molecule environment.

- The sensitivity and dependence of the intensity of peak III/I on the polarity of the microenvironment surrounding the probe are illustrated by comparing the emission spectrum of free pyrene in polar solvent such as acetonitrile and non-polar solvent such as butanol, propanol, ethanol and so on [**Table 3.1.3.1**] .
- The specific feature of pyrene fluorescence emission sensitivity to solvent polarity has been used to assess the changes in probe microenvironment as a result of conformational change during aggregation of HEWL.
- [**Table 3.1.3.2**] represents variations in peak III/I values of pyrene monomer fluorescence. Pyrene fluorescence spectrum in pH 7 corresponds to that in polar solvent with III/I ratio ~ 0.5 which remains fairly constant with incubation time as shown in **[Figure 3.1.4.1 (a)]**. Even in case of protein incubated in pH 7(monomeric condition) the value of peak ratio III/I is ~ 0.58 as depicted in **[Figure 3.1.4.1 (b)]**, remains constant with time which suggests that there is a lack of exposed hydrophobic environment available for the probe to bind. Perhaps, there may be a barrier for entry of probe inside the protein.

- In order to characterize the hydrophobic region of aggregates, pyrene was incubated in 120 μM HEWL aggregates transferred to pH 7 after 144 hrs. Initially at 0 hr. incubation time, value of peak intensity ratio III/I spiked to 0.933 which indicates the presence of pyrene in the exposed interior hydrophobic region of aggregates **[Figure 3.1.4.1 (c)]**. However, with increasing incubation time a sharp decrease in the value of peak ratio was observed implying that pyrene is not able to access the hydrophobic interior of HEWL aggregates due to rearrangements in the structure. Hence, perturbations in vibronic band intensities of pyrene have been successfully used to characterize HEWL aggregates.

The values obtained for HEWL in its native state (aqueous pH 7.0 buffer) range from 0.57 to 0.59 which are typical of an aqueous environment. In acetonitrile, pyrene exhibits a value of 0.523 as I_3/I_1 which is usually the case of pyrene emission in polar solvents. The solvent dependence of emission bands in the fluorescence spectra was observed for symmetrical aromatic pyrene chromophore in different polar and non-polar solvents. Results obtained by us were found to be in good correlation with the solvent polarity scale of pyrene. For the samples containing aggregates transferred to pH 7.0, within 1 hr. of transfer a value of I_3 / I_1 as 0.933 is a clear indication of presence of hydrophobic microdomains in the aggregates which are accessible to pyrene molecule. A drop in value of peak ratio from 0.93 to 0.69 after 24 hours of incubation in pH 7.0 for the transferred sample suggests that pyrene molecules are not able to find any hydrophobic surface in the aggregates to harbour them. It was clearly visible from the solvent polarity ratio that fluorescent emission spectra of pyrene underwent characteristic changes for the protein aggregates which in turn reflect the variation in local hydrophobicity of the probe induced by structural changes occurring within the aggregates. Previously many studies have been carried out by covalently labeling the macromolecules with pyrene dye which provided a lot of information on internal dynamics of macromolecules and their supramolecular assemblies which was possible due to the characteristic pyrene excimer formation[13]. Self-aggregation behaviour of nanohydrogels has been studied where the critical aggregation concentration of the nanosystem was evaluated by using pyrene fluorescence technique[14]. Examples are there where pyrene fluorescence has been used to study hydrophobically modified materials.

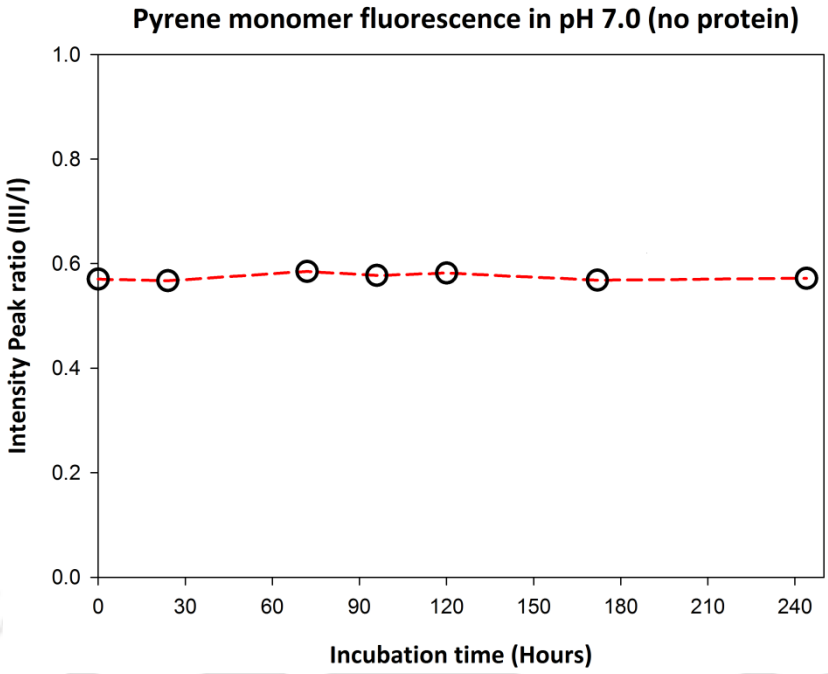

Figure 3.1.4.1 (a): Pyrene monomer fluorescence intensity peak ratio is plotted as a function of incubation time. 2 µM Pyrene is incubated in 100 mM Sodium phosphate buffer, pH 7.

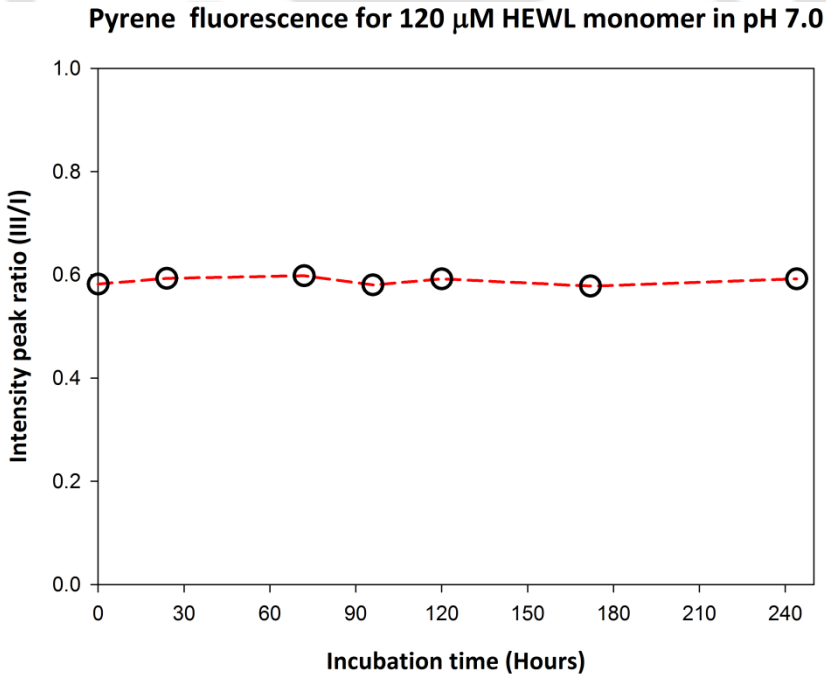

Figure 3.1.4.1 (b): Pyrene monomer fluorescence for 120 µM HEWL incubated in Sodium phosphate buffer, 100 mM, pH 7(under monomeric condition).While recording the fluorescence spectra, protein concentration was diluted to 12 µM and pyrene concentration was kept as 2 µM.

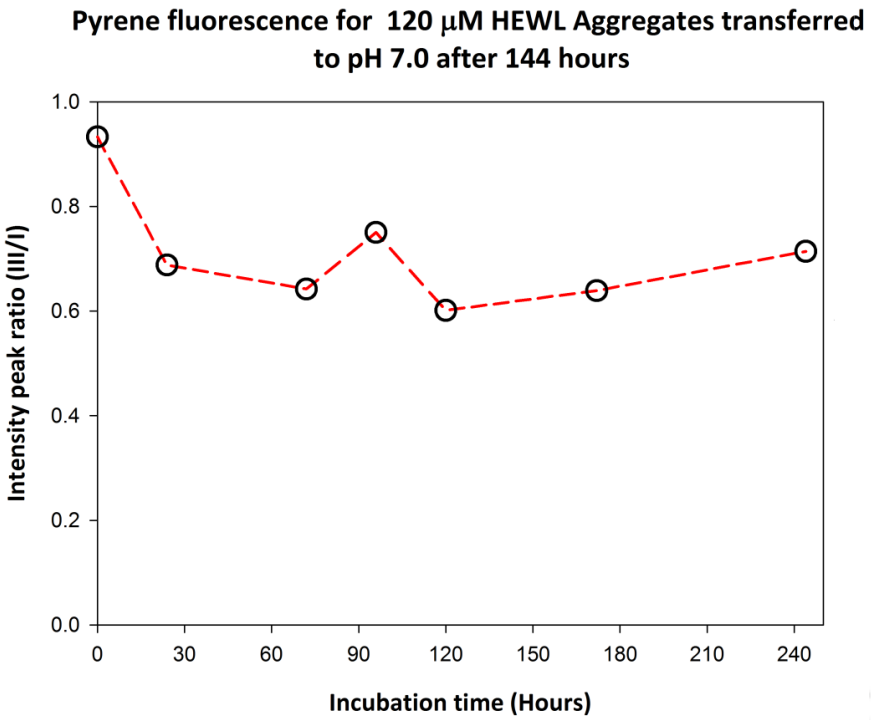

Figure 3.1.4.1 (c): The ratio of pyrene emission intensity (Peak III / Peak I) is represented as a function of incubation time.120 µM HEWL was incubated in 50 mM Sodium phosphate buffer, pH 12.2(HEWL aggregates) and then transferred to pH 7.0. Table 1 refers to the values obtained from emission intensity (peak III / peak I) ratio.

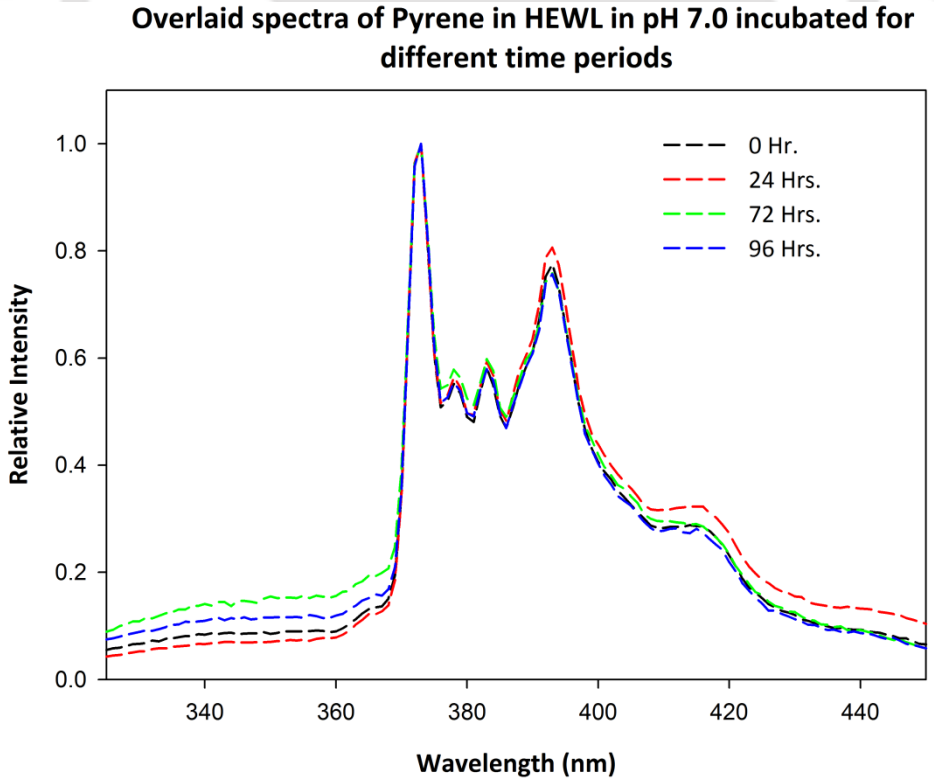

Figure 3.1.4.1 (d): Overlaid Normalised Fluorescence spectra of pyrene observed in aqueous solution of HEWL incubated for different time periods in pH 7.0. At different time points 2 µM Pyrene was incubated with HEWL in its native state (pH 7.0).The spectra are normalized with respect to the bands with maximum intensities.

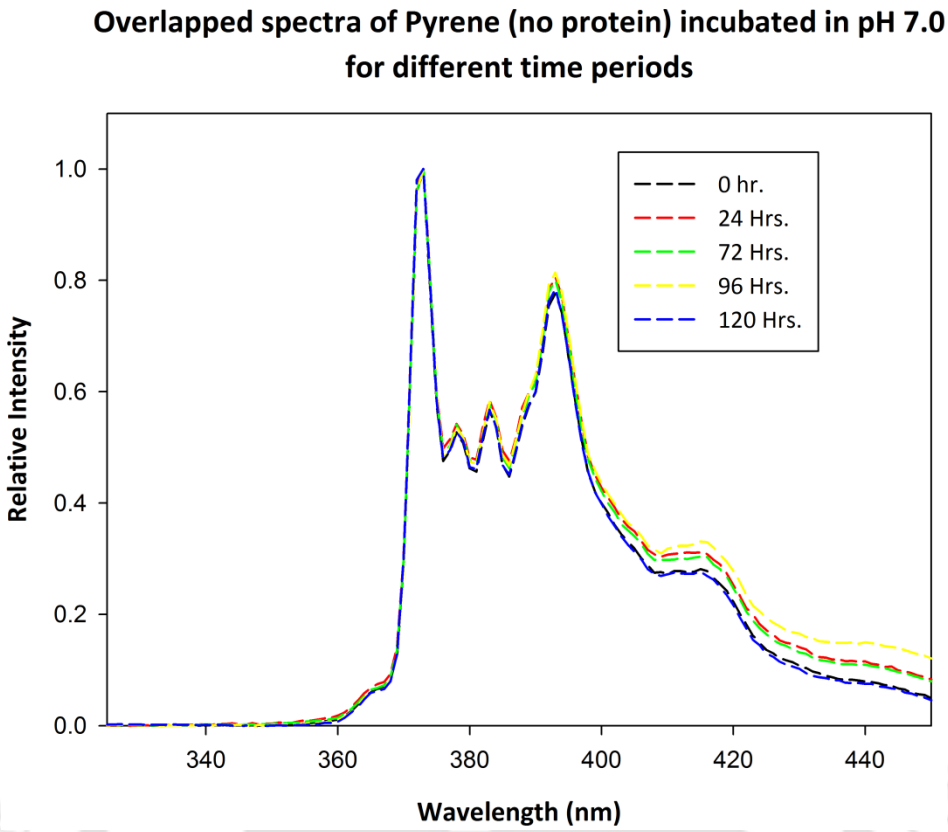

Figure 3.1.4.1 (e): Overlaid normalised fluorescence spectra of Pyrene incubated in pH 7.0 without protein. Spectra were recorded for the incubated aqueous solution at different time points.

In the fluorescence spectra for pyrene in HEWL (native state), a shoulder observed around 340 nm can be attributed to the presence of protein which was not observed in the case of spectra for only pyrene in pH 7.0.

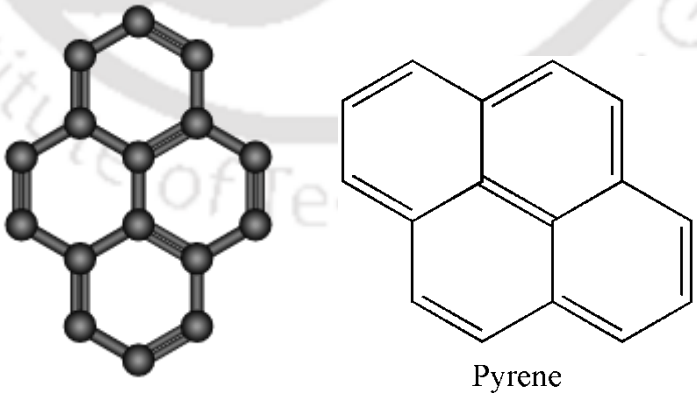

Structure of Pyrene

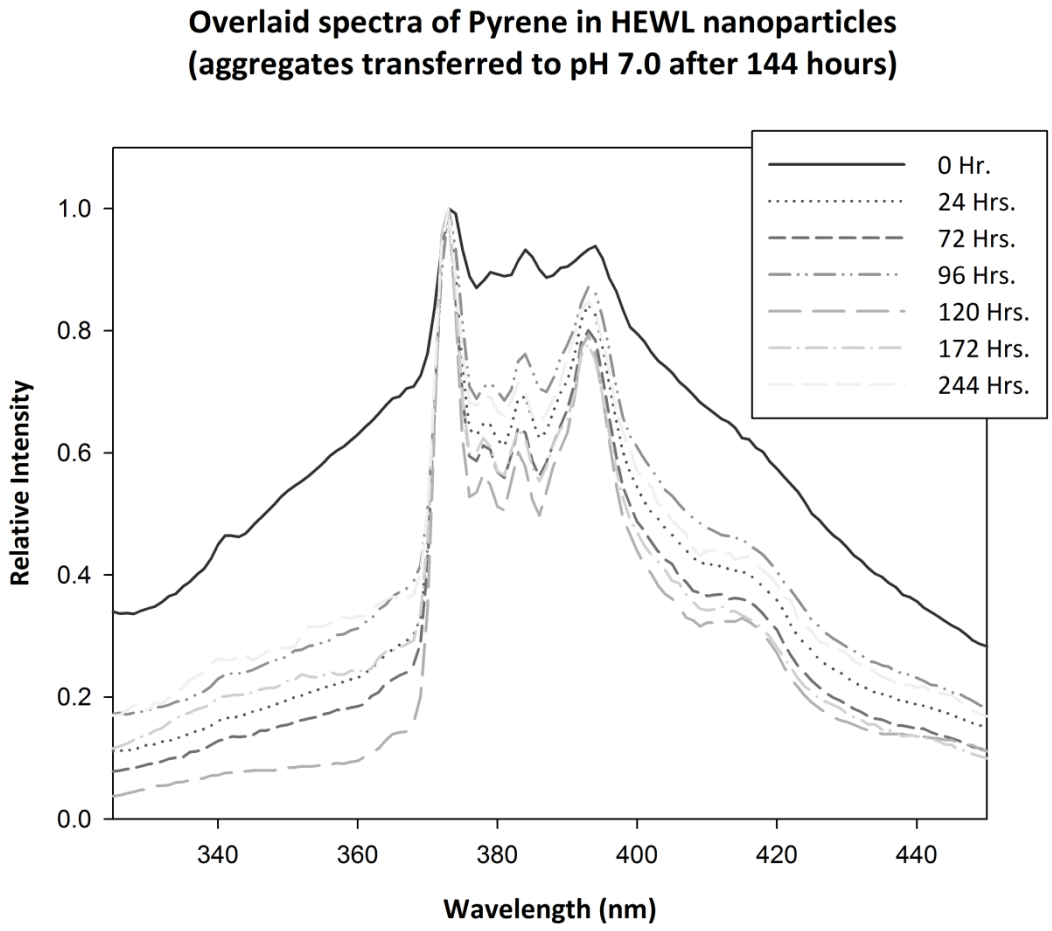

Figure 3.1.4.1 (f): Fluorescence spectra of Pyrene in HEWL nanoparticles (aggregates in pH 12.2 transferred to pH 7.0 after 144 Hrs.) in pH 7.0 at different time points are illustrated.

Overlaid spectra of pyrene in HEWL nanoparticles revealed a major enhancement in intensity of pyrene for 0 Hr. incubated sample which is evident from the [**Figure 3.1.4.1 (f)]**.This particular result confirms the inclusion of pyrene into the hydrophobic microenvironment of the aggregates within a short time period after transfer of aggregates to pH 7.0.When the pre formed aggregates in pH 12.2 suddenly experience a huge change in pH i.e. when transferred to pH 7.0, the aggregates open up partially due to electrostatic repulsions such that pyrene dye gets an access to the hydrophobic environment within the aggregates. Increase in I_3/I_1 ratio for 0hr. incubated sample can be assigned to inclusion of pyrene in the interior of aggregates which appears to have a very low polarity or high hydrophobicity. Enhancement in the intensity clearly seen for 0 Hr. sample in the normalised spectra for HEWL nanoparticles in comparison to longer hours incubated samples may be due to increased distribution of pyrene molecules present in hydrophobic pockets of aggregates.

At later times (24 Hr. onwards), fluctuations in the intensity has been observed but the intensity is many fold less than 0 hr. incubated sample. The value of I_3/I_1 as 0.933 for pyrene in 0 hr. incubated HEWL nanoparticles is almost comparable to that of pyrene in 1-Butanol (I_3/I_1 = 0.925).The intensification of the vibronic bands can be ascribed to the non-polar interior of the nanoparticles. However, there is a considerable difference for the longer hours incubated (24 Hrs.) nanoparticles where the intensity ratio drops to around 0.67 which is somewhat still larger than that of pyrene in water (0.56), a highly polar solvent. From the values obtained for I_3/I_1 ratio for 24 Hrs. incubated nanoparticles it can be interpreted that pyrene is not completely in a polar environment or it might be ascertained that the aromatic dye is lying close to the hydrophobic interior but not able to diffuse into the compact environment of nanoparticles due to structural rearrangements. The size of the pyrene molecule which has been determined previously amounts to a value of 7.1 x 8.9 ($Å^2$)[15].

Variation in I_3/I_1 ratio is also influenced by the fact that whether the hydrophobic pockets present in the nanoparticles are capable enough to incorporate the pyrene molecule because if the size of the pyrene happens to be significantly larger than the diameter of the pockets then it may lead to exclusion of the aromatic dye from the hydrophobic region of aggregates. This can be the possible explanation for the observed apparent polarity in the late hours transferred samples (HEWL nanoparticles). In this case, solvent exposed surface area of pyrene to solvent molecules is larger as compared to 0 Hr. transferred sample due to which the microenvironment turned out to be polar as reflected from I_3/I_1 ratio.

Fluorescence of pyrene was used to investigate the accessibility of the dye to hydrophobic environment of HEWL nanoparticles. Dependence of I_3/I_1 ratio on the polarity of microenvironment is pronounced for a hydrophobic dye such as pyrene. In order to ensure that pyrene is present in monomeric configuration, its concentration was maintained at 2 µM in the final solution for all the samples. As a result, no excimer formation was detected in any of the samples. In view of the importance of the need to keep pyrene concentration very low as such in micromolar concentrations, fluorescence measurements of vibrational bands were possible due to high quantum yield of pyrene (Φ = 0.7)[15] and high sensitivity of fluorescence spectroscopic technique.

3.1.5 Conclusion

Strong dependence of I_3/I_1 vibronic intensity ratio of fluorescent probe, pyrene, on local molecular polarity is well known from literature reports. The technique of pyrene monomer fluorescence to use as a hydrophobic probe has proved to be very efficient at characterizing HEWL monomer in native state (pH 7.0) and HEWL oligomers (aggregates in pH 12.2 transferred to pH 7.0). In the above presented work, the self-assembled nanoparticles were characterized by using pyrene as an interesting tool to assess the hydrophobic microenvironment of nanoparticles. The above reported results will serve as a base for future studies where HEWL oligomers can be used to encapsulate hydrophobic compounds such as non-polar drugs.

It is noteworthy that the system of nanoaggregates under investigation is a heterogeneous polydisperse system which consists of different species of varying sizes, depending upon the number of monomer units associated to form each oligomer unit. Accordingly, differing species will have slightly differing sizes of hydrophobic pockets. In spite of this heterogeneity, pyrene was used as a polarity probe to characterize our system. Thus it can be concluded that change in fluorescence intensity ratio (III/I) of pyrene just gives an idea about the microscopic polarity rather than an average polarity of the whole system.

Interactions of pyrene with protein nanoparticles play a key role in studying the influence of structural transition occurring in nanoparticles due to a change in pH on hydrophobic behaviour of self-assembled aggregates. Structural transitions in HEWL spherical oligomers induced by a change in pH resulting in positively charged species was monitored by pyrene steady state fluorescence. In a polar environment, remarkable enhancement of the 0-0 band emission intensity was observed.

3.2 Intrinsic **tryptophan fluorescence** as a tool to probe the polarity of the environment of HEWL nanoaggregates

3.2.1 Introduction

Trp[1] residues provide peculiar information about protein conformation which is possible due to the high sensitivity of fluorescence spectroscopy technique. Distribution of different Trp residues present in HEWL has been studied in the past by using fluorescence spectroscopy as a tool. Several reports have been published where changes in conformation of biological macromolecules are determined from alterations in the intrinsic fluorophore's emission spectra. Usually tryptophan is the dominant intrinsic fluorophore in a protein[18]. Lysozyme protein has been extensively used to deduce information about tryptophan environments in proteins from fluorescence emission intensity. In fact, the availability of well-studied crystal structure of the native protein and presence of higher no. of tryptophan residues as compared to tyrosine residues makes lysozyme vey suitable for fluorescence studies[19]. Increase or decrease in fluorescence quantum yield of Trp residues in response to variation in local environment yields critical information about various biological processes such as protein folding/unfolding[20], ligand binding[21], protein aggregation etc. Previously, intrinsic tryptophan fluorescence has been widely used to study protein denaturation and renaturation in presence of denaturants such as guanidium hydrochloride, urea etc. It is relatively simple to interpret the data in case of single Trp containing proteins. However, complications arise in a scenario where there are multiple tryptophan residues exist in a protein. Moreover, the various quencher groups inherently present in a protein enormously affect tryptophan fluorescence which further adds to the complexity. **Chen et al.** have elucidated the different quenching mechanisms by which the amino acid side chains effectively quench trp fluorescence[22]. Previously peptide bond has also been reported to quench trp fluorescence by electron transfer mechanism[23]. The side chains of tyrosine (phenol), cysteine (sulfhydryl), positively charged histidine (imidazole) and cystine have been found to be the strong quenchers of the indole ring of tryptophan. Lysine ε-amino group, amide groups of asparagine and glutamine and neutral histidine have been reported to be relatively weak quenchers. Whereas carboxyl groups of glutamic and aspartic acids were apparently considered to have moderate contribution to the quenching of indole fluorescence.

[1] **Trp**- Tryptophan residue

Steady state and time resolved fluorescence techniques were used to derive information about the effects of amino acid functional groups as quenchers of indole chromophore. Various other factors such as a) proximity of amino acid side chains to indole ring b) specific geometry c) local polarity and d) ionization state of the amino acid groups play a very significant role in determining the quenching mechanism followed by these quenchers.

The changes in environment of Trp residues in HEWL in its native state as well as in oligomeric state have been investigated by intrinsic tryptophan fluorescence. The intrinsic fluorescence of lysozyme was studied at different pH conditions (pH 7.0 and pH 12.2) and the spectroscopic observations have been used to monitor the structural transitions in the tertiary structure of lysozyme under aggregating conditions.

The results demonstrate that there is significant difference in the environment of tryptophan residues in HEWL aggregates and HEWL monomer. Various theoretical and experimental studies have been carried out on lysozyme protein containing 6 Trp residues, each having a different location within the protein. However, the changes in Trp fluorescence spectra due to structural transitions occurring inside the lysozyme aggregates at pH 12.2 has not been reported yet. In this work, we have carried out steady state fluorescence measurements in a time dependent way for the protein samples at different concentrations incubated for long hours from 0 hr. reading till 150 hrs.

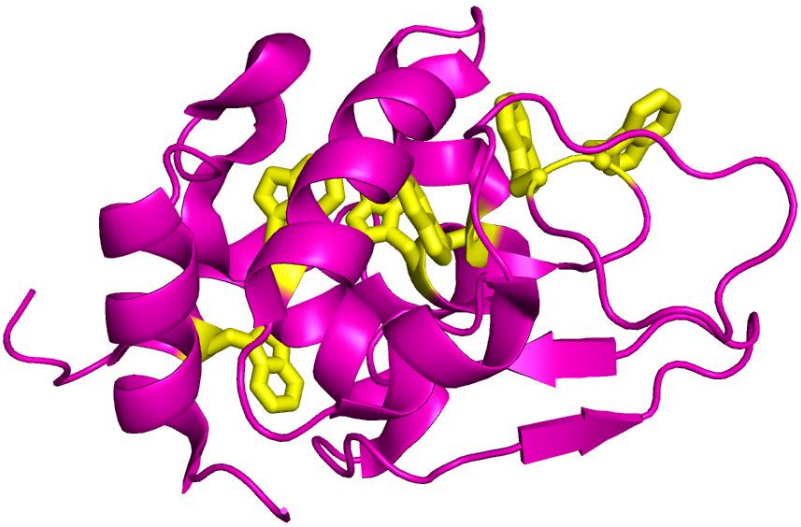

Figure 3.2.1: Tryptophan residues of HEWL (PDB Id- 5f14). Trp 28, Trp 62, Trp 63, Trp 108, Trp 111 and Trp 123 are shown in yellow colour as side chains. Structure of HEWL (PDB Id- 5f14) generated by **Polyview-3D** server using Pymol for visualization of the structure.

3.2.2 Materials and Method

3.2.2.1 Materials

Hen egg white lysozyme was procured from Sigma Aldrich (molecular weight – 14.6 kDa, Cat no. L-6876) in lyophilized powdered form and NATA (N-acetyl-L-tryptophanamide) was purchased from Sigma Aldrich Cat no. A6501.

Sodium phosphate buffers (pH 7.0 and pH 12.0) were prepared in milliQ water with NaH_2PO_4 and Na_2HPO_4 salts respectively. The pH of the buffer solutions were adjusted to their respective pH by adding NaOH solution. The ionic strength of the buffer solutions was maintained at 50 mM.

3.2.2.2 Steady state fluorescence

Steady state fluorescence measurements were performed on Jobin-Yvon Fluoromax-3 spectrofluorometer and fluorescence spectra were recorded in 1.0 cm path length quartz cells. The emission wavelength scan range was recorded from 310 nm to 400 nm at 1 nm wavelength increments. In order to show the spectroscopic behaviour of only Trp residues of HEWL in the emission spectrum, excitation was performed at 295 nm. The reason for employing the excitation wavelength of 295 nm was to minimize excitation of tyrosine residues. Hence, it can be assumed that there are no chances of transfer of energy from tyrosine to tryptophan. Excitation and emission bandwidths were set at 1 nm/5 nm. While processing the intensity data, intensity signal for all the samples were subtracted from the respective buffer blanks.

3.2.2.3 Tryptophan spectra

Excitation is performed at 295 nm to avoid the effects of fluorescence from Tyrosine residues. Intrinsic tryptophan fluorescence intensity can be used to detect hydrophobic exposure due to conformational changes occuring during aggregation. In order to monitor aggregation, samples were incubated for different time periods and Tryptophan spectra were recorded at particular time periods as shown in the plots. HEWL incubated in pH 7 showed negligible change in fluorescence intensity over time. For samples incubated in pH 12.2, fluorescence intensity escalated after 12 hours of incubation followed by a significant increase up to 150 hours.

3.2.3 Results and Discussion

3.2.3.1 Tryptophan emission spectra

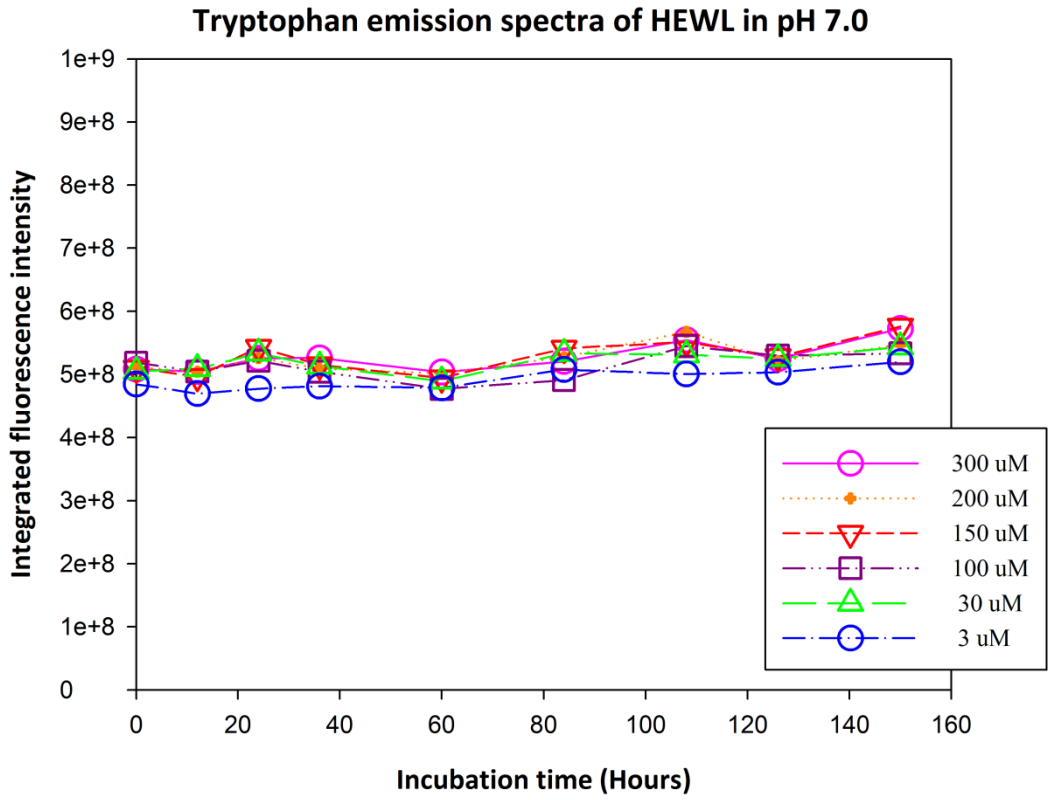

Figure 3.2.3.1 (a): Emission spectra of Tryptophan of HEWL incubated in 50 mM Sodium phosphate buffer, pH 7.Excitation slit-1 nm and Emission slit-5 nm were used to record $\mathbf{I_{295}}$.The different coloured symbols in the figure correspond to the monomer concentration used for incubation of sample.While recording fluorescence measurements,the samples were diluted to 1 µM and the concentration of protein was same in the cuvette for all the samples. Buffer pH 7.0 was used as control and for background subtraction in the experiments

It can be seen [**Figure 3.2.3.1 (a)**] from the fluorescence spectra of HEWL solution in buffer pH 7.0, tryptophan intensity remains more or less unchanged and a significant blue shift in λ_{max} for emission from 350 nm (for **NATA**[2] in pH 7.0) to 336 nm for 0 Hr. incubated pH 7.0 sample (300 µM HEWL).Little variation was observed in the maximum emission wavelength which ranged from 336 nm to 338 nm for the pH 7.0 incubated samples. However, an apparent red shift [**Figure 3.2.3.1 (c) & 3.2.3.1 (e)**] was observed from 339 nm (150 µM HEWL, pH 7.0, 0 hr.) to 342 nm (150 µM HEWL, pH 12.2, 0 Hr.) which suggests that there is an alteration in the conformation of HEWL molecule when the pH is changed from physiological pH 7.0 (native condition) to alkaline pH 12.2 (aggregating condition).

[2] **NATA** – N-acetyl-L-tryptophanamide is an N-terminal and C-terminal blocked analogue of L-tryptophan.

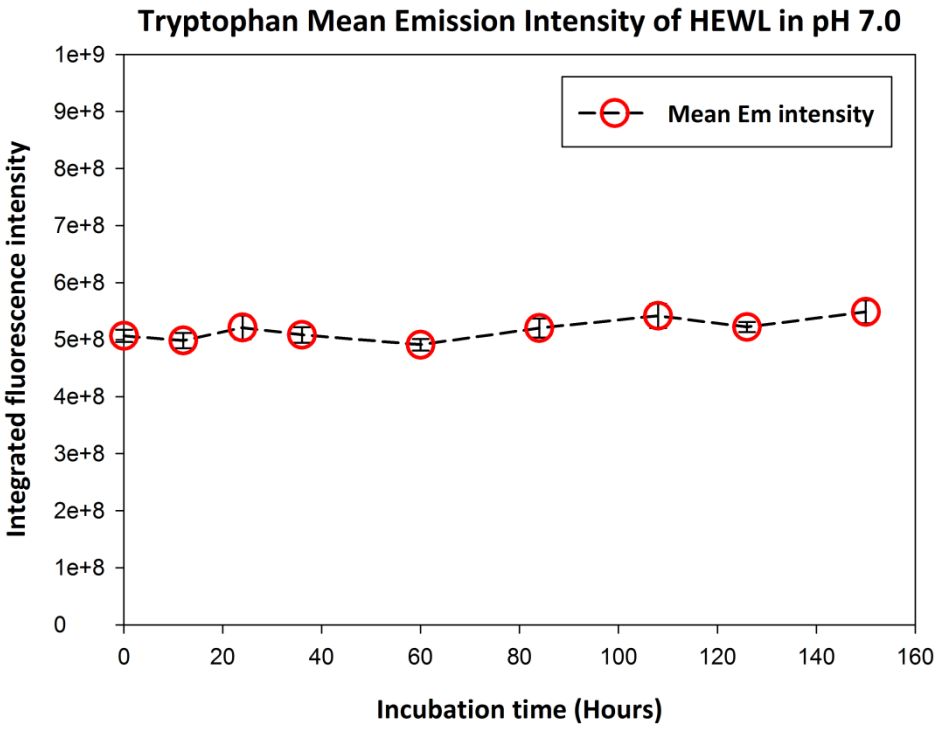

Figure 3.2.3.1 (b): Mean emission intensity for different concentrations of HEWL incubated in pH 7.0. The mean intensity reported is the average of integrated fluorescence intensity of different concentrations of HEWL at different incubation time points in pH 7.0. The time points are: 0,12, 24, 36, 60, 84, 108, 126, 150 hours.

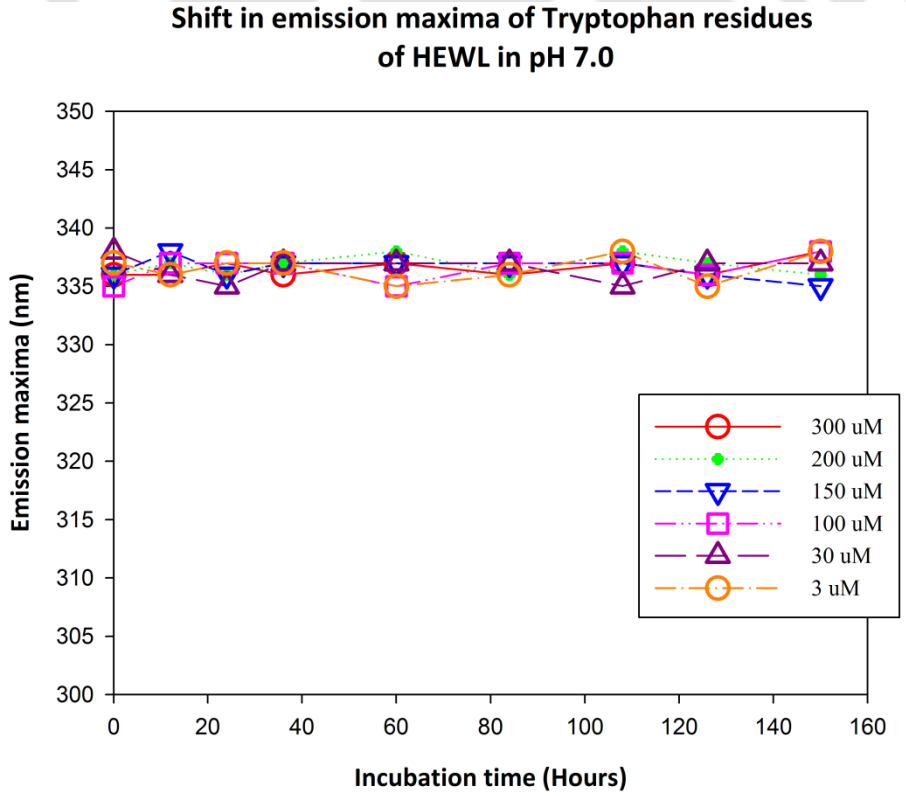

Figure 3.2.3.1 (c): Emission maximum for tryptophan emission spectra of HEWL in pH 7.0.

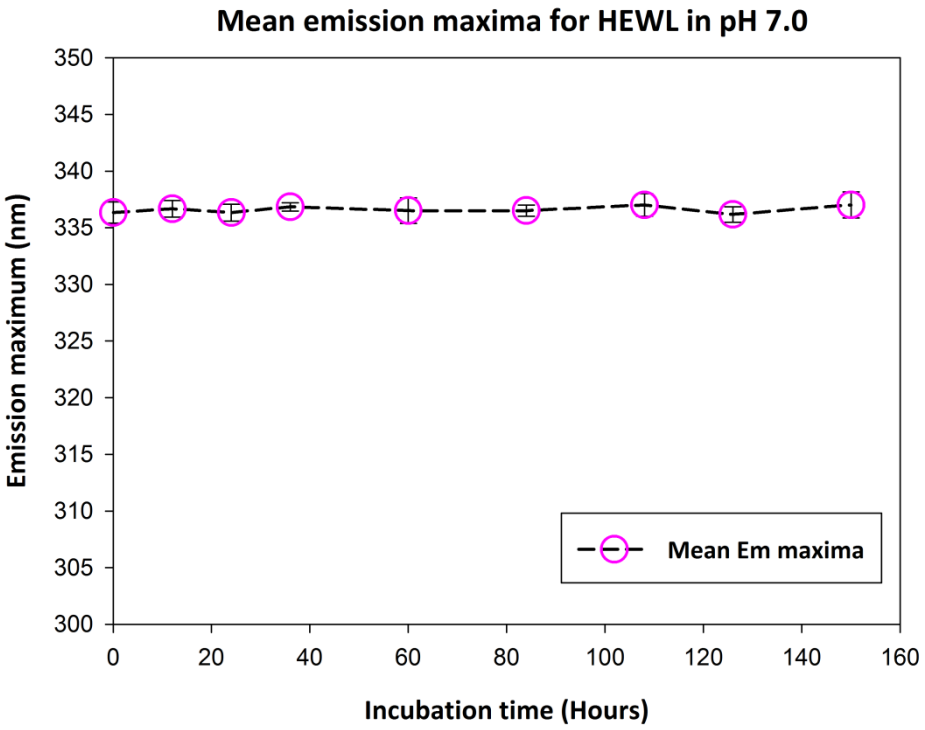

Figure 3.2.3.1 (d): Mean emission maximum for different concentrations of HEWL incubated in pH 7.0. The average value reported here refers to the average of emission maxima of different concentrations of HEWL at a particular incubation time point in pH 7.0. The different concentrations of HEWL used are: 300 µM, 200 µM, 150 µM, 100 µM, 30 M & 3 µM.

Excitation wavelength at 295 nm is used to reveal specifically the spectral properties of tryptophan residues. Spectral overlaps of the tryptophan residues may complicate the interpretation of the data and it is difficult to discriminate the fluorescence of each tryptophan residue from steady state spectroscopy only. The blue shift in the fluorescence maxima observed in case of native HEWL incubated in pH 7.0 **[Figure 3.2.3.1 (d)]** as compared to NATA clearly demonstrates that tryptophan residues are buried in the hydrophobic region of the protein or it can be interpreted as the polarity is reduced in the vicinity of tryptophan residues. The emission spectra of HEWL incubated in pH 7.0 at different concentrations were almost identical in profile and no significant variation in the fluorescence quantum yield was observed.

In order to gather information regarding the environment of tryptophan residues[24] of HEWL, SCAT[3] tool was used for analysis of 6 trp residues present in native structure of HEWL with PDB Id: *5f14*.

[3] **Structural Correlation Analysis Tool**- used for detailed structural analysis of the environment of Tryptophan residues in a protein.

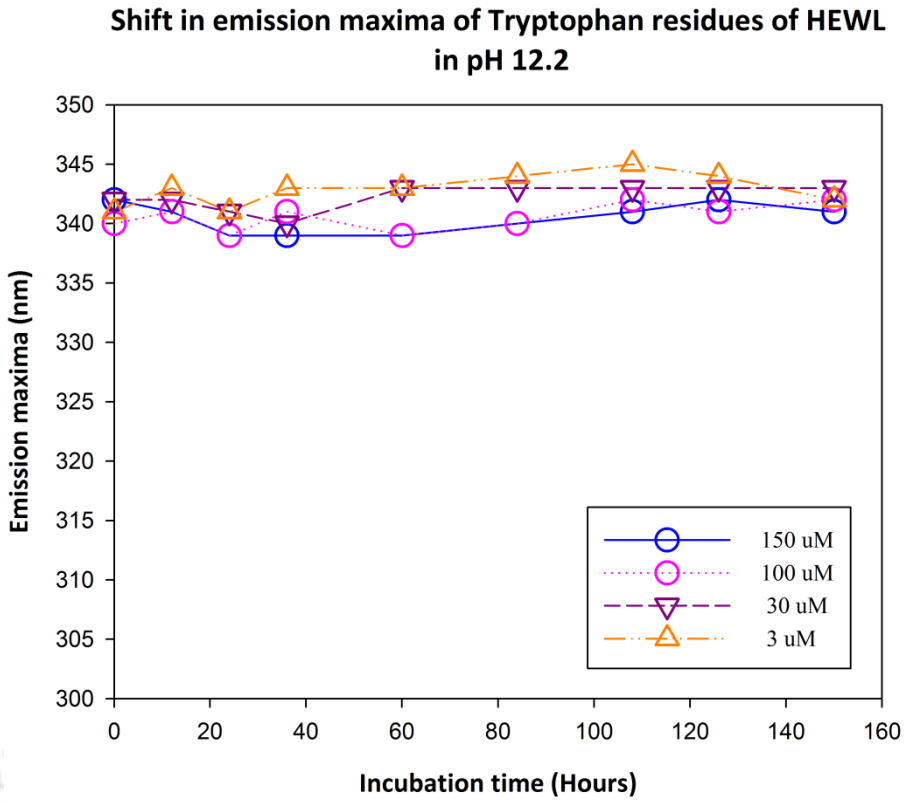

Figure 3.2.3.1 (e): Emission maximum for tryptophan residues of HEWL aggregates in pH 12.2.

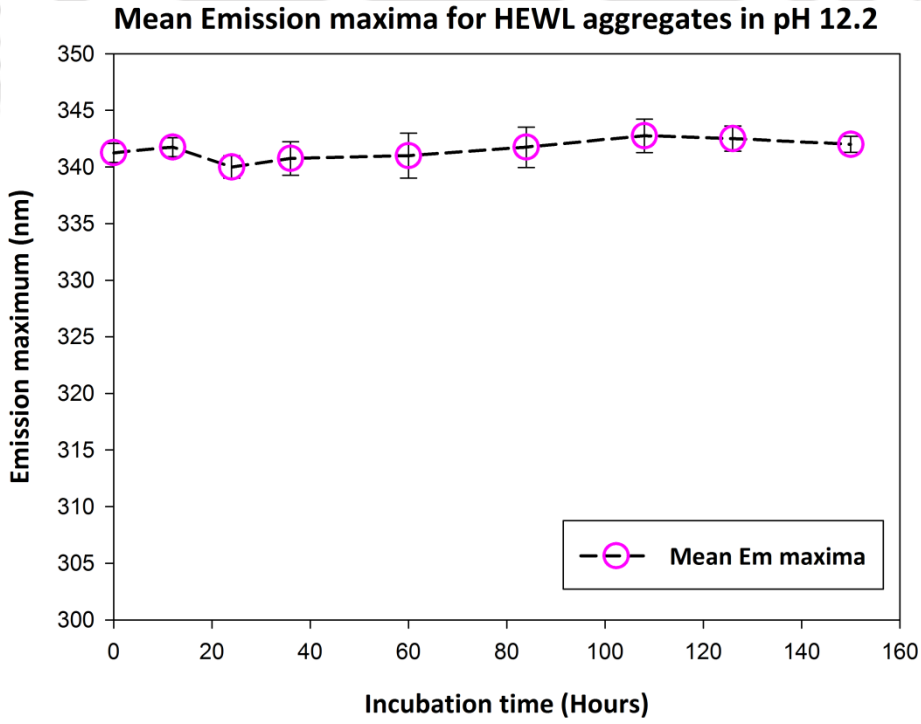

Figure 3.2.3.1 (f): Mean emission maximum for different concentrations of HEWL incubated in pH 12.2. The average value reported here refers to the average of emission maxima of different concentrations of HEWL at a particular incubation time point in pH 12.2.

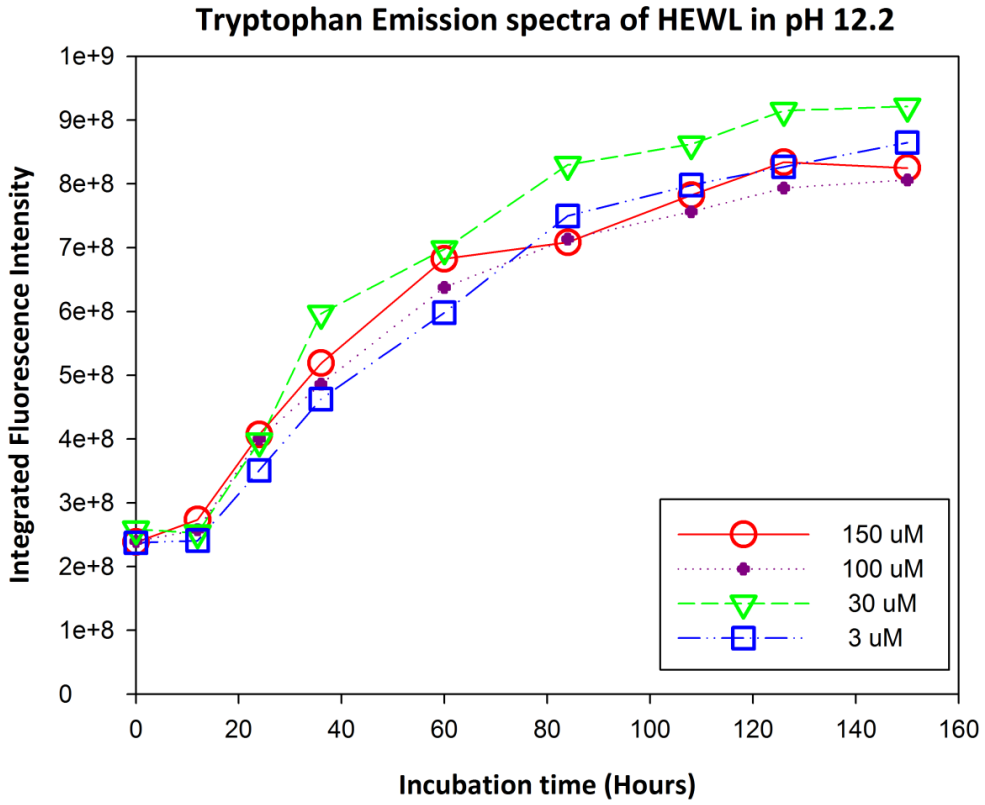

Figure 3.2.3.1 (g): Emission spectra of Tryptophan of HEWL incubated in 50 mM Sodium phosphate buffer, pH 12.2 at room temperature.In order to measure the Trp intensity**(I_{295}),** excitation was performed at 295 nm,Ex/Em slits- 1 nm/5 nm and emission spectra was recorded from 310 nm to 400 nm.Integrated fluorescence intensity was calculated from area under the curve.

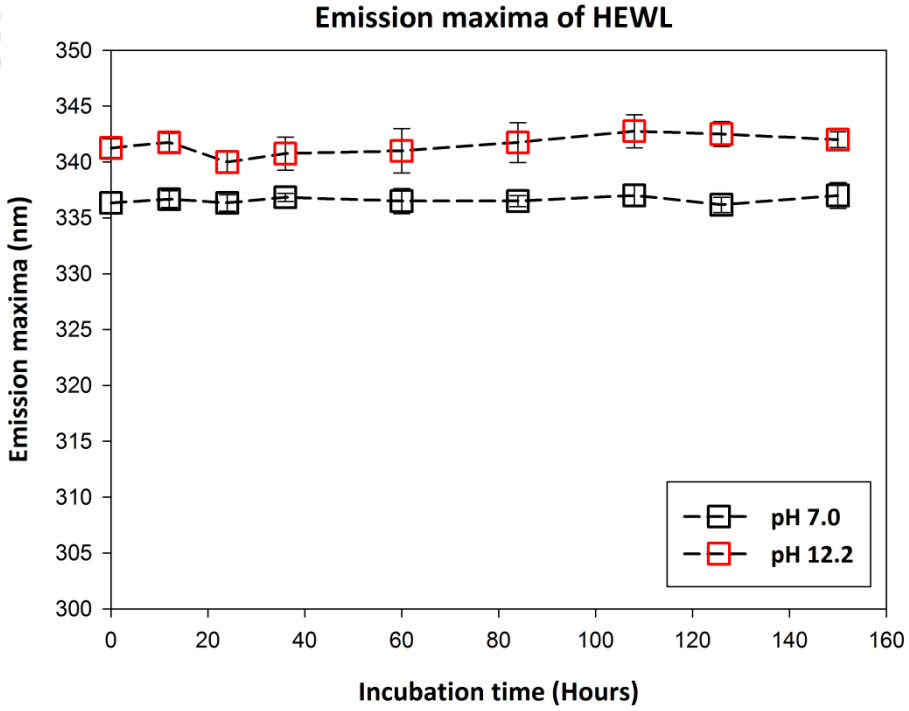

Figure 3.2.3.1 (h): Shift in Mean of emission maxima for HEWL can be clearly distinguished when it is incubated under two different conditions a) pH 7.0 (native state) and b) pH 12.2 (aggregating condition).

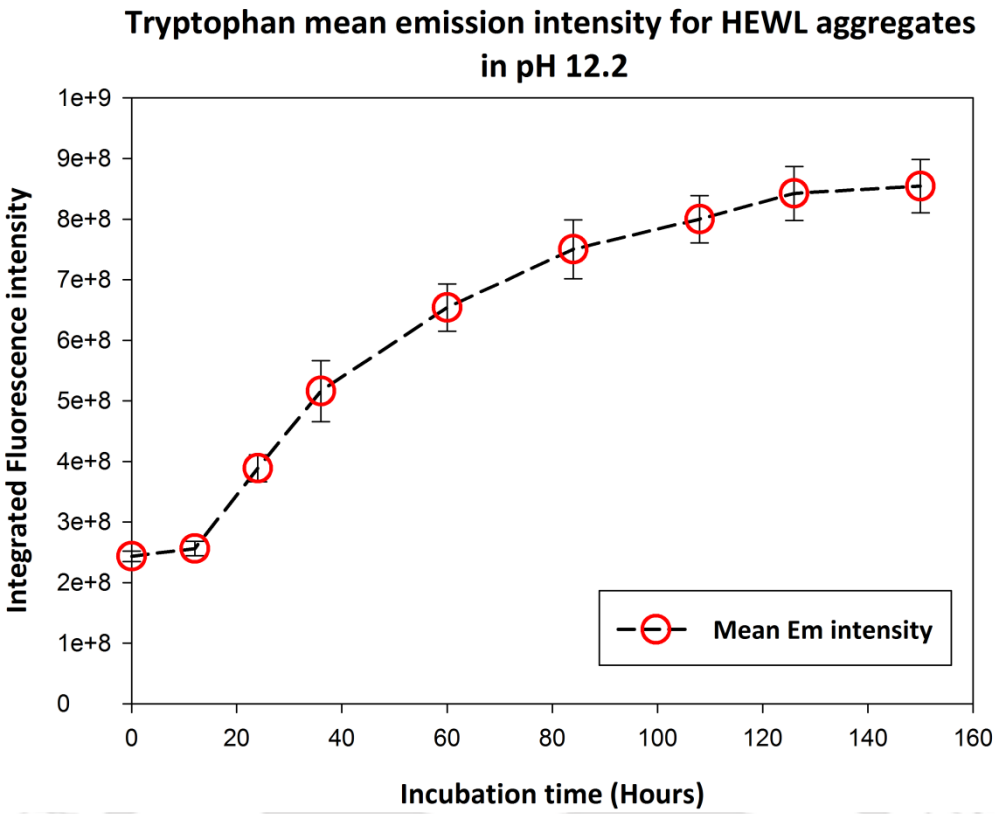

Figure 3.2.3.1 (i): Mean emission intensity for different concentrations of HEWL incubated in pH 12.2. The mean intensity reported is the average of integrated fluorescence intensity of different concentrations of HEWL at different incubation time points in pH 12.2. The time points are: 0,12, 24, 36, 60, 84, 108, 126, 150 hours.

The results for HEWL samples incubated at pH 12.2 show that initially the fluorescence intensity for 0 Hr. incubated sample (150 µM, pH 12.2) gets reduced to 53.2 % [**Figure 3.2.3.1 (i)**] of that of the sample incubated in pH 7.0 (150 µM, 0 Hr.) [**Figure 3.2.3.1 (b)**].In addition, it was also observed that fluorescence intensity escalates gradually for the samples of different concentrations in pH 12.2. Buffer pH 12.2 was used as control and for background subtraction in the experiments. In contrast, the fluorescence intensity for pH 7.0 incubated samples remains fairly unchanged, irrespective of the concentration of protein, without any increase or decrease over a time period of 150 Hrs. [**Figure 3.2.3.1 (b)**]. Data for samples incubated in pH 12.2 at higher concentration of 200 µM and 300 µM are not shown. As precipitation was observed for these samples within 12 Hrs. of incubation, hence no spectral measurements could be recorded.

Surprisingly, the trend observed as rise in fluorescence for HEWL aggregates incubated in pH 12.2 is nearly independent of HEWL concentration. The increase in fluorescence is apparently due to the conformational changes occurring in the aggregates which drift away the trp residues from the quencher groups present in the protein.

Furthermore, it was interesting to note that the shift in emission maximum wavelength[4], λ_{em}, was clearly evident in HEWL solution in pH 12.2. As it is known that when the protein molecule is exposed to alkaline pH, the buried residues are exposed to the surrounding solvent and thus a red shift in the position of λ_{em} occurs corresponding to the changes in conformation of HEWL. The red shift indicates the increase in polarity surrounding tryptophan residues which is consistent with the emission intensity which gets quenched on exposure to alkaline pH as observed in case of 0 Hr. and 12 Hrs. incubated samples. Surprisingly, fluorescence intensity gets enhanced with increasing time of incubation (36 Hrs. to 150 Hrs. samples).The possible explanation for this can be the increasing distance between a) inter tryptophan residues (of different HEWL monomers), b) intra tryptophan residues (within HEWL molecule) and c) tryptophan and different quencher groups due to structural arrangements occurring in aggregation pathway of HEWL which diminishes the effects of quenching. Consequently, which in turn resulted in a significant increase in intensity at later time of incubation as depicted from the integrated fluorescence intensity plots[5].Experimental results indicate that the initial quenched fluorescence of trp residues of HEWL in pH 12.2 becomes comparable to that of quantum yield of trp residues in pH 7.0 for 36th hour incubated sample [**Figure 3.2.3.1 (j)**]. However after 36 hrs. of incubation, a large change is observed in the tryptophan fluorescence yield for HEWL aggregates unlike native protein. The increase in yield can be regarded as a result of the contribution of different quencher groups becomes negligible to tryptophan fluorescence. This occurs due to structural changes in protein under aggregating conditions resulting in placing of trp groups in a different configuration than that of native protein. Analysis of the emission spectra for HEWL aggregates demonstrates that after incubation of 150 Hrs. in pH 12.2, integrated fluorescence intensity increases by 256 % than that of 0 Hr. incubated sample for 30 µM HEWL **[Table 3.2.3.2]**. Here, we have referred sometimes the increase in fluorescence intensity to increase in quantum yield as both the terms go parallel with each other. Variations observed in fluorescence emission intensity due to changes in the environment of a protein are equivalent to changes in the quantum yield of tryptophan emission in the protein[19].

Structural alterations and molecular rearrangements occur during the aggregation pathway of HEWL such as formation of intermolecular disulfide bonds at later times of incubation which

[4] **Shift in maximum emission wavelength** reports about the polarity of the micro environment of tryptophan residues.

[5] **Area under the curve** is calculated by trapezoidal integration.

hold the self-assembled aggregates tightly[1]. Previously, our lab has reported a rise in free thiol groups after incubation of HEWL in pH 12.2 for the first initial 3 days with a saturation over next 3-5 days and finally a decrease after 5 days[25]. From this, it can be inferred that cleavage of disulfide bond under alkaline conditions leads to generation of free thiols which may lead to a change in interaction of tryptophan residues with disulfide bonds. It is already known that when tryptophan residues are in close proximity with disulfide bonds, it results in quenched fluorescence. This can be one of the likely explanations for quenched fluorescence seen in case of 0 Hr. incubated samples (pH 12.2). However, at later times due to cleavage of disulfide bonds and also due to changes in microenvironment of trp residues, there is reduced interaction of trp with the disulfide bond. After 3 days of incubation in pH 12.2, majority of disulfide bonds are reduced. This was evident from the free thiol estimation assay for HEWL aggregates previously performed by our group[25]. Consequently, there is a release of quenching for the tryptophan residues. As a result, a very significant increase in quantum yield is observed after nearly 40 Hrs. of incubation. In addition, the tryptophan residues can be expected to be deeply buried in the inner core of tightly packed aggregates as with increasing time they become more compact. Structural modifications inside the aggregates also change the solvent accessibility around tryptophan residues which has profound effects on fluorescence emission spectra.

It is generally observed that proximity of tryptophan residues to various quencher groups such as disulfide linkages, protonated carboxyl group may lead to a quenched fluorescence[26]. The possibility of resonance energy transfer between aromatic residues especially between tryptophan molecules, when come to close proximity with each other in a protein was proposed first by **Weber**[27]. Even **Imoto et al.** has provided evidence for energy migration between tryptophan residues in case of lysozyme protein. Although lysozyme consists of 6 tryptophan residues, however the major fluorescence emission has been ascribed to only two residues, Trp 62 and Trp 108; the bulk emitters[19].

Nishimoto et al. have utilized time resolved and quenching fluorescence spectroscopy to characterize the spectral properties of tryptophan residues of hen egg-white lysozyme[26]. Spatial location of the trp residues in the multi tryptophan protein has been reported previously by quenching resolved fluorescence spectroscopy which proved Trp 62 to be fully exposed to the solvent and was estimated to be at the active site of HEWL. Tryptophan mutants of lysozyme have been generated; W62Y and W108Y in which tryptophan residues

were replaced by tyrosine. Fluorescence of each of the tryptophan residues have been differentiated successfully by fluorescence quenching studies. Fluorescence lifetime decay data revealed the contribution of Trp 63 and Trp 123 residues to the fluorescence of lysozyme to be negligible even if they are present in the hydrophilic regions of the protein. Dominant electron exchange interactions with disulfide linkages have been stated as the most likely reason behind the quenched fluorescence of these tryptophan residues. Henceforth, they can be referred to as the non-fluorescent residues of lysozyme. Various studies on tryptophyl fluorescence in hen egg-white lysozyme have confirmed the location of Trp 28 and Trp 111 in the hydrophobic region which are responsible for maintaining structural stability of the protein. Trp 108 is believed to be confined in cage of peptide chains and also present at the active site.

Steady state fluorescence parameters for 30 µM HEWL in pH 7

Hours of incubation	λ_{max} (nm)	% Difference[6] in Intensity
0	338	0
12	336	0.81
24	335	5.7
36	337	1.6
60	337	-3.07
84	337	5.6
108	335	5.2
126	337	3.98
150	337	7.6

Table 3.2.3.1: Experimental parameters for HEWL aggregates incubated in pH 7.0.

[6] **% Difference** is calculated from 100 X $[I_A - I_0] / I_0$ where I_0 refers to integrated fluorescence intensity of 0 Hr. incubated sample and 'A' refers to time points of incubation used for experimental analysis.

Steady state fluorescence parameters for 30 µM HEWL in pH 12.2

Hours of incubation	λ_{max} (nm)	% Difference[7] in Intensity
0	342	0
12	342	-2.29
24	341	53.2
36	340	130.7
60	343	169.8
84	343	220.9
108	343	233.6
126	343	253.8
150	343	256.4

Table 3.2.3.2: Experimental parameters for HEWL aggregates incubated in pH 12.2.

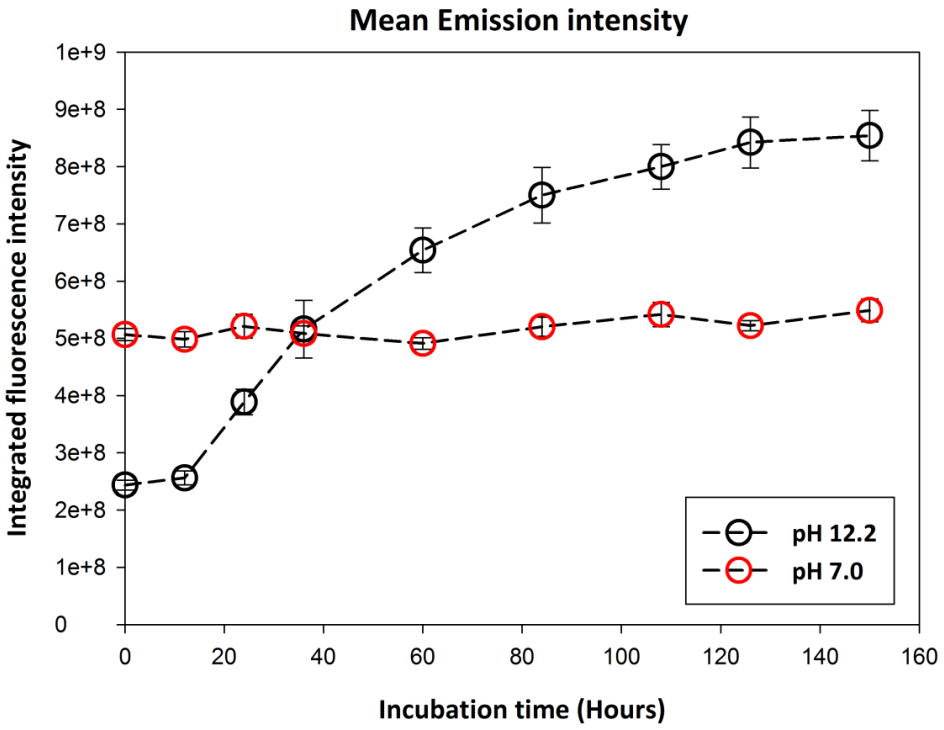

Figure 3.2.3.1 (j): Overlap of mean emission intensity profiles of HEWL incubated in a) pH 7.0 and b) pH 12.2.

[7] **% Difference** is calculated from 100 X $[I_A - I_0] / I_0$ where I_0 refers to integrated fluorescence intensity of 0 Hr. incubated sample and 'A' refers to time points of incubation used for experimental analysis.

3.2.3.2 SCAT analysis results for HEWL (native structure, PDB Id-5F14)

Web based tool for analysis of structural properties of environment of trp residues from atomic structures of protein

Previously, trp-trp energy transfer has been suggested as one of the possible causes for decrease in fluorescence emission. The Forster distance between trp residues for efficient homotransfer ranges between 6 to 12 Å. SCAT analysis was performed for crystal structure of Hen egg white lysozyme under native conditions (PDB 5F14). Distances were determined between different trp residues and the efficiency of energy transfer was calculated from SCAT analysis. This is an online tool kit developed by researchers for generating structural parameters for tryptophan environment in proteins. The structural analysis is performed for 3D atomic structures of proteins provided by the protein data bank (PDB). The output is generated in the form of .txt file which consists of a summary of structural parameters of environment of tryptophan residues.

The structural parameters for 6 tryptophan residues: [W28; W62; W63; W108; W111; W123] (the position of these residues in the protein sequence) are computed. Basically, 6 important structural parameters are calculated which provides information about the microenvironment of tryptophan residues. The relative solvent accessibility of Nε1 and Cζ2 atoms of the indole moieties of each of the tryptophan residues has been calculated. In addition, the averaged value of the relative solvent accessibility of 9 atoms of the whole indole ring of tryptophan fluorophore is also determined from the analysis. From the output generated for native hen egg-white lysozyme (5F14), W62 residue has been found to be the most accessible residue to the surrounding solvent as compared to other tryptophan residues present in the protein. Thus, it can be inferred that except trp 62, all the other 5 trp residues are buried or are somewhat inaccessible to the surrounding solvent in the native state of the protein.

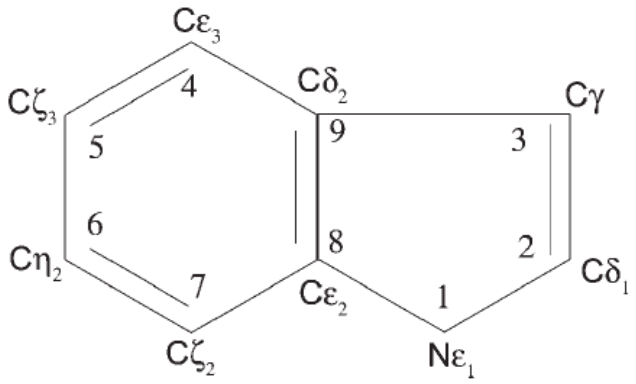

Figure 3.2.3.2 (a): Schematic of the 9 atoms of indole moiety of tryptophan residues[24].

Relative solvent accessibility[8] of trp residues in HEWL

	Accessibility of indole ring (%)
Trp 28	0
Trp 62	46.52
Trp 63	0.79
Trp 108	0
Trp 111	0.77
Trp 123	1.55

Table 3.2.3.3: Accessibility % of tryptophan residues predicted from SCAT analysis. The accessibility of indole ring to the solvent is calculated in presence of bound water molecules which is included in atomic coordinates of PDB files.

The accessibility to solvent molecules for each of the tryptophan residues **[Table 3.2.2.3]** has been calculated by taking into account the water molecules.

Distances between centres of indole ring of all tryptophan pairs in Å	
Tryptophan pairs	**Distance (Å)**
Trp 28 <--> Trp 62	19.27
Trp 28 <--> Trp 63	13.8
Trp 28 <--> Trp 108	**7.38**
Trp 28 <--> Trp 111	**8.28**
Trp 28 <--> Trp 123	12.66
Trp 62 <--> Trp 63	**6.35**
Trp 62 <--> Trp 108	12.96
Trp 62 <--> Trp 111	18.68
Trp 62 <--> Trp 123	27.08
Trp 63 <--> Trp 108	**8.63**
Trp 63 <--> Trp 111	15.54
Trp 63 <--> Trp 123	23.2

[8] **Relative accessibility** can be defined as the percent ratio of the accessible area of an atom in a protein for 1.4 Å spherical probe to that of free tryptophan.

Trp 108 <--> Trp 111	**7.92**
Trp 108 <--> Trp 123	14.63
Trp 111 <--> Trp 123	11.18

Table 3.2.3.4: Distances calculated between centers of the indole rings of tryptophan residues represented in Å.

The **table 3.2.3.4** contains information about the distances between the tryptophan residues of hen egg white lysozyme protein. The probability of energy transfer is greater between those tryptophan pairs where the distances between the indole rings are less than 12 Å (distances are marked in bold black).

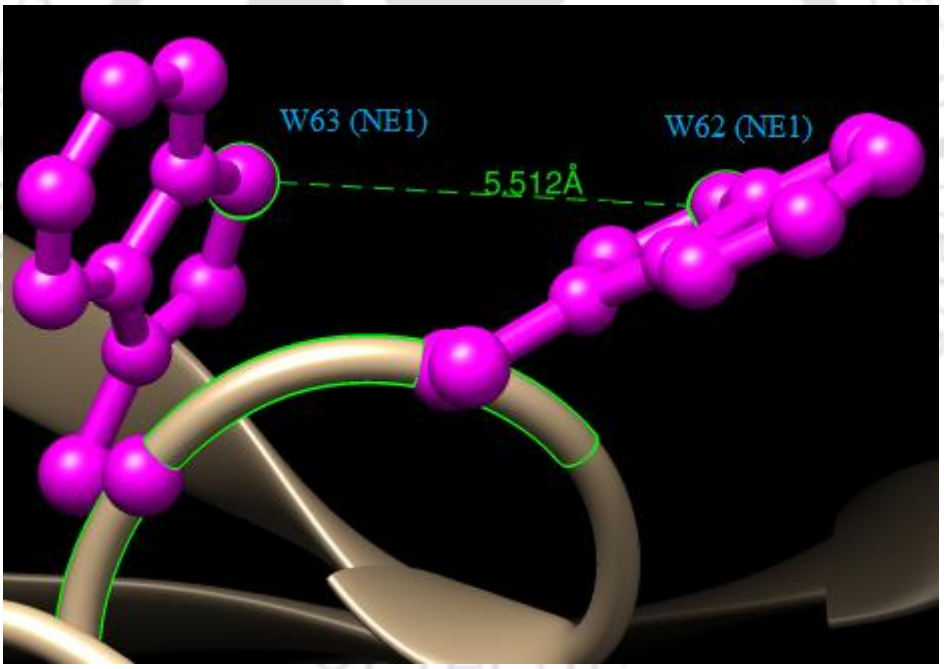

Figure 3.2.3.2 (b): Distance calculated between NE1 atom of indole ring of tryptophan residue 62 and that of Trp residue 63 (generated by Chimera 1.11.2rc).

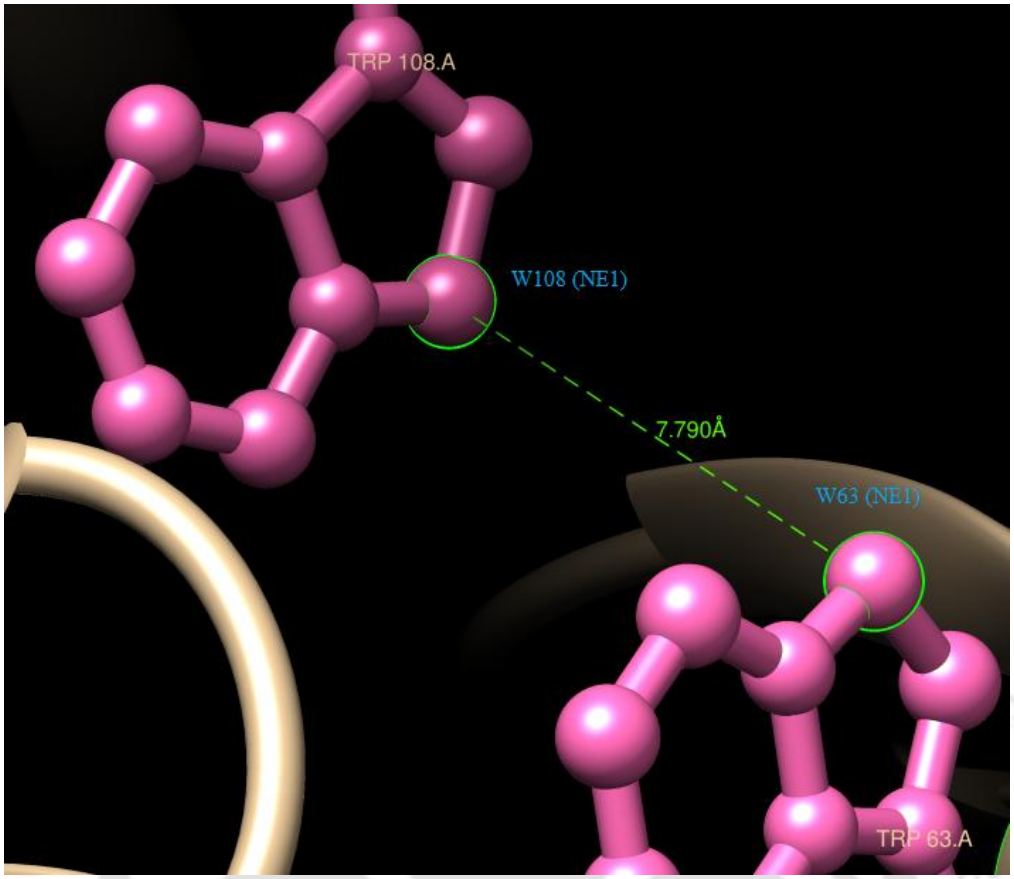

Figure 3.2.3.2 (c): Distance calculated between NE1 atom of indole ring of tryptophan residue 63 and that of Trp residue 108 (generated by Chimera 1.11.2rc).

3.2.4 Concluding Remarks

Although, the steady state emission data provided valuable information about the environment surrounding Trp residues of HEWL in both native state and oligomeric state, but the interpretation of results is difficult from only steady state fluorescence technique. Moreover, heterogeneity and complexity of the microenvironment of multiple trp residues inside the aggregates have to be taken into consideration while drawing any conclusion from the data. We have monitored the changes in quantum yield of tryptophan residues in a time dependent way by incubating the protein solution at both pH 7.0 (monomeric state) and pH 12.2 (oligomeric state).

Significant changes were observed in Trp fluorescence associated with structural alterations occurring during aggregation. We have reported a change in λ_{max} when samples are incubated in pH 12.2 as compared to pH 7.0, thus reflecting upon the collective polarity of the microenvironment of Trp residues. λ_{max} for the HEWL incubated in pH 7.0 represented the Trp residues to be present in a buried state in the native environment of the protein. Finally, the comparison of spectral parameters such as λ_{max} and quantum yield[9] reveals that tryptophan emission spectra show large differences in native and aggregated states. The trend observed was similar for all pH 7.0 samples irrespective of the concentration of the protein used for incubation. Similarly, all the pH 12.2 incubated samples showed an increasing trend for fluorescence intensity, independent of the protein concentration initially used for incubation. It is very important to mention here that although the protein was incubated in alkaline pH at different concentrations but while recording the fluorescence emission spectra, all the samples were diluted to 1 μM. Thus, the concentration of the protein was same in the cuvette for all the samples. As a result, tryptophan fluorescence intensity here is a measure of concentration normalised tryptophan fluorescence quantum yield as a function of aggregate concentration. We have also hypothesized various possible factors such as quenching and trp-trp energy transfer which are responsible for the reduced fluorescence emission of tryptophan residues when exposed to alkaline pH initially. Subsequently, increase in intensity occurs later when these effects are relieved and there is release of quenching due to conformational changes.

[9] **ϕ**- Quantum yield is directly proportional to integrated fluorescence intensity.

3.3 **ANS fluorescence** as a tool to investigate the microenvironment of interior of HEWL nanoaggregates

3.3.1 Introduction

ANS fluorescence undergoes a remarkable change upon binding to the non-polar surfaces resulting in about two-hundred fold enhancement in the intensity accompanied with a blue shift **(Stryer, 1965)**. It is a known fact that ANS exhibits a characteristic environment dependent fluorescence. As polarity of the surrounding solvent decreases, the increase in quantum yield of ANS becomes evident from emission spectra in correlation with blue shift in emission maximum[28]. Several studies have demonstrated the use of ANS (8-anilino-1-napthalenesulfonate) and bis-ANS (1,1′-bis(4-anilino-5-napthalenesulfonic acid)) as polarity sensitive fluorescent probes[29]. ANS binding studies provide a good estimate of exposure of hydrophobic surfaces of the different folding intermediates of a protein.

The solvent dependence of fluorescence emission spectra of ANS fluorophore is basically due to the environmental effects of solvent polarity, the phenomenon is termed as *solvent relaxation* **(Lakowicz et al., 1999)** which usually occurs within a time scale of 10^{-10} sec. This is predominantly observed in case of chromophores which exhibit a higher dipole moment in excited state, μ_e than in ground state, μ_g. Usually, due to redistribution of electrons most of the polarity probes have a larger dipole moment in the excited state than in the ground state ($\mu_e > \mu_g$). Upon interaction with the excited dipole moment of the fluorophore, the surrounding solvent molecules reorient themselves and attain a solvent relaxed state[30]. This leads to lowering of energy of the excited state and results in a huge shift in emission maximum to longer wavelengths i.e., red shifted emission. These solvent effects become more pronounced as the polarity of solvent increases. Hence, higher is the polarity of the medium; greater is the red shift in the emission spectra due to the loss of energy from the relaxed state **(Valeur, 2002)**.

ANS binding has been used previously to monitor aggregation of globular proteins and also to study the kinetics of aggregation[31]. Association of ANS to non-polar surfaces of aggregates gives an idea about the porosity and packing of the aggregates. When a protein undergoes partial or complete unfolding, the hydrophobic surfaces which are otherwise buried in the native state get exposed. Self-association of the partially folded intermediates via solvent exposed hydrophobic patches culminates in formation of aggregates[32]. However, as the aggregation proceeds the exposed hydrophobic patches get buried in the interior of aggregates with time. Dramatic increase in ANS fluorescence intensity, when ANS

incorporates to hydrophobic pockets present in supramolecular complexes of protein aggregates, have been previously reported by the researchers[33]. **Santoro et al.** have studied the binding of ANS to partially folded intermediates of globular proteins which form during denaturation. These authors showed experimentally the presence of intermediates with accessible hydrophobic core in the unfolding pathway. Globular proteins in the native state do not display any affinity towards ANS owing to their well protected, solvent inaccessible, buried hydrophobic core[34]. Surprisingly, even unfolded proteins do not show any preferential binding to ANS in spite of the presence of hydrophobic side chains. On the contrary, molten globule state, a compact partially folded intermediate showed up highest affinity towards ANS due to their exposed hydrophobic clusters.

Hence, ANS can be used as good fluorescent indicator to examine the fraction of exposed hydrophobic surfaces in HEWL aggregates in a time dependent way.

In order to gain insights into structural organization of HEWL amorphous aggregates, ANS was used as a hydrophobic probe. Spectrofluorimetry was used to carry out ANS binding assay. To investigate the hydrophobic clusters present on the surface of the aggregates and in the interior region of HEWL aggregates, the binding assay was carried out in a time dependent way.

The major issue which has been addressed corresponds to the questions: a) **can we ascertain the intactness of HEWL aggregates transferred to pH 7.0 by means of their ability to take up a hydrophobic probe?** b) **Whether bigger aggregates have greater exposed hydrophobic sites as compared to smaller aggregates?** c) **Whether the non-polar pockets are retained in the aggregates after transfer to pH 7.0?**

Here we have presented the experimental data for ANS binding studies for HEWL in native state, aggregates state and HEWL nanoparticles transferred to pH 7.0.

3.3.2 Materials and Methods

3.3.2.1 Steady-state fluorescence measurements

Fluorescence measurements were performed on a Jobin-Yvon Fluoromax-3 spectrofluorometer. For acquisition of emission spectra, excitation was carried out at 380 nm with 1 nm as excitation slit and 8 nm as emission slit. The scanning range for procuring the emission spectra was from 400 nm to 600 nm. While recording the spectra, the protein samples were diluted such that the final concentration of protein was 3 μM in the cuvette. ANS concentration was kept very low as much as 10 μM for all the binding experiments. ANS stock was prepared in water at a concentration of 1 mg/ml. The concentration of the stock solution was estimated by using the extinction coefficient of 4,950 $M^{-1}cm^{-1}$ at 350 nm. The stock was further diluted to desired concentration for all the experiments. A very low concentration of ANS, 10 μM was used as a uniform concentration throughout the experiments in order to avoid the inner filter effect in fluorescence measurements.

The concentration of ANS and protein solutions were determined using Cary 100 UV-Vis spectrophotometer.

3.3.3 Results and Discussion

3.3.3.1 ANS assay for HEWL monomer and HEWL aggregates

A 1 mM stock solution of ANS in water was incubated at room temperature for control experiment. Aliquots from the stock were taken out from the stock solution at different time points and further diluted to 10 μM in 100 mM pH 7.0 sodium phosphate buffer while recording emission measurements. Fluorescence intensity of 10 μM ANS in pH 7.0 buffer was recorded as a function of time in order to confirm that the quantum yield of ANS doesn't alter in absence of any hydrophobic surface to bind, as it may affect the interpretation of results. No significant change in fluorescence of ANS was observed in aqueous buffer pH 7.0. The wavelength of maximum emission (λ_{max}) was 520 nm for ANS in pH 7.0 buffer as revealed from the emission spectra. Average integrated ANS fluorescence in aqueous buffer showed a value close to ~1.2 x 10^8.

Under the similar conditions of excitation as used for control, fluorescence emission spectra were recorded for 40 μM HEWL incubated in pH 7.0 as function of time. Protein solutions were incubated with ANS for 20 minutes prior to acquisition of emission spectra. ANS spectra clearly indicated that it doesn't bind to the native state of the protein due to the absence of any exposed hydrophobic patches **[Figure 3.3.3.1 (a) & 3.3.3.1 (b)]**.

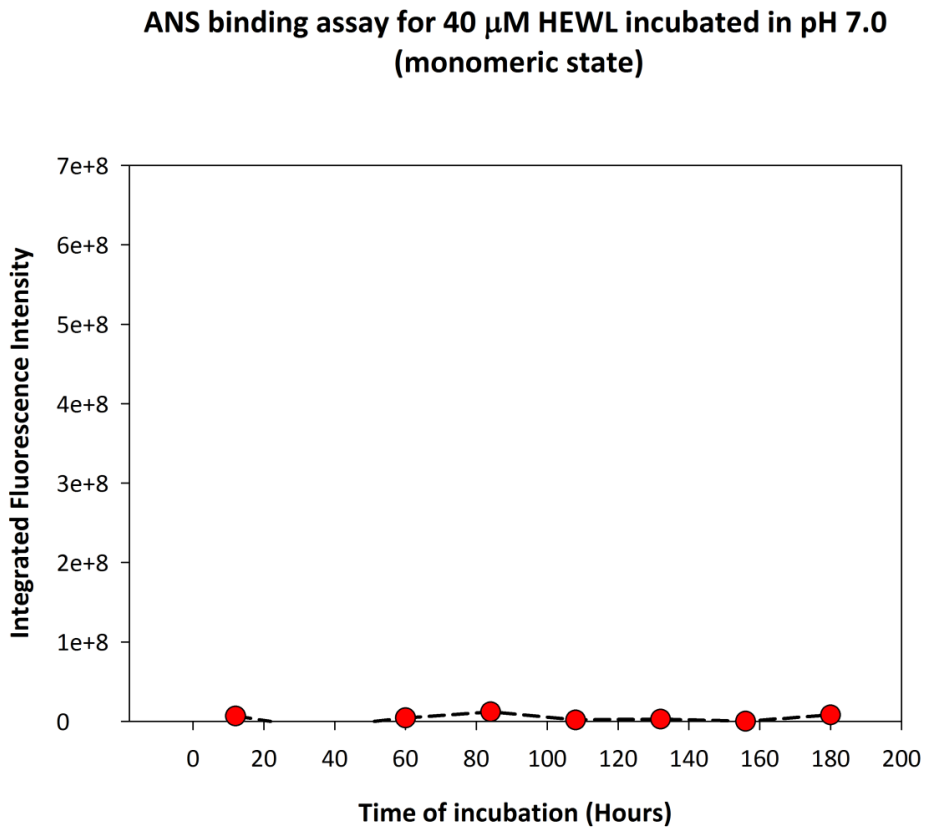

Figure 3.3.3.1 (a): Integrated fluorescence plot for 40 µM HEWL incubated in pH 7.0 (native state).

It can be clearly seen from the figure **[Figure 3.3.3.1 (a)]** that the fluorescence intensity of ANS is quenched in the aqueous buffer due to lack of any hydrophobic surfaces to bind to. HEWL protein retains its native state in pH 7.0 and its hydrophobic core remains occluded from the surrounding solvent, inaccessible to ANS.

[Figure 3.3.3.1 (b)] shows the experimental results obtained for ANS binding to HEWL aggregates incubated in pH 12.2. Immediately after exposure to alkaline pH, there is an increase in ANS fluorescence intensity followed by a rapid rise for 24 hours incubated sample. **[Figure 3.3.3.1 (c)]** represents ANS fluorescence for 120 µM HEWL aggregates incubated in pH 12.2 in a time dependent way.

A sharp rise in ANS fluorescence was observed for 120 µM HEWL incubated in alkaline pH which is in agreement with the formation of aggregates at pH 12.2 with time. In addition, maximal fluorescence was observed for 1 day old aggregate sample which suggests maximum availability of exposed hydrophobic patches to ANS. The results are in accord with those reported previously for HEWL aggregates incubated in pH 12.2[25] **(Kumar et al., 2008)**. It should be noted that the concentration of ANS and protein used for initiating

aggregation was different than being used here. However, the trend observed for ANS fluorescence when it binds to hydrophobic pockets of HEWL aggregates is similar. Gradual increase in fluorescence, initially observed for 6 hours of incubation, can be attributed to the growth of aggregates which results in increase of exposed hydrophobic surfaces.

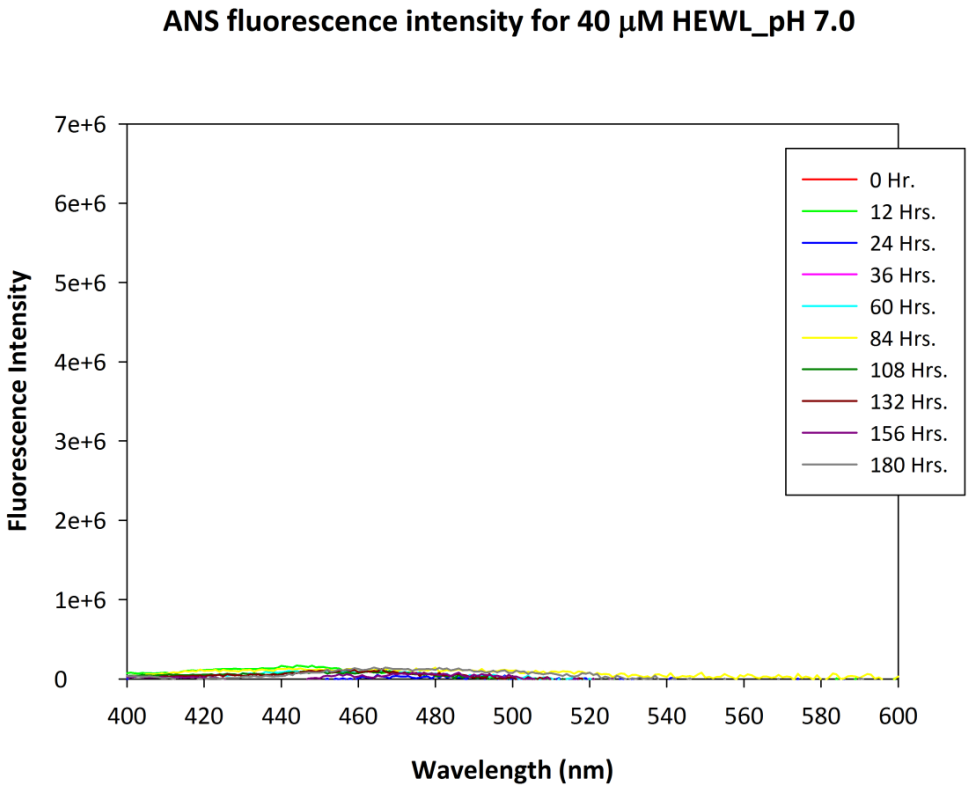

Figure 3.3.3.1 (b): ANS binding to 40 µM HEWL in pH 7.0 (native state) measured by fluorescence intensity (excitation at 380 nm).The samples were incubated with ANS for 10 min. prior to measurement. Excitation and emission slits were fixed at 1 nm and 8 nm. Protein concentration in the cuvette was 3 µM.

Integrated fluorescence intensity plots presented here represents the area under the curve calculated from ANS fluorescence intensity spectra. In case of fluorescence intensity data, each emission spectrum was obtained after averaging over 3 independent acquisitions using identical conditions.

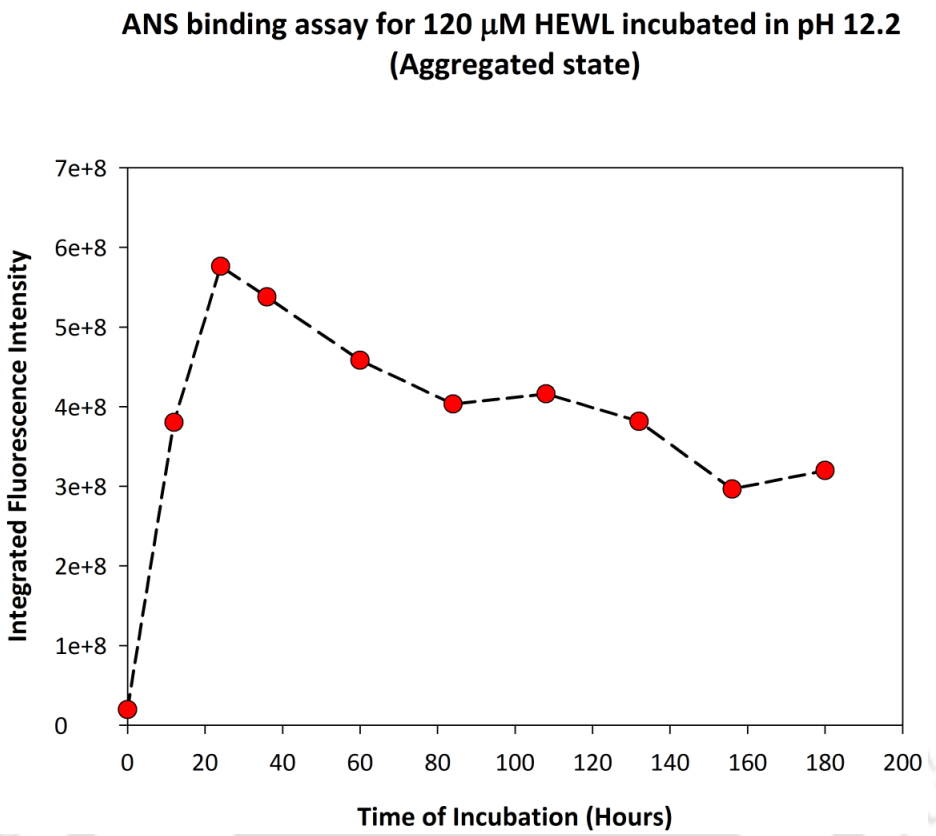

Figure 3.3.3.1 (c): Fluorescence of ANS bound to 120 µM HEWL aggregates in pH 12.2.Here, concentration of protein refers to the monomer concentration at which the protein solution was incubated in alkaline pH.

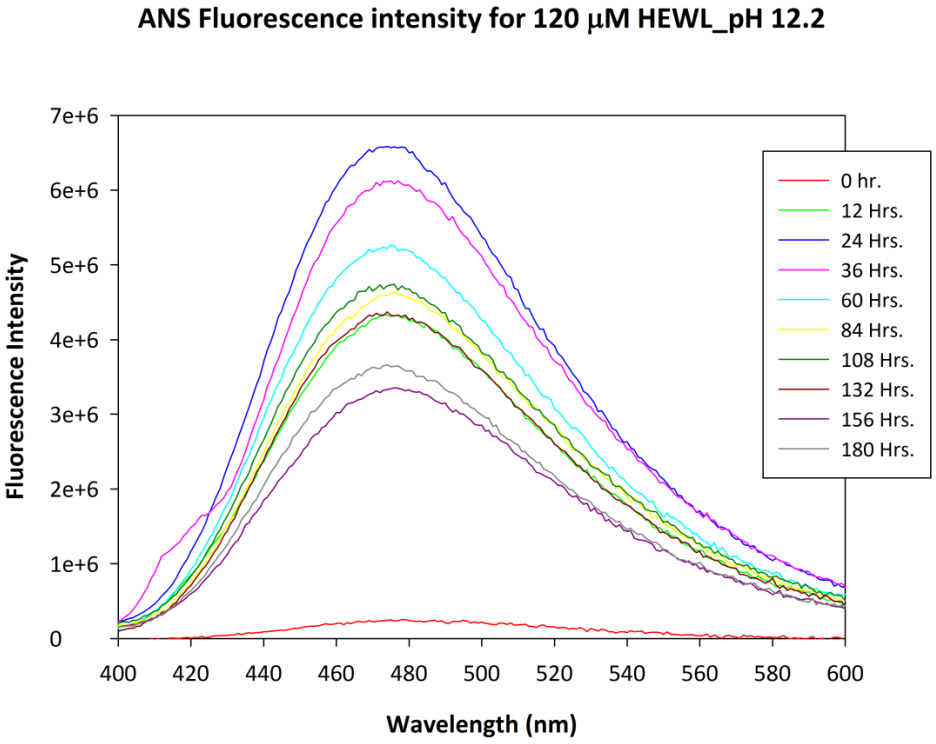

Figure 3.3.3.1 (d): ANS fluorescence intensity for HEWL aggregates incubated in pH 12.2.Protein concentration in the cuvette was 3 µM and conc. of ANS was 10 µM.

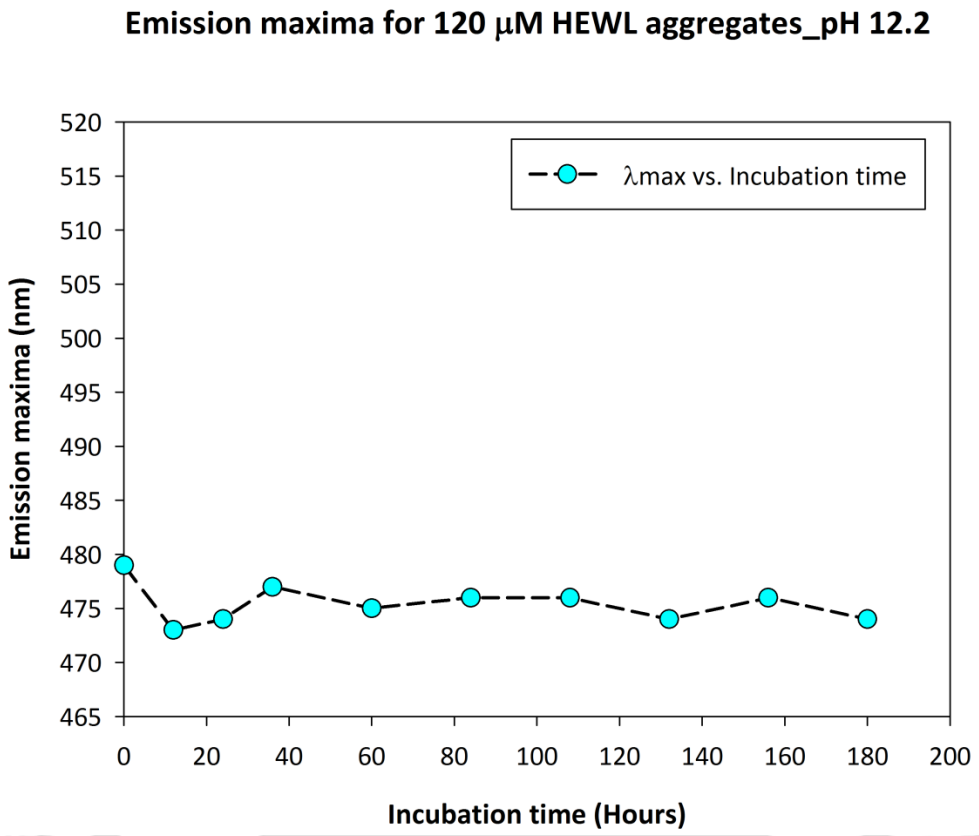

Figure 3.3.3.1 (e): λmax of ANS emission spectra for HEWL aggregates with time.

Increase in ANS fluorescence for HEWL aggregates incubated in pH 12.2 confirms higher affinity of hydrophobic ANS probe to exposed hydrophobic patches of aggregates. In order to know the behaviour of ANS, a freely diffusing probe which binds non-covalently to non-polar regions, aggregates incubated in pH 12.2 were transferred to pH 7.0 at different time points.

3.3.3.2 ANS assay for samples transferred to pH 7.0

We now examine the effect of transferring HEWL aggregates from pH 12.2 to pH 7.0 at different times of transfer (12 hours to 156 hours).

Enhancement in the intensity is rapidly lost after a rise as seen after 0 hour incubation in pH 7.0 (12 hours transferred sample). In case of 24 hours transferred aggregates, initial rise in the ANS intensity is followed by a further decrease in intensity with incubation time. The plot clearly reveals that maximal fluorescence enhancement is seen for one day old aggregates transferred to pH 7.0. As 24 hours old aggregates have maximum exposed hydrophobic patches which give them the capacity to take up ANS maximally.

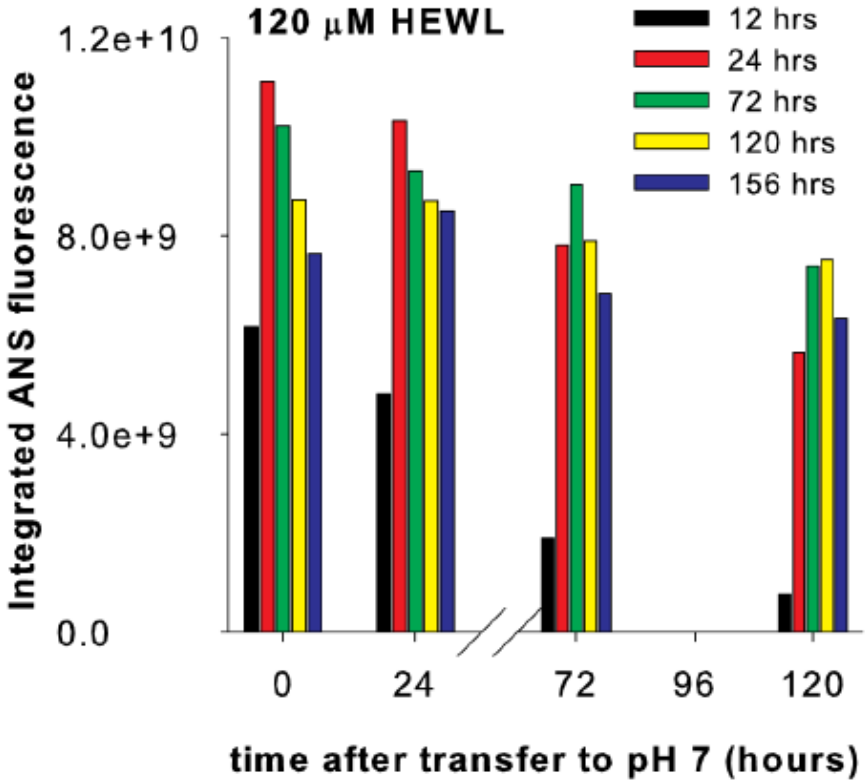

Figure 3.3.3.2 (a): Integrated ANS fluorescence intensity for 120 μM HEWL aggregates transferred to pH 7.0 with 10 fold dilution at different time points: 12, 24, 72, 120 & 156 hours. Fluorescence intensities were recorded at different time points of incubation in pH 7.0 after transfer: 0, 24, 72 & 120 hours. Final concentration of the protein in cuvette was 12 μM.

Finally for late hours transferred samples (120 and 156 hours), there is negligible decrease in intensity with incubation time in comparison to faster drop as seen for early hours transferred samples. The possible explanation for a slower decline in intensity of late hours transferred samples can be the optimal packing of aggregates. The well packed compact aggregates show a tendency of steady binding to ANS. Thus, as illustrated in the **[Figure 3.3.3.2 (a)]** for early hours transferred samples, after an initial rise in the intensity during initial hours of incubation is followed by rapid decline in intensity with time. In contrast, the intensity for late hours transferred samples especially after 120 hours transfer, remains almost unperturbed with time.

The conclusion which can be drawn from the results obtained after ANS binding assay is that late hours transferred aggregates bind strongly to ANS which establishes their robustness **(Ravi et al., 2014)**.

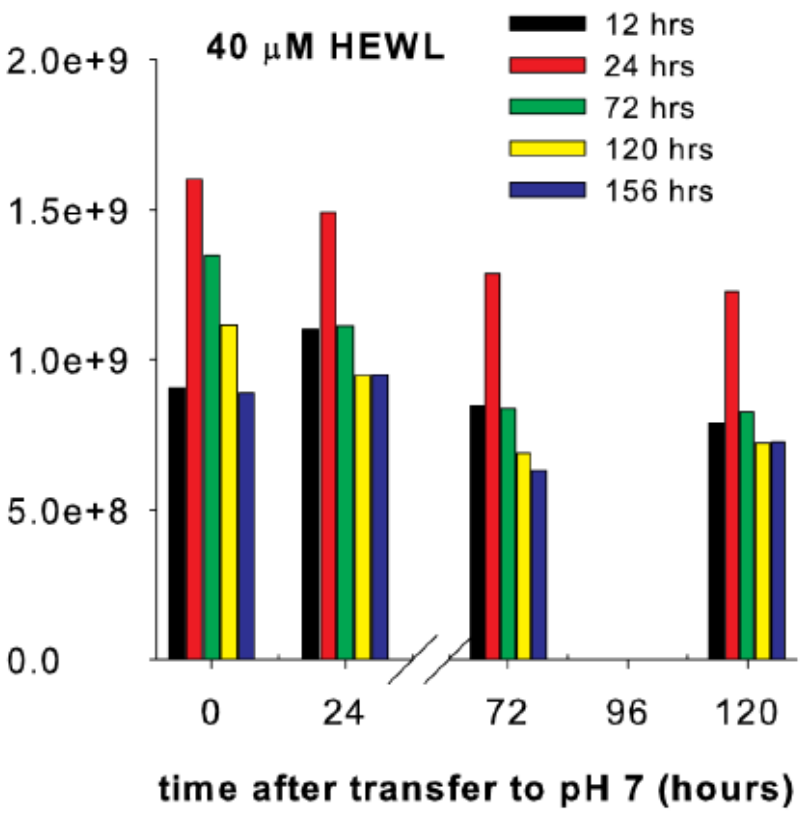

Figure 3.3.3.2 (b): ANS fluorescence intensity for 40 M HEWL incubated in pH 12.2 and then transferred to pH 7.0 with 10 fold dilution after time points: 12, 24, 72, 120 & 156 hours. Final concentration of the protein in cuvette was 4 μM.

The results obtained from **[Figure 3.3.3.2 (a) & 3.3.3.2 (b)]** cannot be used to draw any conclusion especially for comparison of concentration dependent studies as the protein concentration used for ANS binding studies are different in both the cases. Additional information comes from another experiment in which the concentration of protein was kept same in the cuvette. Hence, to further gain a better understanding, HEWL concentration was maintained as 4 μM in cuvette for both 120 μM and 40 μM aggregates transferred to pH 7.0 **[Figure 3.3.3.2 (c) & 3.3.3.2 (d)]**.

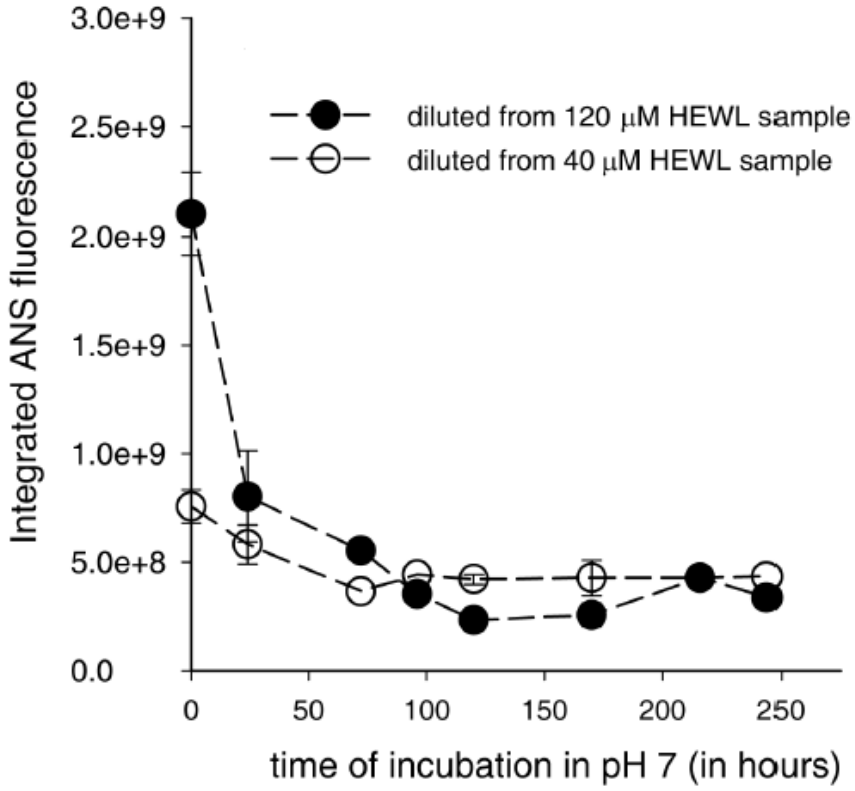

Figure 3.3.3.2 (c): Transfer after 144 hours: Binding of ANS to 120 μM and 40 μM aggregates incubated in pH 12.2 for 144 hours and then transferred to 100 mM Sodium phosphate buffer pH 7.0 with 10 fold dilution. Protein conc. was kept as 4 μM in the cuvette for recording emission spectra in both 40 μM & 120 μM samples.

[Figure 3.3.3.2 (c)] shows a significant increase in fluorescence intensity of ANS probe for 120 μM HEWL aggregates (0 hours incubation after transfer to pH 7.0) as compared to 40 μM HEWL aggregates. In case of 120 μM aggregates transferred after 144 hours, the aggregates open up after suddenly experiencing electrostatic repulsions in pH 7.0.This results in the exposure of hydrophobic surfaces at initial hours of transfer, which renders them more accessible to ANS due to which remarkable enhancement in the intensity was observed. Henceforth, this can be a plausible reason for initial binding which resulted in greater magnitude in enhancement of ANS fluorescence.

Further subsequent drop in fluorescence intensity after 24 hours of incubation (120 μM aggregates) and there on reflects the conformational changes taking place within the oligomeric assembly. This could arise due to optimal packing of the aggregates in order to minimize repulsions upon transfer to pH 7.0 which resulted in sterically inaccessible ANS binding regions.

Another interesting finding which came out from this study is that larger aggregates have a higher affinity to associate with ANS as compared to smaller aggregates. The magnitude of increase in fluorescence intensity of ANS as seen in case of 120 μM aggregates is much greater in comparison to 40 μM aggregates **[Figure 3.3.3.2 (d)]**. The differences between the two plots are quite remarkable even though they represent the ANS fluorescence intensities for aggregates transferred to pH 7.0.The conditions are identical in Figure [**3.3.3.2 (c) & 3.3.3.2 (d)**] except the transfer time to pH 7.0 are different in the experiments.

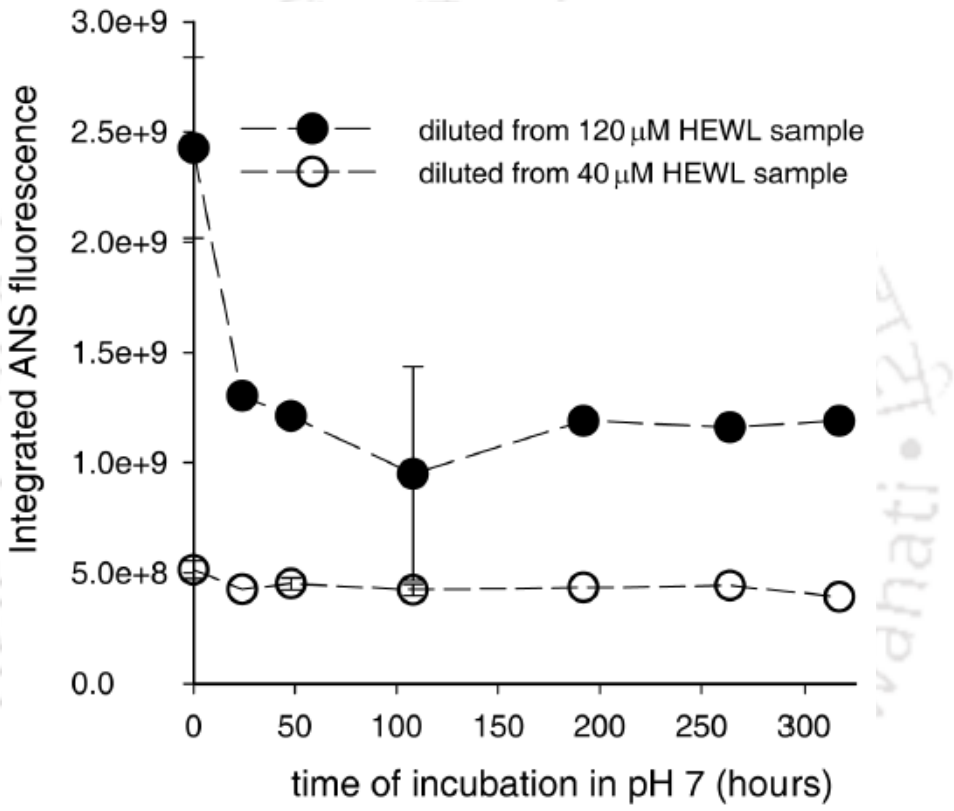

Figure 3.3.3.2 (d): Transfer after 264 hours: Binding of ANS to 120 μM and 40 μM aggregates incubated in pH 12.2 for 264 hours and then transferred to 100 mM Sodium phosphate buffer pH 7.0 with 10 fold dilution. Protein conc. was kept as 4 μM in the cuvette for recording emission spectra.

The results presented here emphasizes on the fact that HEWL aggregates of higher [M][10] concentration have more accessible hydrophobic pockets as compared to aggregates of lower [M] concentration at 0 hr. after transfer to pH 7.0. This is revealed from the ANS intensity data as the emission spectra follow a concentration dependent trend.

[10] **[M]** - here refers to monomer concentration.

It was apparent from the studies that aggregates with higher [M] displayed enhanced fluorescence intensities i.e. an increased binding to ANS as a result of increased hydrophobic interior in case of bigger aggregates.

It seems from the plot that drop in ANS fluorescence for 120 μM HEWL aggregates occurs at later times of incubation in pH 7.0 after transfer. This suggests that the hydrophobic surfaces which were available initially to bind to ANS get diminished with time. At later stages, conformational changes induce formation of tightly packed and compact aggregates which excludes the hydrophobic binding sites for ANS. Consequently, due to the optimal packing of aggregates, ANS is not able to access the buried hydrophobic clusters.

Substantial differences were observed for both 120 μM and 40 μM HEWL aggregates at different transfer times (144 hours and 264 hours of transfer). The results presented here strongly reinforce the view that late hour transferred samples are more stable and retain the capacity of binding to ANS after transfer to pH 7.0. This is due to the role of intermolecular disulfide bonds, formed after 5 days of incubation in pH 12.2, which hold the aggregates together against any repulsion. There is no major variation in ANS fluorescence is seen in case of 40 μM aggregates after transfer to pH 7.0, irrespective of the transfer time. Although major difference seems to be significant in case of 120 μM aggregates (transferred samples). For 144 hours transferred samples, ANS fluorescence intensity after reaching a maximal at early stage (0 hours in pH 7.0 after transfer) is rapidly lost and the drop comes to a level similar to that observed for 40 μM aggregates **[Figure 3.3.3.2 (c)]**.

Whereas for 120 μM aggregates transferred after 264 hours, the intake capacity to take up ANS dye is significantly retained even after longer times of incubation in pH 7.0 after transfer **[Figure 3.3.3.2 (d)]**.

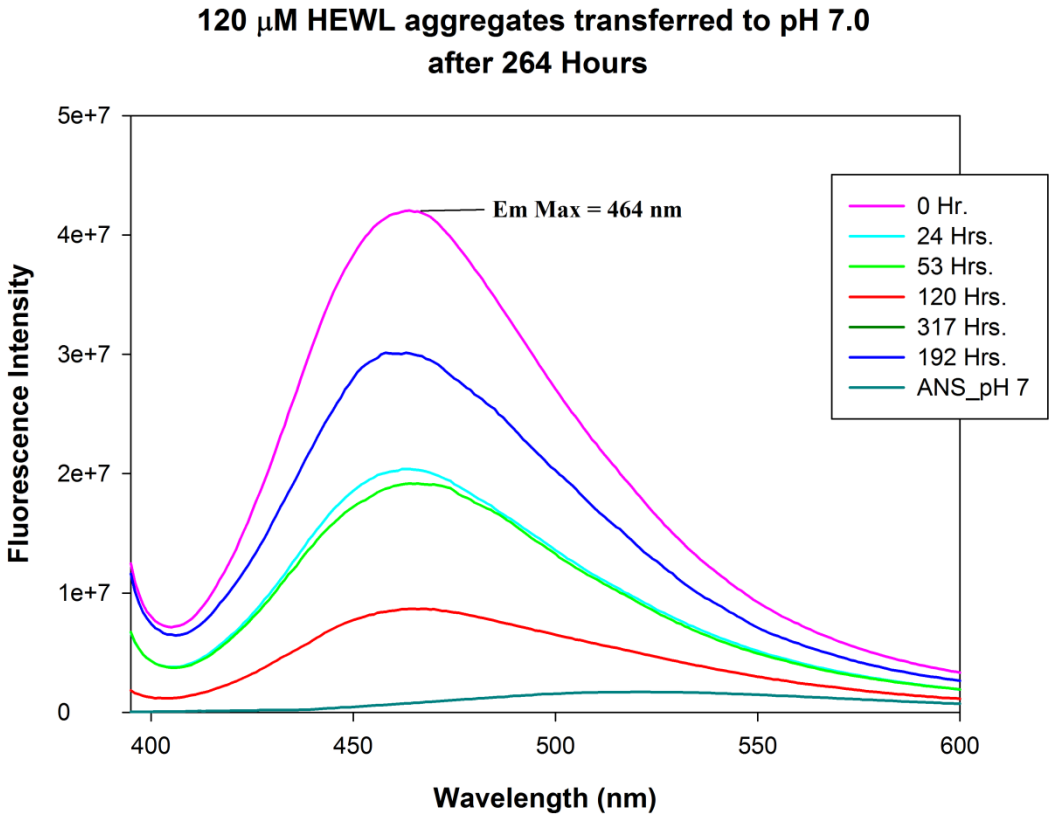

Figure 3.3.3.2 (e): ANS Emission spectra for 120 μM HEWL aggregates in pH 12.2 transferred to pH 7.0 after 264 hours with 10 fold dilution. Em Max or emission maximum for 0 hour incubated transferred sample is at **464 nm** which is blue shifted as compared to Em max for ANS in pH 7.0 buffer which is at **520 nm**.

3.3.4 Conclusion

ANS binding assay suggests that the binding sites in case of 40 μM aggregates differ from 120 μM aggregates. Aggregates from 120 μM show a greater binding capability for ANS than 40 μM aggregates consistent with their larger size. Thus, it can be inferred from the study that aggregates with higher [M] have more accessible hydrophobic pockets as compared to aggregates with smaller molecular volume. Interaction of ANS with transferred samples revealed that 120 μM aggregates displayed higher ANS fluorescence and more blue shifted spectra in comparison to 40 μM aggregates.

The picture that emerges from ANS binding assay gives us a view about the oligomeric species which are incubated for a longer time period in alkaline pH before transfer to pH 7.0. These appear to have more capability of binding to ANS due to different structural organization as compared to the species with shorter incubation period in pH 12.2.

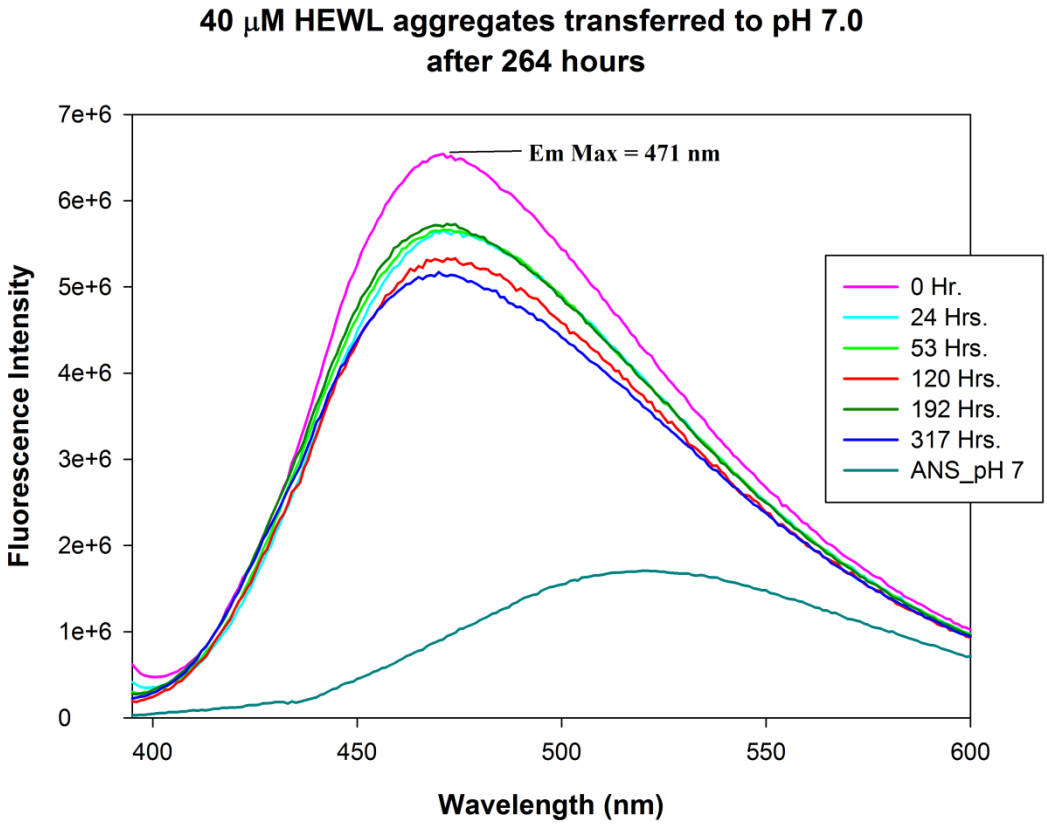

Figure 3.3.3.2 (f): ANS Emission spectra for 40 μM HEWL aggregates in pH 12.2 transferred to pH 7.0 after 264 hours with 10 fold dilution. Em Max or emission maximum for 0 hour incubated transferred sample is at **471 nm** which is blue shifted as compared to Em max for ANS in pH 7.0 buffer which is at **520 nm**.

References

1. Ravi, V. K., Swain, T., Chandra, N. & Swaminathan, R. On the characterization of intermediates in the isodesmic aggregation pathway of hen lysozyme at alkaline pH. *PLoS One* **9,** 1-12 (2014).
2. Nakajima, A. A study of the system of pyrene and β-cyclodextrin in aqueous solution utilizing the intensity enhancement phenomenon. *Spectrochim. Acta Part A Mol. Spectrosc.* **39,** 913–915 (1983).
3. Homchaudhuri, L., Kumar, S. & Swaminathan, R. Slow aggregation of lysozyme in alkaline pH monitored in real time employing the fluorescence anisotropy of covalently labelled dansyl probe. *FEBS Lett.* **580,** 2097–2101 (2006).
4. Mako, T., Marks, P., Cook, N. & Levine, M. Fluorescent detection of polycyclic aromatic hydrocarbons in ternary cyclodextrin complexes. *Supramol. Chem.* **24,** 743–747 (2012).
5. Durocher, G. and Sandorfy, C. On the General Occurrence of the Ham Effect in the Electronic Spectra of Aromatic Hydrocarbons. *J. Mol. Spectrosc.* **20,** 410–424 (1966).
6. Nakajima, A. Intensity enhancement induced by solute-solvent interaction between pyrene and polar solvents. *Spectrochim. Acta Part A Mol. Spectrosc.* **38A,** 693–695 (1982).
7. Nakajima, A. Fluorescence spectra of pyrene in chlorinated aromatic solvents. *J. Lumin.* **11,** 429–432 (1976).
8. Nakajima, A. Fluorescence spectra of anthracene and pyrene in water and in aqueous surfactant solution. *J. Lumin.* **15,** 277–282 (1977).
9. Nakajima, A. Effects of isomeric solvents on vibronic band intensities in fluorescence spectrum of pyrene. *J. Mol. Spectrosc.* **61,** 467–469 (1976).
10. Díaz, a. N., Sánchez, F. G. & Pareja, a. G. Cholic acid behavior in water and organic solvent: study of normal and inverted aggregates. *Colloids Surfaces A Physicochem. Eng. Asp.* **142,** 27–34 (1998).
11. Salonen, A. *et al.* A novel pyrene-based fluorescing amphiphile with unusual bulk and interfacial properties. *ChemPhysChem* **12,** 150–160 (2011).
12. Thomas, J. K. and Kalyanasundaram, K. Environmental effects on vibronic band intensities in pyrene monomer fluorescence and their application in studies of micellar systems. *J. Am. Chem. Soc.* **99,** 2039–2044 (1977).

13. Duhamel, J. New Insights in the Study of Pyrene Excimer Fluorescence to Characterize Macromolecules and their Supramolecular Assemblies in Solution. *Langmuir* **28,** 6527–6538 (2012).
14. D'Arrigo, G. *et al.* Self-assembled gellan-based nanohydrogels as a tool for prednisolone delivery. *Soft Matter* **8,** 11557 (2012).
15. Eddaoudi, M., Coleman, A. W., Prognon, P. & Lopez-mahia, P. Steady state fluorescence studies of the complexes between pyrene and per-6-O-tert-butyldimethylsilyl cyclodextrins. *J. Chem. Soc., Perkin Trans.* **2,** 955–959 (1996).
16. Thomas, J. K. and Kalyanasundaram, K. Environmental effects on vibronic band intensities in pyrene monomer fluorescence and their application in studies of micellar systems. *J. Am. Chem. Soc.* **99**, 2039–2044 (1977).
17. Riaz Waris, Michael A. Rembert, David M. Sellers, William E. Acree, JR., Kenneth W. Street, JR., Colin F. Poole, Prabhakara H. Shetty, & J. C. F. Polycyclic Aromatic Hydrocarbon Solute Probes: Effect of Solvent Polarity on the Ovalene and Benzo[ghi]perylene Fluorescence Emission Fine Structures. *Appl. Spectrosc.* **42,** 1525–1530 (1988).
18. Teale, F. W. J. The Ultraviolet Fluorescence of Proteins in Neutral Solution. *Biochem. J.* **76,** 381–388 (1960).
19. Imoto, T., Forster, L. S., Rupley, J. a & Tanaka, F. Fluorescence of lysozyme: emissions from tryptophan residues 62 and 108 and energy migration. *Proc. Natl. Acad. Sci. U. S. A.* **69,** 1151–1155 (1972).
20. Lasagna, M., Gratton, E., Jameson, D. M. & Brunet, J. E. Apohorseradish peroxidase unfolding and refolding: intrinsic tryptophan fluorescence studies. *Biophys. J.* **76,** 443–450 (1999).
21. James, N. G., Ross, J. A., Mason, A. B. & Jameson, D. M. Excited-state lifetime studies of the three tryptophan residues in the N-lobe of human serum transferrin. *Protein Sci.* **19,** 99–110 (2010).
22. Chen, Y. & Barkley, M. D. Toward understanding tryptophan fluorescence in proteins. *Biochemistry* **37,** 9976–9982 (1998).
23. Chen, Y., Liu, B., Yu, H. T. & Barkley, M. D. The peptide bond quenches indole fluorescence. *J. Am. Chem. Soc.* **118,** 9271–9278 (1996).

24. Shen, C. *et al.* The protein fluorescence and structural toolkit: Database and programs for the analysis of protein fluorescence and structural data. *Proteins Struct. Funct. Genet.* **71,** 1744–1754 (2008).
25. Kumar, S., Ravi, V. K. & Swaminathan, R. How do surfactants and DTT affect the size, dynamics, activity and growth of soluble lysozyme aggregates? *Biochem. J.* **415,** 275–288 (2008).
26. Nishimoto, E., Yamashita, S., Yamasaki, N. & Imoto, T. Resolution and characterization of tryptophyl fluorescence of hen egg-white lysozyme by quenching- and time-resolved spectroscopy. *Biosci Biotechnol Biochem* **63,** 329–336 (1999).
27. G.Weber. Fluorescence-Polarization Spectrum and Electronic-Energy Transfer in Proteins. *Biochem. J.* **75,** 345–352 (1960).
28. Stryer, L. The interaction of a naphthalene dye with apomyoglobin and apohemoglobin: a fluorescent probe of non-polar binding sites. *J. Mol. Biol.* **13,** 482–495 (1965).
29. John, B., D'Silva, P. R. & Lala, A. K. Analysis of protein folding using polarity-sensitive fluorescent probes. *Curr. Sci.* **80,** 287–290 (2001).
30. Valeur, B (2001). Photoinduced charge transfer and solvent relaxation. In *Effect of polarity on fluorescence emission. Polarity probes,* Molecular Fluorescence: Principles and Applications (pp. 206-213). Weinheim: Wiley-VCH.
31. Kundu, B. & Guptasarma, P. Use of a hydrophobic dye to indirectly probe the structural organization and conformational plasticity of molecules in amorphous aggregates of carbonic anhydrase. *Biochem. Biophys. Res. Commun.* **293,** 572–577 (2002).
32. Khurana, R. *et al.* Partially folded intermediates as critical precursors of light chain amyloid fibrils and amorphous aggregates. *Biochemistry* **40,** 3525–3535 (2001).
33. Povarova, O. I., Kuznetsova, I. M. & Turoverov, K. K. Differences in the pathways of proteins unfolding induced by urea and guanidine hydrochloride: Molten globule state and aggregates. *PLoS One* **5,** 1–4 (2010).
34. Martins, N. F. & Santoro, M. M. Partially folded intermediates during trypsinogen denaturation. *Brazilian J. Med. Biol. Res.* **32,** 673–682 (1999).
35. Lakowicz, J.R. (1999) Principles of Fluorescence Spectroscopy, Kluwer Academic/Plenum Press, Newyork.

Chapter 4

Estimation of structural parameters for globular HEWL monomer and heterogeneous HEWL aggregates by Small Angle X-ray Scattering

Estimation of structural parameters for globular HEWL monomer and heterogeneous HEWL aggregates by **Small Angle X-ray scattering**

4.1 Introduction

SAXS (Small Angle X-ray Scattering) is very apt to study the sizes of molecules ranging from 1 nm to 1 μm which makes this technique suitable for various structural studies on biomolecules. It is a solution scattering technique and the wavelength used for x-ray scattering is from 0.5-2.0 Å.

The difference in electron density within a sample causes the incident X-ray beam to scatter resulting in both coherent and incoherent scattering. Out of these two, elastic or coherent scattering (without energy loss) is of major importance. The scattering pattern generated is dependent on the atomic groups present in the sample and thus can be used for structural studies.

The structural characterization method from solution scattering is advantageous for the study of macromolecules in solution which cannot be crystallized easily. Moreover, SAXS provides information about macromolecules in their native state or in physiological environment. Low resolution structural information about overall shape and size of the particles can be extracted easily from the scattering intensity profile. This information provides an edge over other high resolution methods. The presence of any intermolecular interactions can also be investigated from the pattern of scattering intensity profile.

Electron density contrast[1] is a very important parameter which greatly influences SAXS data. The contrast is equal to the difference in density of the particle from that of the solvent. The experimental SAXS data is obtained by subtracting the measured scattering profile of buffer from that of the sample in solution.

Recent interest in potential applications of amyloid fibrils has led to the development of various methods to elucidate the mechanism of fibril formation. SAXS has been used to monitor the kinetics of amyloid fibrils formed by self-assembly. SAXS based studies have been previously carried out to investigate the structural investigation of insulin fibrils.

Resonance occurs when a monochromatic X- ray beam is incident on electrons, leading to oscillation of electron with the same frequency as that of the incident X-ray. As a result, secondary waves are generated which further undergo constructive and destructive interference. The interference of waves give rises to a scattering pattern[2].

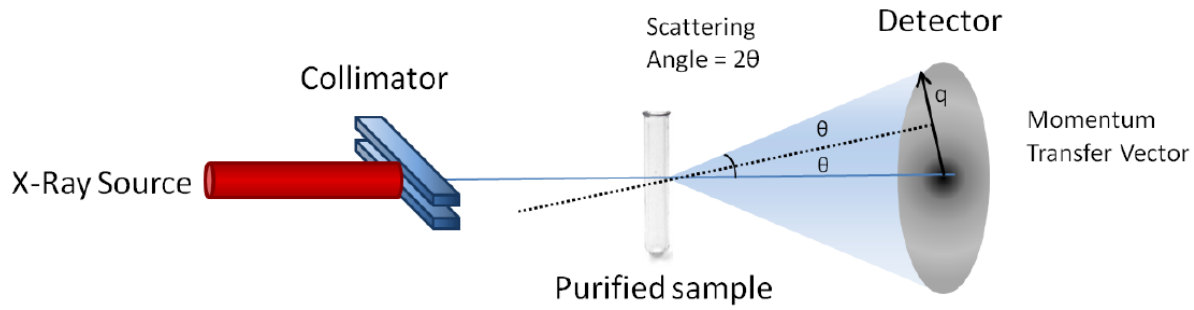

Figure 4.1.1: SAXS set up: Monochromatic X-ray beam of constant λ are focussed by the collimator. This incident X-ray beam when passes through the sample, X-rays are scattered by the electrons in the sample. The scattered X-rays are captured by the detector resulting in 2D scattering pattern. The data is processed to generate SAXS intensity scattering profile (**Putnam et al., 2013**).

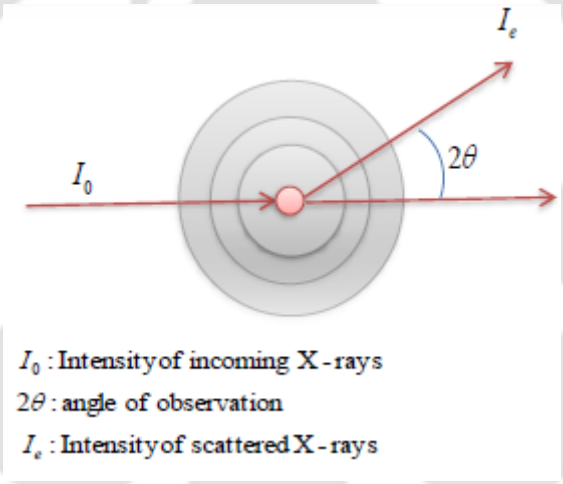

Figure 4.1.2: X-ray scattering showing the incident and scattered rays.

The real space coordinates are converted to reciprocal space of scattering vectors by Fourier transformation. Scattering intensity is equal to square of the x-ray scattering amplitude. Furthermore, these scattering amplitudes are function of momentum transfer vector.

$$I(s) = A(s) * A(s) \quad \ldots\ldots (1)$$

For macromolecules in solution, scattering intensity from a single particle is averaged over all orientations which is proportional to the intensity from the whole sample i.e. $I(s) = \langle I(s) \rangle_{\Omega}$. The above condition holds true in case of dilute monodisperse solution of non-interacting particles (**Svergun et al., 2003**).

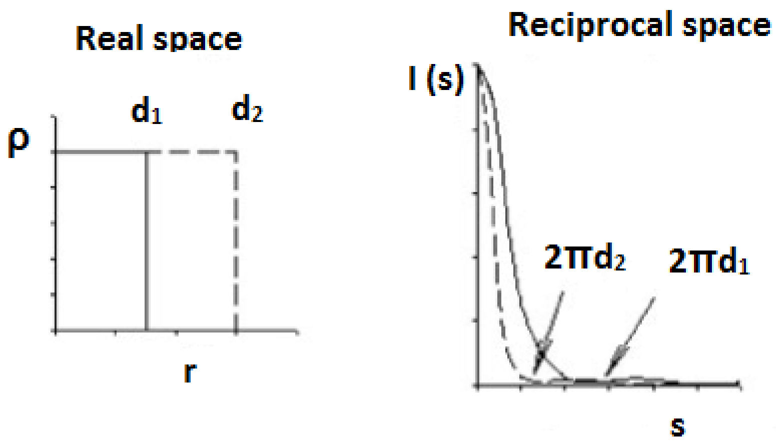

Figure 4.1.3: Fourier transformation from real space to reciprocal space (**Svergun et al., 2003**).

Dimension of q or s is one over length (1/nm) due to which the scattering pattern is called as the structure in *reciprocal space* whereas the particles are said to have a structure in *real space* because they can be measured in units of length (nm).

The intensity scattering profile obtained in reciprocal space is directly related to the real space particle with a resolution equivalent to 2π/s. In case of solution scattering, low resolution data can be obtained in the range of size of the object ≫ λ.

The magnitude of momentum transfer vector is defined as the path difference between the scattered and incident waves multiplied by 2π/λ. The magnitude of scattering vector, q is defined by the equation:

$$|q| = \frac{4\pi \sin\theta}{\lambda} \quad \text{.......................................} (2)$$

2θ is the scattering angle and λ is the wavelength of the incident X-ray beam. The term q is known as the magnitude of the momentum transfer vector. In the literature, sometimes scattering vector is also referred to as 's' where

$$s = \frac{2 \sin\theta}{\lambda} \text{ and } q = 2\pi s.$$

It is a non-destructive technique which provides information on shape and size of the scattering particle in solution. Various parameters which can be extracted from this method include Rg, I_0, Dmax, Porod volume and many more.

The scattering experiments are recorded at very small angles of scattering due to the resolution factor. For the characterization of particles of size in range of d (in nm), with x-ray source constituting rays of λ (usually 0.1 nm), the resolution which can be obtained for the scattering is given by:

$$\frac{2\pi}{d} = \frac{4\pi \sin\theta}{\lambda} \quad \ldots\ldots\ldots\ldots\ldots\ldots\ldots\ldots (3)$$

The data obtained from SAXS experiments can provide information on the molecular weight, shape, size, polydispersity and oligomeric state of a protein. The scattering profile can also be used to generate a 3D structural envelope of a protein. It is also used to decipher structural features of proteins that can't be easily crystallized. We can extract structural parameters such as radius of gyration (Rg) and maximum dimension (D_{max}) of molecules in solution. In a SAXS set up the particles sizes that can be resolved range from 1 to 100 nm by measuring scattering at smaller angles i.e., from 0.1° to 10° . We have used this non-destructive technique to compare the scattering intensities of monomer with that of HEWL aggregates incubated for different time periods in pH 12.2. Moreover, aggregates are amorphous in nature and cannot be crystallized. Hence, SAXS proves to be a valuable tool to study the structural parameters of these globular aggregates in solution.

R_g is defined as: ***Radius of Gyration:*** *Size of a biomolecule* R_g is the root mean square of distances between points in the particle and the centre of gravity of a biomolecule relative to its centre of mass. It is an indicator of how the mass of a particle is distributed around its centre of mass. It can be determined from Guinier fit for data at lowest scattering angles (low q region from scattering profile).Guinier formula is not applicable if the molecule aggregates resulting in interparticle scattering. R_g^2 is the average electron density weighted squared distance of the scatters from the centre of the object.

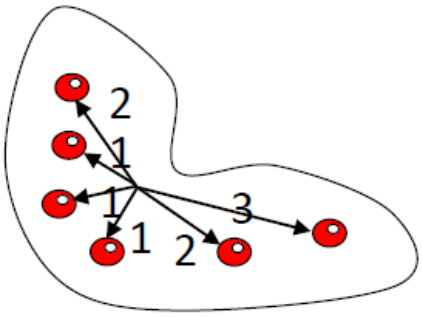

Figure 4.1.4: R_g as radius of gyration for a biomolecule.

4.1.1 Review of literature on SAXS studies of lysozyme

Szymańska et al. have reported SAXS results to show the aggregation and denaturation of hen egg white lysozyme in presence of ethanol. Significant changes in p (r) distribution function and R_g were observed. At low concentrations of ethanol, R_g was reported to be 1.48 nm which corresponds to that of a lysozyme monomer[3]. However, R_g jumped to more than 4 nm for ethanol concentration >80 % (v/v) which confirms substantial amount of lysozyme aggregation. Thus, aggregation of proteins can be detected by changes in SAXS intensity curves as well as by the increase in R_g of the macromolecules in solution. Similar studies on hen egg white lysozyme have been carried out by **Yonezawa et al**. SAXS was employed to study the amyloid fibrils of lysozyme formed in the presence of ethanol. In the pathway of amyloid formation of HEWL, different structural states have been detected and characterized in detail. The different states of HEWL such as monomer form, dimer state and protofilament state have been detected based on the changes observed in the R_g obtained from SAXS experiments[4].

The radius of gyration (R_g) for hen egg white lysozyme in aqueous solution i.e. in different D_2O/H_2O ratio has been reported by **Sangawa et al.** Small angle neutron scattering experiments were performed for lysozyme[5]. Structural parameter, R_{gc}, radius of the gyration of the particle at infinite contrast was estimated to be 13.5 Å. Time-resolved SAXS studies have also been carried out to characterize the different transition states of HEWL induced by thermal denaturation process[6].

The effects of conformational changes in HEWL at pH 5.0, by elevating the temperature were clearly seen in the scattering curves (**Hirai et al., 2000**). Temperature dependent tertiary structural changes were also reflected in p (r), distance distribution function, profile. Significant increase in R_g indicates an expansion in the structure of HEWL molecule caused by thermal denaturation. **Hoshino et al.** have studied the trifluoroethanol (TFE) induced conformational state of hen egg white lysozyme by SAXS[7]. The authors have reported a higher R_g value for TFE state which showed that it has an expanded structure than the native state. From the Guinier plots of scattering curves, R_g was determined to be 18 Å for the native state, 21 Å in TFE state, 23 Å in Gdn-HCL induced denatured state and 38 Å for the disulfide reduced state. The TFE state of lysozyme was shown to be an open helical structure but the presence of disulfide bonds restricts the motion of free chain and makes the structure compact.

SAXS has been used previously as a tool to investigate the structural details of lysozyme protein in H_2O and D_2O solutions by taking the hydration shell into account (**Svergun et al., 1998**). CRYSOL program has been developed to compare the experimental solution scattering curves with that of the obtained from crystallographic structure of the protein[8]. The R_g of lysozyme calculated from the atomic structure, 1.407 nm, correlates well with that of the experimental R_g value of 1.54 nm. Inclusion of the hydration shell resulted in better fit to the experimental data.

4.2 Materials and Methods

4.2.1 Experimental configuration

SAXS measurement were done in transmission geometry using Cu Kα radiation (wavelength λ = 0.154 nm) from a sealed X-ray tube (Source power – 50 Watt). Beam dimensions at sample position were 50 x 200 μm^2.The X-ray scattering data was recorded on a 2D Pilatus detector with a pixel size of 172 x 172 μm^2 at a sample detector distance of 300 mm. The range of momentum transfer (Q range) was 0.003 to 0.6 $Å^{-1}$. Exposure time was 3600s for each sample. Scattering curve for the buffer was also acquired for background subtraction under the same conditions as used for protein samples. Liquid samples were placed inside a thin capillary after washing and drying it under N_2 air. Syringe was used to pump the sample into the capillary tubes. For each experiment, 30 µl of sample was loaded. The scattered intensities were measured as a function of the scattering angle 2θ.

SAXS facility at CCMB (***S3-MICRO Point-Focus system, Hecus X-ray systems, GmbH***) was used for carrying out the experiments.

4.2.2 Sample preparation and data processing

One of the limiting factors in our study was concentration of the protein. In our case, for aggregation experiments we cannot go beyond 150 µM of protein concentration as it leads to precipitation of the sample above that concentration. As a result we had to compromise on the signal to noise ratio. At different time points of incubation of 120 µM and 150 µM samples in pH 12.2, aliquots were taken to obtain SAXS data. Even similar concentrations were used for HEWL monomer in order to have comparable experimental data. Extra caution was taken while loading the sample in sample chamber to avoid the formation of air bubbles. Raw SAXS data is obtained as images and these images are converted to intensity plots before analysis. 2D image data processing is done by using Fit2D program.

ATSAS package is used for data evaluation, buffer subtraction and analysis of the samples. PRIMUS software is used for 1D data processing. The buffer subtracted curves are plotted in primus. Scattering intensity is plotted against q (scattering vector). In SAXS experiments, q-range is the range of scattering angles. Before performing measurements for the sample, every time blank scattering pattern is recorded for only buffer.

In the present work, we have tried to address the question **a) Is it possible to extract information about structural parameters of HEWL protein aggregates, formed at alkaline pH 12.2, from scattering pattern of the protein in aqueous solution?** HEWL aggregates are amorphous in nature and cannot be crystallized. As scattering from amorphous substances yields a distribution of diffuse scattering intensity at small scattering angles and from the scattering pattern size and shape of molecules can be determined. Hence, SAXS is a useful technique to study the properties of such amorphous nanostructures in solution. Using SAXS, the solution structure of the HEWL monomer as well as aggregates was studied. The aggregates were incubated in 50 mM Sodium phosphate buffer, pH 12.2 at two different concentrations, 120 µM and 150 µM for different time points. SAXS was used to investigate time dependent aggregation of HEWL and detectable changes were observed in the overall size of aggregates. In addition, SAXS experiments were performed without the use of any fluorescent dye tagged to the protein. This also confirms that dansyl tag had no role in aggregation.

DATA processing - ATSAS program package is available online which can be accessed from https://www.embl-hamburg.de/biosaxs/software.html.

PRIMUS – It is a primary data processing tool for SAXS. It performs the manipulations with experimental data files such as: averaging, subtraction, merging, extrapolation to zero concentration and curve fitting and evaluates the integral parameters from Guinier and Porod plots such as radius of gyration (for globular, flat and rod-type particles), Porod's volume, zero intensity and molecular weight. Buffer subtraction in PRIMUS – The two .dat files corresponding to sample and buffer are used as input in the PRIMUS interface. After buffer subtraction, scattering curve is generated.

Guinier plot

Guinier plot is generated in PRIMUS using the data of buffer subtracted scattering curve. The data is fitted to the Guinier equation and it is checked that the residuals are minimized.

Rg is estimated from the optimum fit. Guinier plot doesn't work in case of polydisperse or aggregated samples. Hence, it is difficult to estimate Rg and I (0) from Guinier fit.

I (0) or forward scattering parameter is always theoretically computed, at a scattering angle of zero, rather than experimentally observed. I (0) is the zero angle intensity. I (0) is a parameter which enables us to determine the molecular mass of unknown sample with reference to I (0) of that of protein with known molecular mass. A higher value of I (0) in comparison to protein monomer indicates aggregation or oligomerization.

Fourier transformation of I (q) data to P (r) profiles is performed by GNOM.

4.3 Results and Discussion

4.3.1 SAXS intensity profiles

The average density of a protein molecule is of order ρ_p= **0.42 e$^-$/Å^3** while that of the water solvent is ρ_s= **0.33 e$^-$/Å ^{3}**, the scattered intensity is $(\rho_p - \rho_s)^2 / \rho_p^2$ which is only 5 % of the intensity that would be calculated for the molecule in vacuum. For this reason, the acquisition of SAXS data is subjected to signal-to-noise problems.

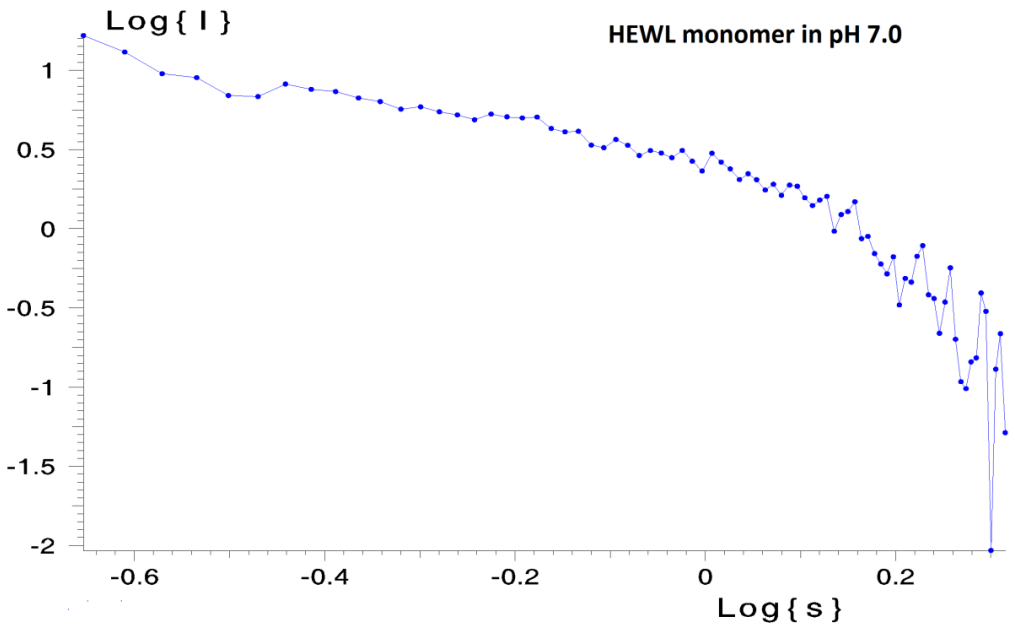

Figure 4.3.1: Concentration of HEWL used for SAXS measurements was 3 mg/ml in 50 mM sodium phosphate buffer pH 7.0. The plot is generated in SASPLOT available in PRIMUS. The intensity scattering curve is plotted with Log (I) as Y-axis vs. Log (s) as X-axis. Unit of s is in nm^{-1}. Intensity is arbitrary units.

The presence of aggregates in the sample gives rise to an upward curve in the scattering intensity plots at low q values. However, for a monodisperse sample the scattering curve becomes parallel across the full q-range (**Sawyer et al., 2013**).

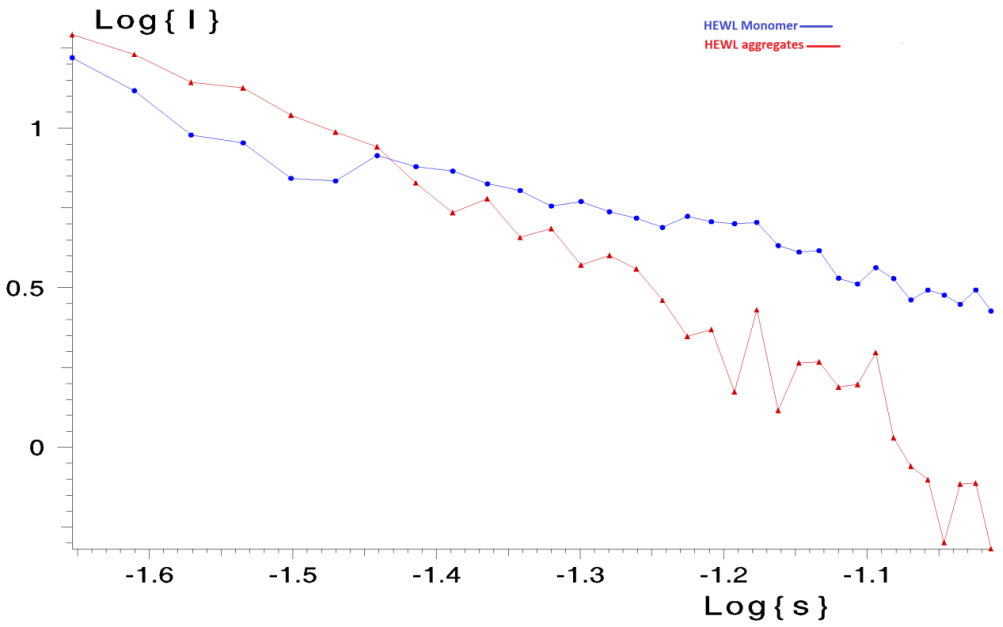

Figure 4.3.2: Units of s are in $Å^{-1}$. The plot is generated in SASPLOT from PRIMUS window. The intensity scattering curves are shown in low q (or s) region. This plot is displaying the difference between intensity scattering curves of HEWL monomer and aggregated sample.

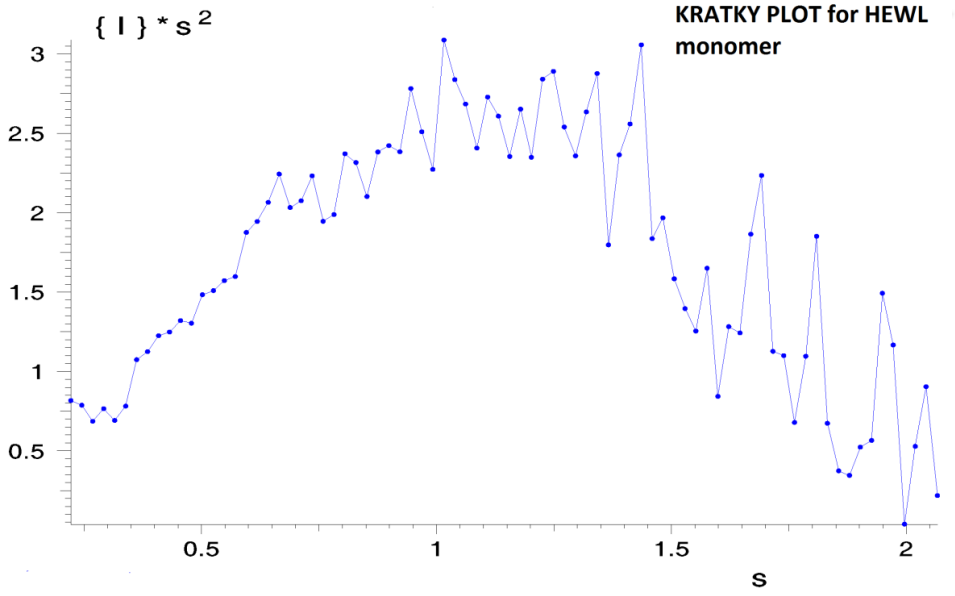

Figure 4.3.3: Kratky plot for HEWL monomer in pH 7.0 was generated in SASPLOT. Concentration of HEWL used was 3 mg/ml in 50 mM Sodium phosphate buffer pH 7.0. The plot is generated as $(I)*s^2$ on Y-axis vs. s on X-axis. Kratky plot reveals that the protein is in the folded form. This plot is an indicator of the folded/unfolded state of the protein. It is sensitive to the degree of compactness of a protein. This plot is generated to reveal the extent of flexibility and unfolding within the sample. Globular particles show as bell shaped curve in the Kratky plot.

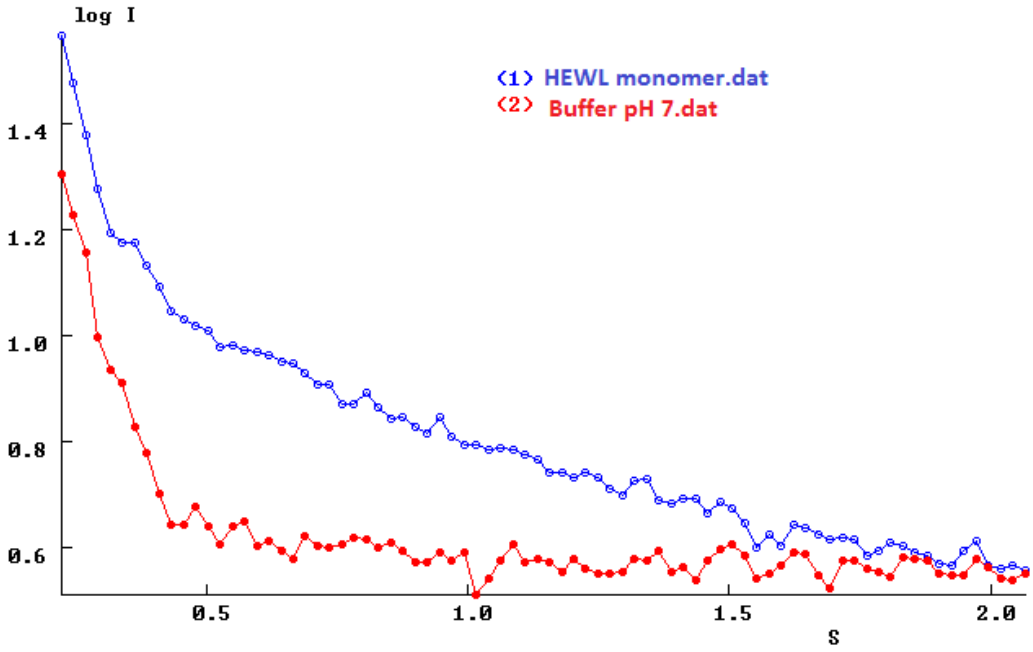

Figure 4.3.4: HEWL monomer (concentration = 3 mg/ml) in 50 mM Sodium phosphate buffer pH 7.0. Unit of s is in nm^{-1}. The plot is generated in PRIMUS with log I on Y-axis and s in X-axis.

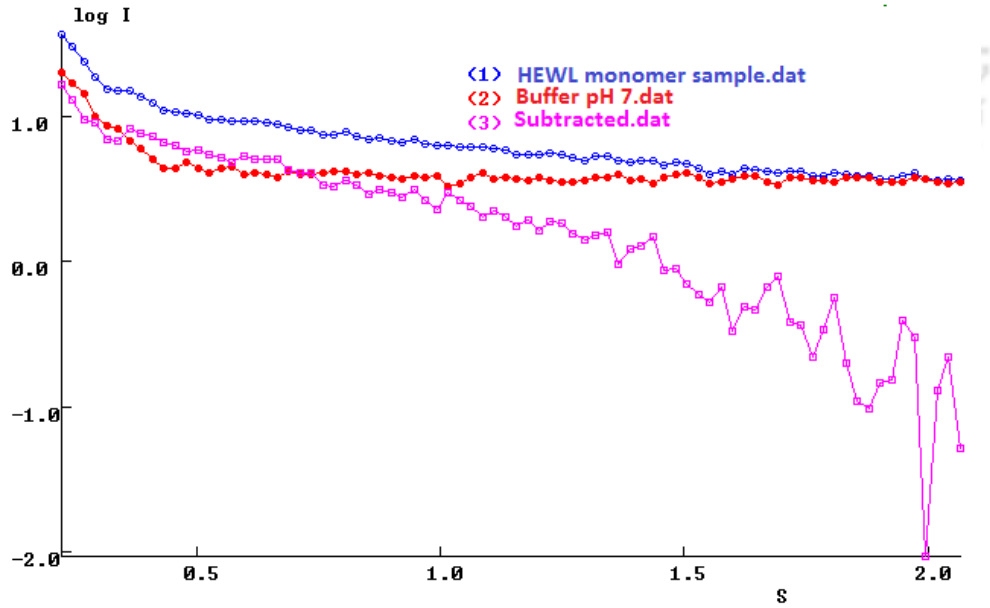

Figure 4.3.5: Combined scattering curve plots: 1) HEWL monomer (3 mg/ml) 2) 50 mM Sodium phosphate buffer pH 7.0 and 3) Subtracted (sample - buffer). Subtraction is performed in PRIMUS software. Unit of s is in nm^{-1}.

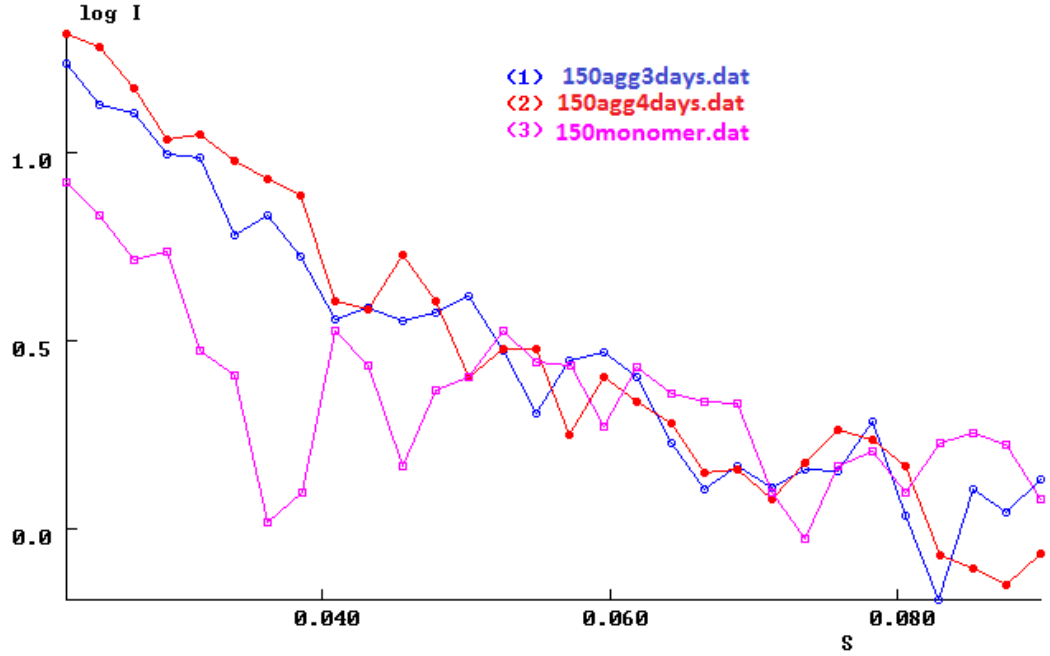

Figure 4.3.6: Combined scattering curve plots: 1) 150 µM HEWL aggregates (3days old) 2) 150 µM HEWL aggregates (4days old) and 3)150 µM HEWL monomer in pH 7.0 (freshly prepared). Subtraction of sample from the respective buffers was performed in PRIMUS software. Unit of s is in $Å^{-1}$.

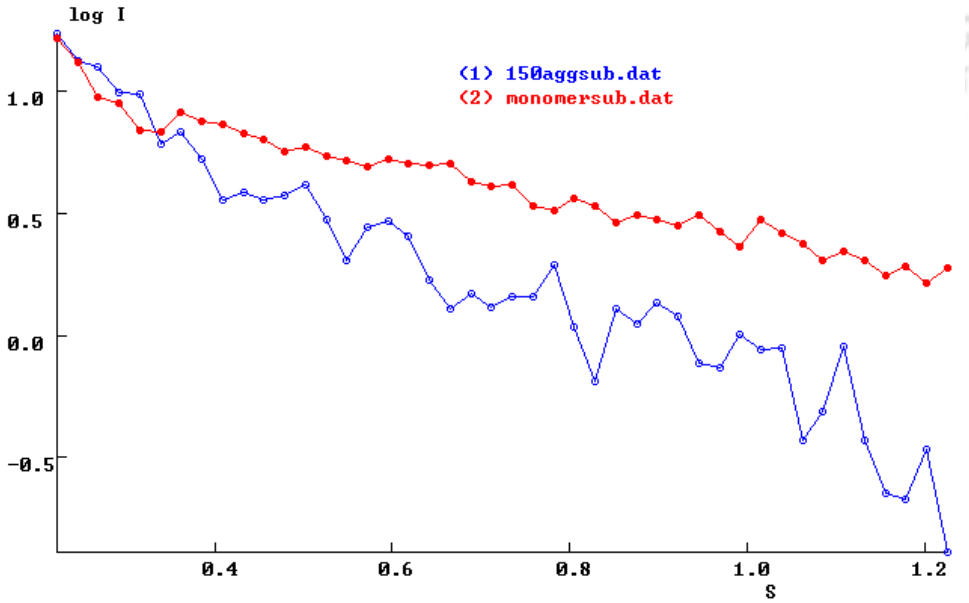

Figure 4.3.7: Intensity scattering curve for 1) 150 µM HEWL aggregates (3 days old) and 2) HEWL monomer (3 mg/ml). Unit of s is in nm^{-1}.

The experimental scattering curves show that I (q) in case of monomer falls slowly as compared to aggregates.

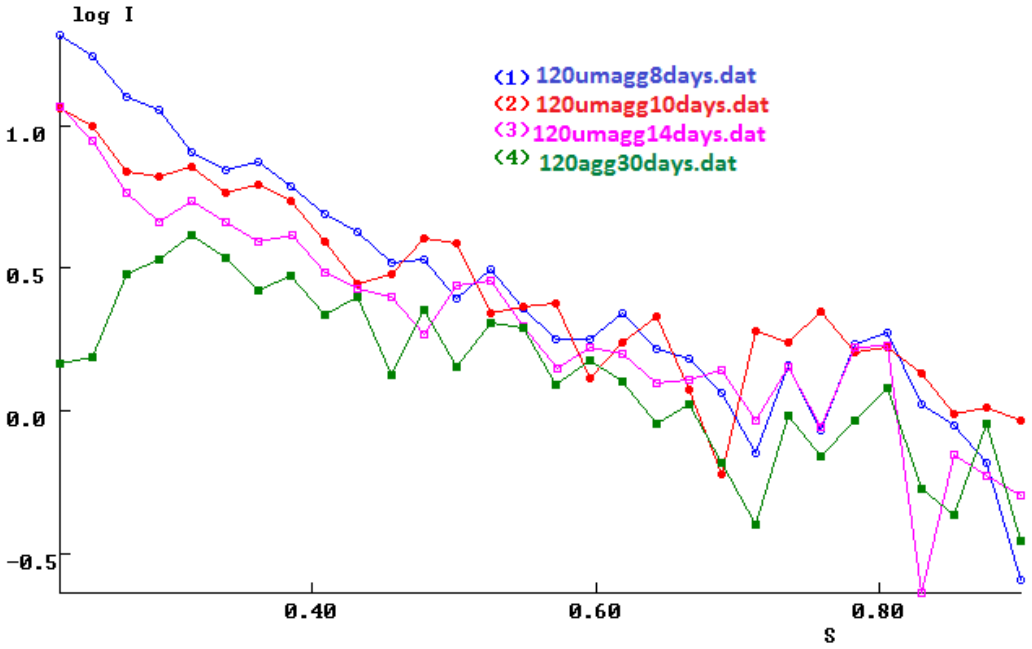

Figure 4.3.8: SAXS intensity curves for 120 µM HEWL aggregates incubated in pH 12.2 for different time periods. X-ray scattering pattern from a solution of 120 µM HEWL aggregates in pH 12.2.The curves are shown as a semi-logarithmic plot. Subtracted curve (sample-solvent scattering) represents the pure scattering from only protein.

Scattering intensity curve for 120 µM HEWL monomer couldn't be plotted as the scattering intensity was very low due to low concentration which resulted in noisy data. However, at the same concentration, aggregates displayed a higher intensity as compared to the monomer which confirms the aggregates as larger scattering bodies [**Figure 4.3.8**]. I (q) for 120 µM HEWL aggregates, 30 days old, showed a bend or decrease at very low q region which is due to interparticle interactions. Thus, a bend in the scattering curve at low q region, below q = 0.02 $Å^{-1}$ indicates the presence of repulsive interparticle interactions.

Scattering intensity, I (s) is usually a decaying function of momentum transfer vector. The solution scattering pattern provides crucial information about the overall shape and structure of biomolecules.

4.4 Distance distribution function P(r)

The P(r) function is an electron density function. This function is defined as histogram of equivalent pairwise atomic distances in a given sample[2]. The pairwise distance distribution function is always defined in real space. P(r) is also called pair- distance distribution function (PDDF) which is a histogram of distances found inside the particle. It is otherwise known as particle distance function or pairwise distance distribution function. The distribution function can otherwise be described as the probability of finding a pair of elements at a distance r within the volume of the scattering particle[9]. This function relates the scattered intensity to a physical characteristic of a molecule, P(r), a histogram of its electron-density-weighted intramolecular distances r. It is the length distribution function which measures the global conformation of molecules. Distance distribution function can be evaluated from Fourier transformation of the scattering curve.

The scattering intensity, I (q) is related to pair distribution function, P(r) by the equation:

$$P(r) = \frac{1}{2\pi^2} \int_0^\infty I(q).qr.\sin(qr).dq \quad \ldots\ldots\ldots\ldots\ldots\ldots (4)$$

Radius of gyration can be calculated from P(r) functions by Glatter's method:

$$(R_g)^2 = \frac{\int_0^{Dmax} r^2 p(r) dr}{2\int_0^{Dmax} p(r) dr} \quad \ldots\ldots\ldots\ldots\ldots\ldots\ldots\ldots\ldots\ldots (5)$$

R_g estimated from P (r) functions is more reliable as compared to R_g determined by Guinier's method. For a monodisperse system of particles, the distribution is known as distance distribution function, P(r) and volume distribution function, D(r) in case of polydisperse system. D_{max} is the maximum dimension of the protein.

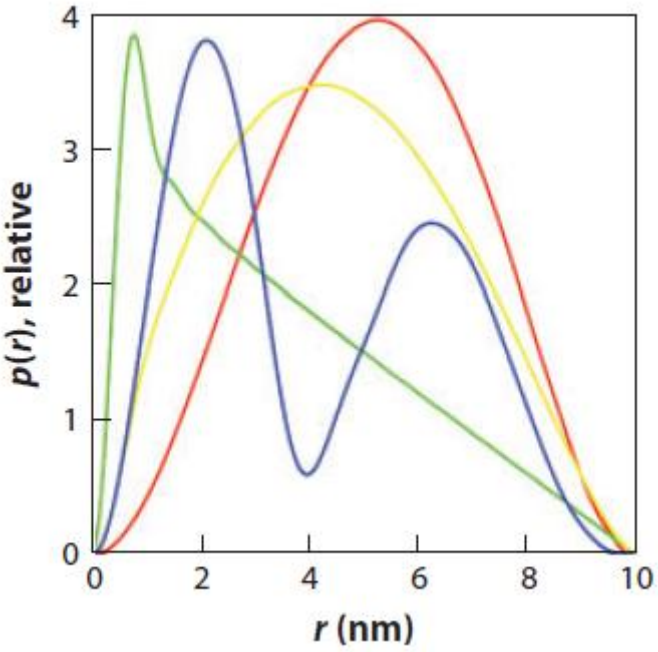

Figure 4.4.1: Pairwise distance distribution, P(r) function for differently shaped objects. The pairwise distances are represented for geometrical bodies: red (solid sphere), cylinder or long rod (green), flat disk (yellow) and dumbbell (blue)[10].

Pair distance distribution functions, P(r), are generated by using GNOM available from ATSAS. P(r) distribution function can be defined as the plot for probability of interatomic distances (r) within the particle. The shape of the P(r) function gives an idea about the shape of the particle. Highly symmetric P(r) distribution function indicates towards the symmetry of the particle.

P(r) functions for HEWL aggregates and monomer were calculated from GNOM, by indirect Fourier transformation of small angle scattering intensity data. Manual for GNOM program run can be accessed on website: https://www.embl-hamburg.de/biosaxs/manuals/gnom.html.

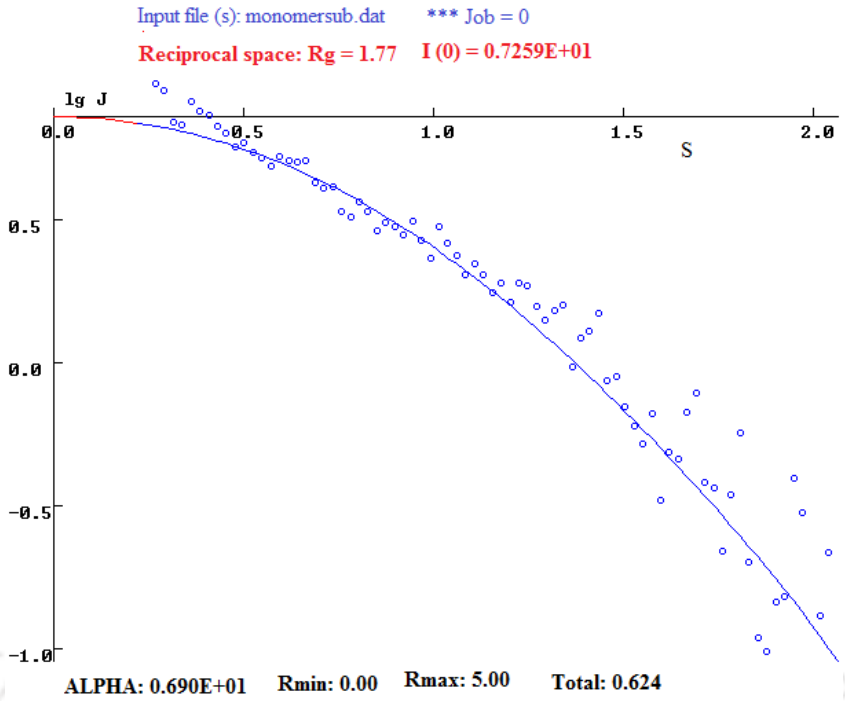

Figure 4.4.2 (a): Fit in reciprocal space. R_g value for **lysozyme monomer** obtained is equal to 1.77 nm. Solution with total estimate value of 0.624 was chosen i.e., a reasonable solution. I (0) value obtained in reciprocal space was 0.7259E+01. Real space range fall within the range of Rmin = 0 nm to Rmax = 5 nm.

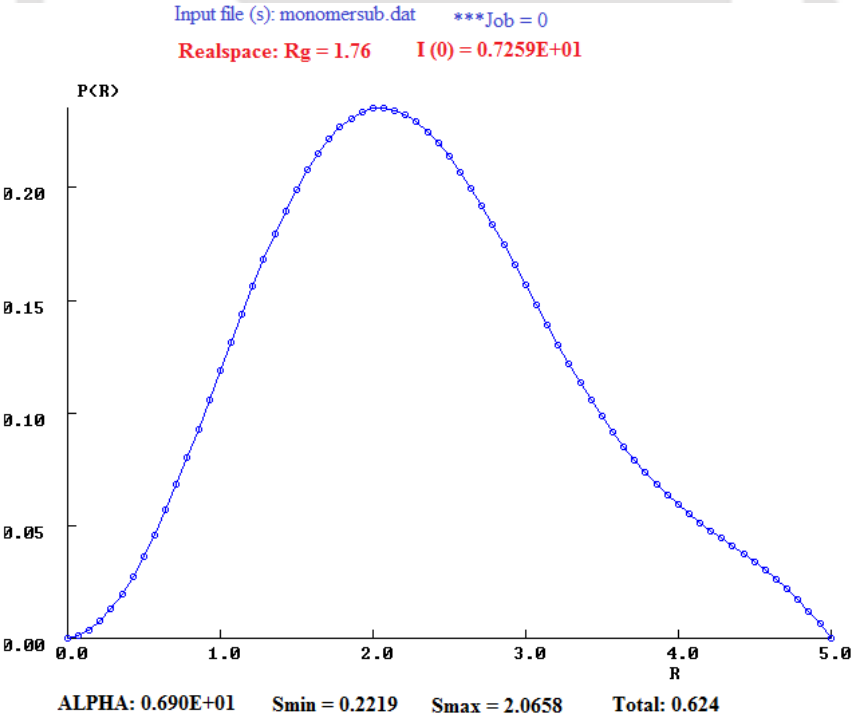

Figure 4.4.2 (b): Distance distribution function of **HEWL monomer** (3 mg/ml in 50 mM sodium phosphate buffer, pH 7.0). Unit of R (on X-axis) is in nm. **Job = 0** corresponds to the assumption that the system under study consists of monodisperse spherical particles. OSCILL value for monomer is equal to 1.193 which represents P(r) as a smooth monomodal function of sphere.

Job as 0 is the default job in GNOM run. It means P(r) function is evaluated for a monodisperse system. Job = 0 was selected for all the HEWL monomer samples in pH 7.0.

Job as 1 was given as input for HEWL aggregated samples in pH 12.2. Job =1 refers to polydisperse system of solid spheres. In case of polydisperse system, volume distribution function, D(R) is computed. Where D(R) = $\frac{4\pi}{3}$ *R^3 N(R) for solid spheres of radius R and N(R) is relative number of particles in the system.

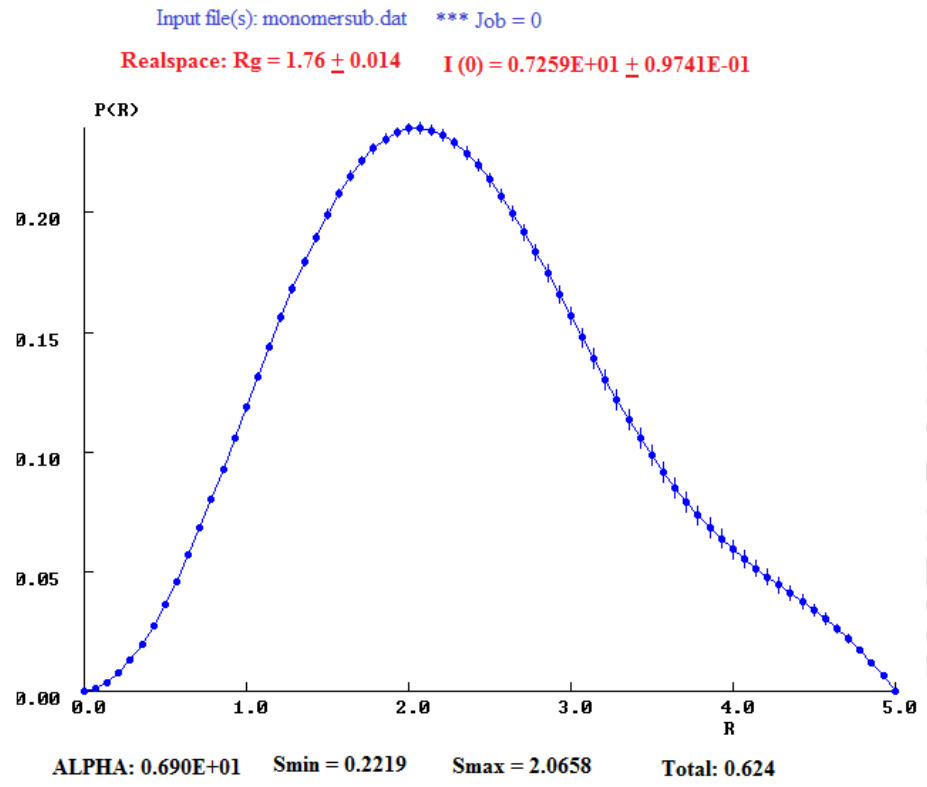

Figure 4.4.2 (c): Figure: P(r) distribution with errors. Angular range is from 0.2219 to 2.0658.The current alpha value is 0.690E+01.

The parameter total estimate tells about the quality of the solution. In the program GNOM, method of indirect transformation of the small angle scattering data is used. Experimental scattering intensity is related to distribution function in real space by integral transformation (**Svergun, 1992**). The relation is defined by the equation[11]:

$$I(q) = 4\pi \int_0^{\infty} p(r) \frac{\sin(qr)}{qr} . dr \quad \text{..... (6)}$$

Here, q is the scattering vector; P (r) is the distribution function in real space and r is the distance such that $D_{min} < r < D_{max}$.

Different values of Rmax for evaluating P(r) are given as input and the program is run with well-defined default parameters. The results are compared from different runs and the most acceptable solution is selected.

Criteria to select an optimal solution

In order to ensure that after GNOM run, the solution obtained is in acceptable range, visual inspection of the distribution in real and reciprocal space is done. Some mathematical parameters or criteria as described by **Svergun et al.** are used to select a particular solution for P(r) distribution function.

Alpha (α) is a critical nonnegative parameter for a specified (D_{max}, D_{min}) range. If the value of alpha obtained is equal to zero, then it results in an unstable solution. However, very high values of alpha indicates the deviation of reciprocal space experimental data from real space.

The **oscillations** (**OSCILL)** criterion obtained for the distribution is equal to 1.19, then it corresponds to the pair distribution function of a sphere. In addition, this value also indicates that the P(r) distribution is a smooth monomodal function. However, if the value of OSCILL is nearly equal to 2 then it represents either a bimodal or oscillating monomodal distribution.

Systematic deviations (SYSDEV) is a very important parameter which is defined in reciprocal space. This measures the deviations from the experimental data and in absence of any deviations; the value is close to 1.

Discrepancy (DISCRP) corresponds to match between residuals and experimental errors. The value should be lower than 1 for an optimal solution.

Stability (STABIL) describes the dependency of the solution on the value of alpha. The value should be << 1 for a correct solution.

Positivity (POSITIV) is a measure of non-negativity of P(r) distribution function.

TOTAL is the total estimate which describes the quality of the solution. The value for total estimate ranges between 0 (totally unacceptable) and 1 (ideal solution).

In case of GNOM program run, D_{max} or maximum dimension of the particle is defined by the user. GNOM was allowed to run for multiple times for a particular sample with multiple D_{max} values. Ultimately, the best solution among the multiple runs was selected by considering all the important criteria.

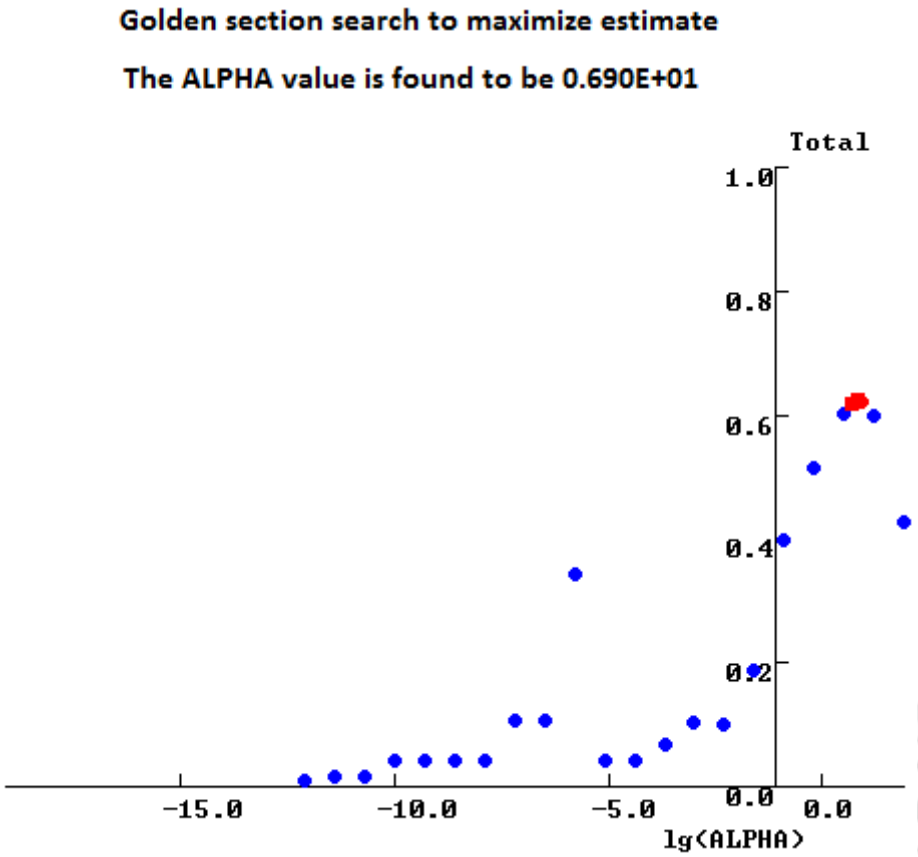

Figure 4.4.3: The value of total estimate is estimated by finding the best solution for the value of α. The search is done to maximize the total estimate.

Alpha is a regularization parameter which ensures the smoothness of P(r) function as well as goodness of fit. For polydisperse system, job = 1 was given as input. It is selected to describe the system as polydisperse solid spheres. I (0) or forward angle intensity is also computed from p(r) distribution functions. If the Total estimate value gives a suspicious solution or a bad solution, then that particular distribution is not accepted.

Here, P(r) distribution functions were computed from scattering curves for HEWL aggregates as well as monomer by GNOM with user defined D_{max}.

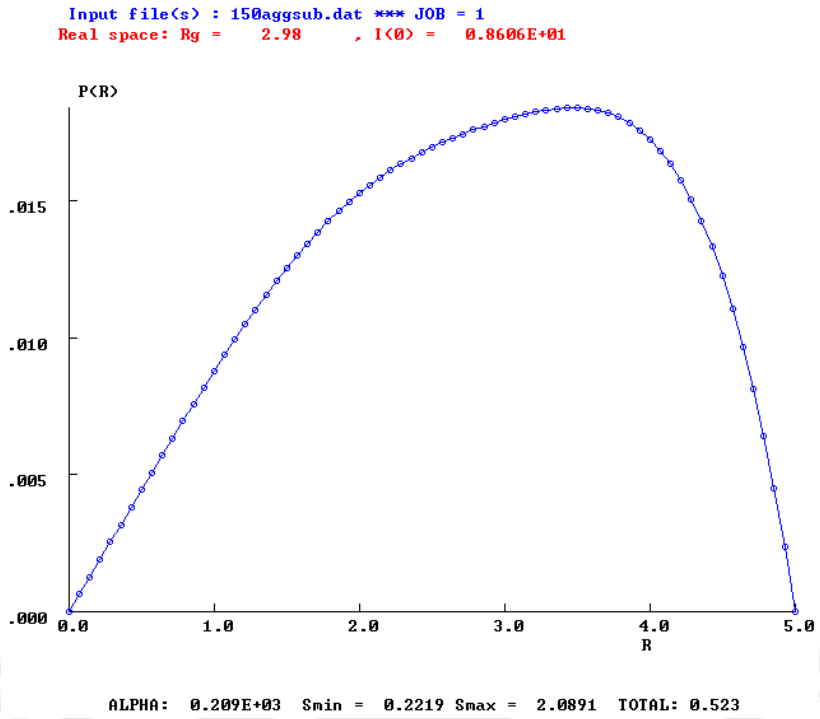

Figure 4.4.4 (a): Real space volume distribution of **150 µM aggregates** incubated in pH 12.2 for **3 days**. R_{max} = 5 was given as input parameter. The solution obtained has a total estimate of 0.523 which is a reasonable solution. R_g value in real space is 2.98 nm and I (0) = 8.606. In reciprocal space (not shown), R_g value obtained is 2.99 nm.

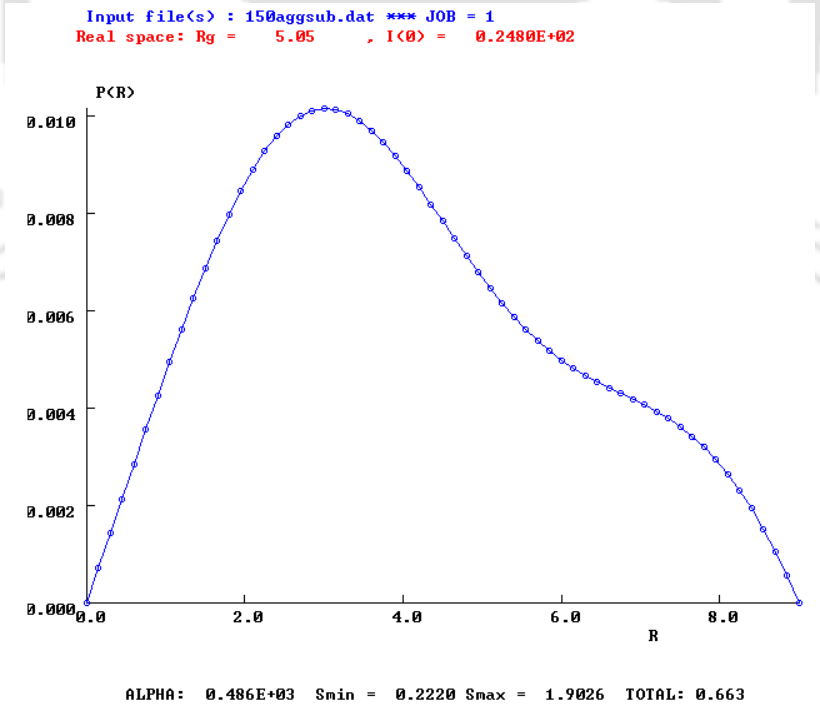

Figure 4.4.4 (b): Real space volume distribution of **150 µM aggregates** incubated in pH 12.2 for **4 days**. R_{max} = 9 was given as input parameter. The solution obtained has a total estimate of 0.663 which is a reasonable solution. R_g value in real space is 5.05 nm and I (0) = 24.80. In reciprocal space (not shown), R_g value obtained is 5.03 nm.

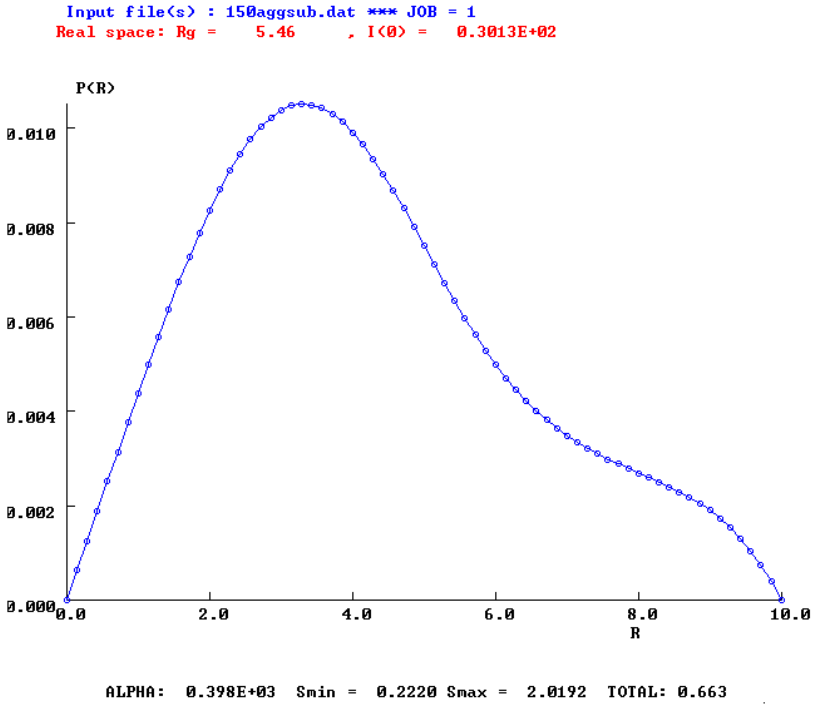

Figure 4.4.4 (c): Real space volume distribution of **150 µM aggregates** incubated in pH 12.2 for **8 days**. R_{max} = 10 was given as input parameter. The solution obtained has a total estimate of 0.663 which is a reasonable solution.

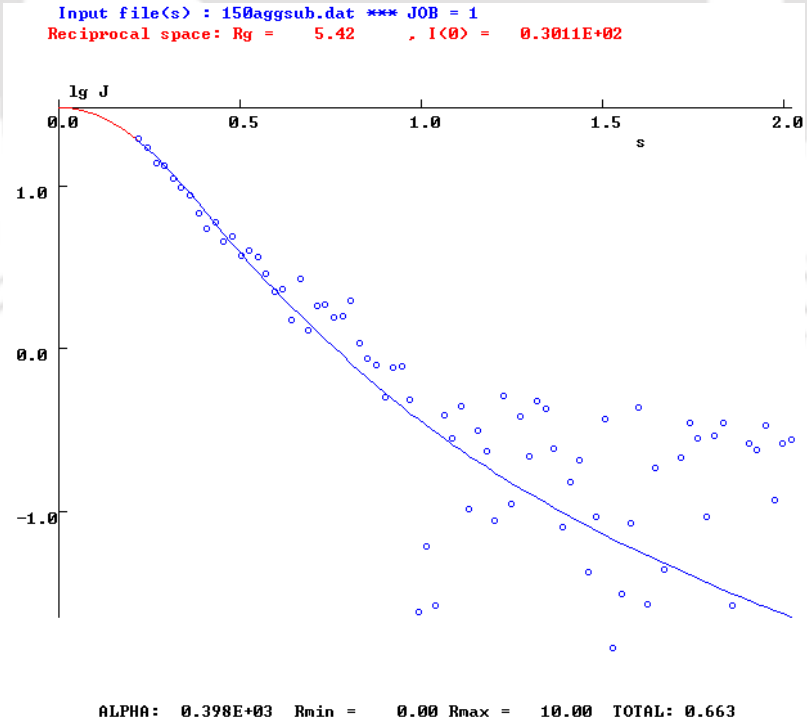

Figure 4.4.4 (d): Reciprocal space volume distribution of **150 µM aggregates** incubated in pH 12.2 for **8 days**. R_{max} = 10 was given as input parameter. The solution obtained has a total estimate of 0.663 which is a reasonable solution. Reciprocal R_g obtained was 5.42 nm and I (0) = 30.11.

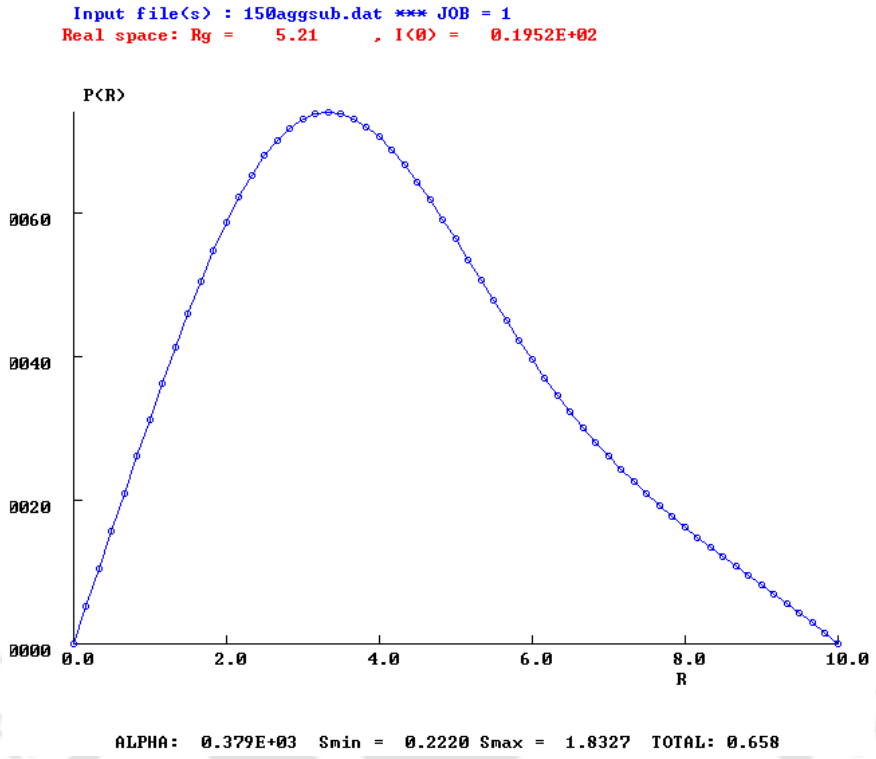

Figure 4.4.4 (e): Real space volume distribution of **150 µM aggregates** incubated in pH 12.2 for **30 days**. R_{max} = 10 was given as input parameter. The solution obtained has a total estimate of 0.658 which is a reasonable solution. R_g value in real space is 5.21 nm and I (0) = 19.52.

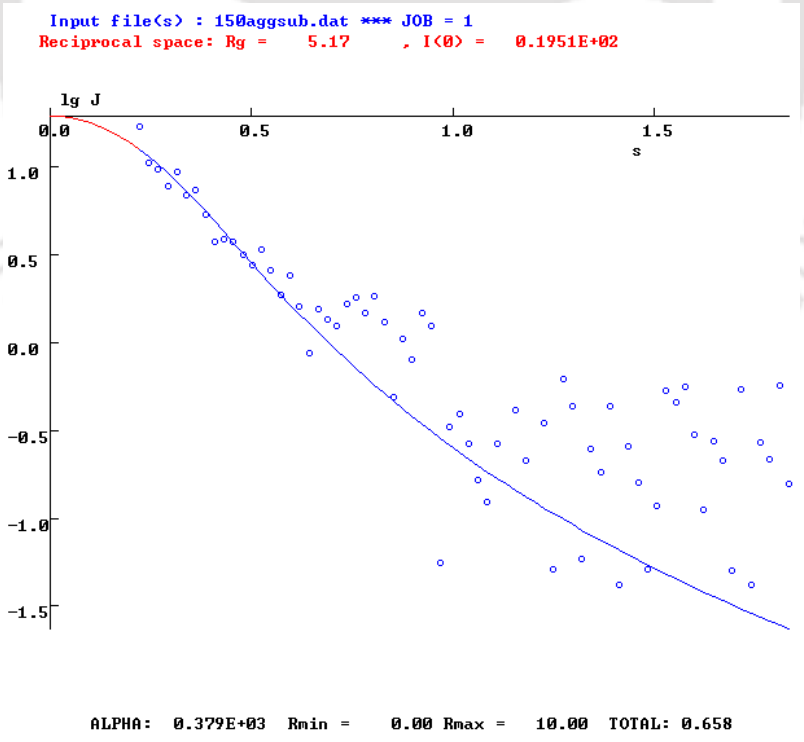

Figure 4.4.4 (f): Reciprocal space volume distribution of **150 µM aggregates** incubated in pH 12.2 for **30 days**. R_{max} = 10 was given as input parameter. The solution obtained has a total estimate of 0.658 which is a reasonable solution. Reciprocal R_g obtained was 5.17 nm and I (0) = 19.51.

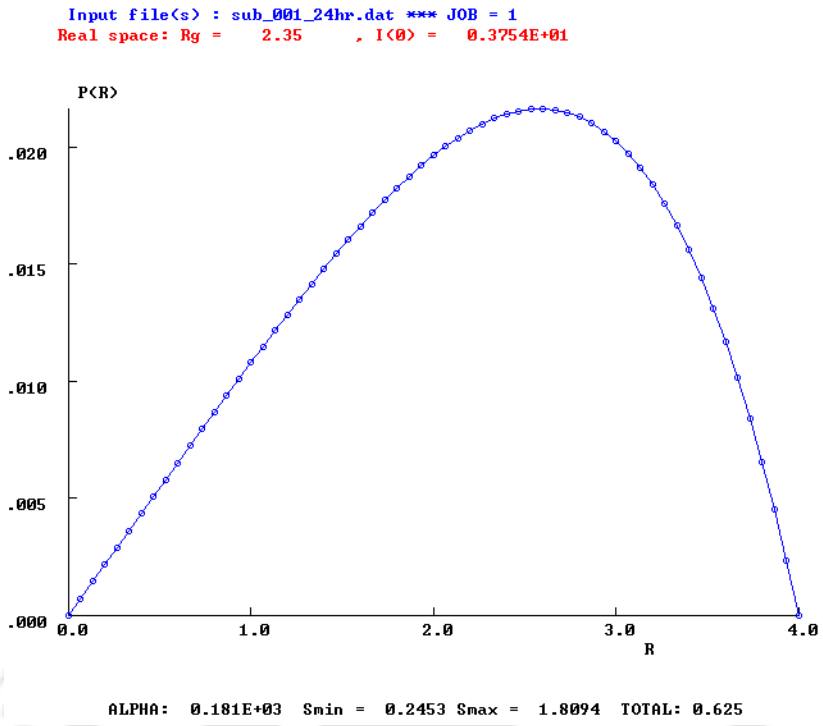

Figure 4.4.5 (a): Real space volume distribution of **120 µM aggregates** incubated in pH 12.2 for **24 hours**. R_{max} or maximum dimension of the particle = 4 was given as input parameter. The solution obtained has a total estimate of 0.625 which is a reasonable solution. R_g value in real space is 2.35 nm and I (0) = 3.754. In reciprocal space (not shown), R_g value obtained is 2.35 nm.

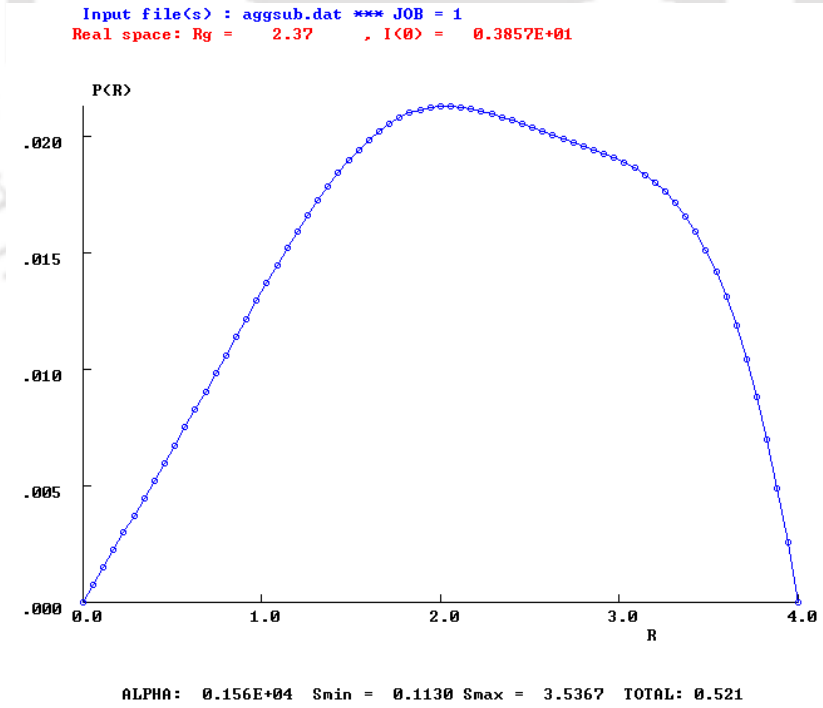

Figure 4.4.5 (b): Real space volume distribution of **120 µM aggregates** incubated in pH 12.2 for **5 days**. R_{max} or maximum dimension of the particle = 4 was given as input parameter. The solution obtained has a total estimate of 0.521 which is a reasonable solution. R_g value in real space is 2.37 nm and I (0) = 3.857. In reciprocal space (not shown), R_g value obtained is 2.37 nm.

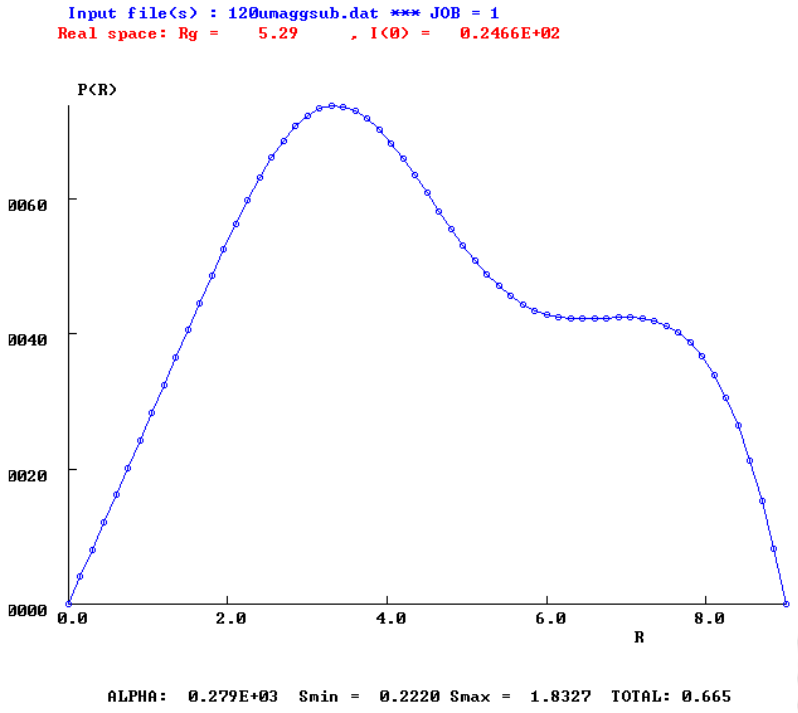

Figure 4.4.5 (c): Real space volume distribution of **120 µM aggregates** incubated in pH 12.2 for **8 days**. R_{max} = 9 was given as input parameter. The solution obtained has a total estimate of 0.665 which is a reasonable solution. R_g value in real space is 5.29 nm and I (0) = 24.66. In reciprocal space (not shown), R_g value obtained is 5.28 nm.

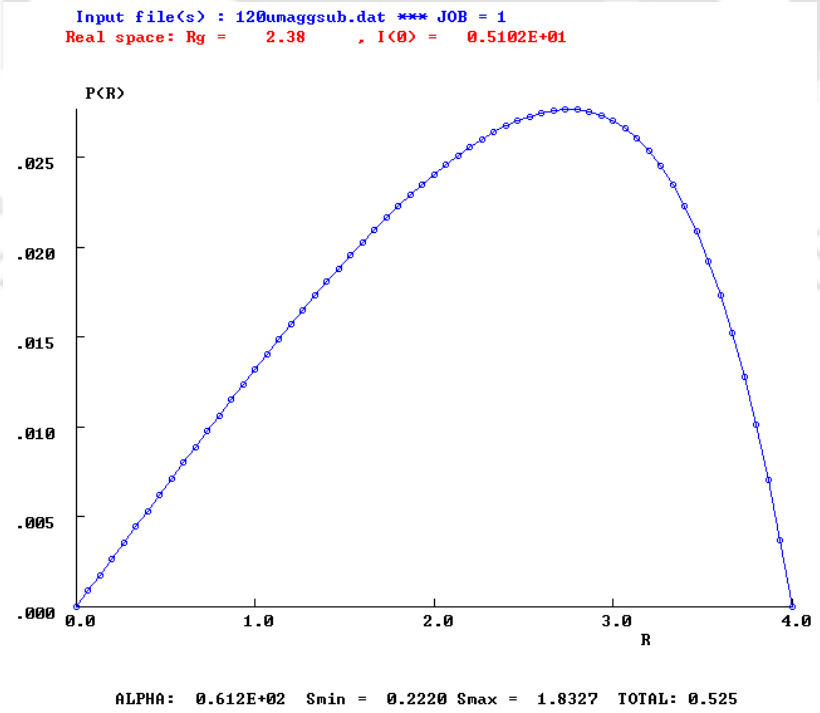

Figure 4.4.5 (d): Real space volume distribution of **120 µM aggregates** incubated in pH 12.2 for **10 days**. R_{max} or maximum dimension of the particle = 4 was given as input parameter. The solution obtained has a total estimate of 0.525 which is a reasonable solution. R_g value in real space is 2.38 nm and I (0) = 5.102. In reciprocal space (not shown), R_g value obtained is 2.39 nm.

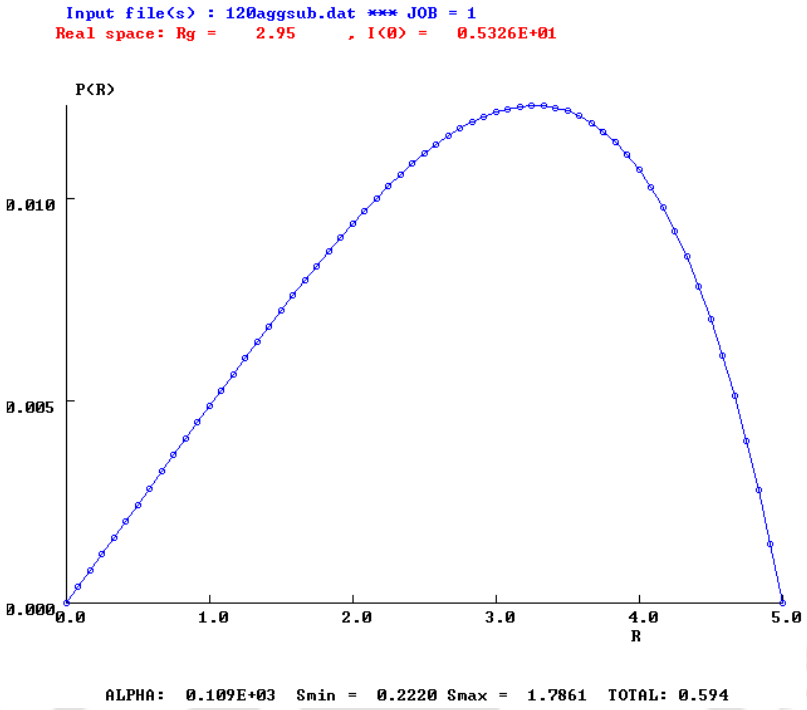

Figure 4.4.5 (e): Real space volume distribution of **120 µM aggregates** incubated in pH 12.2 for **14 days**. R_{max} or maximum dimension of the particle = 5 was given as input parameter. The solution obtained has a total estimate of 0.594 which is a reasonable solution. R_g value in real space is 2.95 nm and I (0) = 5.326. In reciprocal space (not shown), R_g value obtained is 2.96 nm.

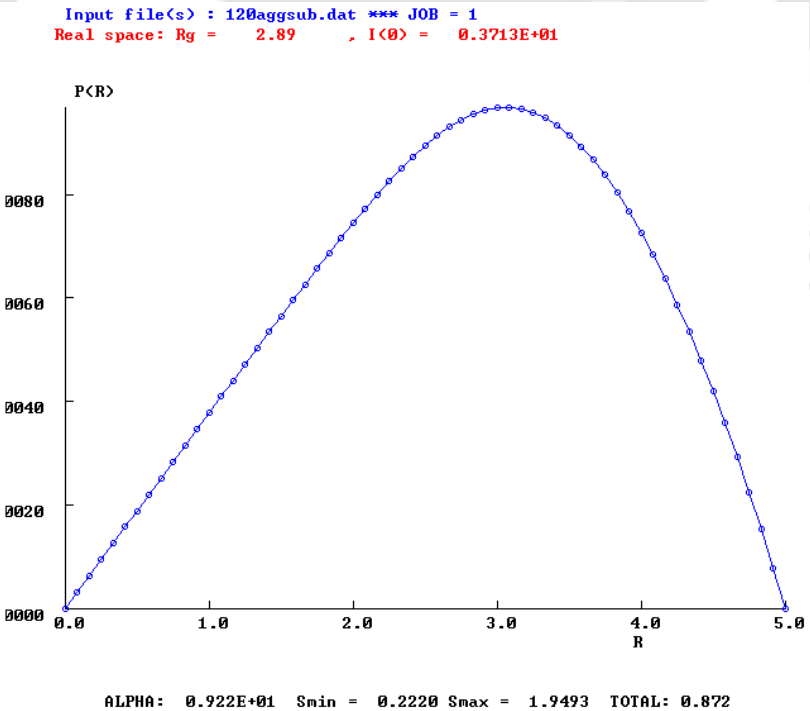

Figure 4.4.5 (f): Real space volume distribution of **120 µM aggregates** incubated in pH 12.2 for **30 days**. R_{max} = 5 was given as input parameter. The solution obtained has a total estimate of 0.872 which is a good solution. R_g value in real space is 2.89 nm and I (0) = 3.713. In reciprocal space (not shown), R_g value obtained is 2.9 nm.

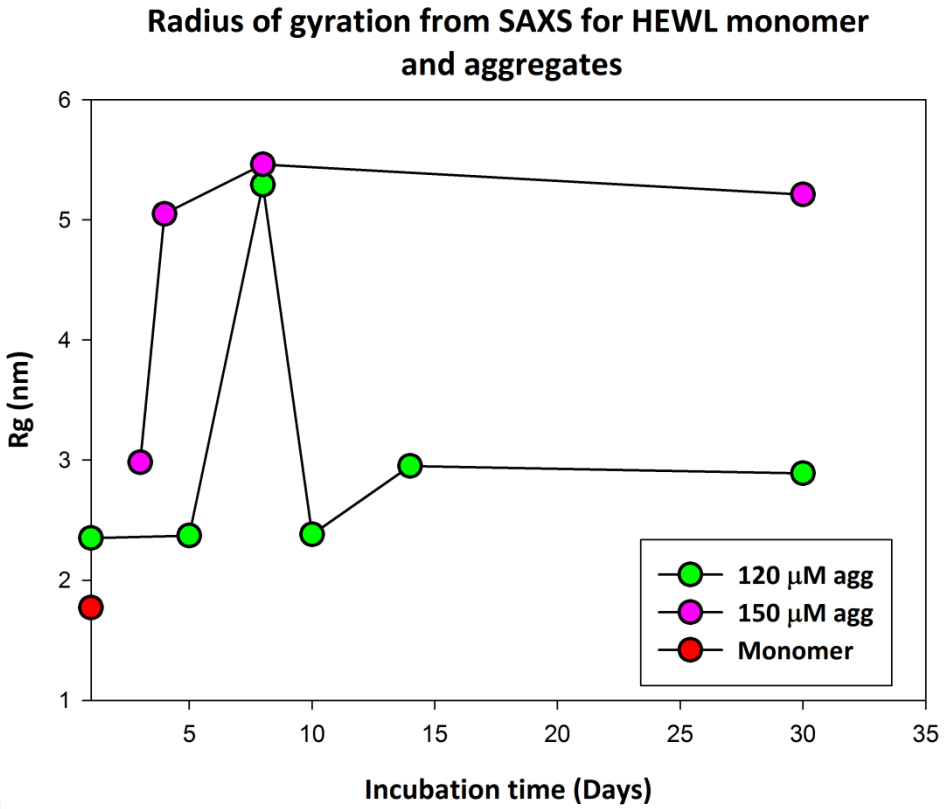

Figure 4.4.5 (g): Radius of gyration was obtained from P (r) distribution profiles of 1) 120 μM HEWL aggregates 2) 150 μM HEWL aggregates & 3) HEWL in native state (pH 7.0). For aggregates, samples were incubated in alkaline pH 12.2. HEWL monomer sample was freshly prepared in 50 mM sodium phosphate buffer, pH 7.0.

4.5 CRYSOL for HEWL monomer

CRYSOL is a program for evaluating the solution scattering from macromolecules with known atomic structure and fitting it to experimental scattering curves from Small-Angle X-ray Scattering. CRYSOL is used for fitting the SAXS data to atomic coordinates. Hydration shell around the protein is considered in CRYSOL. It is a program used to fit the experimental SAXS data to theoretical scattering curve obtained from existing atomic structure of the macromolecule. The theoretical SAXS profiles are computed from atomic coordinates[12]. SAXS experimental data is given as input, CRYSOL fits the theoretical scattering curve by minimizing the discrepancy (chi-square value).

SAXS profile is predicted from the crystal structures and as a result the crystal structures are validated in solution. Spherically averaged scattering pattern is computed from the known atomic structures of macromolecule by taking the hydration shell into account (**Svergun et al., 1995**).

The experimental scattering curve is fitted with the predicted solution scattering curve from atomic coordinates of crystallographic structure available in PDB bank. This comparison reveals the structural similarity between crystal form of protein and its solution state.

SAXS intensity for particles in solution is directly related to the average scattering by a single particle and the equation governing this is:

$$I(s) = \langle |A(s)|^2 \rangle_\Omega = \langle |A_a(s) - \rho_0 A_c(s) + \delta\rho A_b(s)|^2 \rangle_\Omega \quad \ldots\ldots\ldots\ldots [1]$$

$A_a(s)$ = Atomic scattering amplitude of particle in vacuum (*in vacuo*)

$A_c(s)$ = Scattering amplitude from the excluded volume (volume occupied by the biomolecule in solution that is inaccessible to the solvent)

$A_b(s)$ = Scattering amplitude from the border layer (hydration layer)

$\langle \quad \rangle_\Omega$ represents the average over all orientations and Ω is the solid angle in reciprocal space.

$\delta\rho$ is given by the difference of ρ_b and ρ_0 $(\rho_b - \rho_0)$. ρ_0 is defined as the average scattering density of the solvent surrounding the macromolecule. ρ_b is the density of hydration shell or border layer.

Scattering intensity is equal to the absolute square of the amplitude. Three different amplitudes are used as parameters while calculating the SAXS profile. One is atomic scattering amplitude in vacuum; second is scattering amplitude from the excluded volume of the solvent and the third is scattering amplitude of the hydration shell.

The mathematical approach used to calculate scattering intensity from atomic models is spherical harmonic approximation as provided by the program CRYSOL (**Svergun et al., 1995**).

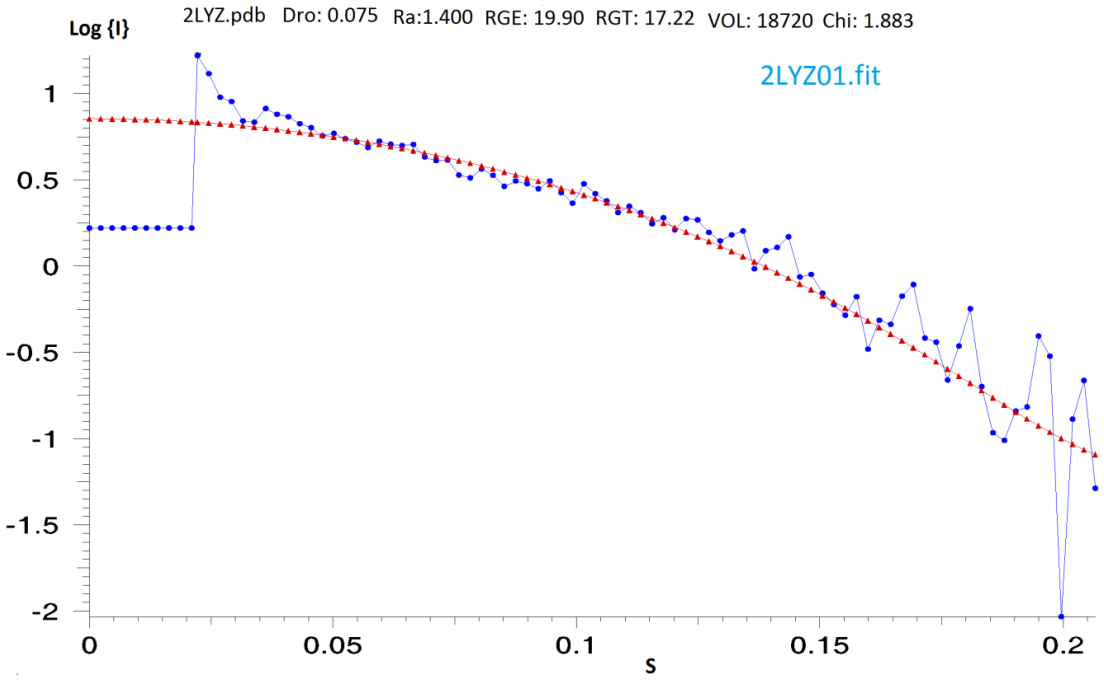

Figure 4.5.1: Experimental curve for HEWL monomer and fitting with theoretical curve from HEWL PDB file (2LYZ.pdb) generated in SASPLOT. **Dro:** Optimal contrast of hydration shell, **Ra:** Optimal radius of atomic group, **RGE:** Radius of gyration estimated from experimental curve (in Å), **RGT:** Radius of gyration estimated from theoretical curve (in Å), **Vol:** Optimal excluded volume and **Chi:** Discrepancy between theoretical and experimental curves

4.5.1 CRYSOL program run

PDB data file for lysozyme with PDB Id 2LYZ.pdb was given as input and the atomic coordinates were read from the input file. Experimental SAXS intensity scattering file (monomer.dat) in .dat format was provided as input for experimental data. The .dat file is the subtracted scattering profile (sample-buffer) for HEWL (3mg/ml) in 50 mM sodium phosphate buffer pH 7.0 as extracted from the SAXS experiment. Reciprocal space grid was tabulated in terms of a range of momentum transfer ($s = 4*\pi*\sin\theta/\lambda$) and units for the same were in 1/Å.

Parameters were computed from the PDB file: 2LYZ.pdb such as: Average atomic radius of atomic groups and atoms for HEWL calculated was 1.607 Å and Displaced solvent volume per atomic group was identified as 0.1741E+05 ($Å^3$). The different scattering amplitudes and envelope function were evaluated. SAXS intensity was calculated for theoretical curve using the parameter ρ_0 as electron density of the solvent equal to 0.334 e/$Å^3$ (number of electrons per unit volume). Certain fitting parameters were adjusted so as to fit the experimental curve.

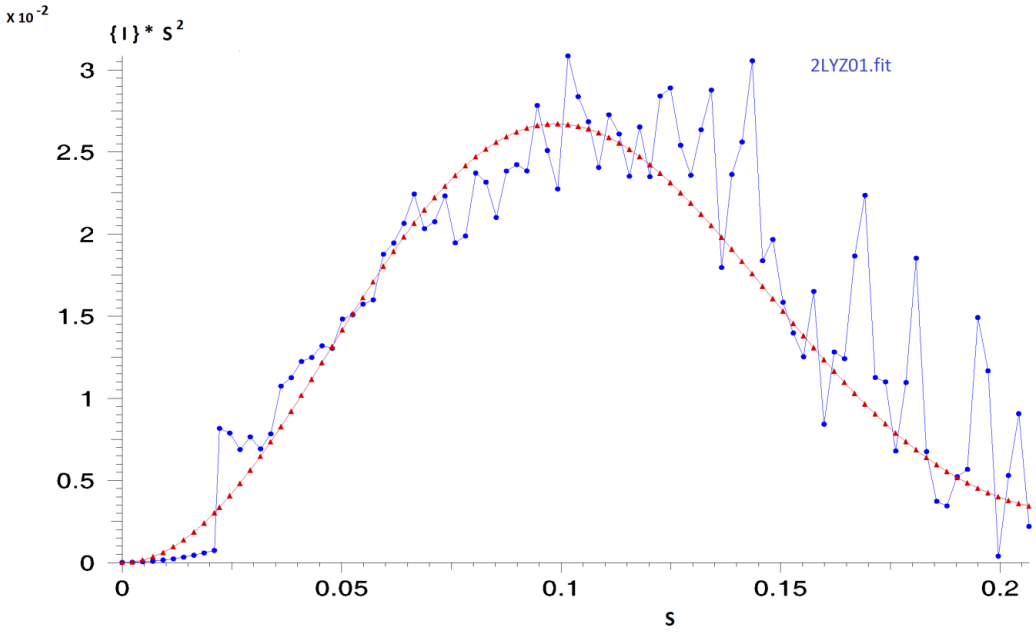

Figure 4.5.2: Kratky plot which is the plot of I (s^2) vs. s tells about folded and unfolded states of the macromolecule.

Experimental radius of gyration for HEWL monomer was found to be 19.90 ± 0.29 Å. Rg computed for theoretical curve was 17.22 Å. The best fit to the experimental data was obtained at Chi value equal to 1.883 corresponding to hydration of 0.593 g g^{-1}(grams of water per gram of protein).

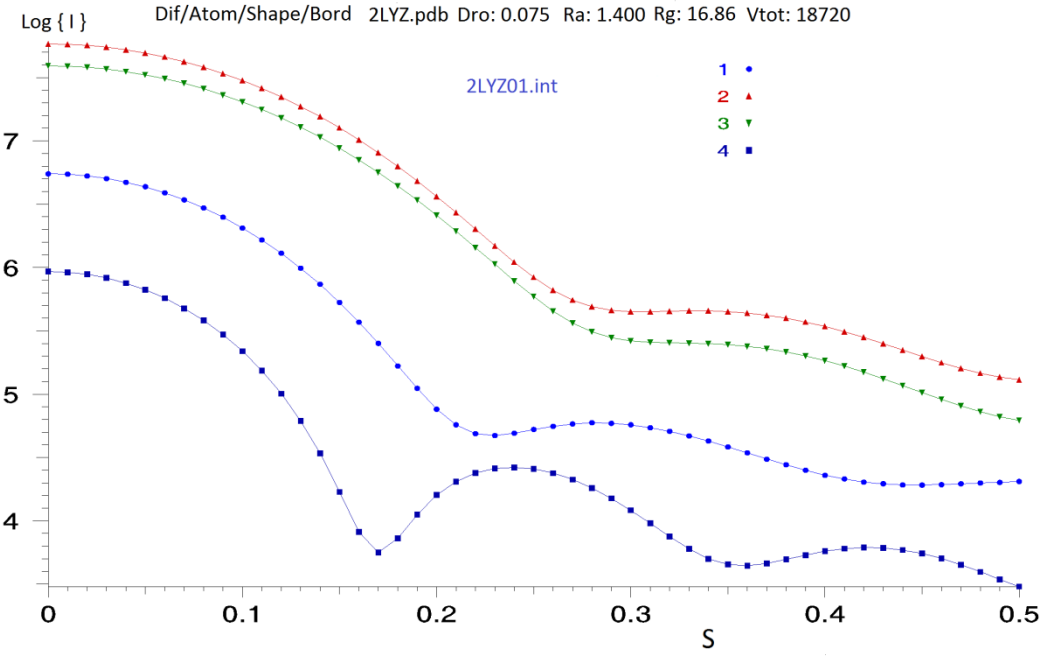

Figure 4.5.3: The figure represents scattering intensity profiles from the atomic structure of lysozyme as: 1) Difference 2) scattering from Atomic structure in vacuum 3) Shape scattering and 4) Border layer scattering.

Dro is a parameter which defines the contrast of the hydration shell. It represents the difference in electron density between free and bound water molecules. SAXS intensity profile is dependent on this parameter. It has been observed previously that consideration of hydration shell improves the fit to the experimental data. Hence, CRYSOL program includes the hydration shell while computing the SAXS profile. The hydration shell surrounding a macromolecule has a different e^- density than the bulk solvent. Contribution from the hydration shell to x-ray scattering is incorporated in CRYSOL.

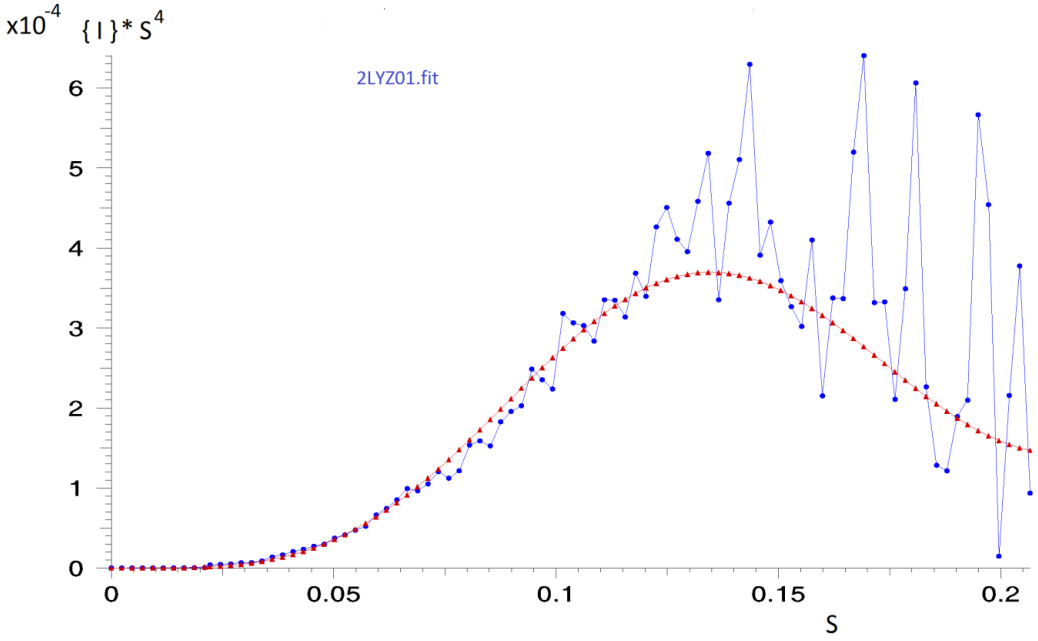

Figure 4.5.4: Porod plot is a plot between I (s)*s^4 vs. s. This graph is generated in SASPLOT.

Experimental radius of gyration (RGE) for HEWL obtained is 19.90 Å and the theoretical value (RGT) obtained is 17.20 Å. Radius of gyration calculated from atomic structure (Atoms- excluded volume + hydration shell) generated a value of Rg as 16.21 Å.

Experimental SAXS data was fit to PDB model of the protein which was given as an input. Some of the default input parameters were used while running the program. The output of CRYSOL run consists of different output files such as intensities, net amplitudes, envelope function and data fit to the experimental SAXS profile. The files are saved in .int, .alm, .flm and .fit formats respectively.

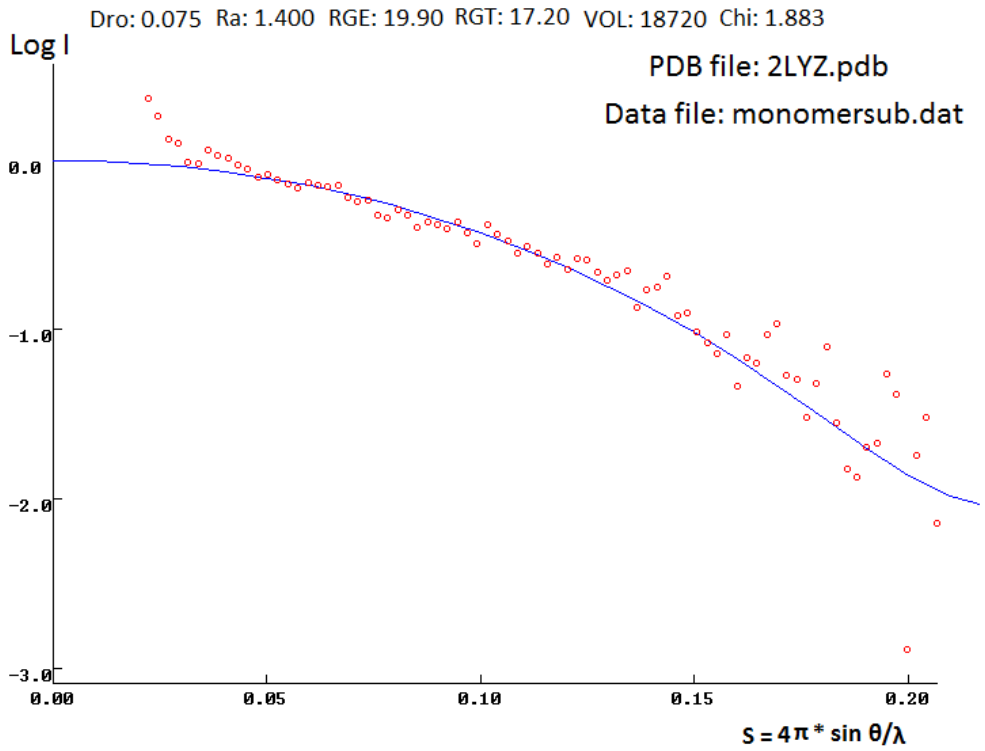

Figure 4.5.5: The Experimental solution scattering of protein solution of HEWL (3 mg/ml) in Sodium phosphate buffer pH 7.0 was measured. The graphical plot displays the fit between the experimental solution scattering of HEWL and the best fit predicted by CRYSOL. Experimental curve for HEWL monomer and fitting with theoretical curve from HEWL PDB file (2LYZ.pdb)

4.5.2 Lysozyme envelope generated in MASSHA

Visualisation of low resolution models such as smooth envelopes of the protein is one of the main features of the program. Three dimensional model of the envelope can be displayed as well as manipulated for better visual representation (**Konarev et al., 2001**). The files containing information about angular envelope function, ***.flm**, are generated by the program CRYSOL. Subsequently, ***.flm** files are transformed into surface representation ***.sld** format files by inbuilt program FLM2SLD in MASSHA[13]. The particle surface envelopes can be displayed in form of shaded surfaces or wire frames.

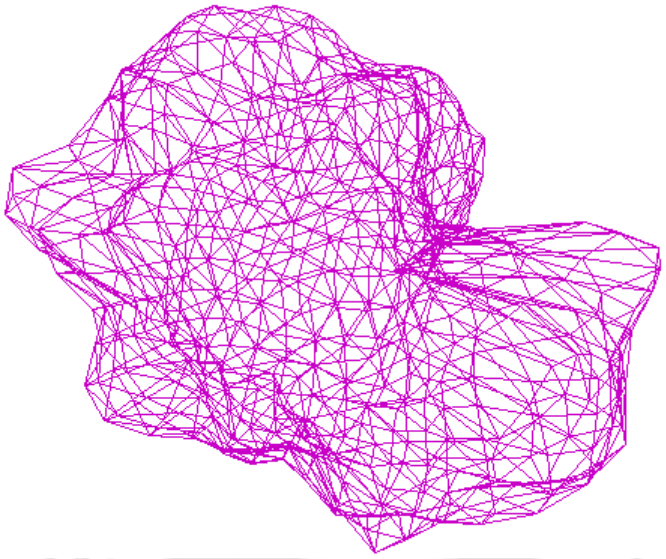

[A]

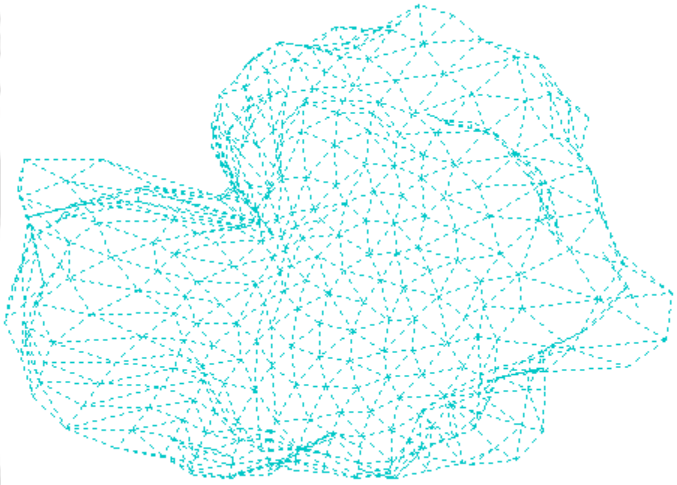

[B]

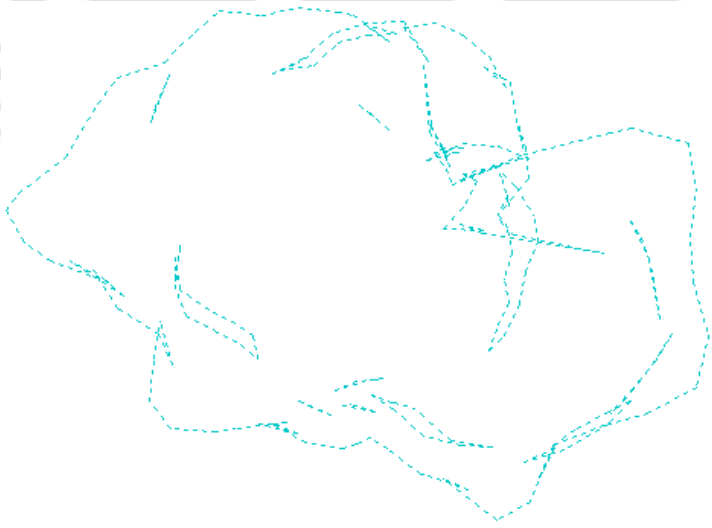

[C]

Figure 4.5.6: Surface representation of the protein envelope of HEWL monomer displayed in MASSHA.

GUINIER PLOT

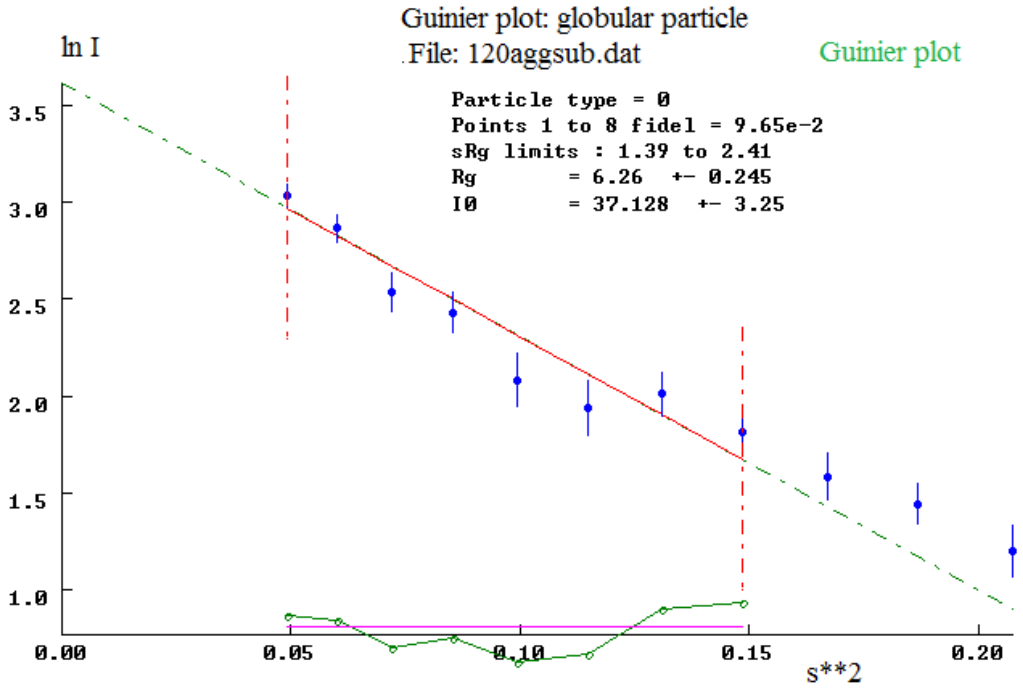

Figure 4.5.7: The graph displays the Guinier plot for 120 µM HEWL aggregates in pH 12.2. The graph is plotted with ln I on Y-axis vs. s^2. Unit of s^2 is in nm^{-2}.

Linearity of the Guinier plot indicates ideal monodisperse system. Intercept yields the parameter I (0) and R_g is calculated from the slope. However, it can be observed from the aggregated samples that deviation from the linearity indicates polydispersity of the sample as well as interparticle interactions.

4.6 Conclusion

Here we have studied the protein HEWL in its native state and in aggregated state by using the SAXS technique. As HEWL aggregates are polydisperse, a different approach was used to compute R_g. For aggregates, change in size and shape as well as maximum dimension of the particle was observed. Aggregates displayed a higher scattering intensity, I (0) as compared to HEWL monomer. However, concentration of protein was a limiting factor for us due to which the quality of the data was not the best.

Experimental SAXS profiles were obtained for HEWL aggregates in pH 12.2 for two different concentrations (120 µM & 150 µM). The intensity scattering profile for HEWL monomer at this low concentration resulted in a noisy data as the scattering intensity was very low as compared to aggregates of similar concentration. Shapes of the scattering bodies

were computed using GNOM program. CRYSOL program has been employed to compute SAXS intensity scattering profiles from atomic coordinates.

- HEWL in native state has a substantially different pair distribution function than the aggregated samples in pH 12.2. Difference in R_g values in both the cases reflects the difference in dimensions and shape of the protein under two different conditions.

- Increase in the maximum dimension of protein and gyration radius from SAXS indicates the loss of globular native structure. Modifications or changes in the protein conformation were followed from P(r) distribution functions. Changes in shape of the P(r) distribution plots for HEWL aggregates revealed the changes in shape of the aggregates in solution.

- P(r) distribution for monomer represents homogeneous spheres as estimated from SAXS data.

- Increase in forward scattering, I ($q \rightarrow 0$) in case of aggregates was observed due to difference in volumes of monomer and aggregates.

- R_g (Radius of gyration) estimated from SAXS data for monomeric HEWL yields a value of 1.77 nm close to the R_g values as reported in literature.
- Polydispersity for the aggregates was detected from Guinier plot. Instead of a straight line as seen in case of monodisperse solutions, a nonlinear decrease in low q region occurs for polydisperse systems. Thus, a nonlinear shape of Guinier plot indicates the presence of aggregates.
- The radius of gyration jumped to 2.35 nm for 120 µM HEWL aggregates (24 hour old) obtained from P(r) distribution plots.

- A significant increase was observed in radius of gyration for 150 µM HEWL aggregates (30 day old) i.e., R_g = 5.21 nm indicating the formation of bigger aggregates as compared to 120 µM aggregates (R_g = 2.89 nm).

- Scattering due to larger aggregates in case of 150 µM HEWL (pH 12.2) is reflected in the SAXS curve and also in the corresponding P(R) functions.

- Kratky plot for HEWL monomer confirms that the protein is in folded form.

References

1. Svergun, D. I. & Koch, M. H. J. Small-angle scattering studies of biological macromolecules in solution. *Reports Prog. Phys.* **66,** 1735–1782 (2003).

2. Putnam, D. K., Lowe, E. W. & Meiler, J. Reconstruction of SAXS Profiles from Protein Structures. *Comput. Struct. Biotechnol. J.* **8,** 1–12 (2013).

3. Szymańska, A., Hornowski, T., Kozak, M. & Ślósarek, G. The SAXS and rheological studies of HEWL amyloid formation. *Acta Phys. Pol. A* **114,** 447–454 (2008).

4. Yonezawa, Y. *et al.* An insight into the pathway of the amyloid fibril formation of hen egg white lysozyme obtained from a small-angle X-ray and neutron scattering study. *J. Mol. Biol.* **323,** 237–251 (2002).

5. Sangawa, U. & Niimura, N. Small-angle thermal neutron scattering lysozyme in aqueous solution. *Phys. B* **181,** 756–758 (1992).

6. Hirai, M., Arai, S. & Iwase, H. Concentration dependence of thermal structural transition of hen egg-white lysozyme under constant heating rate studied by time-resolved SAXS. *Thermochim. Acta* **344,** 95–102 (2000).

7. Hoshino, M., Hagihara, Y., Hamada, D., Kataoka, M. & Goto, Y. Trifluoroethanol-induced conformational transition of hen egg-white lysozyme studied by small-angle X-ray scattering. *FEBS Lett.* **416,** 72–76 (1997).

8. Svergun, D. I. *et al.* Protein hydration in solution: experimental observation by x-ray and neutron scattering. *Proc. Natl. Acad. Sci. U. S. A.* **95,** 2267–2272 (1998).

9. Campana, P. T., Barbosa, L. R. S. & Itri, R. Conformational stability of peanut agglutinin using small angle X-ray scattering. *Int. J. Biol. Macromol.* **48,** 398–402 (2011).

10. Blanchet, C. E. & Svergun, D. I. Small-angle X-ray scattering on biological macromolecules and nanocomposites in solution. *Annu. Rev. Phys. Chem.* **64,** 37–54 (2013).

11. Svergun, D. I. Determination of the regularization parameter in indirect-transform methods using perceptual criteria. *J. Appl. Crystallogr.* **25,** 495–503 (1992).

12. Svergun, D., Barberato, C. & Koch, M. H. J. CRYSOL – a Program to Evaluate X-ray Solution Scattering of Biological Macromolecules from Atomic Coordinates. *J. Appl. Crystallogr.* **28,** 768–773 (1995).

13. Konarev, P. V. *et al. MASSHA* – a graphics system for rigid-body modelling of macromolecular complexes against solution scattering data. *J. Appl. Crystallogr.* **34,** 527–532 (2001).

14. Sawyer, B. E. and Gras, L. S. (2013). Self-Assembling Nanomaterials: Monitoring the formation of Amyloid Fibrils, with a focus on Small-Angle X-Ray Scattering. In Juliet A. Gerrard (ed.), *Protein Nanotechnology: Protocols, Instrumentation, and Applications*, Methods in Molecular Biology (pp. 77-101). New York: Springer Science.

Chapter 5

Chromatography based approaches to observe the heterogeneity of HEWL aggregates on the basis of charge, size and shape

5.1 Separation of different intermediate species present in aggregation pathway of HEWL by *Ion exchange chromatography*

5.1 Introduction

To extensively characterize the protein aggregates; in this work we report the separation of polydisperse nanoaggregates on the basis of charge by anion exchange chromatography in a time dependent manner. The isoelectric point (pI) of HEWL as reported in the literature is 11.3. HEWL aggregation was carried out under conditions such as pH 12.2 (which is ~1.0 pH unit above the isoelectric point) which is apt for binding of molecules to the anion exchanger as the molecules would be negatively charged. Since a single protein is used, so separation of aggregates is possible due to changes on the surface charge of the protein which is not identical with the total net negative charge. To ensure strong binding, elution and binding steps were performed at pH 12.2.

In order to know the therapeutic significance of the aggregation species, structural characterization of oligomers is important. HEWL is a well-studied model system which forms amyloid *in vitro* and has been widely used in research due to its low cost and well characterized structure. Despite the extensive studies on HEWL aggregation pathways, detailed information on the characterization of oligomers formed in the pathway is still lacking. An additional attempt is required to understand the aggregation mechanism of HEWL and the heterogeneity of the system. The issue of separation of protein aggregates into higher order oligomers and lower order oligomers has been addressed here. In this study, we have employed various techniques such as ion exchange chromatography (IEC), SDS-PAGE, AFM imaging and Steady state fluorescence anisotropy (r_{ss}) to tackle this issue. Furthermore, a time dependent study has been performed on the oligomers obtained by room temperature incubation of HEWL under alkaline conditions. Understanding of intermediate aggregate species involved in the self-assembly mechanism is critical. Isolation of oligomeric species is a very challenging issue due to their polydispersity and their existence in dynamic equilibrium with monomers, oligomers of different sizes and higher molecular weight species. Hence, the approach to isolate the target molecules on the basis of charge was appropriate for our work.

Direct imaging of morphology of aggregates as well as quantitative measurements of aggregates heights can be obtained from AFM (Atomic Force Microscopy). It is a technique used for characterization of aggregate geometries[1].

Steady state anisotropy: It is a technique used for observing changes in the overall size of the macromolecules by measuring the changes in rotational motion due to aggregation.

Ion exchange chromatography has been widely used for separating proteins depending on charge heterogeneity. Characterization of different oligomeric species, dimers, monomers and fibril has gained considerable attention due to their potential applications.

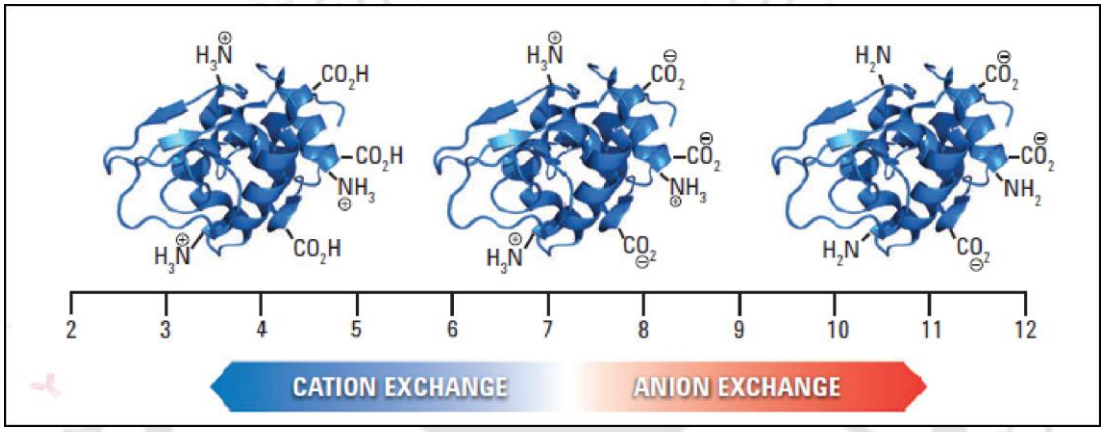

Figure 5.1 (a): Effect of pH on net protein charge (Adapted from Ion exchange chromatography for biomolecule analysis, Agilent technologies)

Protein contains different groups which give rise to differences in charge depending upon the pH of the surrounding solution. Charge on the acidic groups such as C-terminal carboxylic acids, side chains of glutamic and aspartic acid, and on the basic groups such as N-terminal amines, side chains of arginine, lysine, and histidine determines the overall net charge of a molecule which in turn is dependent on the pH of the mobile phase. The buffer pH and salt concentration in the elution buffer are important variable parameters for maintaining a consistent charged state of the molecules being analyzed and for resolution (**Tsai, 2007**). In order to perform elution of the biomolecules from the column, a competing ion is introduced which is accomplished by a linear gradient of NaCl of higher ionic strength. Proteins containing few anionic or cationic charges will be weakly bound to the column and get eluted at the onset of the salt gradient but those with large no. of charges get strongly bound to the column and elute at a higher salt gradient.

5.1.1 Motivation for the work

We represent use of a simple and quick technique i.e., anion exchange chromatography to analyze the intermediate species of HEWL aggregation on the basis of charge which is dependent on the number of monomers associated with the aggregates. Charge distribution on protein molecule plays a dominant role in determining the binding of protein to IEC column. Ion exchange is suitable for separating proteins with different isoelectric points but can also be used for separating the charged variants of a single protein. Aggregation occurring due to conformational changes of tertiary structure of protein culminates in an alteration of net ionization state, charge density and charge accessibility of the protein surface, which can be detected by IEC[2] **(Withka et al., 1986)**. Heterogeneity in charge distribution on protein molecules play a very crucial role in chromatographic separations as they can be represented as a uniformly charged planar surface or a sphere with centred net charge depending on different protein shapes. In case of large oligomers, size and structure of the species is important as the charge distribution around the species will vary depending on the no of monomers associated and also on the structure because here chromatographic interactions particularly occur with surface charges. To the best of our knowledge no report has been published on the use of IEC for characterization of HEWL aggregates.

5.1.2 Objectives

- Separation of different species involved in aggregation of HEWL by anion exchange chromatography.
- To probe the conformational changes occurring at different steps of aggregation of HEWL, responsible for differences in charge distribution, on the overall structure.
- To carry out a comparative analysis on the charge variants of the same protein arising due to interplay between charge distribution (due to association of monomers) and change in the overall geometry of the oligomers in the due course of time of 5 days.

5.1.3 Review of Literature

Role of charge distribution and the influence of protein structure on binding in IEC have been studied by Yan Yao et al. They have studied cytochrome c variants from different species with similar structures but minimal difference in the residues by modeling electrostatic interactions of protein-adsorbent surface considering the full 3D protein structure[3] **(Yao et al., 2004)**. Contributions of both protein-surface attraction and repulsive protein – protein interactions, which are electrostatic in nature, have been explored on Ion exchange media for basic charged proteins such as lysozyme, cytochrome c and ribonuclease A. These interactions play a major role in predicting the adsorption behaviour of the proteins on the adsorbent surface[4] **(Xu et al., 2008)**. There are very few reports about the characterization of protein aggregates by IEC. Previously a report has been published on characterization of aggregates of enzyme trehalose 6-phosphate synthase using ion exchange chromatography. Fractions were eluted at different ionic strength of KCl and effects of pH and temperature on enzyme stability and activity from the fractions were studied[5]. Researchers have analysed milk whey proteins by using a mixed bed IEC column packed with 1:1 ratio of weak cation exchange and weak anion exchange material[6]. Many studies have shown AEC (anion exchange) to be a reliable technique for isolation and purification of globular proteins[7] **(Nadal et al., 2011)**. Moreover IEC has been also employed for structural characterization of different variants such as deamidated, oxidized and heterodimeric (covalent dimer) forms of recombinant human interferon γ[8] by **Maleksabet et al.**

Cao et al. have shown the conversion of fully reduced HEWL to highly organized amyloid fibrils at low pH by adding ethanol at different concentrations. To achieve full purity of fully reduced HEWL, cation exchange chromatography was used to separate the partially reduced protein from the fully reduced sulfhydryl blocked, positively charged HEWL[9]. Detailed studies have been carried out to understand the nature of aggregation process of human lysozyme by introducing site specific biotin moiety into the protein. Singly labelled biotinylated lysozyme was purified from unlabelled lysozyme and doubly labelled lysozyme using cation exchange chromatography[10]. Several studies have reported IEC as a method to characterize the protein-protein interaction. However, we have carried out this study to separate the amorphous aggregates of HEWL into higher order compact oligomers, held together by strong intermolecular disulfide bonds and weakly associated lower order oligomers.

5.1.4 Advantages of IEC over other techniques

It is a mild non-denaturing liquid chromatography which can be used to detect conformational changes of protein structure, to quantitate protein and for characterization of proteins in their native state. Ion exchange chromatography has been previously used for the measurement of protein conformational change and stability[2]. Sample preparation is not tedious unlike other techniques used for protein analysis. When compared to other techniques, IEC allows higher sample loading capacity.

Oligomers formed during the aggregation pathway of HEWL are non-uniform in size, that's why it is important to understand the nature of these self-assembled species. IEC, AFM in combination with steady state anisotropy and SDS-PAGE techniques have been used to characterize multiple aggregate species.

The study carried out by us here mainly concerns with the question **a) whether it is possible to differentiate the early aggregates from late aggregates on the basis of their morphology and physical dimensions? b) Is it possible to separate the oligomeric species from monomeric species which are in dynamic equilibrium?**

5.1.5 Materials and Methods

5.1.5.1 Materials

HEWL (Hen Egg White Lysozyme) (EC 3.2.1.17)

Lysozyme from chicken egg white was procured from Sigma-Aldrich (**Cat no. L6876**) stored at -20 $^{\circ}$C and was used directly without any purification. We have used deionized water (18.2 mΩ cm) water from Millipore Milli-Q system throughout for all the experiments. NaOH and NaCl were obtained from MERCK. Sodium phosphate buffer was prepared using disodium hydrogen phosphate (Na_2HPO_4) of ionic strength 50 mM and pH was adjusted to 12.2 using 1 N NaOH.

5.1.5.2 Preparation of HEWL aggregates (preparation and incubation conditions)

150 µM HEWL solutions were prepared in 50 mM pH 12.2 Sodium Phosphate buffer (previously reported for preparation of HEWL oligomers) and incubated at room temperature (23-25 °C) without any agitation or shaking[11]. HEWL concentration was determined by absorbance UV measurements (Cary 100 UV-Vis spectrophotometer) using the extinction coefficient of 38,400 M^{-1} cm^{-1} at λ = 280 nm. Aliquots of the HEWL aggregate solution were extracted out of incubation at different time points for characterization. The protein samples were filtered with a 0.45 µm pore size syringe filter **(Syringe filter sterile Uniflo™, GE healthcare life sciences Whatman™ Cat no. 9908-2504)** to avoid any loss of large aggregates.

5.1.5.3 Chromatographic system

All the Ion exchange experiments were carried out on **ÄKTApurifier™** FPLC system **(GE Healthcare)**. It is equipped with a multi wavelength UV-VIS detector (UV-900). For gradient elution, there are two buffer lines A and B, fed with buffers (equilibration and elution) which are mixed to attain the required salt concentration. It is provided with UNICORN software, a simple and user-friendly interface which gives a real time control of chromatography operation.

5.1.5.4 Separation of aggregates by ion exchange chromatography

Experimental conditions for running the column: All experiments and data processing were performed using **FPLC ÄKTA** purifier **UNICORN™5.0** software. **Mono Q™ 5/50 GL, GE Healthcare** ion exchange pre-packed column was chosen to perform the separation due to its high selectivity and strong binding. The strong anion exchange membrane consisted of a trimethyl ammonium (- CH_2 – N^+ $(CH_3)_3$) charged group bonded to a polystyrene/divinyl benzene matrix. The column was equilibrated with 20 CV[1] of **buffer A** (50 mM Sodium phosphate buffer, pH 12.2) prior to injecting the sample. The samples were filtered through a syringe filter (0.4 µm, GE Healthcare) before loading onto the column in order to avoid any contamination and the samples were checked carefully for the presence of air bubbles which might disrupt the column.

[1] **CV** – Column Volume

200 µL of the sample (at different time points of incubation) was loaded onto the column and the samples were run through the column at a flow rate of 1.0 mL/min using FPLC ÄKTA prime system. Sample loading was followed by a washing step up to 10 CV so that all the unbound fractions get washed out from the column using the buffer A. The ionically bound protein was eluted using a linear gradient of **buffer B** (50 mM Sodium phosphate, 1M NaCl, pH 12.2) from 0 to 100 % (an increasing ionic strength up to 1 M NaCl) over 40 min and multiple fractions were collected. Absorbance at 280 nm was used to monitor protein fractions eluted from the column. Binding and elution steps, both were performed at pH 12.2 (alkaline condition, room temperature). Buffers used for experiment were degassed and filtered prior to use. At the end of each analysis or protein elution, the column was equilibrated back with buffer A in order to ensure reproducibility, so that in the next run protein doesn't interact differently with the column.

HEWL aggregates carry a net negative charge at alkaline pH 12.2 as previously reported by our lab[12] **(Homchaudhuri et al., 2006)**, hence anion exchange column was used for separation. Ion exchange resin used is polystyrene divinylbenzene copolymers. The functional group is a quaternary amine group which is negatively charged under basic conditions. Quaternary amines are attached through a derivatization of the phenyl rings of polystyrene. The strong anion exchange column, covalently linked to a porous chemically stable polymer has a wide pH operating range. Short column length (or small bed volume i.e. 1 mL) was efficient for achieving faster analysis and speedy separation. Particle size is an important factor in IEC columns and smaller particle sizes (10 µm) of Mono Q column provides efficient separation and high resolution. Porous, rigid and spherical particles have the advantage of providing greater surface area and hence greater loading capacity.

5.1.6 Results and Discussion

5.1.6.1 Ion exchange Chromatogram profile Changes in Ion exchange chromatograms of HEWL (incubated in pH 12.2) as a function of incubation period. Samples were injected into Mono Q^{TM} 5/50 GL anion exchange column and eluted with NaCl (0-1 M) linear gradient as described under Materials and Methods.

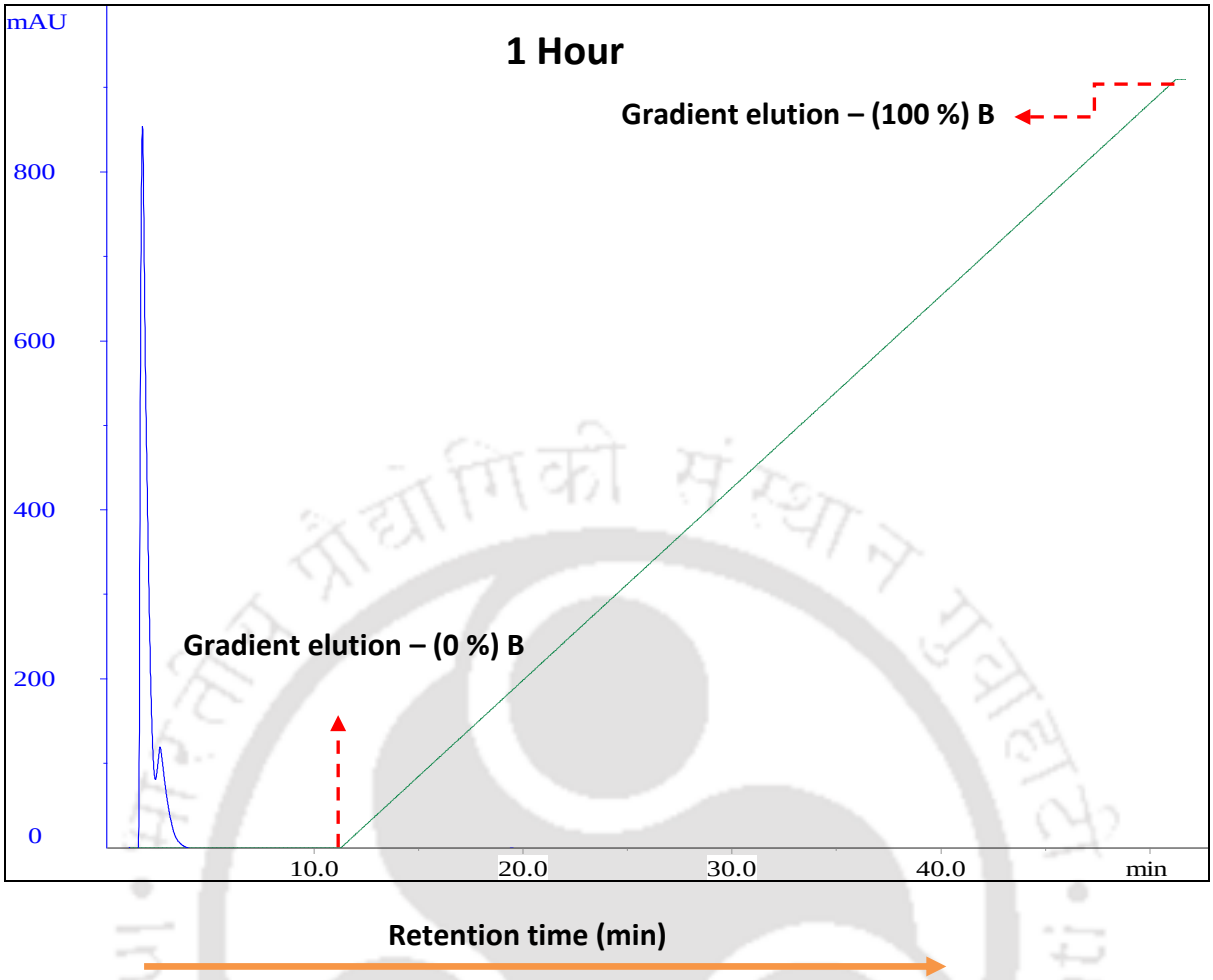

Figure 5.1.6.1(a): Ion exchange chromatogram profile of 150 µM HEWL aggregates. The samples were introduced to the column after **1 hour** incubation of HEWL aggregates at pH 12.2, room temperature. Y-axis represents UV absorbance at 280 nm in mAU units.

Mobile phase: **Buffer A:** 50 mM sodium phosphate buffer, pH 12.2

Buffer B: A + 1 M NaCl

Flow rate: 1 mL/min

Gradient: 0 min- 100% A: 0% B

40 min- 0% A: 100% B

Detector: 280 nm

Protein: Hen egg white lysozyme, 14.3 kDa, pI – 11.35

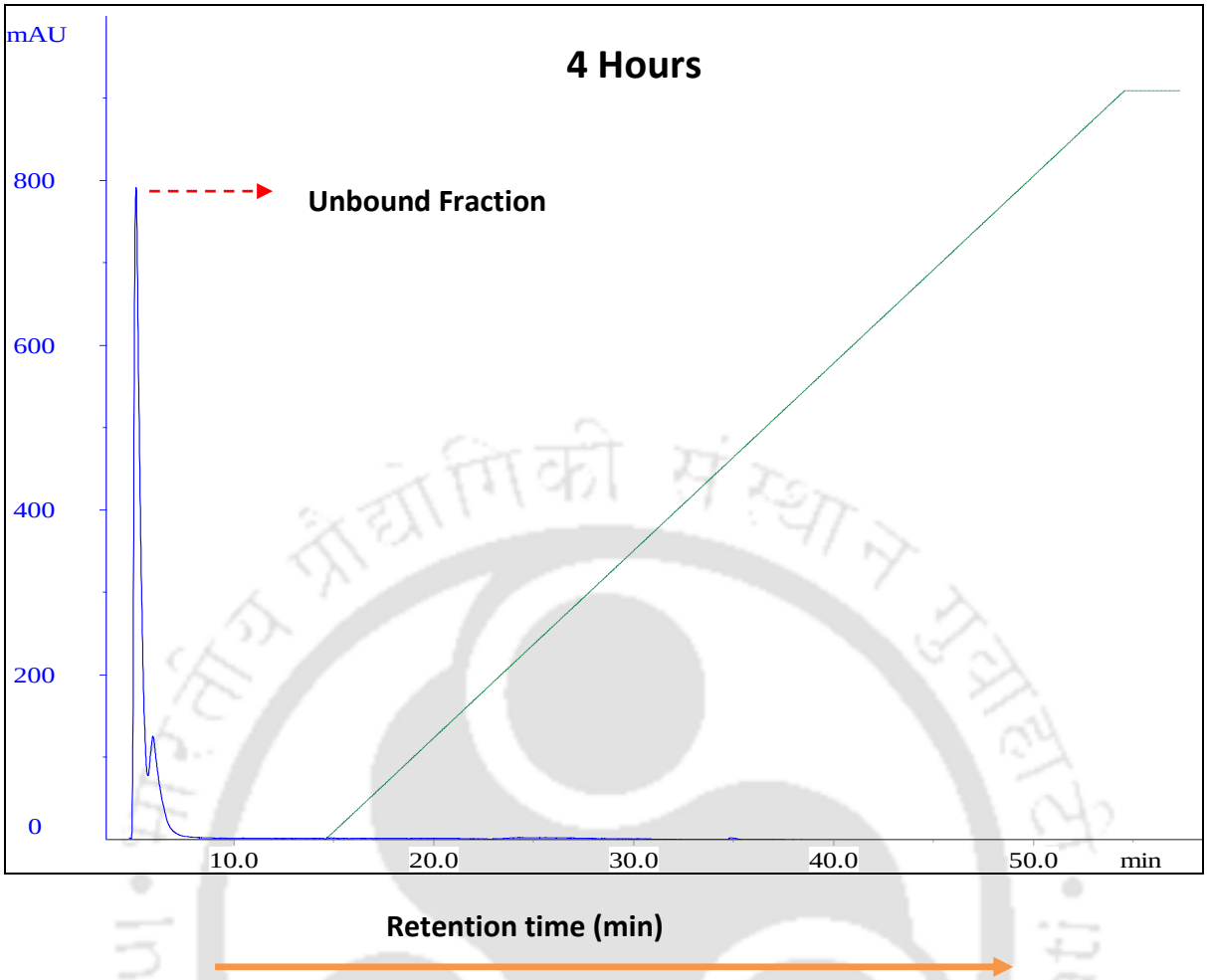

Figure 5.1.6.1(b): Chromatogram profile of 150 µM HEWL aggregates (**4 hours** incubation). Dashed line is used to depict the gradient elution with 1 M NaCl. Y-axis represents UV absorbance at 280 nm in mAU units.

Comparisons of chromatograms showed that the peaks were resolved based on the extent of negative charges carried by the different species which depends on the no of monomers associated with the aggregates. In an ion exchange chromatogram, each peak represents different species with different charges. Area under each peak can be correlated to the concentration of a particular species. Larger area correlates with a higher concentration of a particular ion species. Variation in peak width and peak height can be observed in chromatograms. The unbound fractions have very short retention time; consistent with the low net charge of monomer and dimers at pH 12.2. Significant difference in the chromatographic elution profiles was observed.

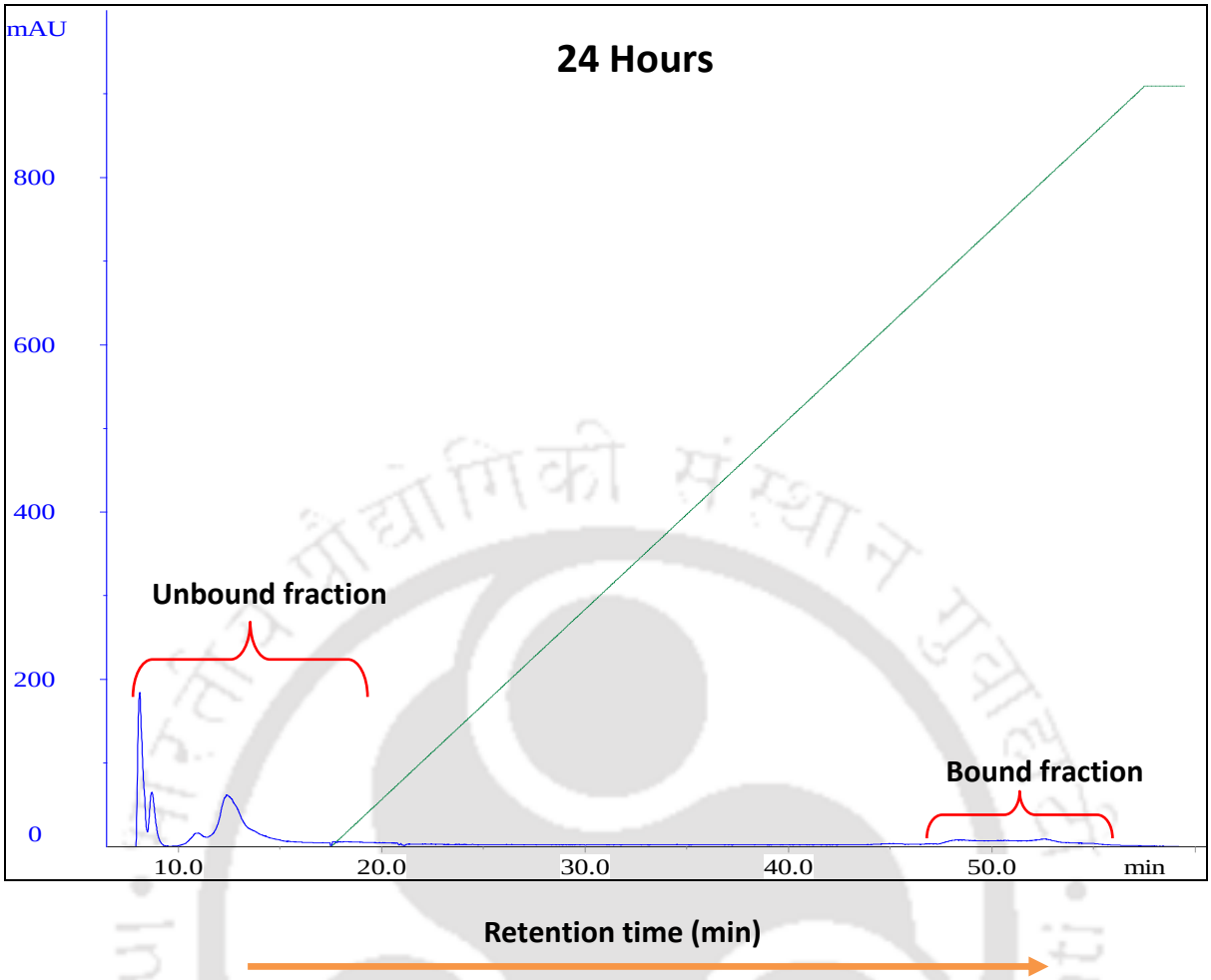

Figure 5.1.6.1(c): Chromatogram profile of 150 µM HEWL aggregates (**24 hours** incubation) showing the emergence of both bound and unbound fractions. Y-axis represents UV absorbance at 280 nm in mAU units.

During the initial hours of incubation i.e. after 1 hour and 4 hours, very sharp and intense peak accompanied with a small peak is observed referring to the dominant monomer population(or conformationally altered monomeric species) and a few dimeric species respectively. As depicted from [**Figure 5.1.6.1(a) & 5.1.6.1(b)]**, it was observed that in case of 1 hour as well as 4 hours incubated samples, the predominant peak displayed was that of unbound fractions and no peak was observed after gradient elution which indicates the absence of species possessing enough anionic binding sites to get bound to the matrix of the column.

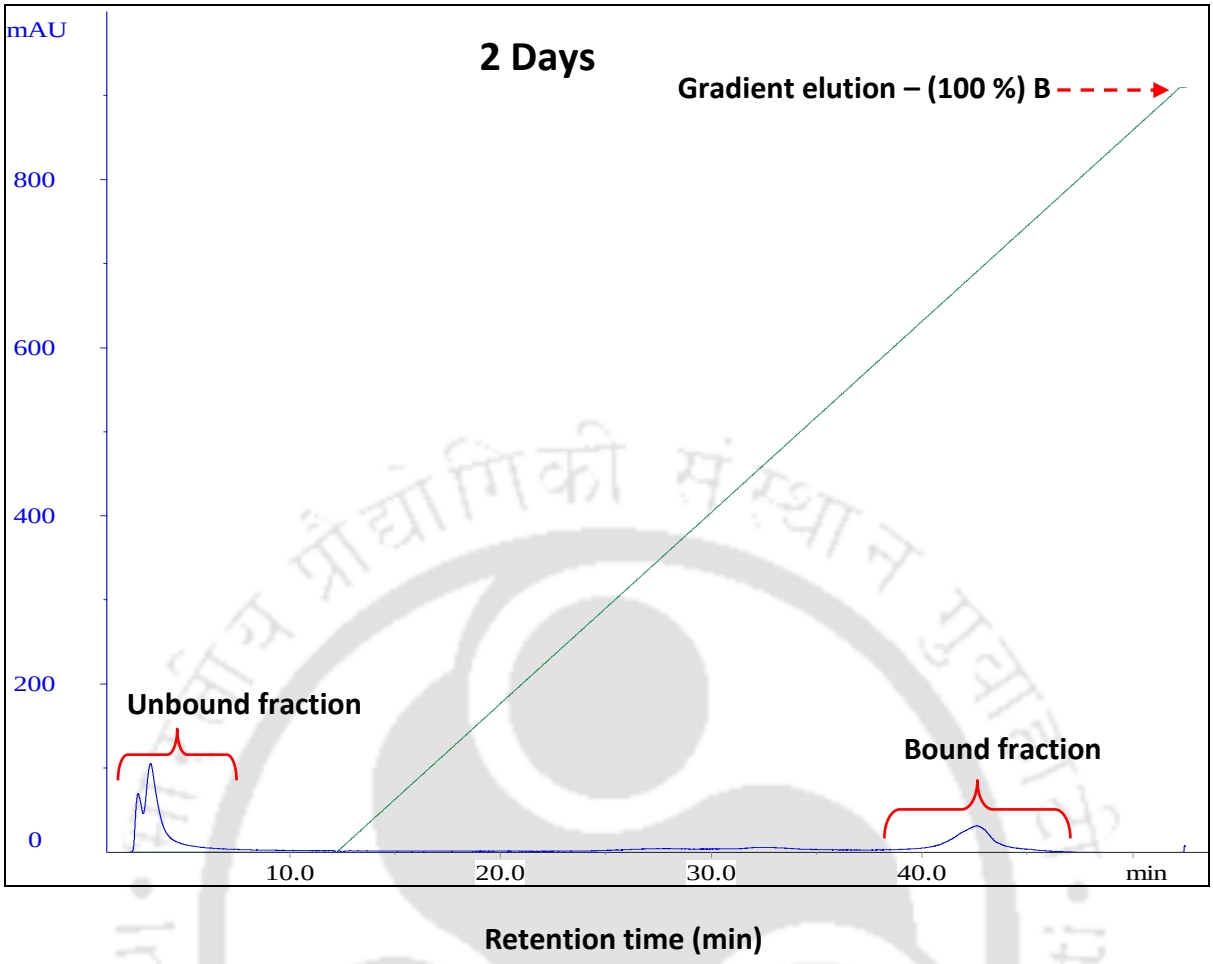

Figure 5.1.6.1(d): Chromatogram profile of 150 µM HEWL aggregates (**2 Days** Incubation) showing the emergence of both bound and unbound fractions. UV absorbance is recorded in milli absorbance units (mAU) which is represented on Y-axis.

After nearly 24 h of incubation **[Figure 5.1.6.1(c)]**, peak corresponding to monomeric population gets diminished i.e., a decrease in peak height as well as area occurs with a concomitant emergence of another broad and continuous peak which indicates the formation of a population of multiple intermediate aggregates which do not carry sufficient negative charges on their surface to get bound to the column, hence they get washed out as unbound fraction. Significantly, after 24 Hrs. of incubation **[Figure 5.1.6.1(c)]**, the appearance of a broad low intensity peak for bound fractions are seen in the chromatogram, while peak for unbound fractions begin to diminish gradually.

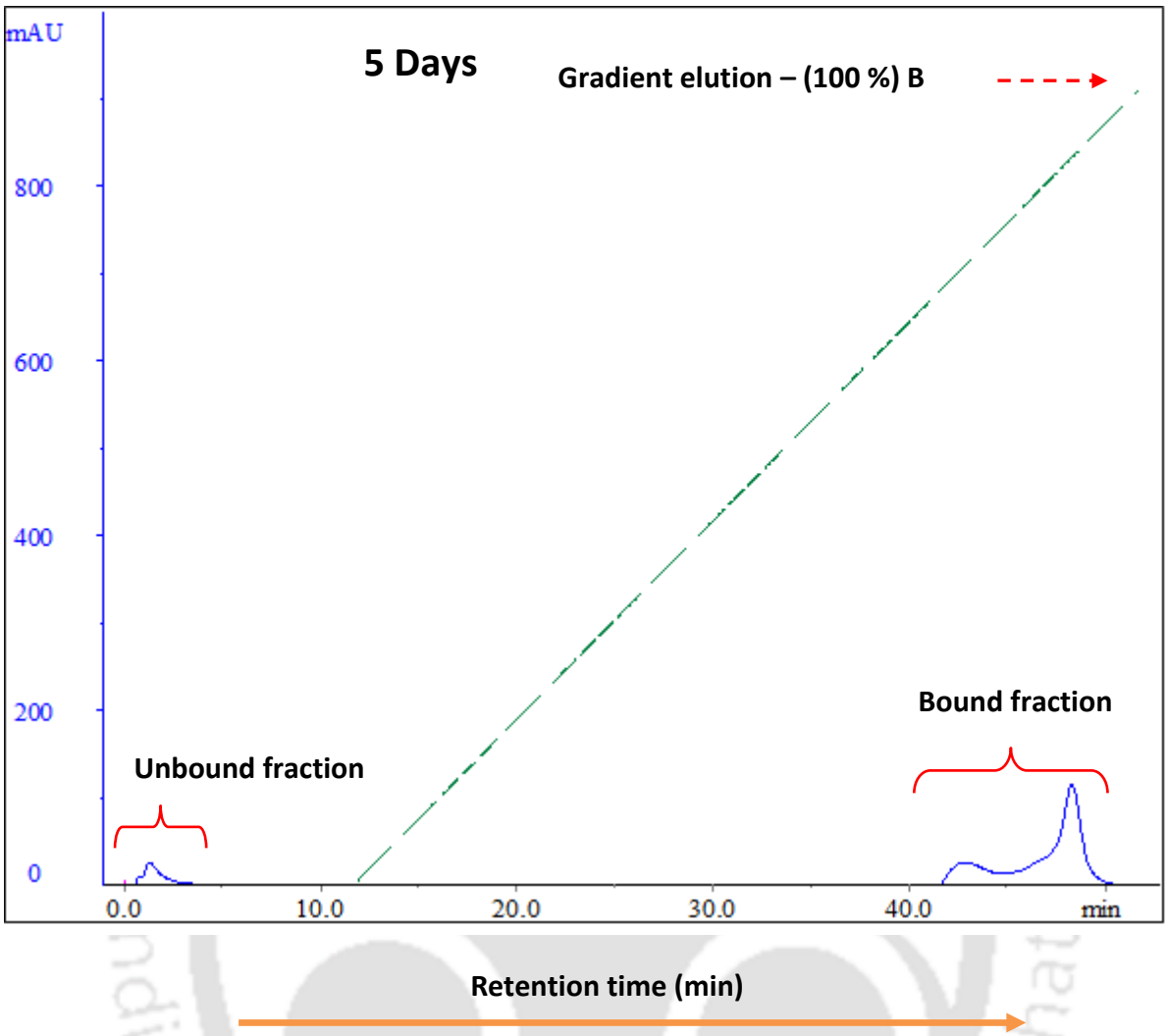

Figure 5.1.6.1(e): Chromatogram profile of 150 µM HEWL aggregates (**5 Days** Incubation) showing the emergence of both bound and unbound fractions. Symbol :(-- -- -- --) is used for representation of gradient elution. (- - - - →) indicates the endpoint of gradient elution. Y-axis represents UV absorbance at 280 nm in mAU units.

5th day sample**[Figure 5.1.6.1(e)]** displays a longer retention time of bound fractions which is due to a large net charge on the aggregates formed by the 5th day. Importantly, population of unbound fraction appears negligible at this incubation time.

5.1.6.2 Peak Area

The amount of protein content or the concentration of a particular species can be correlated to area under each peak, where a larger area correlates with a higher concentration of the species. The area under the peak was used for evaluation of % increase or % decrease in bound and unbound fractions with increasing days of incubation.

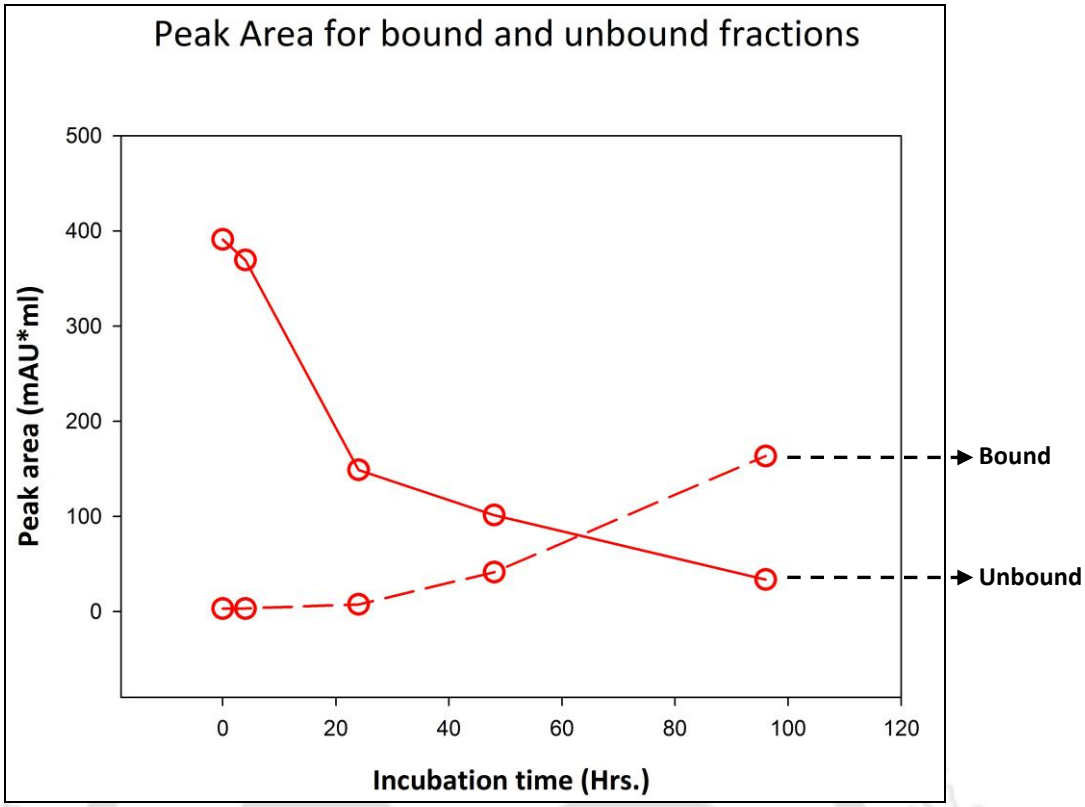

Figure 5.1.6.2: Peak area calculated for unbound and bound fractions from ion exchange chromatogram.Red circles (o) represent different time points of incubation of sample.

Superposition of the two peak area curves of bound and unbound fractions as a function of incubation time **[Figure 5.1.6.2]** displays an upward trend for amount of bound fractions and corresponding downward trend for unbound fractions with time. Both the curves intersect at approximately 65 hours of incubation indicative of equal amount of bound and unbound fraction to be present at that particular time point. The relative decrease in peak area of unbound fractions is 62 % over the 24 hours period incubation which is remarkably higher as compared to a small 6 % decrease in case of 4 hours incubation period**.** But we found that by the end of 5 days of incubation, peak area of unbound fractions dramatically reduced by 93 % which is in correlation with increase in peak area for bound fractions. With increasing days of incubation, the decreasing peak area of unbound fractions and appearance of steadily growing peak for bound fractions suggest that number and size of larger aggregates are increasing as the monomeric population is getting depleted as the aggregation proceeds. This observation encourages us to look at the results obtained from SDS-PAGE run for IEC eluted fractions.

5.1.6.3 Electrophoresis (Tricine SDS-PAGE)

After each chromatographic elution, fractions collected were analysed by Tris Tricine SDS-PAGE (16.5 %) under reducing conditions (β-Mercaptoethanol). Protein standards were 1.06, 3.5, 6.5, 14.2, 17.0, and 26.6 kDa (**Sigma, Ultra low range Molecular weight Marker, Cat no. M3546**).To prevent the aggregation from proceeding further, all the eluted fractions were stored at 4°Celsius and then analysed by Tricine SDS-PAGE. Gel electrophoresis was performed on **mini-PROTEAN® Tetra Cell mini gel electrophoresis system**. The gels were run at 95 V for 2.5 h followed by staining with Coomassie Brilliant Blue solution containing 0.25% (w/v) brilliant blue R/40% (v/v) methanol/ 7% (v/v) acetic acid/water (**Brilliant Blue R Concentrate, Electrophoresis reagent, Sigma, Cat no. B8647-1EA**) and destained in the same solution without the dye. Gels were analysed using **Image Lab™ 4.1 software.**

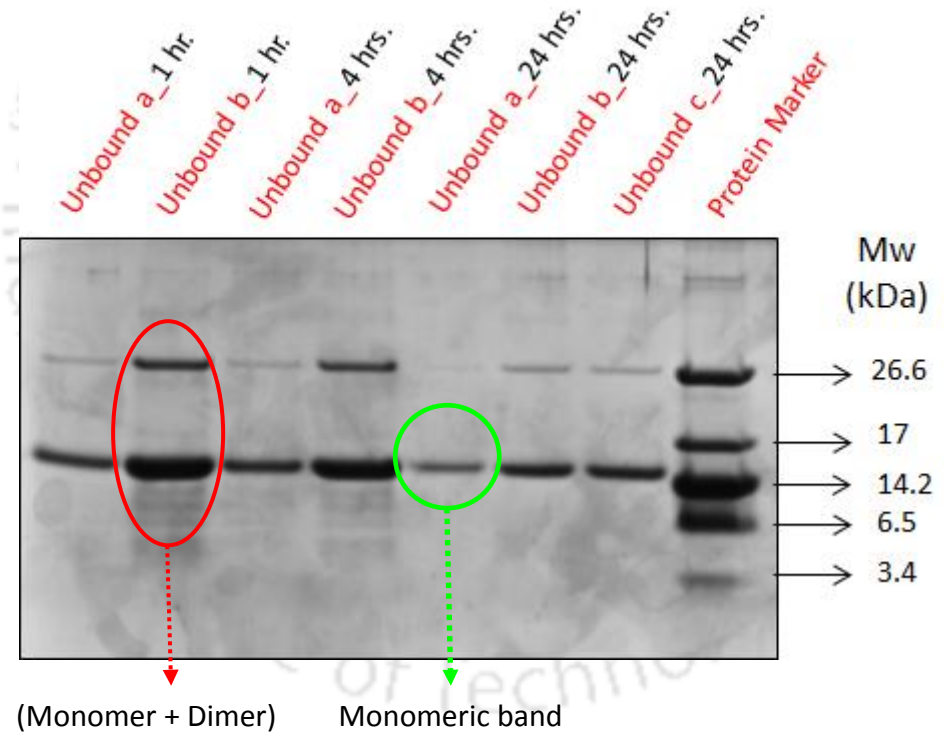

Figure 5.1.6.3 (a): SDS-PAGE for IEC unbound (**U**) fractions of **1 hour**, **4 hours** and **24 hours** incubated aggregates. **Ua_1hr:** 1.68-2.18 mL, **Ub_1hr:** 2.32-2.82 mL, **Ua_4hrs:** 0.48-0.98 mL, **Ub_4hrs:** 1.44-1.94 mL, **Ua_24 hrs:** 0.6-1.1 mL, **Ub_24 hrs:** 1.2-1.7 mL, **Uc_24hrs:** 4.95-5.45 mL & **Ud_24 hrs:** 5.51-6.01 mL.

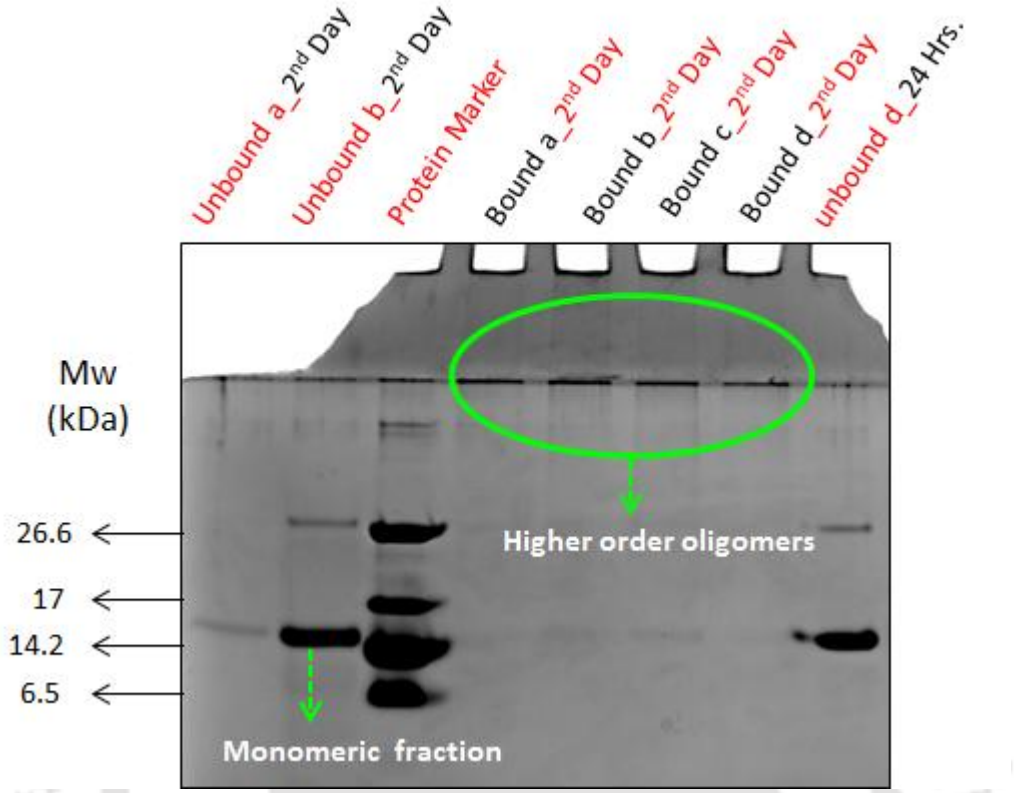

Figure 5.1.6.3 (b): SDS-PAGE for IEC unbound (**U**) and bound (**B**) fractions for 2 days old aggregates. **Ua_2nd day:** 0.50-1.0 mL, **Ub_2nd day:** 1.23-1.73 mL, **Ba_2nd day:** 39.06-39.56 mL, **Bb_2nd day:** 39.86-40.36 mL, **Bc_2nd day:** 40.6-44.1 mL, **Bd_2nd day:** 41.44-41.94 mL.

From SDS-PAGE data, we can infer that bound fractions mostly consists of compact aggregates or oligomers as compared to loosely bonded or expanded aggregates seen in case of unbound fractions. SDS-PAGE for 5th day- Bound fractions which eluted at very high ionic strength of elution buffer (bound fractions eluted at 91.5 % of buffer B and at 94.5 % of buffer B) are seen as bands on Tricine SDS-PAGE stuck to the wells (in resolving gel) and were apparently seen as smear in stacking gel. As evident from the gel images, all the bound fractions for the 5th day incubated sample were seen at the interface of the resolving and stacking gel **[Figure 5.1.6.3(c)]**.

Lanes indicated the formation of soluble oligomeric aggregates (High molecular weight) on prolonged incubation of 5 days. This could lead us to conclude the formation of compact and higher order (high molecular weight) oligomers stabilized by inter disulfide bonds by the 5th day of incubation, hypothesis which was proved in our earlier work is strongly supported by current data.

This in agreement with an article published **(Yang et al., 2015)** on formation of amorphous aggregates of lysozyme promoted by disulfide bond scrambling in presence of disulfide reducing agents[13]. They have demonstrated how the integrity of disulfide bonds affects aggregation of HEWL and BSA proteins by the use of disulfide reducing agents. Scrambled disulfide bonds (inter- / intramolecular) resulted in high molecular weight species. Presence of these species could be observed on SDS-PAGE.

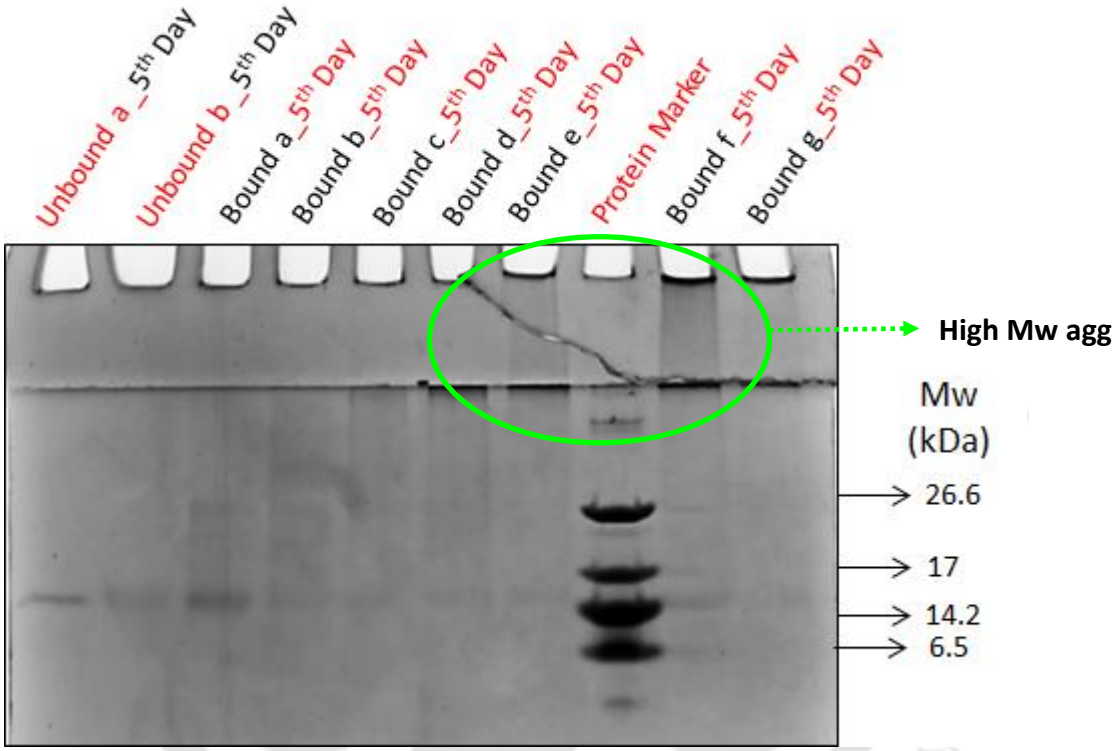

Figure 5.1.6.3: Tricine SDS PAGE of IEC eluted fractions: Unbound (**U**) and Bound (**B**) fractions of **5 days old** aggregates. **Ua_5th day:** 0.93-1.43 mL, **Ub_5th day:** 1.59-2.09 mL, **Ba_5th day:** 41.85-42.35 mL, **Bb_5th day:** 42.67-43.17 mL, **Bc_5th day:** 44.76-45.26 mL, **Bd_5th day:** 46.78-47.28 mL, **Be_5th day:** 47.6-48.1 mL, **Bf_5th day:** 48.2-48.7 mL, **Bg_5th day:** 49.42-49.92 mL.

In case of bound fractions for 5th day old aggregates, appearance of higher molecular weight species in the gel increased with the order of elution. In other words, late eluted fractions showed a decrease in electrophoretic mobility with respect to early eluted fractions. The late eluted fractions were observed as smear of protein stuck to the stacking gel. The condition which we have used (heating the sample at 95 °C and addition of β-Mercaptoethanol to the sample) are not sufficient enough to disrupt the bonds between oligomers as the bands are seen stuck to the well, thus indicating that there is no disassembly of the disulfide bonded aggregates **[Figure 5.1.6.3 (b)]**.

As seen from the electrophoresis pattern of eluted fractions, bands corresponding to 14.2 kDa and an additional 26.6 kDa (in some cases) which can be ascribed to HEWL monomers and covalent dimers were consistently present for the unbound or non-retained fractions **[Figure 5.1.6.3(a)]** and in few cases, only the monomer band was seen and no other protein band was visible in these lanes. The major protein band (14 kDa) was observed in the entire unbound fraction but was absent in the bound fractions. Amorphous aggregates held intact by intermolecular disulfide bonds were found to be thermally stable.

5.1.6.4 AFM Imaging

To further explore the morphology of aggregates, AFM imaging was performed. Eluted fractions stored at 4°Celsius (to arrest aggregation) were diluted 5X times with Sodium phosphate buffer, pH 12.2 and $MgCl_2$ was added such that the final concentration was 2 mM. The samples for AFM measurement were dropped onto freshly cleaved mica sheets and then the sheets were left to dry in air and were stored in a desiccator before imaging. All the raw images obtained were analysed and processed using the open access software, **WSxM v5.0 Develop 7**. Most of the images were acquired at a 512 x 512 pixel resolution and some were acquired at a 1024 x 1024 pixel resolution.

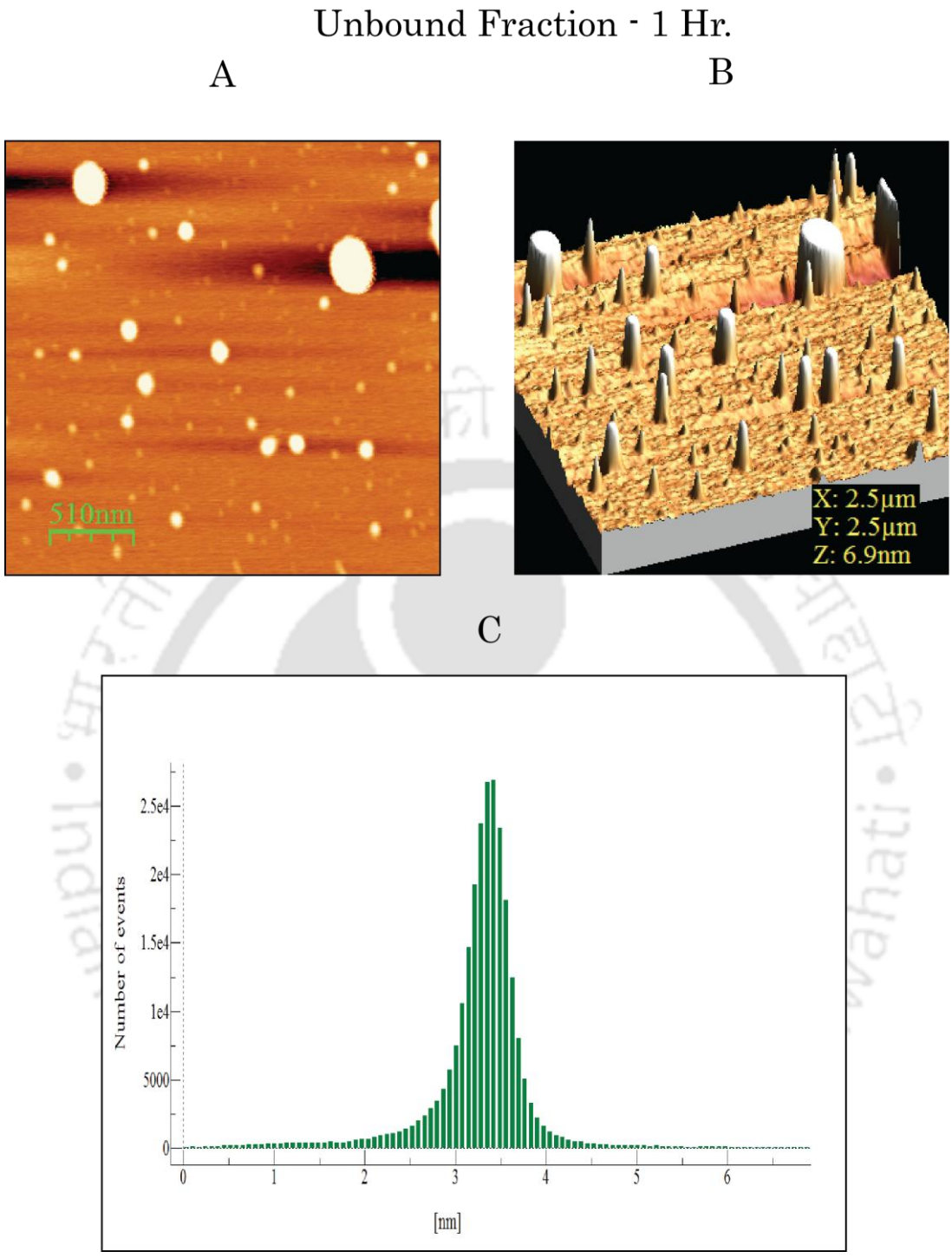

Figure 5.1.6.4 (a) : AFM images of unbound fraction 1 hr.(510 nm scale)

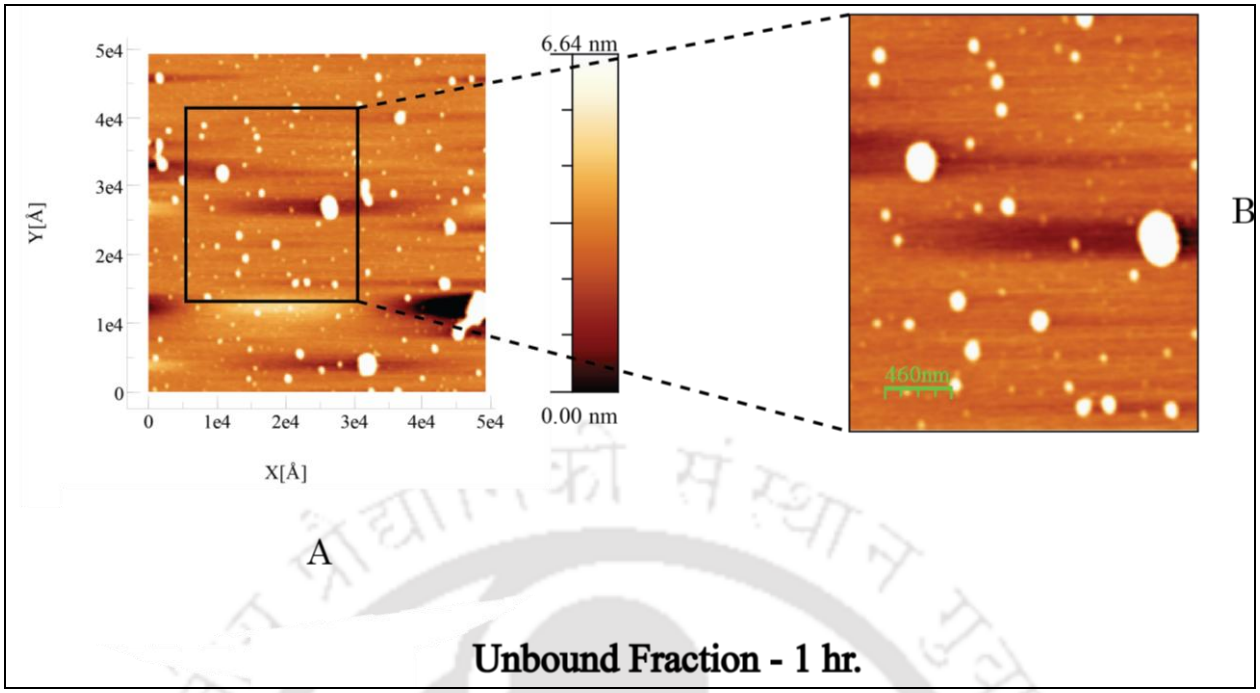

Figure 5.1.6.4 (b) : AFM images of unbound fraction 1 hr.(980 nm-Zoom)

In order to carry out comparative structural analysis on bound and unbound fractions, AFM imaging was performed to reveal the change in morphology of aggregates. Particle dimensions for nanoaggregates were extracted from AFM imaging line scans. The shape of histogram profiles was highly symmetric around the peak height. One of the interesting features of the aggregates observed on 5th day is that the structure and morphology of early eluting aggregates are different from late eluting aggregates as evident from the AFM images. Previous work in our laboratory **(Ravi et al., 2014)** has shown that HEWL nanoaggregates after 5 days of incubation are stabilized by inter disulfide bonds between the oligomers.. AFM images displayed characteristic morphologies for the bound fractions. The unbound fractions displayed higher values for average height as compared to bound fractions. This may be due to the rapid dissociation of oligomeric aggregates for incubation periods of 1 h, 4 h and 24 h. Unbound fractions collected for 5th day and 2nd day incubation displayed average height of 14.7 nm and 6.6 nm respectively in AFM but they didn't show up as larger aggregates in SDS-PAGE which confirms that unbound fraction mostly comprises of unstable aggregates i.e. they can dissociate into monomers easily.

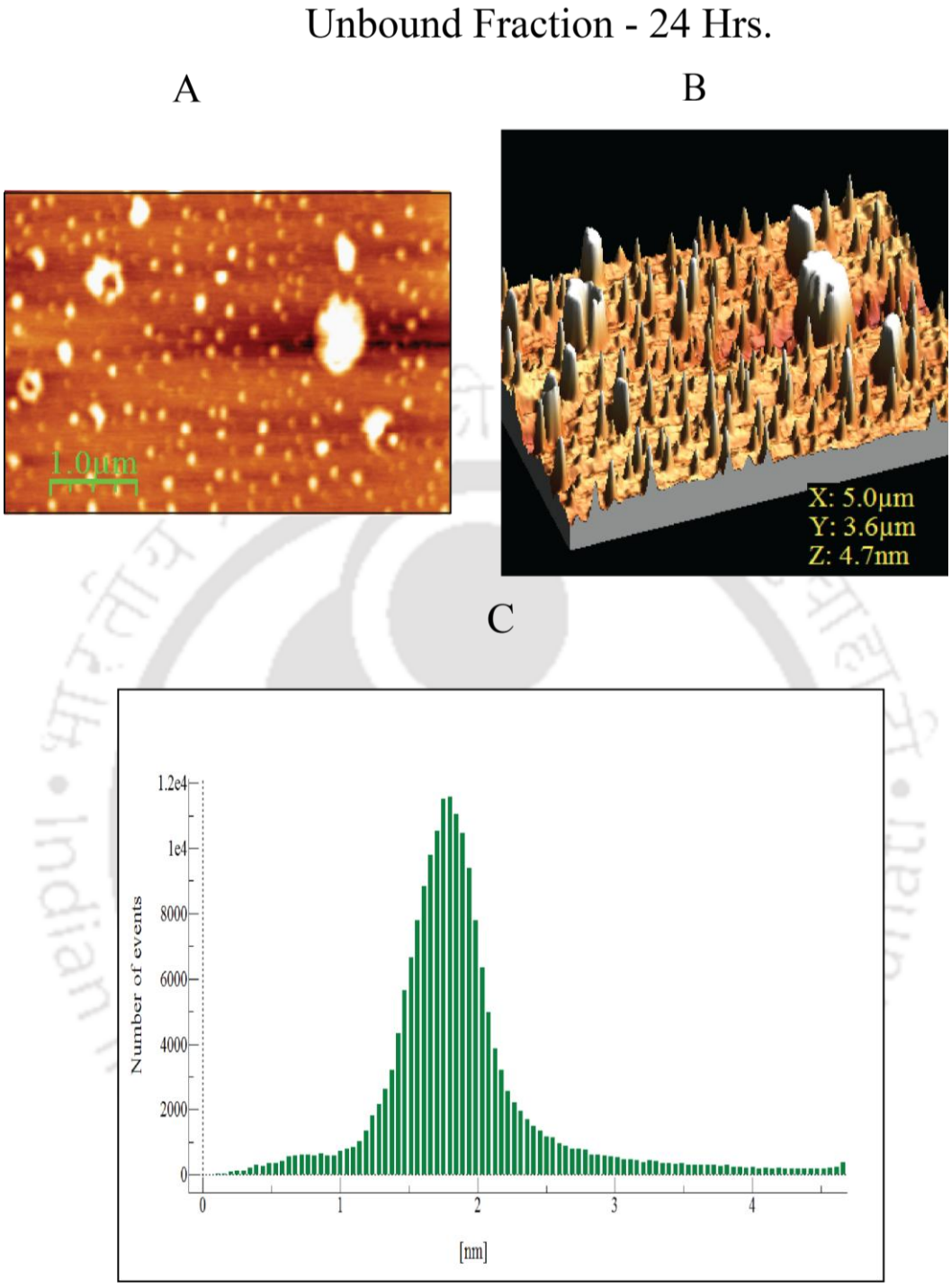

Figure 5.1.6.4 (c): AFM images of unbound fraction 24 Hrs.(1.0 µm scale)

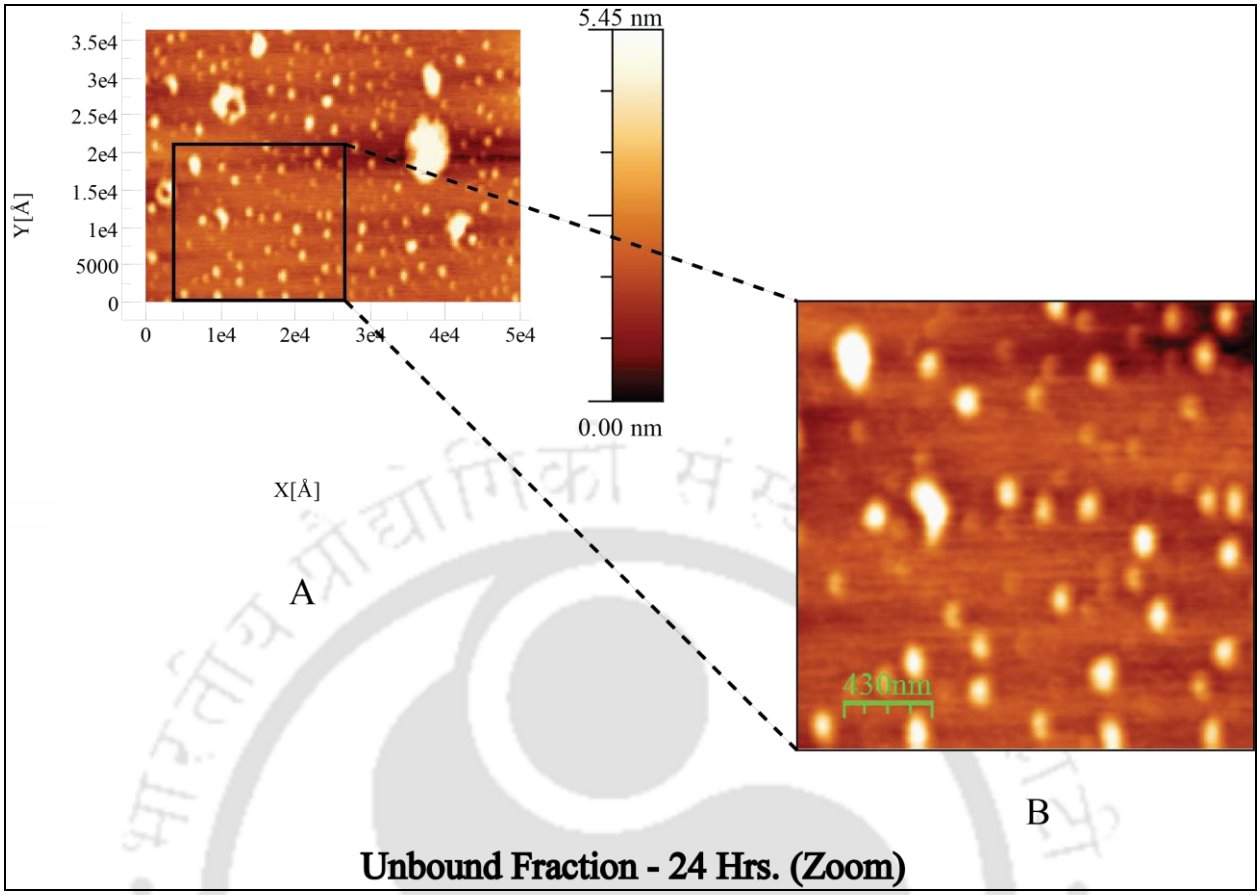

Figure 5.1.6.4 (d): AFM images of unbound fraction 24 Hrs.(1.0 µm- Zoom)

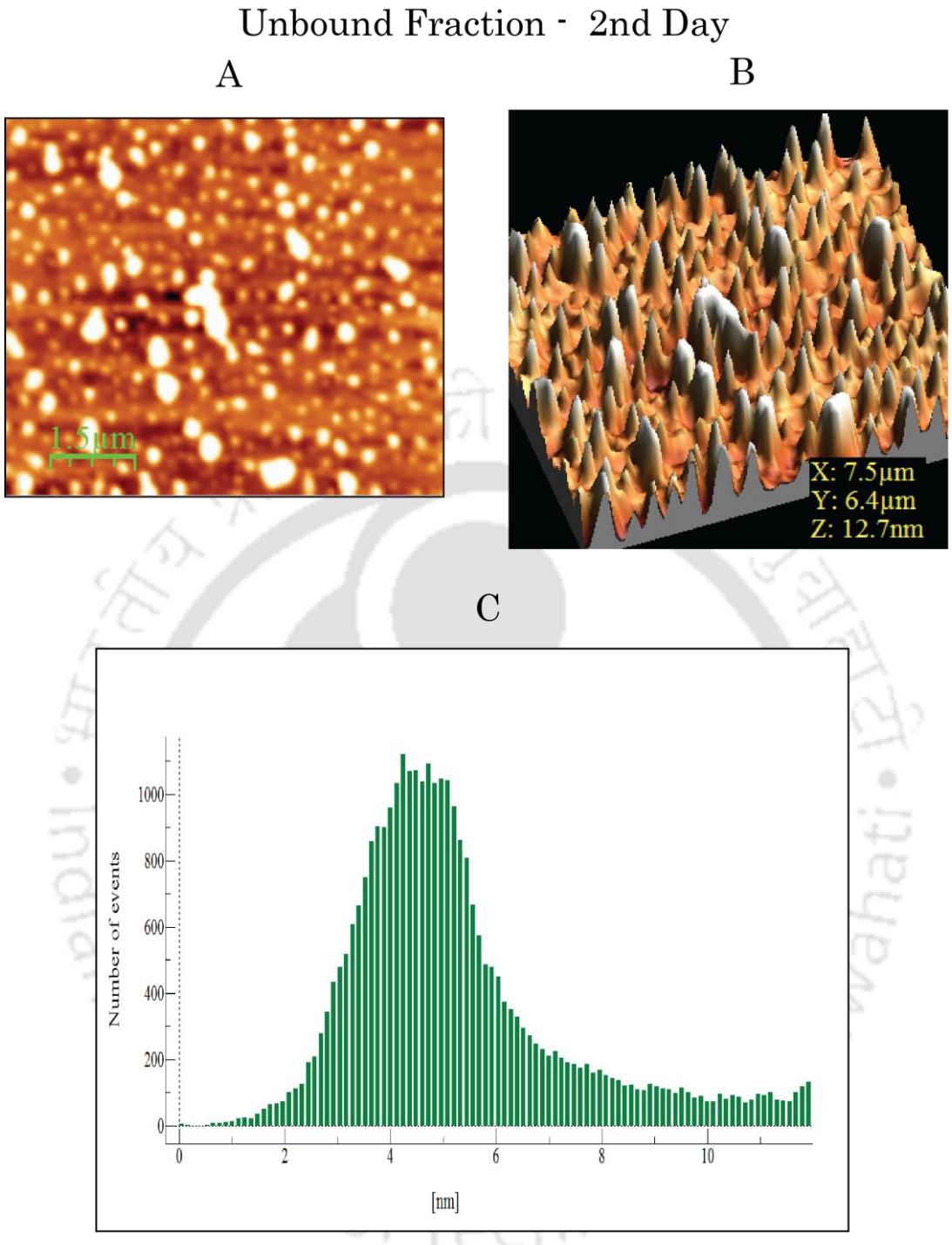

Figure 5.1.6.4 (e): AFM images of unbound fraction 2nd day(1.5 µm scale)

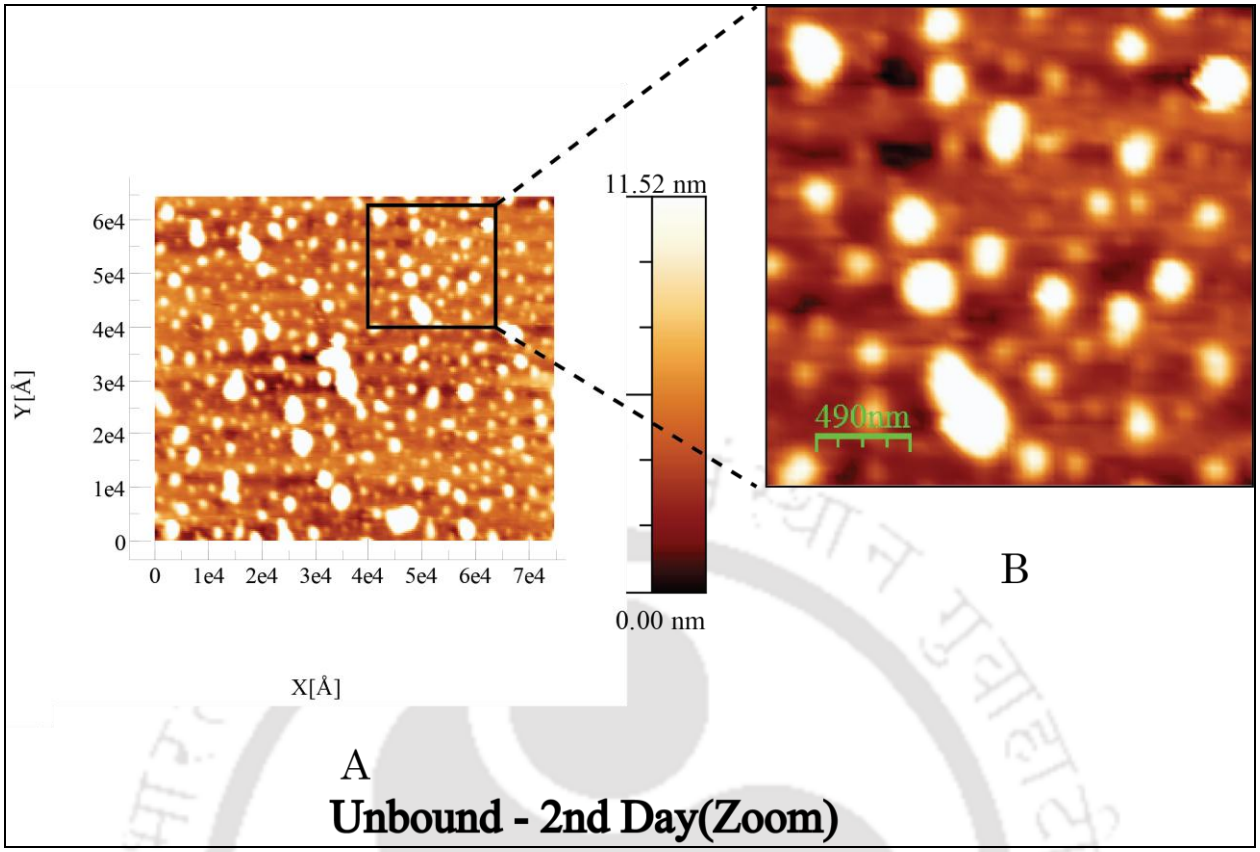

Figure 5.1.6.4 (f): AFM images of unbound fraction 2nd day(1.5 µm- Zoom)

HEWL aggregates or oligomers are retained in the column depending on their anionic character. Aggregates with few anionic binding sites were weakly bound to the column and eluted at the onset of salt gradient whereas aggregates with a large number of anionic binding sites were strongly retained by the column and eluted at high salt gradient concentration. The main purpose of the study is to separate the higher order oligomers from lower order monomeric and dimeric fractions. As our system is known to be a heterogeneous and highly polydisperse. We have to take into consideration the effects of protein – protein interactions at pH 12.2 while running the protein sample in the column and heterogeneous charge distribution.

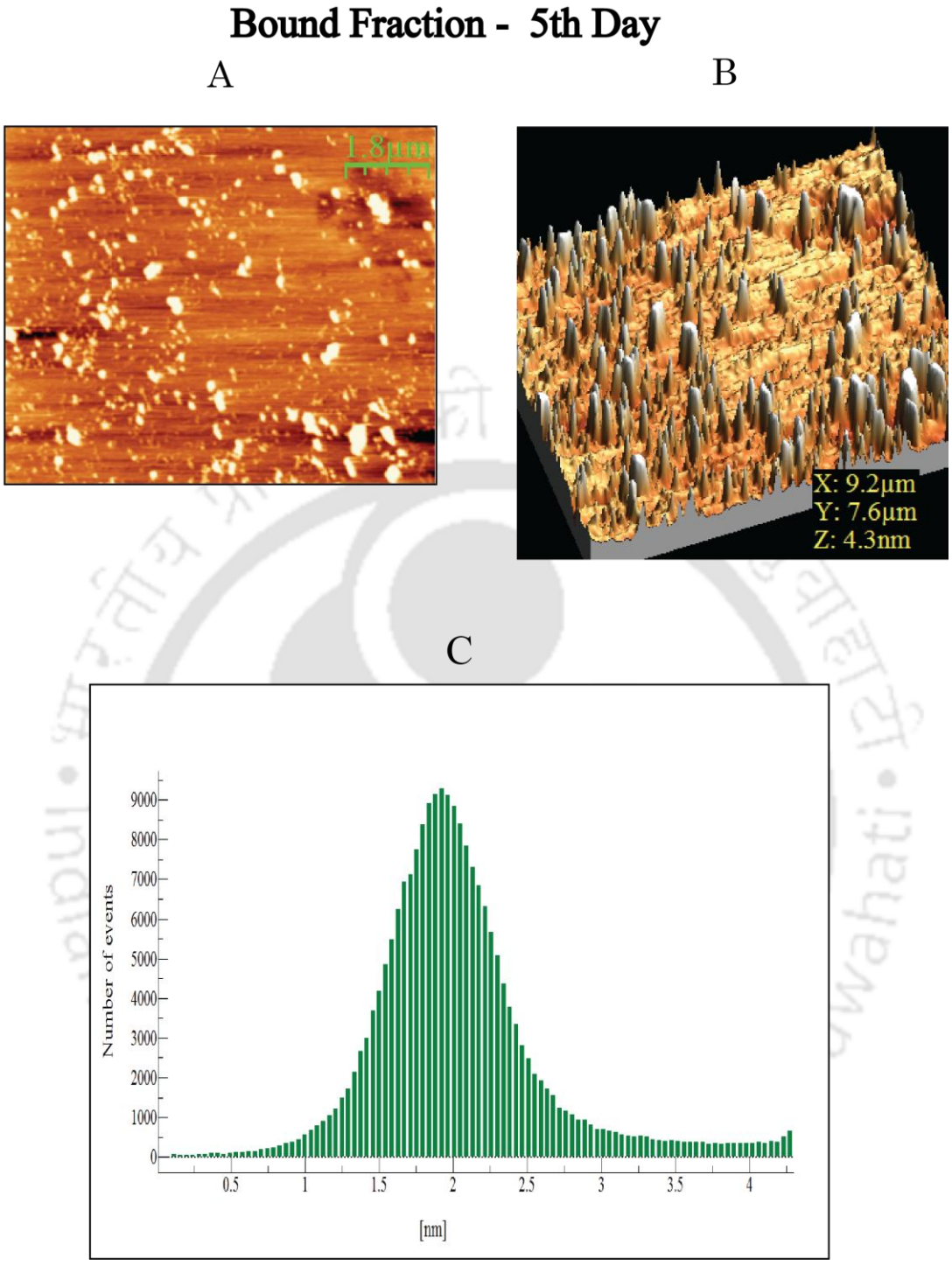

Figure 5.1.6.4 (g): AFM images of bound fraction 5th day(1.8 µm scale)

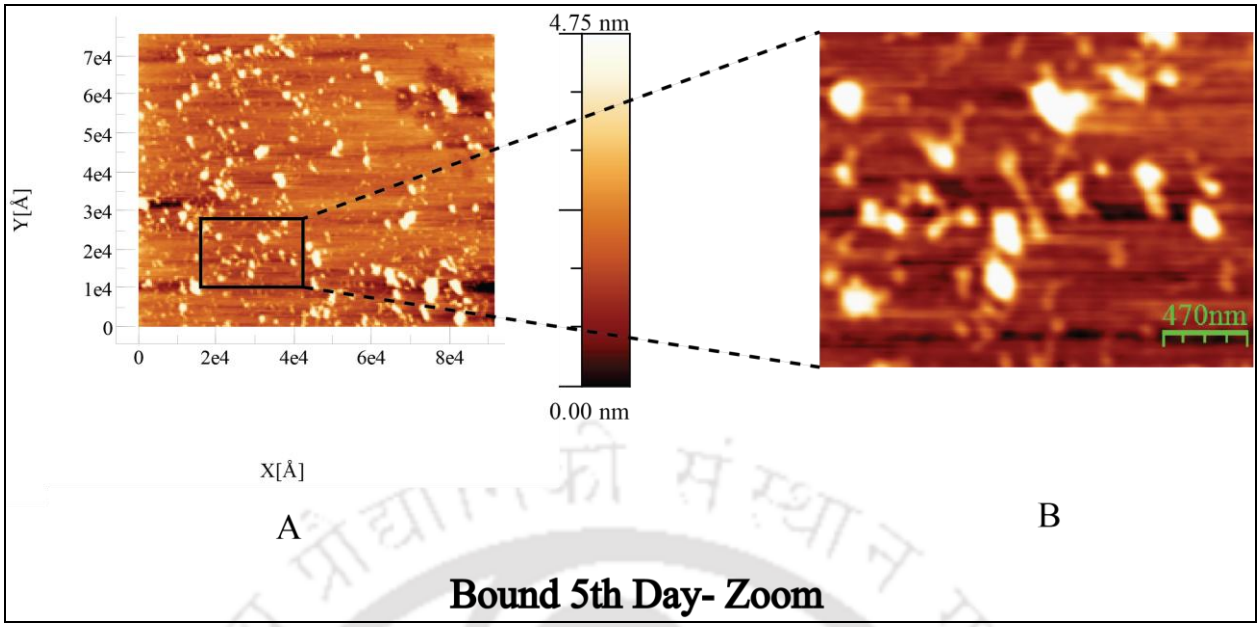

Figure 5.1.6.4 (h): AFM images of bound fraction 5th day(1.8 µm- Zoom)

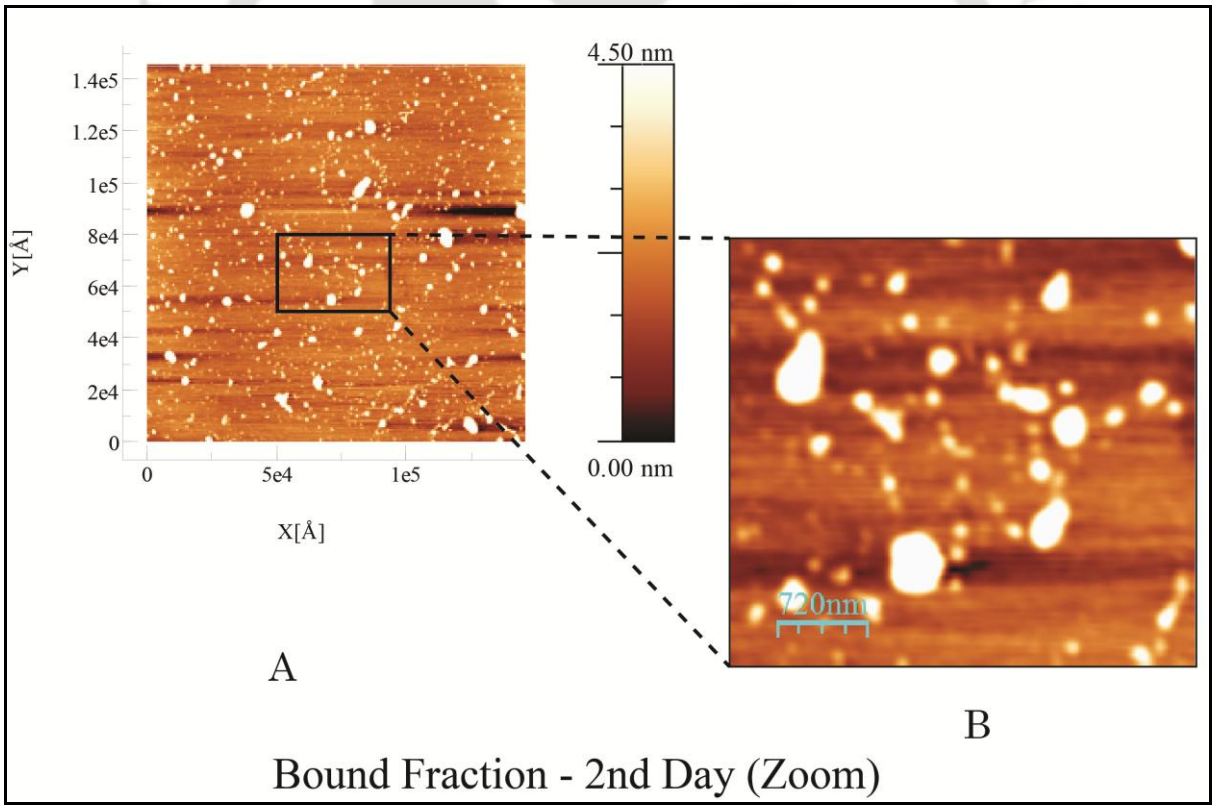

Figure 5.1.6.4 (i): AFM images of bound fraction 2nd day(2.9 µm- Zoom)

5.1.6.5 Steady state anisotropy

Steady state anisotropy measurements were performed with a Spectrofluorometer **(FluoroMax®-4 Horiba Scientific Jobin-Yvon)** equipped with a Xe-lamp**.** Measurements are performed using auto polarizers in L-format **(FM4-2000 model no.)** geometry. Data acquisition and analysis was performed by the use of **FluorEssence™ software**. An excitation wavelength of 295 nm with a slit width of 1 nm and an emission wavelength of 350 nm with different slit widths (depending on intensity) were used for recording tryptophan steady state anisotropy values. Three acquisitions were averaged to give a final value of r_{ss}. Error bars represent the standard deviation of the anisotropy measurements. All the measurements were performed at room temperature. This methodology eliminates the use of external probes for recording the $\mathbf{r_{ss}}$ values for aggregates. NATA(N-Acetyl-L-tryptophanamide) in pH 12.2 buffer was used as a standard control for experiments.

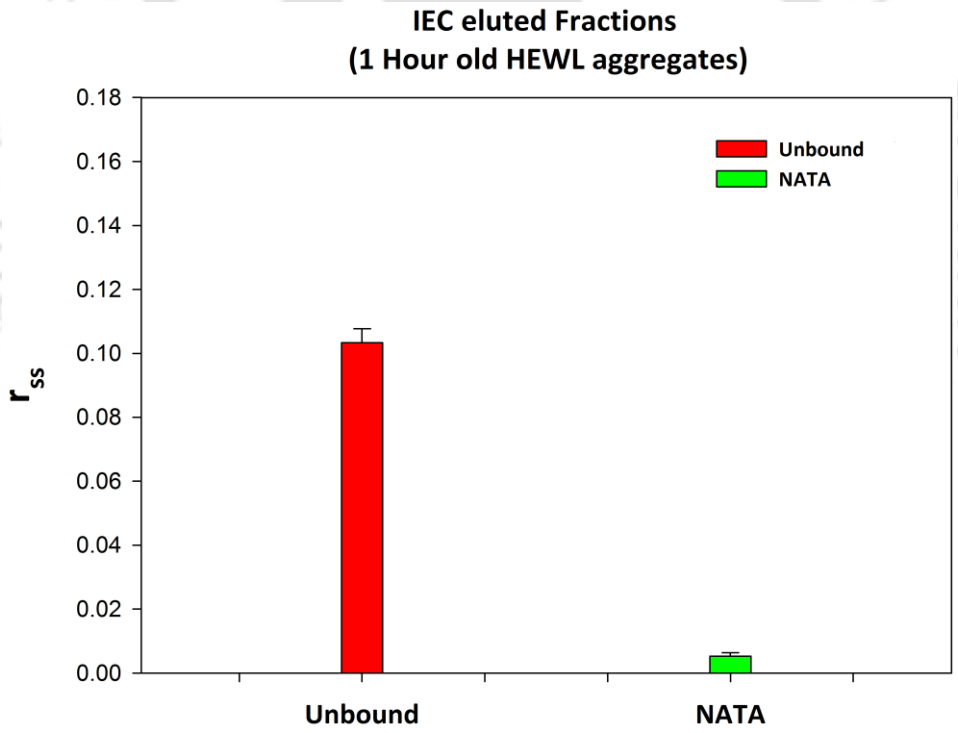

Figure 5.1.6.5 (a): Tryptophan steady state anisotropy of IEC eluted fractions for **1 hour** old HEWL aggregates in pH 12.2. Unbound (**U**) for 1 hour represents 2.32-2.82 mL of fraction.

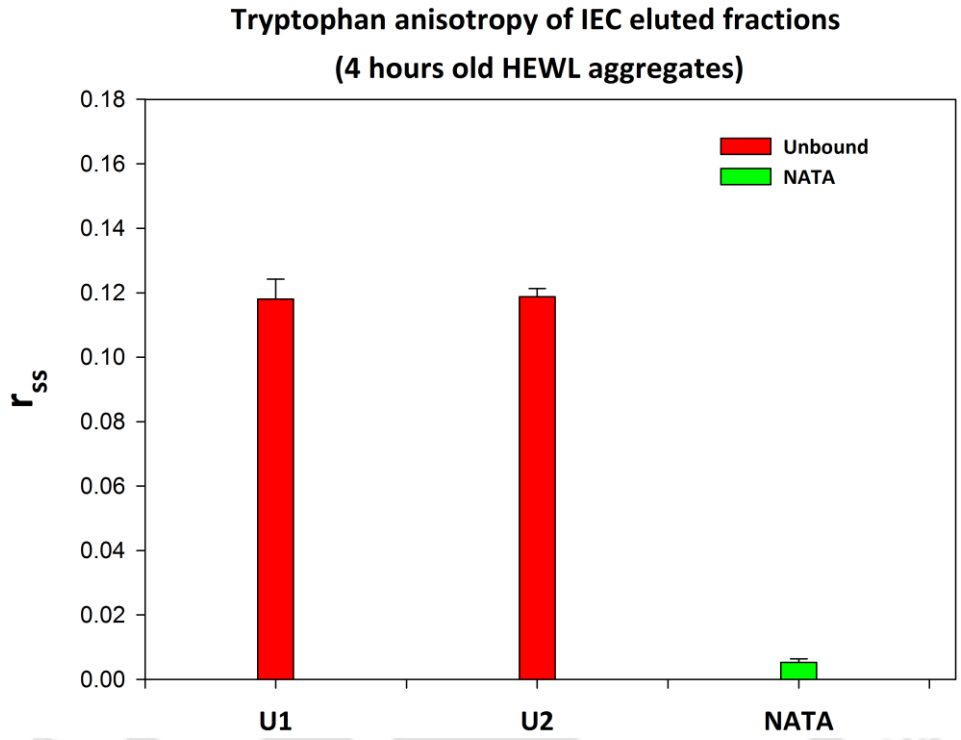

Figure 5.1.6.5 (b): Tryptophan steady state anisotropy of IEC eluted fractions for **4 hours** old aggregates. **U1:** 0.48-0.98 mL & **U2:** 1.44-1.94 mL.

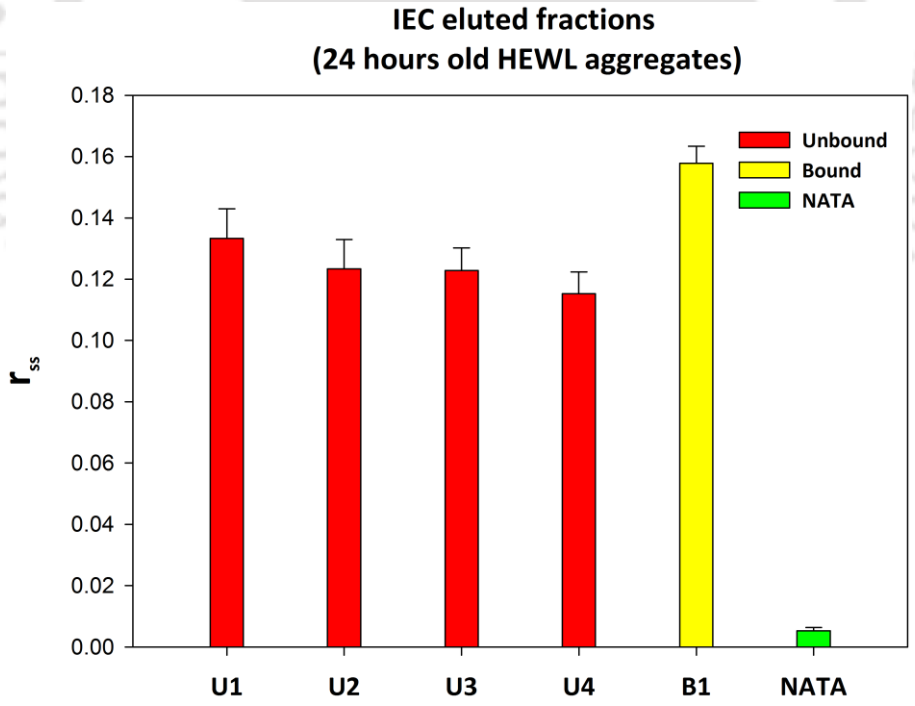

Figure 5.1.6.5 (c): Tryptophan steady state anisotropy of IEC eluted fractions of HEWL aggregates incubated for **24 hours** in alkaline pH 12.2. Fractions are numbered as per their order of elution. Unbound **(U)** fractions: **U1:** 0.1-1.1 mL, **U2:** 1.2-1.7 mL, **U3:** 4.95-5.45 mL & **U4:** 5.51-6.01 mL. Bound **(B)** fraction: **B1:** 45.25-45.75 mL.

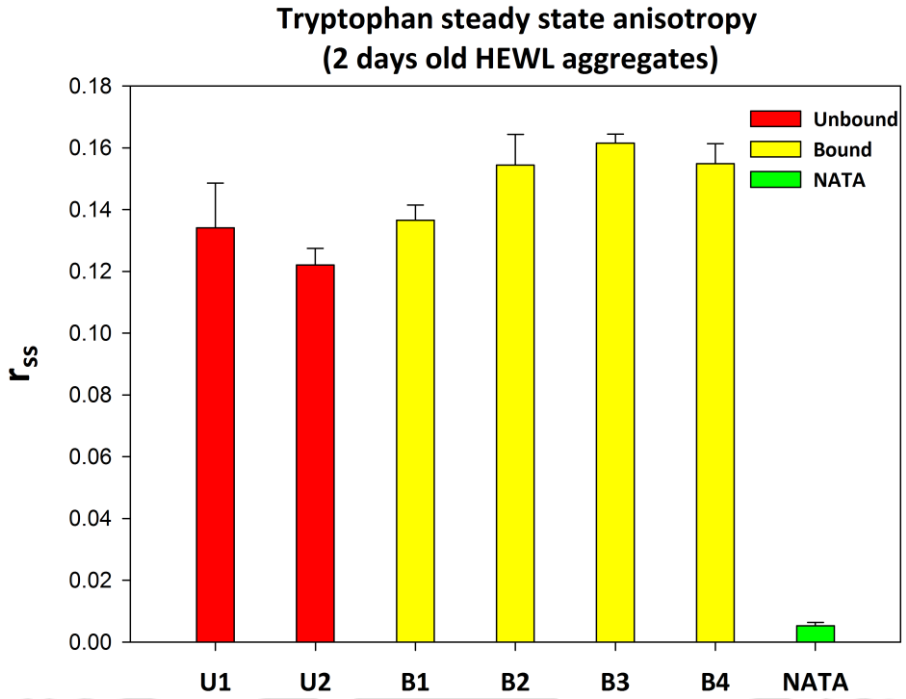

Figure 5.1.6.5 (d): Tryptophan steady state anisotropy of IEC eluted fractions for **2 days** old HEWL aggregates. Unbound **(U)** fractions & Bound **(B)** fractions: **U1:** 0.5-1.0 mL, **U2:** 1.23-1.73 mL, **B1:** 39.06-39.56 mL, **B2:** 39.86-40.36 mL, **B3:** 40.6-41.1 mL & **B4:** 41.44-41.94 mL.

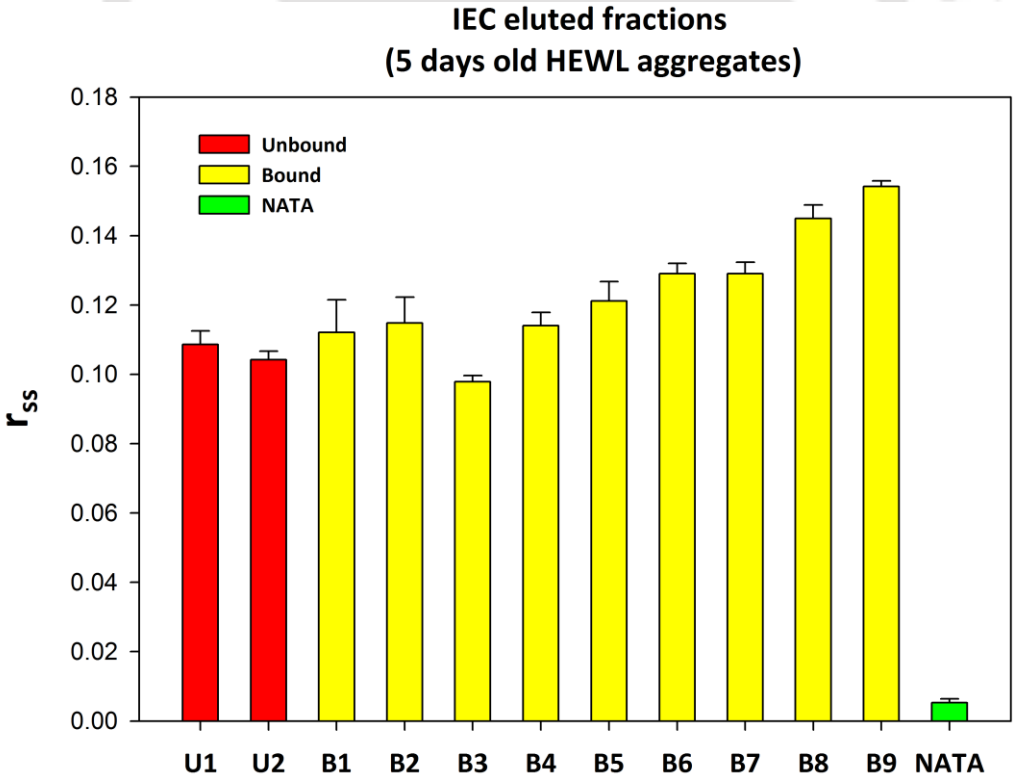

Figure 5.1.6.5 (e): Tryptophan steady state anisotropy of IEC eluted fractions for **5 days** old HEWL aggregates. Unbound **(U)** fractions & Bound **(B)** fractions: **U1:** 0.93-1.43 mL, **U2:** 1.59-2.09 mL, **B1:** 41.85-42.35 mL, **B2:** 42.67-43.17 mL, **B3:** 43.6-44.1 mL, **B4:** 44.76-45.26, **B5:** 46-46.5 mL, **B6:** 46.78-47.28 mL, **B7:** 47.6-48.1 mL, **B8:** 48.2-48.7 mL & **B9:** 49.42-49.92 mL.

Tryptophan steady state anisotropy can be used as attractive measure of aggregation. Steady state anisotropy data indicates a higher r_{ss} value for unbound fractions of 4 hours old aggregates than that of 1 hour old aggregates [**Figure 5.1.6.5 (a) & (b)**]. This is due to the formation of larger aggregates as a result of longer incubation period of HEWL in alkaline pH 12.2. In case of 24 hours and 2 days old aggregates, bound fractions display comparatively higher r_{ss} value than unbound fractions [**Figure 5.1.6.5 (c) & (d)**]. This suggests that the bound fractions mainly constitute of larger aggregates and the unbound fractions are composed of relatively smaller aggregates. The larger aggregates as observed in bound fractions can be referred to as compact and interlinked by disulfide bonds. This is confirmed from SDS-PAGE results for bound fractions of 2 days and 5 days old aggregates. However, aggregates present in unbound fractions break down to monomer or dimer units when subjected to high temperature which is visible in SDS-PAGE.

The possible explanation for this result can be that the unbound fractions represent loosely associated aggregates or loosely associated monomeric units. The increasing trend seen in r_{ss} for bound fractions in 5 day old aggregates, with the order of elution, reflects an increase in size of the aggregates [**Figure 5.1.6.5 (e)**]. This shows that larger aggregates, due to higher anionic binding sites, elute later i.e. at a high concentration of salt.

5.1.7 Conclusion

Ion exchange chromatography has been used as a characterization technique to quantify aggregation kinetics of HEWL in pH 12.2, in terms of rate of disappearance of native monomer from the population. Various techniques have been used to carry out a detailed structural investigation of the species formed during aggregation process. Chromatographic profile of unbound protein fractions showed a decrease in peak area with time. Broad observation time frame allowed us to carry out a detailed characterization as the longer time scale (5 days incubation) resulted in significant amount of oligomer species to be populated. The experiment demonstrates the changes in peak shape and peak intensity as well as the % of fractions bound to the column with different incubation period during aggregation of HEWL.

Interestingly, it was found that different species formed on the aggregation pathway of HEWL have different charge distribution since they eluted at different ionic strengths. Elution profiles clearly confirm the polydispersity of the aggregates as expected. The charge differences could be due to heterogeneity in the system arising due to conformational change in the species and the no of monomers associated with them. The difference in size and shape of different oligomers leads to heterogeneous charge distribution which is reflected in the elution profile. Hence, the charge differences on surface of intermediate species formed in the aggregation pathway predominantly determines the interactions of unique molecular assemblies with the IEC matrix. Our results give us an in-depth exploration of different intermediate oligomeric species involved in the aggregation pathway. All high molecular weight oligomeric species were observed only in bound fractions for samples incubated for more than 24 hours. This shows the formation of covalently bonded, thermally stable and high molecular weight oligomers as they didn't disintegrate after subjecting to heat and disulfide reducing agent (β-ME) while performing SDS-PAGE.

References

1. Hill, S. E., Robinson, J., Matthews, G. & Muschol, M. Amyloid protofibrils of lysozyme nucleate and grow via oligomer fusion. *Biophys. J.* **96,** 3781–3790 (2009).

2. Withka, J., Moncuse, P., Baziotis, A. & Maskiewicz, R. Use Of High-Performance Size-Exclusion, Ion-Exchange, And Hydrophobic Interaction Chromatography For The Measurement Of Protein Conformational Change And Stability. *J. Chromatogr.* **398,** 175–202 (1987).

3. Yao, Y. & Lenhoff, A. M. Electrostatic Contributions to Protein Retention in Ion-Exchange Chromatography. 1. Cytochrome C Variants. *Anal. Chem.* **76,** 6743–6752 (2004).

4. Xu, X. & Lenhoff, A. M. A predictive approach to correlating protein adsorption isotherms on ion-exchange media. *J. Phys. Chem. B* **112,** 1028–1040 (2008).

5. Márquez-Escalante, J. a, Figueroa-Soto, C. G. & Valenzuela-Soto, E. M. Isolation and partial characterization of trehalose 6-phosphate synthase aggregates from Selaginella lepidophylla plants. *Biochimie* **88,** 1505–1510 (2006).

6. Le, A., Barton, L. D., Sanders, J. T. & Zhang, Q. Exploration of bovine milk proteome in colostral and mature whey using an ion-exchange approach. *J. Proteome Res.* **10,** 692–704 (2011).

7. Nadal, P., Canela, N., Katakis, I. & O'Sullivan, C. K. Extraction, isolation, and characterization of globulin proteins from lupinus albus. *J. Agric. Food Chem.* **59,** 2752–2758 (2011).

8. Maleksabet, N., Masoumian, M. R., Saeedinia, A. & Mohammadi, R. The structural characterization of Recombinant Human Interferon Gamma. *J. Biol. Sci.* **8,** 1087–1091 (2008).

9. Cao, A., Hu, D. & Lai, L. Formation of amyloid fibrils from fully reduced hen egg white lysozyme. *Protein Sci.* **13,** 319–324 (2004).

10. Ahn, M. *et al.* Analysis of the Native Structure, Stability and Aggregation of Biotinylated Human Lysozyme. *PLoS One* **7,** (2012).

11. Ravi, V. K., Swain, T., Chandra, N. & Swaminathan, R. On the characterization of intermediates in the isodesmic aggregation pathway of hen lysozyme at alkaline pH. *PLoS One* **9,** 1-12 (2014).

12. Homchaudhuri, L., Kumar, S. & Swaminathan, R. Slow aggregation of lysozyme in alkaline pH monitored in real time employing the fluorescence anisotropy of covalently labelled dansyl probe. *FEBS Lett.* **580,** 2097–2101 (2006).

13. Yang, M., Dutta, C. & Tiwari, A. Disulfide-Bond Scrambling Promotes Amorphous Aggregates in Lysozyme and Bovine Serum Albumin. *J. Phys. Chem. B* **119,** 3969–3981 (2015).

14. Tsai, C. (2007). Purification and Characterization. In *Introduction to Structure, Function and Informatics*, Biomacromolecules (pp. 34-38). Newyork: John Wiley & Sons.

5.2 Molecular weight distribution analysis of Hen Egg-White Lysozyme nanoparticles by *Size exclusion chromatography*

5.2 Introduction

Size exclusion chromatography is otherwise referred to as molecular sieve, gel filtration or gel permeation chromatography. The sieving properties of a porous matrix are used to achieve separation on the basis of size and shape of the molecules. In gel filtration chromatography, the sorting of macromolecules occurs on the basis of their size such that the larger molecules migrate faster as compared to the smaller ones.

Characterization of aggregates in terms of their molecular weight or size is a necessary step. The correlation between elution volume or residence time to molar mass can be used to determine molar mass distribution of aggregates[1].

We have used SEC to demonstrate the polydisperse nature of HEWL aggregates, indicating the presence of higher order oligomers as well as monomers. In this study we have shown the chromatographic pattern obtained for HEWL aggregates transferred to pH 7, at both ionic strength of 20 mM and 50 mM Sodium phosphate buffer. The nanoparticles synthesized were analyzed by SEC. In the present work, we have analyzed the wide distribution of 7-day old HEWL soluble aggregates transferred to pH 7.0 by means of size exclusion chromatography. Previously, our lab has reported HEWL aggregates to be globular in shape. DLS results have shown the z- average hydrodynamic radius for 7 day old aggregates to be ~ 17.33 nm.

Size exclusion chromatography is characterized by separation based on molecular size of the sample. Our objective was to achieve the separation of different intermediate and oligomeric species involved in HEWL aggregation pathway on the basis of their hydrodynamic volume.

In this part of the thesis, the research question which we have addressed: **a) what information can be obtained from average molecular weight distribution of HEWL aggregates transferred to pH 7.0?**

5.2.1 Materials and methods

5.2.1.1 Synthesis of HEWL nanoparticles

120 µM HEWL was incubated in 50 mM Sodium phosphate buffer, pH 12.2 for 7 days at room temperature.

5.2.1.2 Transfer to pH 7.0

Sample A: Buffer exchange was performed by means of a centrifugal concentrator **(Vivaspin® 15R, 5000 Da MWCO GE Healthcare)**. The sample containing 120 µM HEWL aggregates in pH 12.2 incubated for 7 days was finally replaced to 20 mM Sodium phosphate buffer, pH 7 (Ionic strength changed). Buffer exchange and sample concentration was done simultaneously with the help of concentrator. There were no visible precipitates after buffer but the sample appeared turbid. Before injecting into the column, the sample was filtered through 0.22 µm filter **(Syringe filter sterile Uniflo^{TM}, GE healthcare life sciences Whatman^{TM} Cat no.9908-2502).** Final concentration of the sample was found to be 72 µM after filtration.

Sample B: Sample constituting of 120 µM HEWL aggregates incubated in pH 12.2 for 7 days was transferred to 50 mM Sodium phosphate buffer, pH 7.White precipitates were observed in large amounts after the buffer exchange which were removed by filtering the protein sample through 0.22 µm filter. Hence, it is expected that very large aggregates were separated out as precipitates by filtration. Final concentration of the sample was found to be 68 µM.

Oligomer concentration here refers to the original monomer protein concentration incubated for aggregation at pH 12.2.

5.2.2 Experimental Chromatographic conditions

Mobile phase: 50 mM Tris-HCl, pH 7.5, 0.1 M KCl buffer was used for equilibration, calibration as well as elution from the column. KCl salt is added to the buffer in order to avoid any non-specific interactions with the column matrix.

Equilibration of the column: The column was equilibrated with 1 CV (column volume) of running buffer. Degassed and filtered buffers were used to avoid the formation of air bubbles in the packed column during the run.

Flow rate: Volumetric flow rate of 1 mL/min or linear flow rate of 11.31 cm/h was maintained throughout the experiment.

Sample volume: Approximately 1 % of column volume (CV) i.e. 3.3 mL of sample volume was injected into the column.

Column pressure: 0.25 – 0.28 MPa was maintained while running the sample in the column. Maximum operating back pressure for the column is 0.3 MPa, 3 bar, 42 psi. Upper pressure limit for the column was set at 0.4 MPa.

Degassed and filtered buffers were used to avoid the formation of air bubbles in the packed column during the run. The column was equilibrated with 1 column volume (CV)[1] of running buffer. Sample was applied through a syringe to the column. Pump was used in the chromatography system to pump the buffer onto the column. For elution, there is no requirement of any gradient and molecules are eluted in order such that molecules with largest hydrodynamic volume elutes first. It should be noted that the buffer used for equilibration and elution are the same i.e. isocratic elution was performed. While equilibrating the column with the buffer, baseline was monitored at 280 nm until a stable baseline is achieved. The column was requilibrated with 1 CV of running buffer before every run. The transferred samples were applied to the column equilibrated with running buffer. At the end of each run, column was washed with 1 CV of 0.5 M NaOH solution at a flow rate of 1 ml/min to remove any non-specifically bound proteins. For long term storage, the column was washed with 1 CV of distilled water followed by 1 CV of 20 % ethanol.

5.2.2.1 Column characteristics

Cross-linked polymers such as agarose gels are very efficient in separation of proteins and other macromolecules due to their appreciable swelling properties. Even gels of dextran polymer, Sephadex, polyacrylamide has been proved to be useful in separation of proteins and polymers. In case of Superdex, cross linked agarose based matrix ensures high mechanical strength of the medium. In addition, covalently linked dextran chains endow the matrix with excellent gel filtration properties. Superdex is the suitable choice among the wide variety of gel filtration media available due to high stability, high recovery and high selectivity with wide M_r range. Long columns are better for performing size exclusion as the separation depends on the column length. Resolving power of a column increases with the

[1] **CV** – it is the total column volume and is equivalent to the volume of the packed bed.

square root of the column length. Thus, longer columns effectively increase the resolution power and a better separation is achieved.

Hiload® 26/60 Superdex 200® Prepgrade (**GE Healthcare, Life Sciences**)

Hiload® 26/60 Superdex 200® Prepgrade	
Matrix	Dextran covalently linked to highly cross-linked agarose
Mean particle size	34 µm(Average) Narrow particle distribution
Column volume	330 ml
Column length(bed height)	60 cm
Column bore(inner diameter	26 mm
Fractionation range for globular proteins	10 – 600 kDa
Theoretical plates(N/m)	> 13,000
pH stability	3-12

Table 5.2.2.1: Column specifications of Superdex 200 used for SEC are listed in the table. It provides high resolution with a broad fractionation range for globular proteins.

One of the key features of the Superdex column is the size-cut off values or the fractionation range which has a lower limit of 10 kDa and upper limit of 600 kDa. Molecules with molecular weight range which falls within the fractionation range will be separated. However, molecules with size beyond the fractionation range will be excluded from entering the pores of the matrix and will elute in the void volume. In order to resolve HEWL monomer and higher order oligomers which are copopulated in the distribution, column with correct operating range of size is mandatory. Selectivity of the gel filtration medium is largely dependent on the molecular weight range cut off for separation of molecules. High resolution fractionation is essential to separate monomers from aggregates. Spectroscopic UV detectors were used to continuously monitor the concentration of protein in the eluted fractions. UV absorption at 280 nm was used to detect protein in the eluent volume.

Chromatography separation was achieved with a controlled flow rate by the use of **ÄKTApurifier™** FPLC **(GE Healthcare)** chromatography system.

5.2.3 Calibration of the column with protein standards

5.2.3.1 Molecular weight markers kit for Gel filtration

Size exclusion chromatography was performed by connecting the column to FPLC apparatus AKTA. Standardization of the column was performed using molecular weight markers kit for gel filtration **(Sigma Aldrich, Catalog no. MWGF 200 kit)** consisting of proteins with a range of molecular masses from 12.4-200 kDa. The elution peak at 258.3 ml corresponds to monomeric HEWL (molecular mass-14.3 kDa) which was used as a standard for comparative analysis.

For calibration, protein samples of a broad range of molecular weight distribution were used. Individual protein standards were dissolved in equilibration buffer at recommended concentrations (1.5 mL of each was prepared freshly) and the standards were mixed well before injecting into the column. HEWL in the calibration mix served as external standard for monomer molecular weight. Calibration standards were run in the same running buffer as that used for the sample run for accurate molecular weight determination. Calibration curve was used as a standard to determine or to get an estimate of the molar masses of HEWL nanoaggregates. The height of the peaks depends on the relative concentration of the different protein standards loaded into the column. The elution peak of the proteins with high molecular weight showed up at a lower value of Ve as compared to those with low molecular weight. Mixture of molecular mass standards was used as listed in table:

Standards	Elution volume(Ve) ml	Molecular weight (kDa)
β-Amylase	171.2	200
Alcohol Dehydrogenase from yeast	182.7	150
Bovine serum albumin	202.3	66
Carbonic anhydrase from bovine erythrocytes	236.8	29
Hen egg white lysozyme	258.3	14.3
Cytochrome c from horse heart	289.1	12.4

Table 5.2.3.1: Calibration of Superdex column with molecular weight standards.

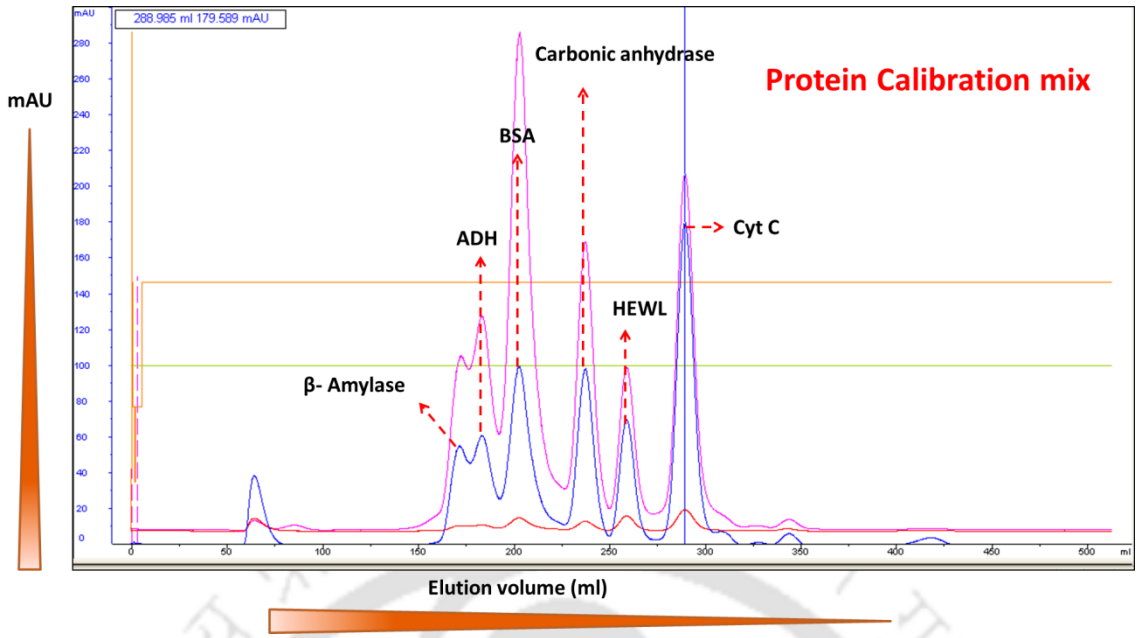

Figure 5.2.3.1 (a): Chromatogram of protein standard mix. Colour codes: —— depicts the profile for mAU measured at 215 nm and —— represents mAU recorded at UV 280 nm. —— is for mAU recorded at 254 nm.

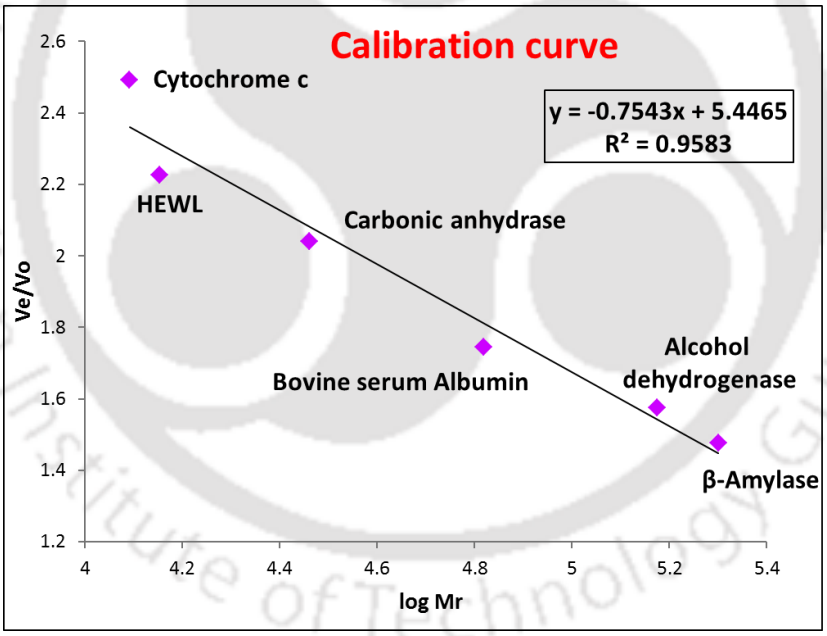

Figure 5.2.3.1 (b): Calibration curve for Superdex column. Ve/Vo is plotted as a function of log of molecular weight. Flow rate = 1 ml/min.

Calibration curve is required to establish a relationship between Ve[2] and mass or molecular weight (M_r)[3] of the solute. Molecular sizes of unknown proteins can be estimated from the calibration curve which is constructed with proteins of known molecular weight. In order to determine the molecular weight, calibration standards are first run into the gel

[2] **Ve** – Elution volume measured from the chromatogram. It is related to molecular size of the molecule.
[3] **M_r** – Relative molecular weight.

chromatography system. Calibration curve is plotted between Ve/Vo and log M_r. Void volume of the column was estimated with blue dextran which was found to be 116 ml. The molecular weight calibration was done by using proteins: β-Amylase (200 kDa), alcohol dehydrogenase (150 kDa), bovine serum albumin (66 kDa), carbonic anhydrase (29 kDa), and hen egg white lysozyme (14.3 kDa) and cytochrome c (12.4 kDa). Elution volume was determined for each of the respective protein standards.

The dependence of elution volume on molecular weight (M) can be expressed as:

$$\text{Log } M = A - B.Ve \quad \ldots\ldots (1)$$

or it can be represented as:

$$\text{Log } M = f(Ve) \quad \ldots\ldots (2)$$

Relationship was established between log M_r and V_e/V_o in the calibration curve. Peaks of interest are well resolved as depicted from the chromatogram of protein standard mixture [**Figure 5.2.3.1 (a)**]. Proteins were fractionated with good resolution and no peak broadening effect was observed. Size calibration of the column was performed in order to determine Mw of oligomers present in HEWL nanoparticles. No aggregates were detectable in SEC standards run. Protein molecules of smallest molecular weight such as cytochrome c (12 kDa) are retained for longer time in the column as compared to other proteins and are eluted as the last fraction in the standard run.

5.2.3.2 Calculation of K_{av}

Partition coefficient, K_{av} can be defined by the equation:

$$K_{av} = (Ve - Vo) / (V_t - Vo) \quad \ldots\ldots (3)$$

V_t = total volume of the column which is equivalent to 330 ml.

Vo = Column Void volume which is equal to elution volume for Blue Dextran 2000.

Ve = Measured elution volume of the protein

$V_t - Vo$ = Volume of the buffer inside the matrix which is available for diffusion of small molecules. This term also includes the volume of the solid material which forms the matrix.

K_{av} is an elution volume parameter which is calculated from calibration curve. This parameter is very useful in molecular weight determination of unknown species.

K_{av} is calculated for each of the protein standards from their elution volume using eq^{n} (3). It is plotted against corresponding molecular weight (log scale). It is fitted with straight line equation and linear regression value is obtained.

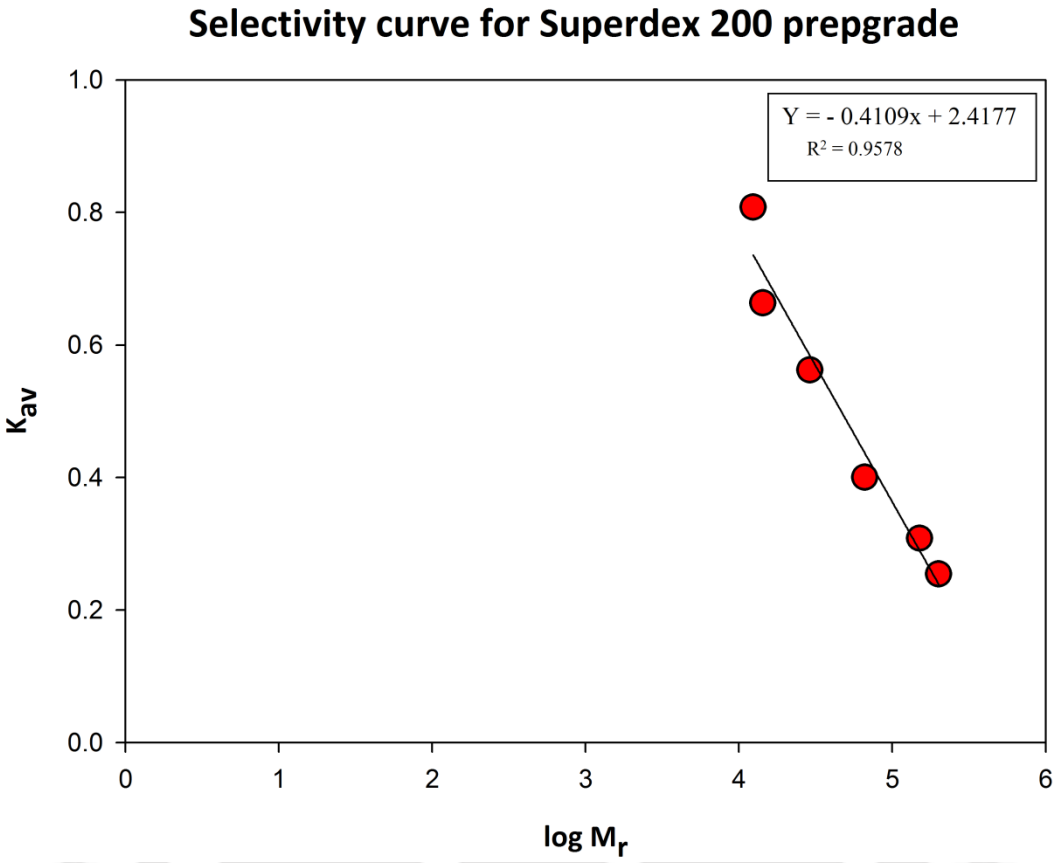

Figure 5.2.3.2 (a): Selectivity curve of Superdex 200 prepgrade for globular proteins. It is represented by a plot of K_{av}, partition coefficient vs. log of the molecular weight for a set of standard proteins.

As depicted from the selectivity curve, linearity is observed in the range of K_{av} = 0.25 to K_{av} = 0.67. This linear part of the curve is used to determine the fractionation range of the column. Molecules which fall within the fractionation range will be separated with high resolution. In case of low molecular weight protein such as cytochrome c, K_{av} value obtained was 0.81 which is close to 1. Whereas, in case of high molecular weight protein such as β–amylase, K_{av} value obtained was 0.25.

5.2.4 Void volume determination

Blue Dextran was dissolved in equilibration buffer at a concentration of 2 mg/mL. It forms a blue coloured solution in aqueous buffer. Sample volume[4] used was less than 2 % of total gel bed volume (4 mL). Sample volume is one of the critical parameters which affect the resolution of separation. In order to achieve maximum resolution, sample volume should not be more than 2 % of the total column volume. Flow rate while running the dextran in the column was maintained at 1 mL/min. Molecular weight of blue dextran is 2000 kDa, due to very high molecular weight they do not enter the matrix and get eluted in the void volume. The void volume was determined from the leading peak. Void volume[5], Vo for the column was estimated to be 116.76 mL.

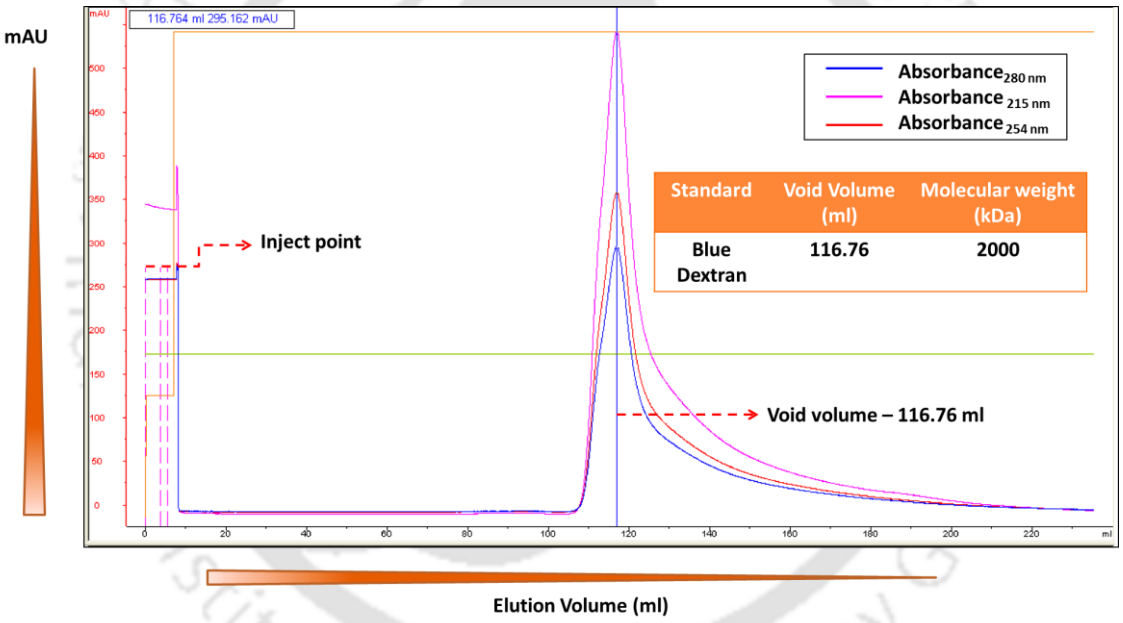

Figure 5.2.4.1: Estimation of void volume Vo for Superdex column with blue dextran. The void volume peak is observed at Ve of 116 mL.

[4] **Sample volume** – It is expressed as % of the total column volume.

[5] **Vo** – Void volume is the elution volume for larger molecules which are excluded from the gel filtration matrix as they are larger than the largest pores of the matrix.

5.2.5 Review of Literature

Size exclusion chromatography has been employed previously as a characterization tool for extracting information about large oligomeric structures of HEWL[2]. Both monomeric species as well as pre fibrillar oligomeric species were clearly evident from the SEC chromatogram in the distribution. Two distinct peaks corresponding to very high molecular weight oligomers and HEWL monomer were visible in the chromatogram. In order to induce fibril formation, 1 mM concentration of HEWL was incubated in pH 2.2, at 57˚C.

Previously, a single step isolation method of lysozyme from egg white by gel-filtration chromatography was reported[3] (**Islam et al., 2006**). Sephadex, a dextran based matrix was used to purify the protein by exploiting the pH dependent interactions. The efficient and fast chromatographic method resulted in yielding a pure form of lysozyme with 99 % activity. A report was published on the structural studies of Hen egg white lysozyme in which a comparative study was carried out between the dimer and monomer. Size exclusion FPLC was used to separate the cross linked dimer from monomer[4].

Muneeruddin and co-workers have shown in their study the significance of SEC as an analytical tool in combination with native ESI MS[5]. It made possible the detection of heterogeneous protein oligomers of serum albumin in solution. The critical analysis of mass profile as well as charge state distribution revealed the conformational identity of multiple species present in dynamic equilibrium with each other. It aided in separation of small oligomers on the basis of size. However, one of the factors which limits the applicability of this method is the use of volatile electrolytes as solvent.

There are numerous problems associated with characterization of aggregates by SEC which arises due to the transient nature of these aggregates. Moreover, the possibility of dissociation of aggregates while undergoing fractionation by SEC also exists. Henceforth, we have addressed these issues by allowing the aggregates to be incubated in alkaline pH for 7 days before transfer to pH 7.0. Incubation of HEWL protein assemblies for longer days in alkaline pH 12.2 strengthens them against any kind of repulsive destabilizing forces due to the formation of intermolecular disulfide bonds[6] **(Ravi et al., 2014)**.

Previously our lab has reported the heterogeneity of HEWL aggregates at pH 12.2. Gel filtration chromatogram revealed the heterogeneous distribution of HEWL aggregates[7].

5.2.6 Results and discussion

The chromatogram as shown in the [**Figure 5.2.6.1**] clearly represents the heterogeneous distribution of HEWL nanoaggregates. Higher order oligomers are discernible from the native population even though the peaks are overlapping and continuous. SEC analysis shows that the aggregate population of HEWL after transfer to pH 7.0 is polydisperse and the distributions overlap considerably. SEC was used as means to quantify the population of non-native aggregates and fraction of native population present in HEWL nanoparticles.

For samples transferred to pH7, 20 mM sodium phosphate buffer: The most significant elution peak appears at 256.3 ml (63.7 mAU) corresponding to HEWL monomer indicating a molecular mass of approximately 14 kDa. The second major elution peak appears at 285 ml (56.5 mAU).The data suggests the presence of monomeric fraction with altered conformation which shows up as the second major peak in the chromatogram. The eluents were monitored at 280 nm.

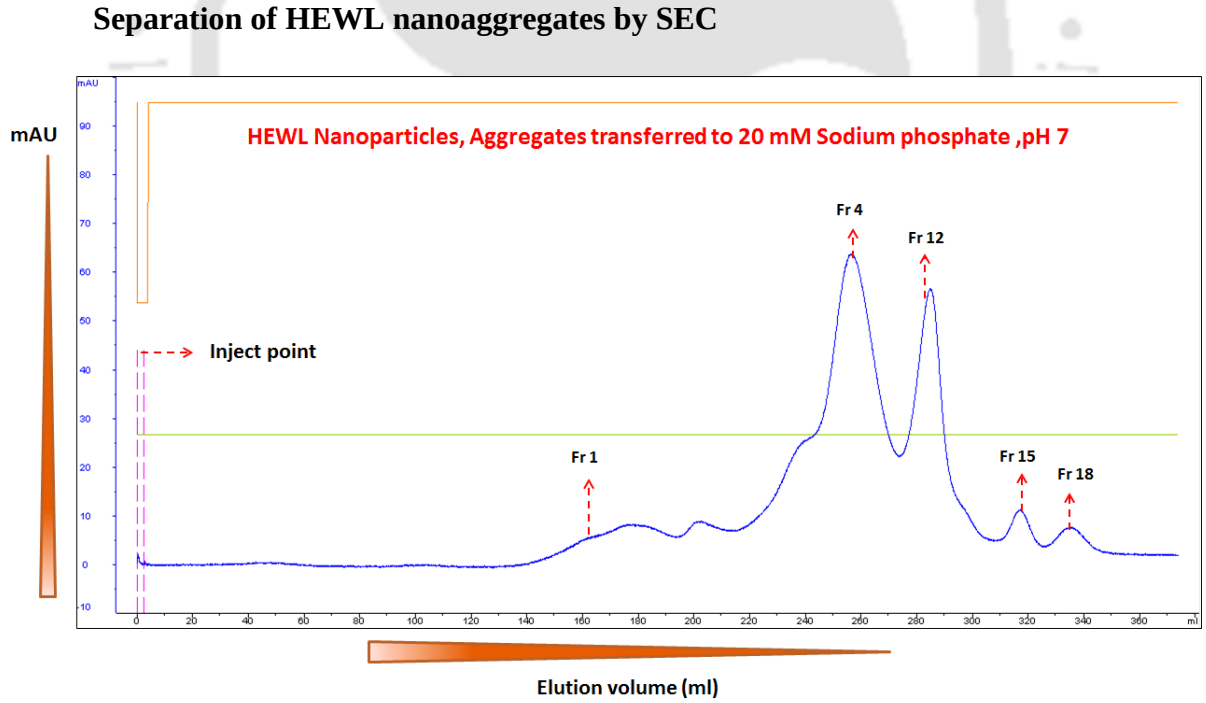

Figure 5.2.6.1: Conformational characterization of HEWL aggregates transferred to pH 7.0 (SEC).The peak for fraction 4 eluted at Ve equal to 255 ml which corresponds to that of HEWL monomer.

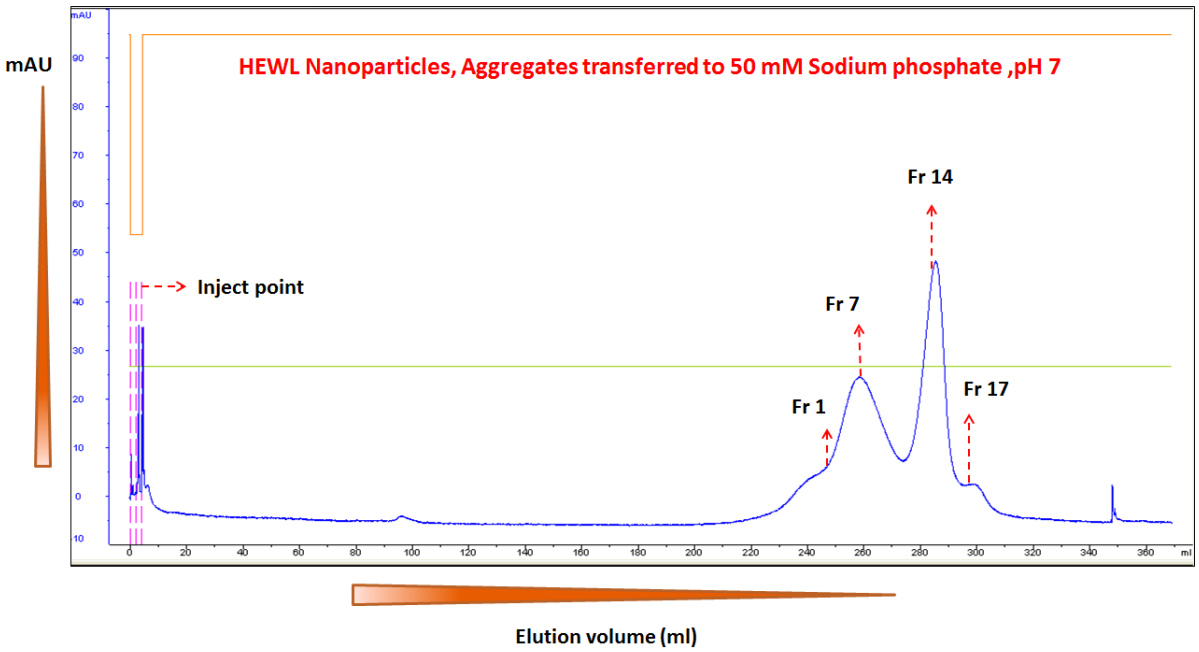

Figure 5.2.6.2: SEC chromatogram of HEWL nanoparticles. Elution profile-The X- axis represents elution volume i.e. the volume passed over the column (in mL) and Y- axis represents absorbance at 280 nm (in milliabsorbance units).

In case of aggregates transferred to pH 7.0 (20 mM, sodium phosphate buffer), it can be clearly figured out from the elution profile that high molecular weight oligomers are retained in the population after transfer. Presence of native monomeric population was predominantly observed in the chromatogram. The elution peak was broader but coincided to that of the standard HEWL in native state **[Figure 5.2.3.1 (a)]**.For the standard HEWL run in gel filtration chromatography, elution peak was observed at Ve equal to 258 ml. Similarly, in the chromatogram of transferred samples, elution peak for native monomer was seen at Ve equal to 255 ml **[Figure 5.2.6.1]**. The second major population is marked as fraction 12 which eluted at Ve of 285 ml. Surprisingly, even though this fraction eluted later than the native monomer but they appeared at the same monomeric band in SDS PAGE. Hence, it is reasonable to conclude that fraction eluted at 285 ml constitutes of monomer population but with altered conformation (non-native). The peak for fraction 1 at Ve of 165 ml represents high molecular weight aggregates **[Figure 5.2.6.1]**. K_{av} value obtained for fraction 1 as calculated from its measured elution volume is 0.22 which is almost close to K_{av} value for β-amylase (K_{av} = 0.25). This confirms the presence of high molecular weight oligomers in fraction 1 with Mw close to 200 kDa as estimated from K_{av} value.

Large protein aggregates have a wide size distribution as interpreted from the experimental data. The earliest eluting fractions were mostly composed of high Mw aggregates.

It is very unlikely that aggregate peak is monodisperse because the peaks are not completely resolvable. They seem to be broad and continuous in the elution profile. SEC chromatogram for transferred samples gave us a relative estimate of the polydispersity for size distribution of HEWL aggregates. Presence of multiple oligomers in the distribution results in broadening of the peaks for larger aggregates. But the large fractionation range of the column makes it possible to discern the contributions from different species in the SEC chromatogram.

Higher order oligomers were mostly excluded when aggregates were transferred to pH 7.0 buffer of higher ionic strength (50 mM) as precipitates. The broad aggregate peaks which were clearly visible in case of samples transferred to pH 7.0, 20 mM ionic strength are lost for samples transferred to pH 7.0 of higher ionic strength (50 mM).

The elution data from the chromatogram can also be presented in terms of Ve/Vt which is the ratio of measured elution volume to total column volume[8]. In case of blue dextran, the total excluded volume gave a value of Ve/Vt ~ 0.35. Native monomer in the chromatogram for protein nanoparticles **[Figure 5.2.6.1]** has an elution position of Ve/Vt ~ 0.77.As anticipated for larger aggregates, elution shifts to Ve/Vt ~ 0.5.

The inference which can be drawn from the chromatogram for HEWL nanoparticles is that higher order oligomers, intermediate species, native monomer and monomer with altered conformation are present at equilibrium in the solution.

The eluted samples were checked for their integrity by SDS-PAGE. It was carried out under reducing conditions. The eluted samples were analyzed by 16.5 % Tricine SDS-PAGE.

The chromatogram profile for HEWL nanoparticles transferred to pH 7.0 (20 mM sodium phosphate buffer) indicated bimodal population of monomer. One of them constitutes of partially folded monomer and the other one reflects the presence of compact or native state monomer. **[Figure 5.2.6.1]** demonstrates from the elution profile that the two forms of the native population i.e. compact and partially unstructured monomer are in equilibrium with each other. This is further complemented by SDS-PAGE data **[Figure 5.2.6.3]** under reducing conditions which revealed no differences between the two different forms of protein monomer.

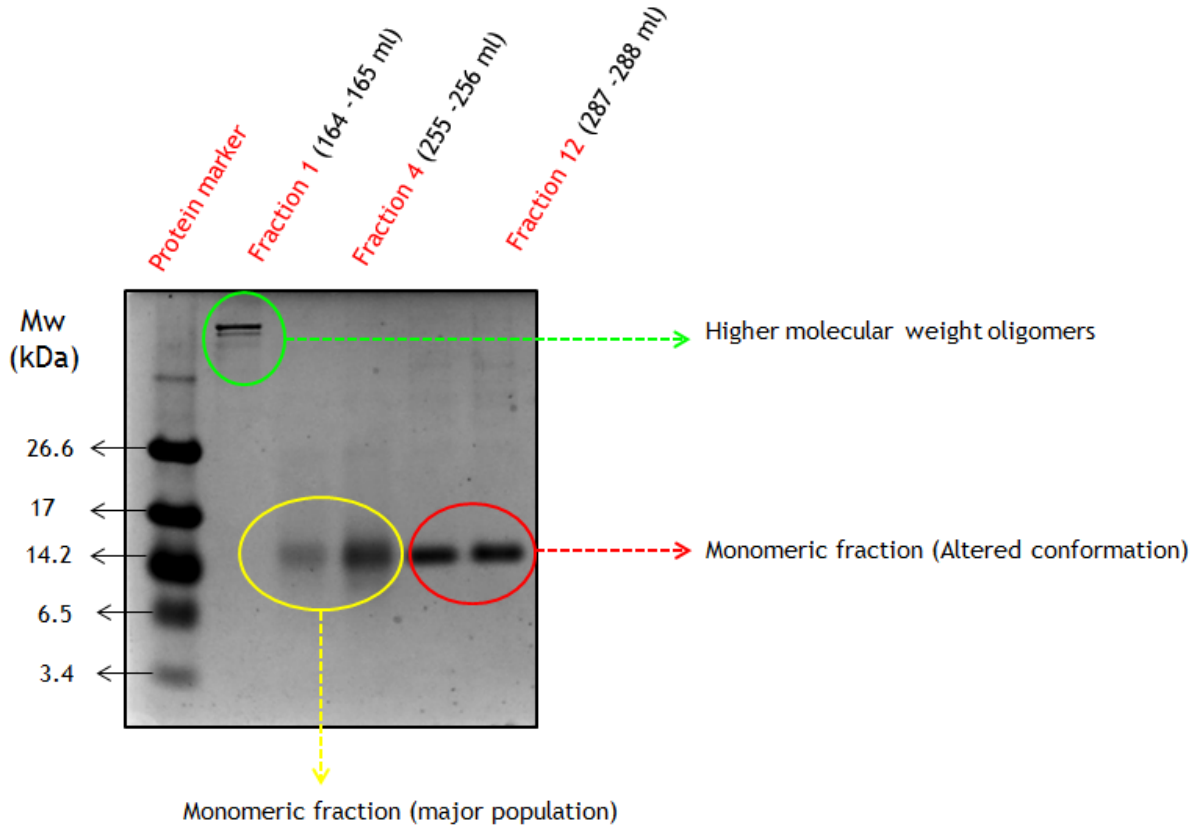

Figure 5.2.6.3: The electrophoretic pattern of SEC eluted fractions for HEWL aggregates transferred to **20 mM** sodium phosphate buffer, pH 7.0 on 16.5 % Tricine SDS PAGE. **Lane1:** protein marker, **Lane 2:** Fraction 1**, Lane 3:** Fraction 2(250-251 mL), **Lane 4:** Fraction 4, **Lane 5:** Fraction 10 (283-284 mL) & **Lane 6:** Fraction 12.

A good correlation was observed between the SEC chromatogram profile and SDS PAGE pattern for aggregates transferred to pH 7.0, higher ionic strength (50 mM). No higher order aggregates could be detected in the SEC eluted profiles as well as in the gel. All the fractions showed up as monomer band in the gel [**Figure 5.2.6.4 & 5.2.6.5**].

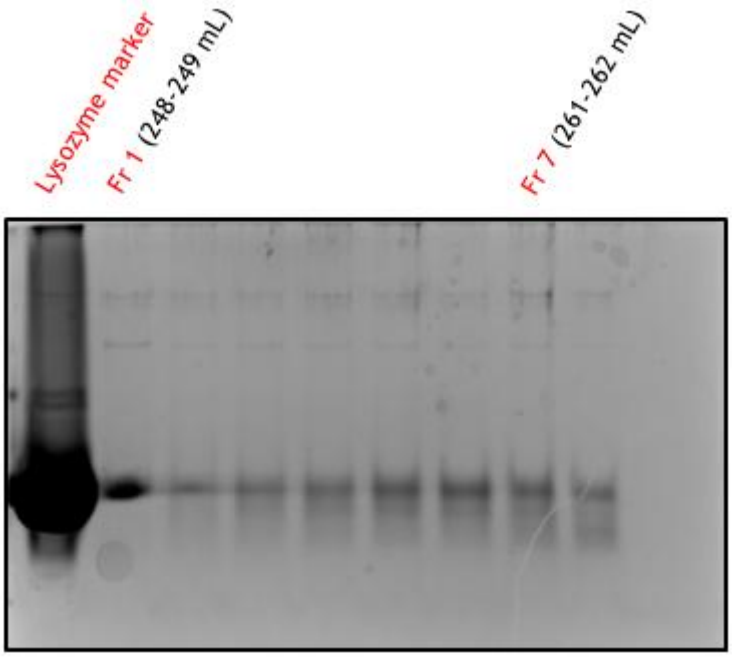

Figure 5.2.6.4: The electrophoretic pattern of SEC eluted fractions for HEWL aggregates transferred to **50 mM** sodium phosphate buffer, pH 7.0 on 16.5 % Tricine SDS PAGE. **Lane 1:** Lysozyme in water, **Lane 2:** Fraction 1, **Lane 3:** Fraction 2(250-251 mL), **Lane 4:** Fraction 3(253-254 mL), **Lane 5:** Fraction 4(255-256 mL), **Lane 6:** Fraction 5(257-258 mL), **Lane 7:** Fraction 6(259-260 mL), **Lane 8:** Fraction 7(261-262 mL), **Lane 9:** Fraction 8(264-265 mL).

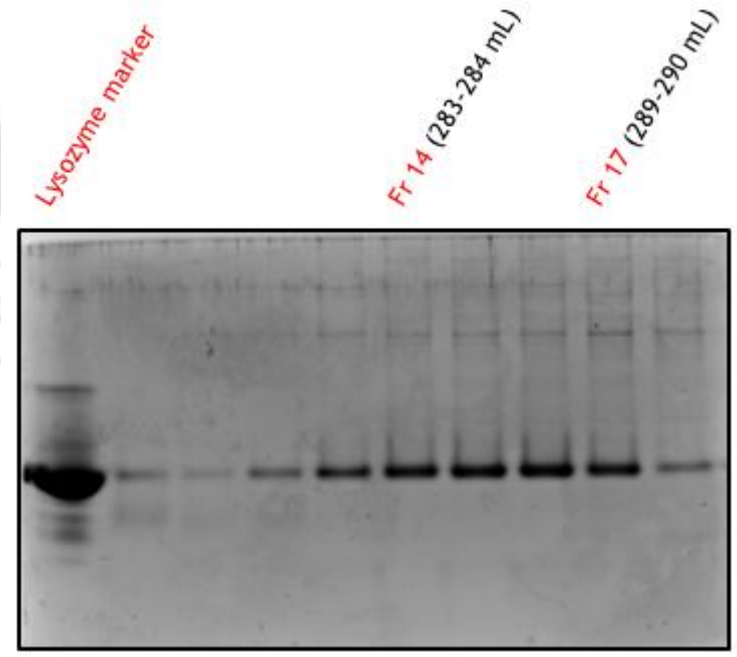

Figure 5.2.6.5: The electrophoretic pattern of SEC eluted fractions for HEWL aggregates transferred to **50 mM** sodium phosphate buffer, pH 7.0 on 16.5 % Tricine SDS PAGE. **Lane 1:** Lysozyme in water, **Lane 2:** Fraction 10(270-271 mL), **Lane 3:** Fraction 11(274-275 mL), **Lane 4:** Fraction 12(278-279 mL), **Lane 5:** Fraction 13(281-282 mL), **Lane 6:** Fraction 14, **Lane 7:** Fraction 15(285-286 mL), **Lane 8:** Fraction 16(287-288 mL), **Lane 9:** Fraction 17.

5.2.7 Concluding remarks

Here we describe the characterization of HEWL nanoparticles in terms of their molecular mass and hydrodynamic volume by SEC. Our data supports the fact that HEWL nanoparticles are polydisperse as a consequence of which they appear as very broad and continuous as well as in form of multiple peaks in the SEC chromatogram. Self-associated soluble high molecular weight oligomers were separated successfully from monomers. The protein samples after transfer to pH 7.0 were analyzed by size-exclusion chromatography. Aggregation elution profiles were obtained from the chromatograms. SEC chromatograms were compared in order to demonstrate the relative population of oligomers and monomers in the transferred samples. In this study, SEC has proved to be a very robust method to characterize the heterogeneity of protein nanoparticles.

Previously, our lab has performed gel filtration experiments for 120 μM HEWL aggregates incubated in pH 12.2 for different time durations (**Kumar et al., 2008**). SEC proved to be a useful tool in characterizing the aggregates formed at pH 12.2 as it revealed the size and shape heterogeneity in aggregate population. Elution profile for aggregates in pH 12.2 clearly showed presence of multiple aggregate species with varying size and shape. Elution profiles for longer incubation period samples (288 and 144 hours) were fairly similar thus indicating the irreversible nature of the aggregates. Hence, SEC was critical in deducing information regarding the distribution of population of different aggregate species. This technique has an edge over other techniques such as dansyl labeled steady-state or time-resolved fluorescence which are limited by ensemble averaging and data analysis complexity respectively.

The two different monomeric peaks which were observed in the elution profile for transferred samples were not present in that of aggregates. However, for aggregates incubated in pH 12.2, the elution was carried out at pH 7.0. Thus, it is difficult to say whether the two different monomer conformations exist or not in pH 12.2.

We have successfully used SEC for quantitative characterization of polydispersity of HEWL nanoparticles. We show in this study that due to differences in hydrodynamic radii of different species involved in HEWL aggregation enabled to achieve high chromatographic resolution. Oligomeric forms were clearly distinguishable from the native monomeric population.

References

1. Trathnigg, B. (2000). Size-exclusion Chromatography of Polymers. In R. A. Meyers (ed.), *Encyclopedia of Analytical Chemistry* (pp. 8008–8034). Chichester: John Wiley & Sons Ltd.

2. Meratan, A. A., Ghasemi, A. & Nemat-Gorgani, M. Membrane integrity and amyloid cytotoxicity: A model study involving mitochondria and lysozyme fibrillation products. *J. Mol. Biol.* **409,** 826–838 (2011).

3. Islam, R., Kite, J., Baker, A. S., Ching, A. & Islam, M. R. Affinity purification of hen egg lysozyme using sephadex G75. *African J. Biotechnol.* **5,** 1902–1908 (2006).

4. Maroufi, B., Ranjbar, B., Khajeh, K., Naderi-Manesh, H. & Yaghoubi, H. Structural studies of hen egg-white lysozyme dimer: Comparison with monomer. *Biochim. Biophys. Acta* **1784,** 1043–1049 (2008).

5. Khaja, M., Thomas, J. J., Salinas, P. A. & Kaltashov, I. A. Characterization of small protein aggregates and oligomers using size exclusion chromatography with online detection by native electrospray ionization mass spectrometry. *Anal. Chem.* **86,** 10692–10699 (2014).

6. Ravi, V. K., Swain, T., Chandra, N. & Swaminathan, R. On the characterization of intermediates in the isodesmic aggregation pathway of hen lysozyme at alkaline pH. *PLoS One* **9,** 1-12 (2014).

7. Kumar, S., Ravi, V. K. & Swaminathan, R. Suppression of lysozyme aggregation at alkaline pH by tri-N-acetylchitotriose. *Biochim. Biophys. Acta - Proteins Proteomics* **1794,** 913–920 (2009).

8. Rosmarie, R. & Stevens, F. J. Small zone, High-speed Gel Filtration Chromatography to detect protein aggregation associated with light chain pathologies. *Methods in Enzymology* **309,** 318–332 (1999).

Chapter 6

Exploring the self-quenching phenomenon of Fluorescein and Fluorescein derivative in HEWL oligomers

6.1 HOMO-FRET as a tool to study the self-quenching due to conformational changes in **FITC** labeled HEWL aggregates

6.1.1 Introduction

The emission spectrum of fluorescein overlaps extensively with its absorption spectrum, which makes this fluorescent dye suitable for HOMO-FRET experiments. Probability of HOMO-FRET or auto RET i.e. energy transfer occurring within the same molecule is higher in case of fluorescein dye. Fluorescence quenching as observed in this dye can be widely used to study intermolecular interactions.

The fluorescent properties of fluorescein are strongly pH dependent i.e. it exists in different protolytic forms depending upon the pH of the aqueous solution[1]. Fluorescein exists in cationic, neutral, anionic and dianionic forms with different pKa values and each of these forms exhibit pH dependent fluorescence. From all these different forms, only anionic and dianionic forms are the fluorescent species at neutral pH.

We have focussed on the use of the phenomena of self-quenching seen usually in case of fluorescein dye. Protein labeled with fluorescent dyes facilitates analysis of conformational changes associated with aggregation. FITC (fluorescein isothiocyanate) dye[2] is used extensively to study the behaviour of proteins in different assemblies. One of the major drawbacks of this dye is self-quenching due to which its use as a fluorescent dye in biological systems is underestimated. However, in our study this dye has been used to analyze the aggregation behaviour of HEWL in alkaline pH.

Due to the proximity between dyes covalently conjugated to protein monomer units in an oligomeric assembly, there exists the possibility of HomoFRET to occur. If the distance between these units in aggregates falls in the range of Förster radius of the fluorophore, then quenching of fluorescence of these dyes can be used to track aggregation. FRET can be expected to occur when protein molecules covalently tagged with fluorescein dye undergo aggregation but not when in the native state. However, if the protein molecule is labeled with more than 2 dye molecules, then it may elicit autoRET even in absence of aggregation.

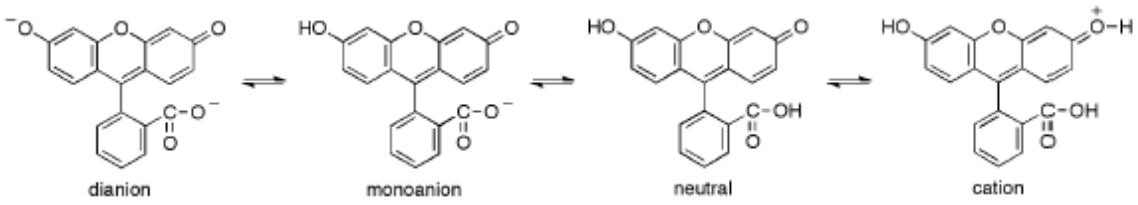

Figure 6.1.1: Ionization equilibria of Fluorescein. Fluorescein exists in dianionic form in alkaline pH **(Ferrari et al., 2013)**[3].

The pH sensitivity and high quantum yield of fluorescein makes this dye as an attractive dye label for different applications. In acidic pH, fluorescein exists in almost non-fluorescent form. However, in alkaline pH fluorescein starts displaying higher fluorescence due to the formation of dianionic structure[4]. This dianionic form fluoresces strongly with emission maxima observed at 515 nm.

In case of fluorescein molecule, for homo RET to occur, Förster distance[5] is about 42 Å. In this study, we have used homo RET or self-quenching of fluorescein to probe HEWL aggregation in alkaline pH 12.2. We have carried out a comparative analysis with HEWL labeled with FITC incubated under native condition (pH 7.0). Another approach which we have used is to vary the degree of labeling i.e. with different no. of dye molecules per protein.

6.1.2 Materials and Methods

6.1.2.1 Materials

Fluorescein (Cat no. F-6377, Sigma Aldrich), FITC (Cat no. F7250, Sigma Aldrich), 5-IAF (Cat no. 130451, Invitrogen).

6.1.2.2 Methods

6.1.2.2.1 Lifetime measurement by **TCSPC (Time correlated single photon counting)** method

Time resolved fluorescence intensity measurements were carried out in LIFE SPEC II spectrometer (**Model-FSP920, Edinburgh instruments, Livingston, UK**). The instrument was operated in TCSPC mode. The emission decay was collected in 4096 channels by means

of microchannel plate PMT detector. Lifetime data analysis was performed with F900 software. Lifetime of fluorescein was measured by exciting the samples with 475 nm (Nanosecond pulse, pulsed laser diode). The emission was collected at 518 nm with a temporal resolution of 0.01221 ns/channel. Identical conditions were kept while recording lifetime for HEWL labeled with FITC samples.

The deconvolution method was used to fit the data and obtain the fluorescence lifetime, τ. The lifetime was calculated from the intensity decay curves with the help of F900 decay analysis software. The goodness of the fitted data was determined from chi-squared value.

Time resolved fluorescence spectroscopy is a technique which is very useful to track the events which occur during the lifetime of the fluorophore in the excited state[6]. In case of time domain measurements, excitation of the sample is performed with pulsed light which is shorter than the decay time (τ) of the sample. The decay time is calculated as slope from the fluorescence intensity decay profile, a plot of log I (t) vs. time. The slope of the plot is equal to -1/τ. The fluorescence emission intensity decay profile for fluorophores from the excited state results in an exponential decay. Time resolved emission spectra provide information about the distinct population of fluorophores in the excited state. This is an advantage over steady state measurements as the steady state spectra represent the intensity weighted average of the decay process.

Single exponential decay function for a fluorophore is given by the eqn:

$$I(t) = I_0 \exp(-t/\tau) \qquad \ldots\ldots\ldots\ldots\ldots\ldots\ldots\ldots \quad (1)$$

The measured fluorescence lifetime is equivalent to the average time a fluorophore remains in the excited state. This statement holds true for single exponential fluorescence decay.

The value for lifetime is obtained by averaging the intensity decay over time, t which is given by the eqn:

$$\langle t \rangle = \frac{\int_0^\infty t\, I(t) dt}{\int_0^\infty I(t) dt} = \frac{\int_0^\infty t \exp(-t/\tau)\ dt}{\int_0^\infty \exp(-t/\tau)\, dt} \qquad \ldots\ldots\ldots\ldots (2)$$

Where I (t) is the fluorescence intensity at time t and I_0 is the intensity at time zero. 'τ' is the lifetime which represents the inverse of the total decay rate.

Hence, for a single exponential decay, fluorescence lifetime τ is:

$$\langle t \rangle = \tau \quad \ldots\ldots\ldots\ldots\ldots\ldots\ldots\ldots\ldots\ldots\ldots\ldots \quad (3)$$

However for multi-exponential decays,

$$I(t) = \sum_i \alpha_i \exp(-t/\tau_i) \quad \ldots\ldots\ldots\ldots\ldots\ldots\ldots\ldots \quad (4)$$

Where τ_i is the lifetime of the i^{th} decay component and α_i is the fractional amplitude and $\sum_i \alpha_i = 1$(the value is normalized to 1).

The fractional contribution of each component to the steady state intensity is described by the eqn:

$$f_i = (\alpha_i \tau_i) / \sum_j \alpha_j \tau_j \quad \ldots\ldots\ldots\ldots\ldots\ldots\ldots\ldots \quad (5)$$

In case of a multi-exponential decay, average lifetime is calculated and this is given by the eqn:

$$\bar{\tau} = \frac{\sum \alpha_i \tau_i^2}{\sum \alpha_i \tau_i} \quad \ldots\ldots\ldots\ldots\ldots\ldots\ldots\ldots\ldots\ldots\ldots\ldots\ldots\ldots \quad (6)$$

$$\bar{\tau} = \sum_i f_i \tau_i \quad \ldots\ldots\ldots\ldots\ldots\ldots\ldots\ldots\ldots\ldots\ldots\ldots\ldots\ldots\ldots \quad (7)$$

Amplitude-weighted lifetime or $\langle \tau \rangle$ which is proportional to area under the decay curve is given by the equation:

$$\langle \tau \rangle = \sum_i \alpha_i \tau_i \quad \ldots\ldots\ldots\ldots\ldots\ldots\ldots\ldots\ldots\ldots\ldots\ldots\ldots\ldots \quad (8)$$

6.1.2.2.2 Labeling of HEWL with FITC

3 mM HEWL was freshly dissolved in 1 mL of freshly prepared 0.1 M $NaHCO_3$ buffer, pH 9.25. A stock solution of FITC dye (10 mg/mL or 5 mg FITC/500 µL of DMSO) was prepared in DMSO solvent as described in Molecular probes. The dye solution was prepared in amber coloured tubes to protect from light. Assuming two different molar ratio (molar ratio of dye: protein) i.e. one at lower MR=3:1 and other at higher MR=10:1, reaction was carried out. Here, MR is referred to as molar labeling ratio.

For MR=3, 351 µL of dye stock solution (10 mg/mL) was added drop wise to 1 mL of freshly prepared HEWL solution with constant stirring in dark at room temperature. The reaction

mixture was incubated for 2 hours in room temperature with continuous stirring. For MR=10, 1170 µL of dye stock solution was added to 1 mL of HEWL solution. Subsequently, the reaction mixture was incubated for 1 hour at room temperature with continuous stirring. The labeled protein was separated from unreacted probe or free dye by passing the reaction mixture over PD-10 gel filtration column. The column was pre-equilibrated with 50 mM sodium phosphate buffer, pH 7.0. All the fractions were eluted in pH 7.0 buffer. While recording the absorbance of the eluted fractions, all the fractions were diluted in 0.1 M $NaHCO_3$ buffer, pH 9.25.

Volume of the reactive dye to be added to reaction mixture was calculated by:

$$\text{Volume of dye stock solution } (\mu L) = \frac{\frac{mg}{mL} \text{ of protein x } 0.2 \text{ mL}}{MW_{protein}} \text{ x } 389 \text{ x } 100 \text{ x MR}$$

MR is the ratio of dye to protein in the reaction mixture.
Molecular weight of FITC = 389 g/mol.
100 is unit conversion factor
0.2 mL is volume of protein solution

The ratio of FITC/HEWL in eluted fractions was determined by measuring the absorbance at 280 nm (A_{280}) and 494 nm (A_{494}). HEWL concentration was calculated as [HEWL] = $[A_{280} - (A_{494} \text{ x } 0.3)]$x dilution factor/ ε. Where 0.3 is the correction factor and ε is the molar extinction coefficient of protein at 280 nm. Dye per protein molecule $= \frac{A_{494} \text{ x dilution factor}}{68{,}000 \text{ x [HEWL]}}$. HEWL concentration is in M and 68,000 $M^{-1}cm^{-1}$ is the extinction coefficient of FITC at 494 nm, pH 8.0.

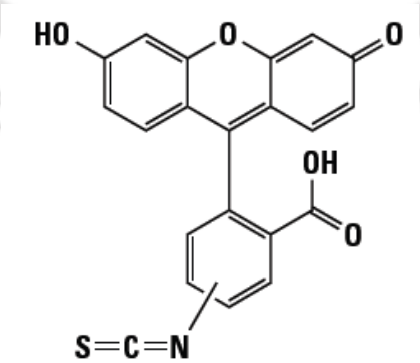

Figure 6.1.2.2 (a): Amine reactive FITC dye which is a derivative of fluorescein dye. It is functionalized with isothiocyanate reactive group by replacing the H-atom on the bottom ring structure.

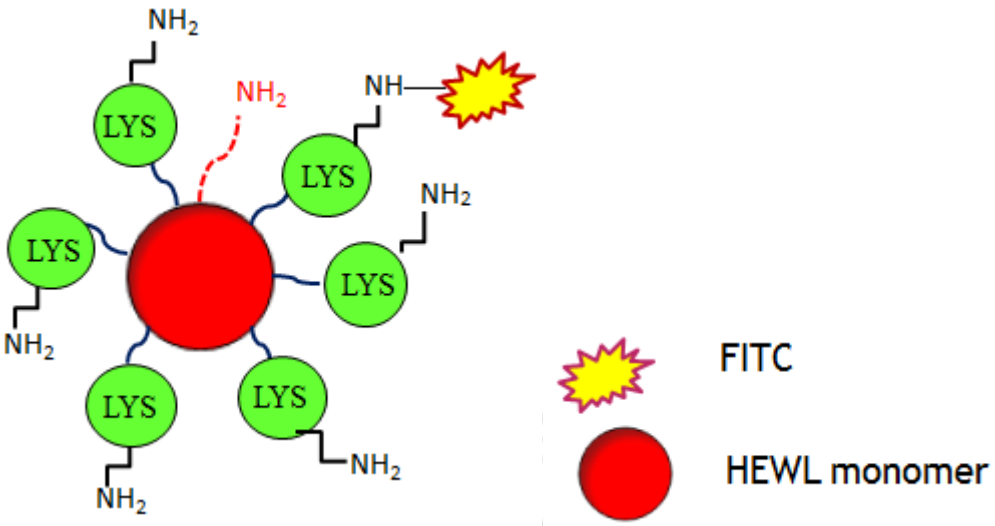

Figure 6.1.2.2 (b): Labeling of HEWL protein with FITC dye. This dye is used to label the proteins via amine group. FITC reacts with terminal amine and primary amine groups of the protein, forming a covalent amide bond.

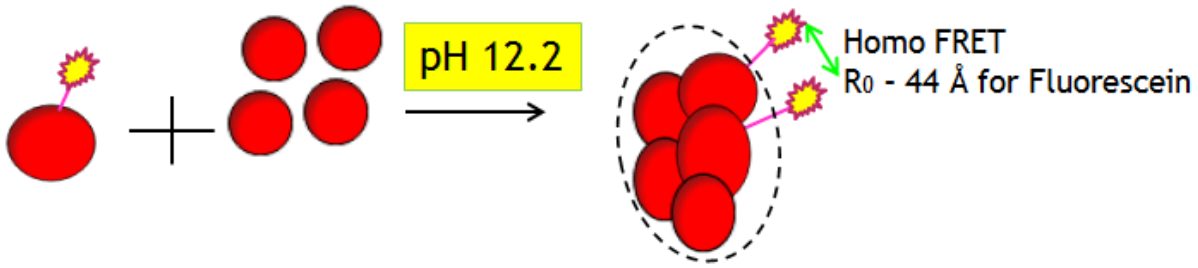

Figure 6.1.2.2 (c): Mixing of labeled and unlabeled protein at different ratios to study the self-quenching in HEWL aggregates.

6.1.2.2.3 Fluorescence steady state intensity

While recording intensity for FITC labeled samples, it was ensured that all the samples were diluted in respective buffers to have same absorbance at 494 nm. This was done to negate the effect of concentration. All the samples were diluted such that the dye concentration was 0.5 μM in the cuvette for fluorescence steady state measurements. The fluorescence spectra were recorded using Jobin-Yvon Fluoromax-3 spectrofluorometer. Fluorescence intensity spectra were recorded 3 times independently and averaged to get the final average spectra.

6.1.3 Results and Discussion

6.1.3.1 Overlap of absorption and emission spectra in Fluorescein

Absorption spectrum of fluorescein was recorded in 0.1 M Sodium bicarbonate buffer, pH 9.0. Emission spectra of fluorescein- Fluorescein was dissolved in different concentrations in 0.1 M $NaHCO_3$ buffer. Excitation was performed at 430 nm. Excitation and emission slit widths were set at 1 nm and 3 nm respectively. Emission spectra were measured from 445 nm to 600 nm.

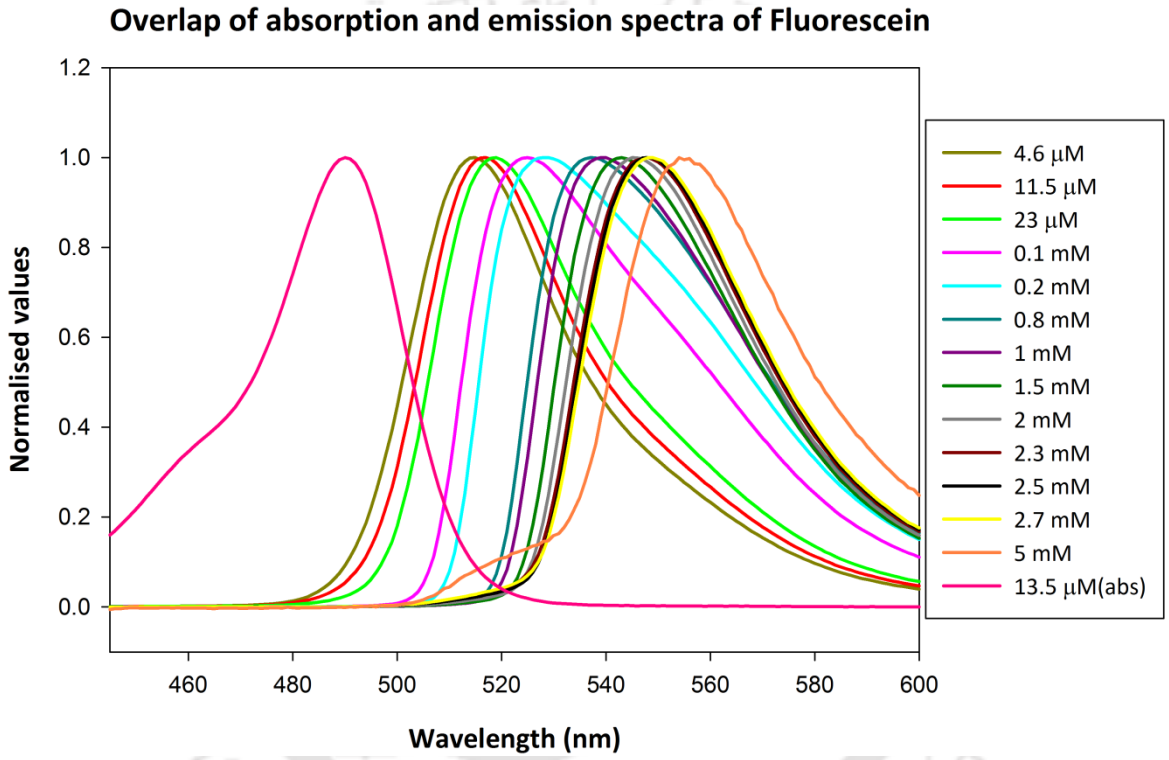

Figure 6.1.3.1 (a): Overlap of absorption and emission spectra of fluorescein. Emission spectra were recorded for different concentrations of fluorescein in 0.1 M $NaHC0_3$, pH 9.0. The absorbance values as well as emission intensity were normalised to a maximum value of 1.

The emission spectra of fluorescein showed a marked reduction in fluorescence intensity with increasing concentration of the dye in aqueous buffer. The maximum emission wavelength (λ_{max}) shifted from about 515 nm for 4.6 µM fluorescein to 554 nm for 5 mM fluorescein. The shift of the emission spectra towards longer wavelengths is very much pronounced for high concentration of the dye. Moreover, the absorption and emission spectra were normalised to a value of 1, due to which the shift of emission spectra as well as overlap of absorption and emission spectra are clearly revealed.

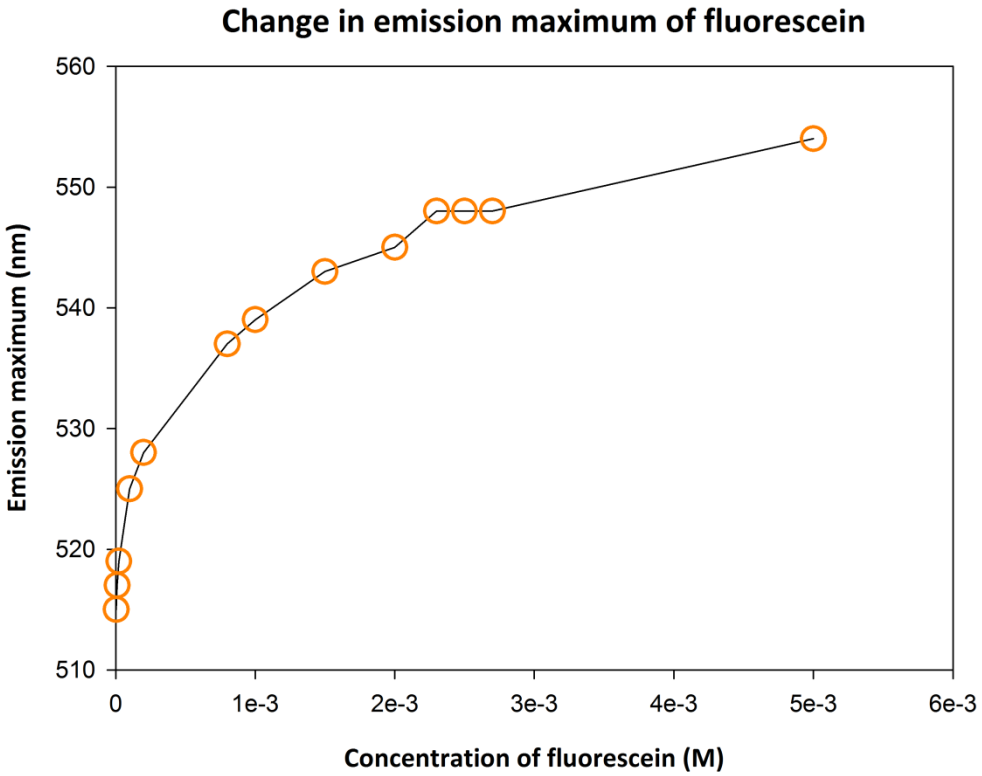

Figure 6.1.3.1 (b): Change in emission λ_{max} of fluorescein at different concentration in 0.1 M $NaHCO_3$ buffer, pH 9.0.

In highly concentrated solutions of the fluorescein dye, fluorescein-fluorescein interactions lead to energy transfer and self-quenching. These results in reduced fluorescence intensity or luminescence yield. Consequently, red shift in emission maximum is observed for fluorescein with increasing concentration **[Figure 6.1.3.1 (b)]**. Self-quenching is clearly evident for concentrated solution **[Figure 6.1.3.1 (c)]** of fluorescein (> 2 mM). In case of self-quenching, fluorophore and quencher are the same fluorophore species. Fluorescein exhibits the property of self-quenching because its emission spectrum substantially overlaps with the absorption spectra.

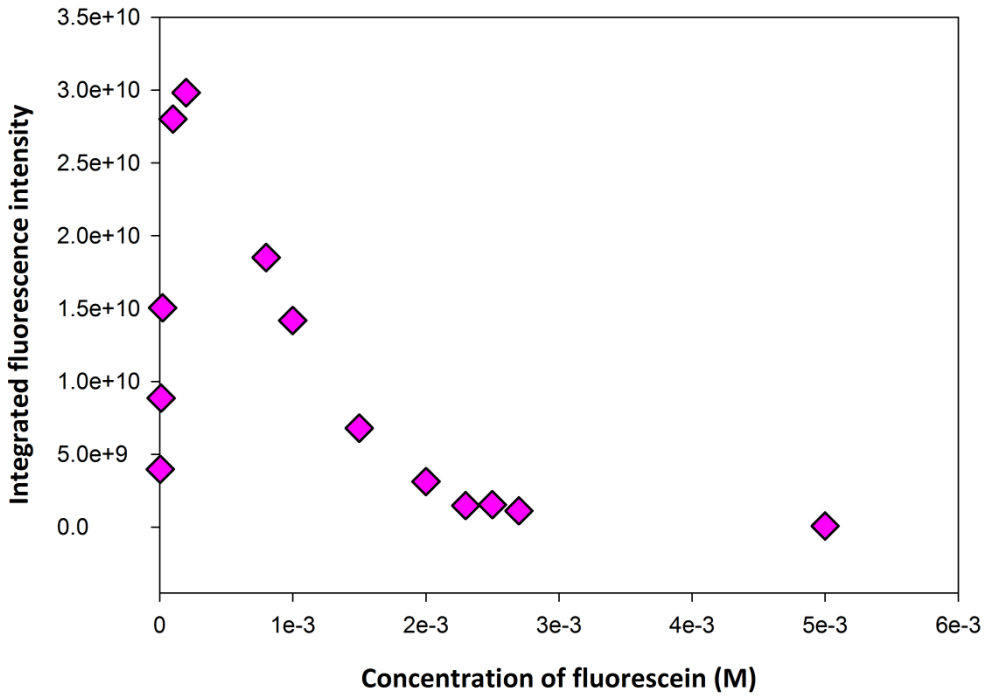

Figure 6.1.3.1 (c): Change of quantum yield in fluorescein with increasing concentration. Area under the curve was calculated by considering the region of emission spectra from 490 nm to 580 nm. Integrated fluorescence intensity was calculated for 4.6 µM, 11.5 µM, 23 µM, 0.1 mM, 0.2 mM, 0.8 mM, 1 mM, 1.5 mM, 2 mM, 2.3 mM, 2.5 mM, 2.7 mM & 5 mM of fluorescein in 0.1mM $NaHCO_3$ buffer, pH 9.0.

6.1.3.2 Application of fluorescein homo-transfer to HEWL aggregation at alkaline pH 12.2

Labeling of protein with the dye was performed at two different molar ratios of dye to protein. Labeling with FITC was carried out at a) low molar ratio of dye to protein (**3:1**) and b) High molar ratio of dye to protein (**10:1**). After labeling with FITC, the labeled fractions were separated from free dye by gel filtration. Absorbance was measured for the eluted fractions. Absorbance was measured at 280 nm for protein (HEWL) and at 494 nm (FITC dye).

Fractions	Protein conc. (µM)	Dye conc. (µM)	Dye per protein
1	0.64	0.083	0.13
2	14.5	17.1	1.18
3	**51.4**	**76**	**1.47**
4	**27**	**47.3**	**1.75**
5	**21.7**	**47.2**	**2.17**

Table 6.1.3.2 (a): Fractions of HEWL labeled with FITC (**low molar ratio i.e. 3:1**) eluted from gel filtration, PD-10 column. Fractions 3, 4 & 5 were used further for experiments.

Labeled and unlabeled protein was mixed in different ratios such that final concentration of the protein in the mixture was 120 µM. Labeled mixed with unlabeled protein (l+u) samples were incubated for 10 days at room temperature (298 K) before recording fluorescence emission spectra.

The samples for FITC labeled HEWL (**low molar ratio**) mixed with unlabeled HEWL were:

1) **30 % L_F3_pH 12.2 -** 30 % labeled protein (fraction 3) + 70 % unlabeled protein in pH 12.2.
2) **10 % L_F4_pH 12.2** – 10 % labeled protein (fraction 4) + 90 % unlabeled protein in pH 12.2
3) **10 % L_F5_pH 12.2** – 10 % labeled protein (fraction 5) + 90 % unlabeled protein in pH 12.2
4) **10 % L_F4_pH 7.0** – 10 % labeled protein (fraction 4) + 90 % unlabeled protein in pH 7.0
5) **8 % L_F3_pH 12.2** – 8 % labeled protein (fraction 3) + 92 % unlabeled protein in pH 12.2
6) **5 % L_F5_pH 7.0** – 5 % labeled protein (fraction 5) + 95 % unlabeled protein in pH 7.0

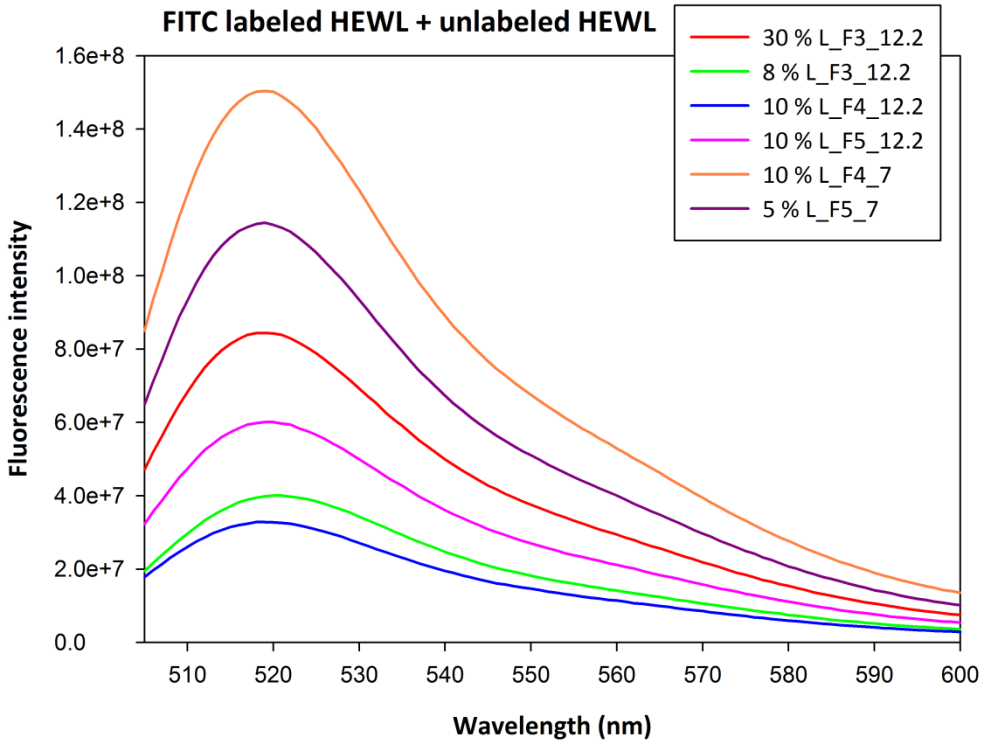

Figure 6.1.3.2 (a): Fluorescence emission spectra for FITC labeled HEWL mixed with unlabeled HEWL. Fluorescence intensity was recorded with excitation at 490 nm. Excitation and emission slit were set as 1 nm and 3 nm respectively. All the samples were diluted such that final concentration of [dye] in the samples was 0.5 µM. Samples incubated in pH 12.2 were diluted in 50 mM sodium phosphate buffer, pH 12.2 for fluorescence measurements. Samples incubated in pH 7.0 were diluted in 0.1 M, $NaHCO_3$ buffer, pH 9.0 for fluorescence measurements.

The maximum intensity is observed for samples incubated in pH 7.0. In case of 10 % FITC labeled HEWL mixed with unlabeled protein, where the average fluorescein dye per HEWL protein molecule is 1, maximum intensity was seen. This is the intensity which is displayed by the sample in absence of any self-quenching of fluorescein.

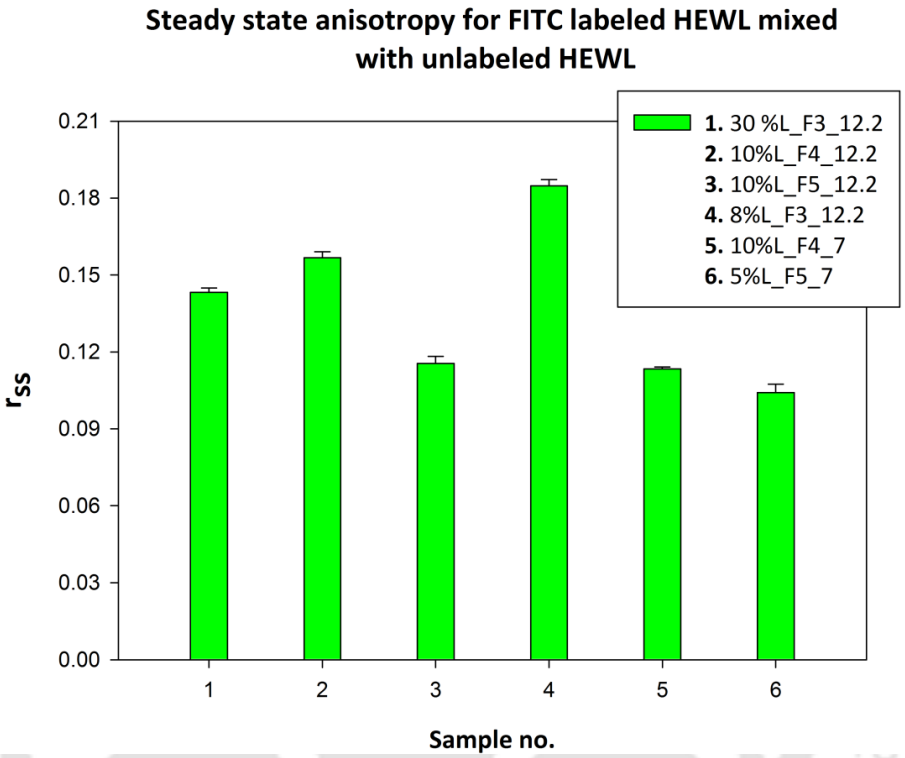

Figure 6.1.3.2 (b): Steady state anisotropy of FITC labeled HEWL (**low molar ratio**) mixed with unlabeled HEWL at different ratios. Excitation was done at wavelength of 494 nm and emission at 518 nm. Excitation and emission slit widths were set as 1 nm and 5 nm respectively. Samples incubated in pH 12.2 were diluted in 50 mM sodium phosphate buffer, pH 12.2 for fluorescence measurements. Samples incubated in pH 7.0 were diluted in 0.1 M, $NaHCO_3$ buffer, pH 9.0 for fluorescence measurements.

Samples	rss
30 %L_F3_pH 12.2	0.143
10 %L_F4_pH 12.2	0.157
10 %L_F5_pH 12.2	0.115
8 %L_F3_pH 12.2	0.185
10 %L_F4_pH 7	0.113
5 %L_F5_pH 7	0.1042

Table 6.1.3.2 (b): Steady state anisotropy values are summarised in the table for FITC labeled HEWL (**low molar ratio**) mixed with unlabeled protein in different ratios and incubated in two different pH conditions: alkaline (12.2) & native (7.0).

In case of FITC labeled HEWL (low molar ratio), only one of the samples incubated in pH 12.2 i.e. 10 % labeled sample which consists of an average of 2 dye molecules per protein showed a drop in r_{ss}. The value dropped to a level similar to that of pH 7.0 incubated samples. The decrease in steady state anisotropy confirms resonance energy transfer between fluorescein molecules which occurs due to the aggregation of protein in pH 12.2. However, all the other samples incubated in alkaline pH which consist of an average of 1 dye per protein displayed higher anisotropy.

Fractions	Protein conc. (µM)	Dye conc. (µM)	Dye per protein
5	15.5	84.5	**5.45**
6	34.6	237	**6.84**
7	31.5	283	**9**
8	7.44	225	**30.25**

Table 6.1.3.2 (c): Fractions of HEWL labeled with FITC (**high molar ratio i.e. 10:1**) eluted from gel filtration, PD-10 column. Fractions 5, 6, 7 & 8 were used further for experiments.

The samples for FITC labeled HEWL (**high molar ratio**) mixed with unlabeled HEWL were:

1) **20 % L_F6_pH 12.2 -** 20 % labeled protein (fraction 6) + 80 % unlabeled protein in pH 12.2.
2) **10 % L_F5_pH 12.2** – 10 % labeled protein (fraction 5) + 90 % unlabeled protein in pH 12.2
3) **10 % L_F7_pH 12.2** – 10 % labeled protein (fraction 7) + 90 % unlabeled protein in pH 12.2
4) **5 % L_F6_pH 12.2** – 5 % labeled protein (fraction 6) + 95 % unlabeled protein in pH 12.2
5) **1 % L_F5_pH 12.2** – 1 % labeled protein (fraction 5) + 99 % unlabeled protein in pH 12.2
6) **1 % L_F7_pH 12.2** – 1 % labeled protein (fraction 7) + 99 % unlabeled protein in pH 12.2
7) **1 % L_F8_pH 12.2** – 1 % labeled protein (fraction 8) + 99 % unlabeled protein in pH 12.2
8) **10 % L_F7_pH 7.0** – 10 % labeled protein (fraction 7) + 90 % unlabeled protein in pH 7.0
9) **1 % L_F7_pH 7.0** – 1 % labeled protein (fraction 7) + 99 % unlabeled protein in pH 7.0
10) **1 % L_F8_pH 7.0** – 10 % labeled protein (fraction 8) + 99 % unlabeled protein in pH 7.0

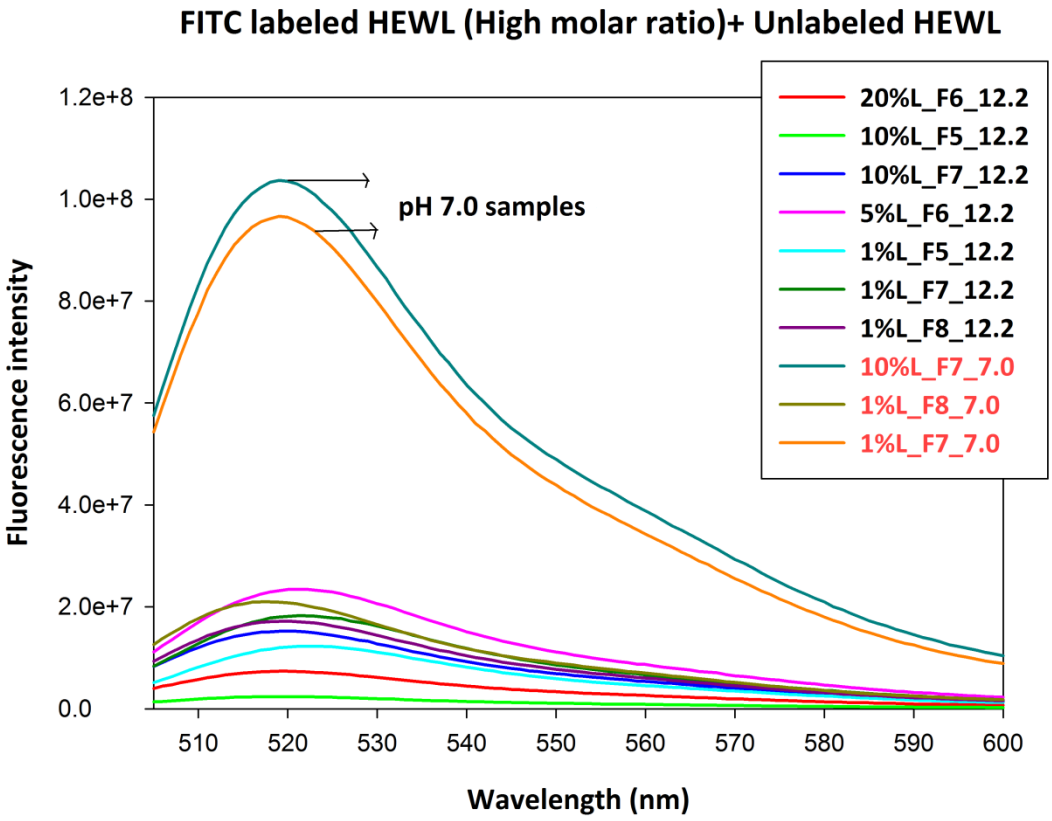

Figure 6.1.3.2 (c): Fluorescence emission spectra for FITC labeled HEWL (**high molar ratio**) mixed with unlabeled HEWL. Fluorescence intensity was recorded with excitation at 490 nm. Excitation and emission slit were set as 1 nm and 3 nm respectively. All the samples were diluted such that final concentration of dye in the cuvette was 0.5 µM. Samples incubated in pH 12.2 were diluted in 50 mM sodium phosphate buffer, pH 12.2 for fluorescence measurements. Samples incubated in pH 7.0 were diluted in 0.1 M, $NaHCO_3$ buffer, pH 9.0 for fluorescence measurements.

In the samples containing protein labeled with higher no. of fluorescein molecules (High molar ratio) displayed significantly lower fluorescence intensities in comparison to low molar ratio samples. This is mainly due to the increase in self-quenching with enhancement in degree of labeling. Especially the effect of self-quenching can be distinctly observed for samples incubated in pH 7.0 where there is no possibility of protein aggregation.

Significant drop in the fluorescence intensity for pH 12.2 incubated samples was observed in comparison to pH 7.0 samples. Irrespective of the % of the labeled fraction in the mixture, all the samples incubated in pH 12.2 displayed quenched intensity.

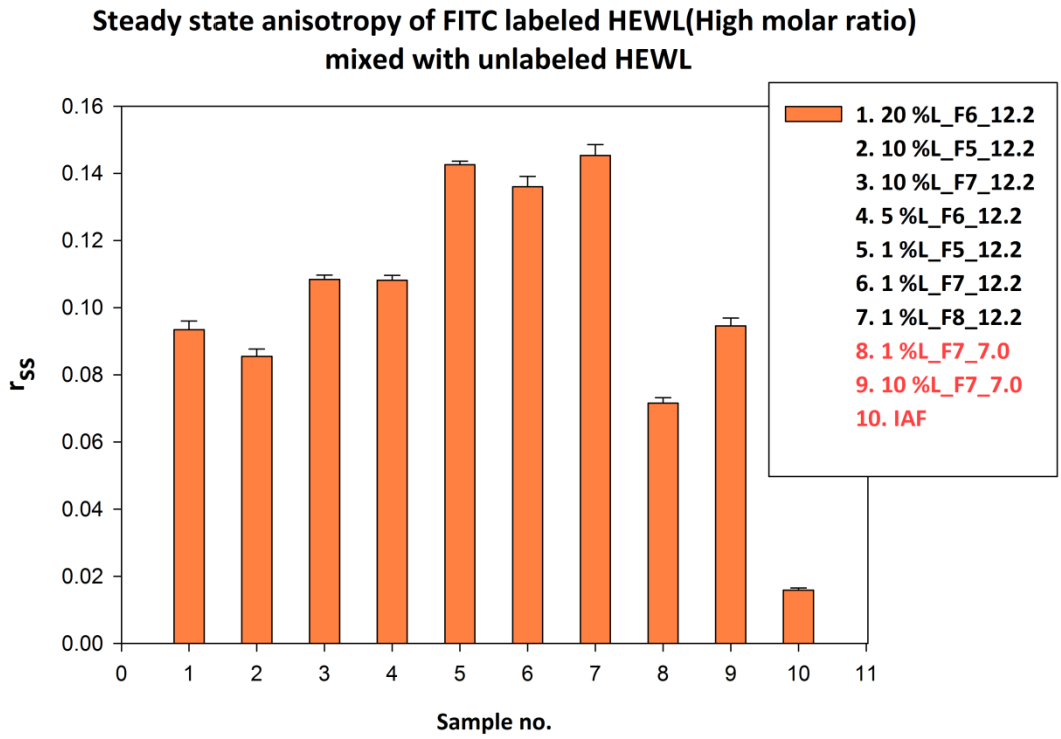

Figure 6.1.3.2 (d): Steady state anisotropy of FITC labeled HEWL (**high molar ratio**) mixed with unlabeled HEWL at different ratios. Excitation was done at wavelength of 494 nm and emission at 518 nm. Excitation and emission slit widths were set as 1 nm and 5 nm respectively. Samples incubated in pH 12.2 were diluted in 50 mM sodium phosphate buffer, pH 12.2 for fluorescence measurements. Samples incubated in pH 7.0 were diluted in 0.1 M, $NaHCO_3$ buffer, pH 9.0 for fluorescence measurements.

Decrease in the value of fluorescence steady state anisotropy or fluorescence depolarization is one of the indicators for homo-FRET[7]. Previously, researchers have demonstrated change in anisotropy value with increase in labeling ratio[2] of FITC:BSA. The anisotropy decreases with increase in labeling ratio due to the possibility of energy migration (**Hungerford et al., 2007**). Steady state anisotropy vales have been measured for FITC labeled samples, both high and low molar ratios. The samples which were incubated in pH 7.0 displayed lower anisotropy as compared to those in alkaline pH 12.2, condition which favours aggregation of HEWL. However, in some of the samples incubated in pH 12.2, drop in r_{ss} value was observed similar to the value seen in pH 7.0 incubated samples. This demonstrates the phenomenon of homo-transfer in fluorescein labeled samples which occur as a consequence of aggregation of the protein in pH 12.2. Previously, similar studies has been carried out where homotransfer between fluorescein molecules tagged to protein subunits has been applied to monitor oligomerization[8] of labeled melittin peptide (**Scarlata et al., 1995**).

Samples	r_{ss}
20 %L_F6_pH 12.2	0.093
10 %L_F5_pH 12.2	0.085
10 %L_F7_pH 12.2	0.108
5 %L_F6_pH 12.2	0.108
1 %L_F5_pH 12.2	0.143
1 %L_F7_pH 12.2	0.136
1 %L_F8_pH 12.2	0.145
1 %L_F7_pH 7.0	0.071
10 %L_F7_pH 7.0	0.094
IAF	0.016

Reduced value of r_{ss}

Table 6.1.3.2 (c): Steady state anisotropy values for FITC labeled (**High MR**) HEWL mixed with unlabeled protein in different ratios. The samples after mixing were incubated at two different pH conditions: 12.2 & 7.0 at room temperature.

It can be clearly noticed from the table that as the labeling ratio increased (higher no. of dye molecules per protein); drop in the values of r_{ss} was seen in 20 %, 10 % & 5 % labeled samples incubated in pH 12.2. However, in case of 1 % labeled samples incubated in pH 12.2, higher r_{ss} was observed. Even though labeled fractions which were used in 1 % labeled samples consist of an average of > 5 dye molecules per protein, drop in r_{ss} was minimal. In case of 1 % labeled sample (fraction 7) incubated in pH 7.0, the r_{ss} showed a value of 0.071. However, when the same sample (1% labeled_F7) was incubated in pH 12.2, an increase in the value of anisotropy i.e. 0.136 was observed. This observation is in agreement with the fact that samples incubated in alkaline pH will exhibit a higher value of r_{ss} due to aggregation of HEWL. Here, the effect of self-quenching was not noticeable as a very low percentage of labeled fraction was used i.e. 1 %. In contrast, 10 % labeled sample (Fraction 7) when incubated under two different conditions i.e. pH 7.0 and pH 12.2, displayed similar values for r_{ss}. Surprisingly, 10 % labeled sample (Fraction 7) displayed a much lower value of r_{ss} (0.108) in comparison to 1 % labeled sample (0.136) when incubated in pH 12.2. Here, the drop in r_{ss} for 10 % labeled sample, incubated in alkaline pH was prominent which confirms the phenomenon of self-quenching in fluorescein moieties.

6.1.3.3 Self-quenching studies in HEWL labeled with FITC mixed with unlabeled protein by TCSPC

Fluorescence lifetime was measured for fluorescein as well as FITC labeled HEWL mixed with unlabeled protein incubated in two different conditions (pH 7.0 & pH 12.2). Time correlated single photon counting was used to record the lifetime for these samples. Deconvolution method was used to fit the data and obtain the fluorescence lifetime.

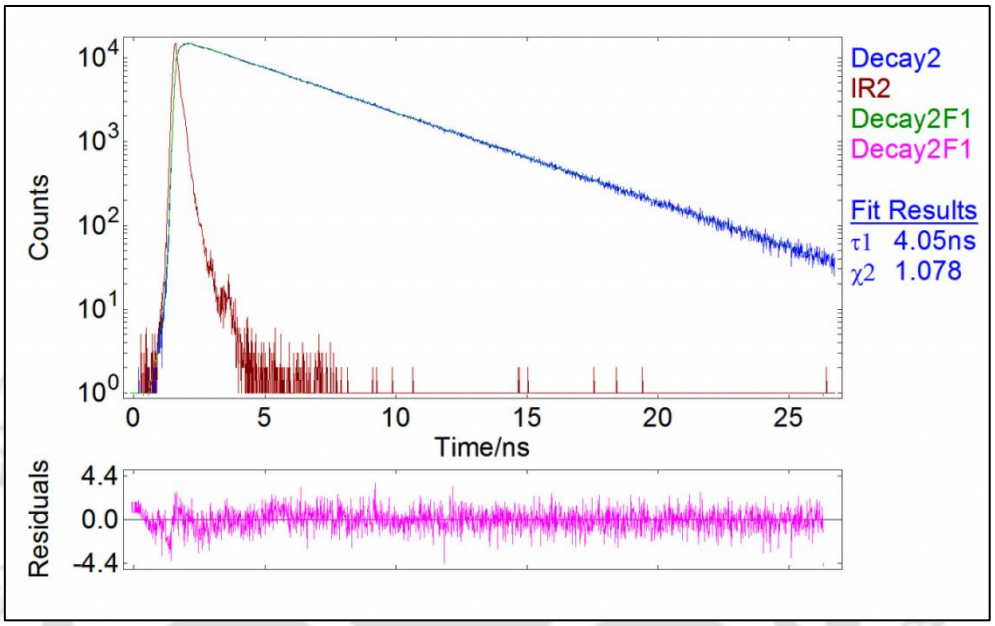

Figure 6.1.3.3 (a): Lifetime decay of Fluorescein in 0.1 M NaHCO3 buffer, pH 9.0. IRF (Instrument response curve), fluorescence decay curve and curve fitting line of fluorescein are displayed in the figure. Excitation source: 475 nm pulsed laser diode. Emission λ: 518 nm. Chi squared value is equal to 1.07.

Experimental fluorescence decay curve for fluorescein was well fitted to mono-exponential equation with a chi-square value of 1.07. Lifetime measurement of fluorescein in 0.1 M $NaHCO_3$ buffer yielded a value of τ = 4.05 ns which correlates well with the value reported in the literature[9]. Fluorescence lifetime of the excited fluorescein dianion has been determined previously which is close to 4 ns. At pH 9.0, dianionic form of fluorescein is the dominant fluorescent species. Previously, lifetime of uncoupled[2] or free FITC has been reported to be 4.05 ns.

FITC labeled fraction with low molar ratio of dye: protein (3:1) was used to prepare the samples for lifetime measurements. The labeled fraction with an average of 1 dye per protein molecule was mixed with unlabeled protein at different ratios and then further incubated in pH 12.2. Samples incubated in pH 7.0 were used as control for the experiment. For lifetime

measurements, low labeling ratio was selected. The reason behind this is to negate out the possibility of self-quenching when there is more than one FITC tag on HEWL protein. This also may cause a reduction in fluorescence lifetime.

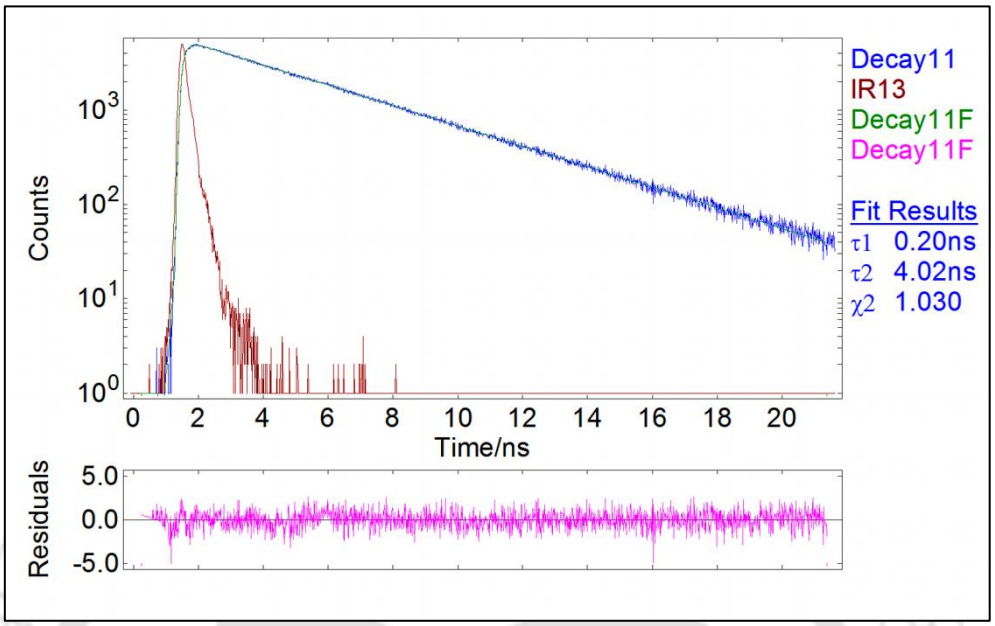

Figure 6.1.3.3 (b): 10% of FITC labeled HEWL mixed with 90% unlabeled HEWL. The sample was incubated in pH7.0. The intensity decay was fitted with two exponential fit.

Bi-exponential fitting was required for FITC labeled HEWL mixed with unlabeled protein incubated in pH 7.0. Fluorescence decay curve displayed a biexponential decay with a longer lifetime ($\tau_2 = 4.02$ ns) and a shorter one ($\tau_1 = 0.20$ ns).

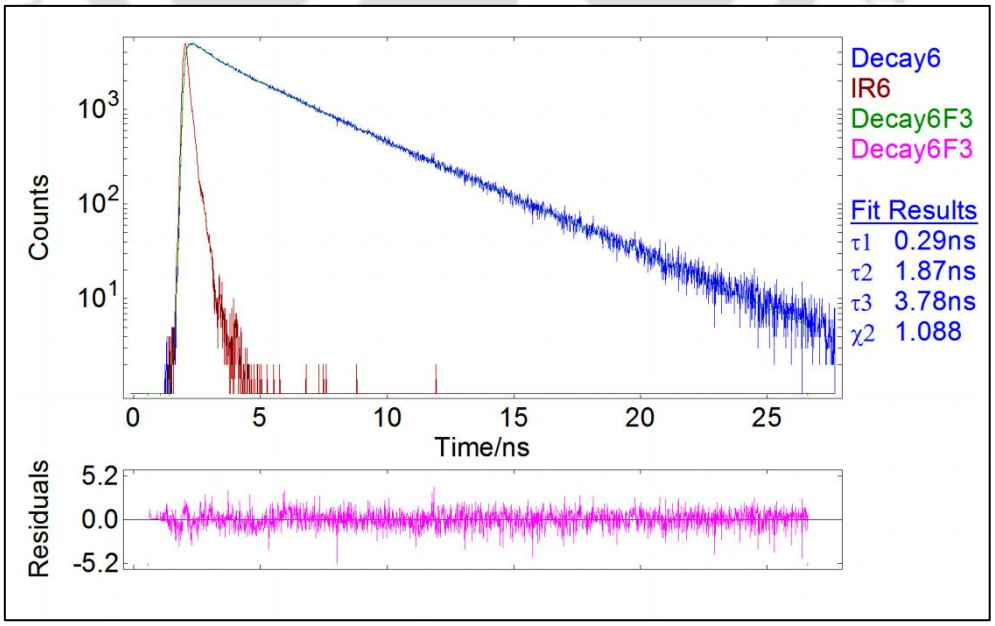

Figure 6.1.3.3 (c): 5% of FITC labeled HEWL mixed with 95% unlabeled HEWL. The sample was incubated in pH12.2. The intensity decay was fitted to three exponential model.

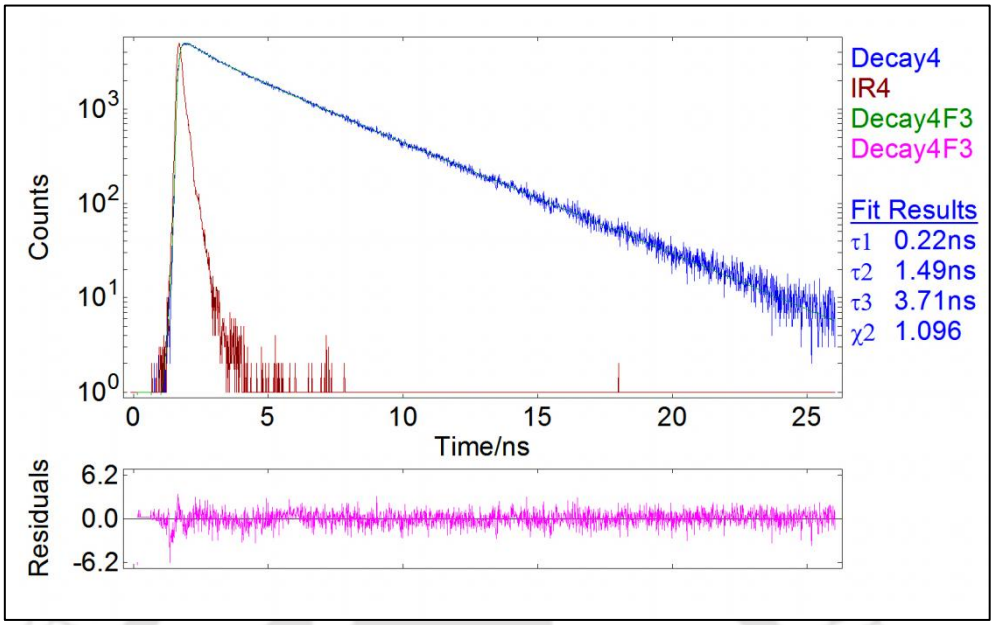

Figure 6.1.3.3 (d): 10% of FITC labeled HEWL mixed with 90% unlabeled HEWL. The sample was incubated in pH12.2. The intensity decay was fitted to three exponential fit model.

Samples incubated in pH 12.2 did not fit to the double exponential model. Assumption of a three exponential decay provided a better fit which is revealed by the χ^2 value.

Fluorescence life time data

Samples	Fitting model	Lifetime, τ (ns)	Chi-square	Lifetime Average (ns)
Fluorescein_1	Single exponential	4.06	1.174	**4.055**
Fluorescein_2	Single exponential	4.05	1.078	

Table 6.1.3.3 (a): Lifetime data for **Fluorescein in 0.1 M NaHCO3** buffer, pH 9.0. The lifetime data was fitted to single-exponential decay model.

τ_1(ns)	α_1	Rel %	τ_2(ns)	α_2	Rel %	Chi-square	τ_1(ns) avg	τ_2(ns) avg
0.22	0.009	1.01	4.02	0.048	98.99	1.142	**0.12**	**4.02**
0.02	0.01	1.02	4.02	0.047	98.98	1.03		

Table 6.1.3.3 (b): Lifetime data for **10% FITC labeled HEWL mixed with 90% of unlabeled protein incubated in pH 7.0 buffer**. The lifetime data was fitted to Bi-exponential decay model.

Fitting model	τ_1(ns)	α_1	τ_2(ns)	α_2	τ_3(ns)	α_3	Chi-square
3-exponential model	**0.29**	0.021	1.87	0.012	3.78	0.03	1.088

Table 6.1.3.3 (c): Lifetime data for **5 % FITC labeled HEWL mixed with 95 % of unlabeled protein incubated in pH 12.2 buffer**. The lifetime data was fitted to three-exponential decay model.

τ_1(ns)	α_1	τ_2(ns)	α_2	τ_3(ns)	α_3	Chi-square	τ_1(ns) avg	τ_2(ns) avg	τ_3(ns) avg
0.22	0.022	1.49	0.0106	3.71	0.034	1.096	**0.245**	**1.63**	**3.725**
0.27	0.0206	1.77	0.0107	3.74	0.032	1.092			

Table 6.1.3.3 (d): Lifetime data for **10 % FITC labeled HEWL mixed with 90 % of unlabeled protein incubated in pH 12.2 buffer**. The lifetime data was fitted to three-exponential decay model.

The table summarizes lifetime values together with the corresponding values for pre-exponential factors, α. The value of reduced χ^2 for 3-exponential fit shows that our assumption was correct in case of samples incubated in pH 12.2.

Average lifetime of the decay process was calculated by the eqn:

$$\langle\tau\rangle = (\alpha_1\tau_1{*}\tau_1 + \alpha_2\tau_2\ {*}\tau_2 + \alpha_3\tau_3\ {*}\tau_3) / (\alpha_1\tau_1 + \alpha_2\tau_2 + \alpha_3\tau_3)$$

Average lifetime for 10 % FITC labeled HEWL mixed with 90 % unlabeled protein incubated in pH 7.0 buffer calculated was **4.015 ns**. Average lifetime for 5 % FITC labeled HEWL mixed with 95 % unlabeled protein incubated in pH 12.2 buffer calculated was **3.328 ns**. Average lifetime for 10 % FITC labeled HEWL mixed with 90 % unlabeled protein incubated in pH 12.2 buffer calculated was **3.347 ns**.

Self-quenching phenomenon of fluorescein has been shown previously to result in a decrease in lifetime[7] (**Lakowicz et al., 2003**). Hence, in our case as expected decrease in average lifetime was evident in case of samples incubated in pH 12.2. The average lifetime decreased from 4.01 ns for pH 7.0 incubated samples to 3.328 ns (5 % labeled FITC) and 3.347 ns (10 % labeled FITC) for pH 12.2 incubated samples.

The intensity decay became more complex for pH 12.2 samples as three-exponential equation was needed to fit the data. In contrast, intensity decay for pH 7.0 samples was fitted to bi-exponential equation. Moreover, average lifetime value for pH 7.0 samples correlated well with unquenched lifetime of free fluorescein i.e. 4.05 ns. Multi-exponential decay was observed in case of samples incubated in pH 12.2.

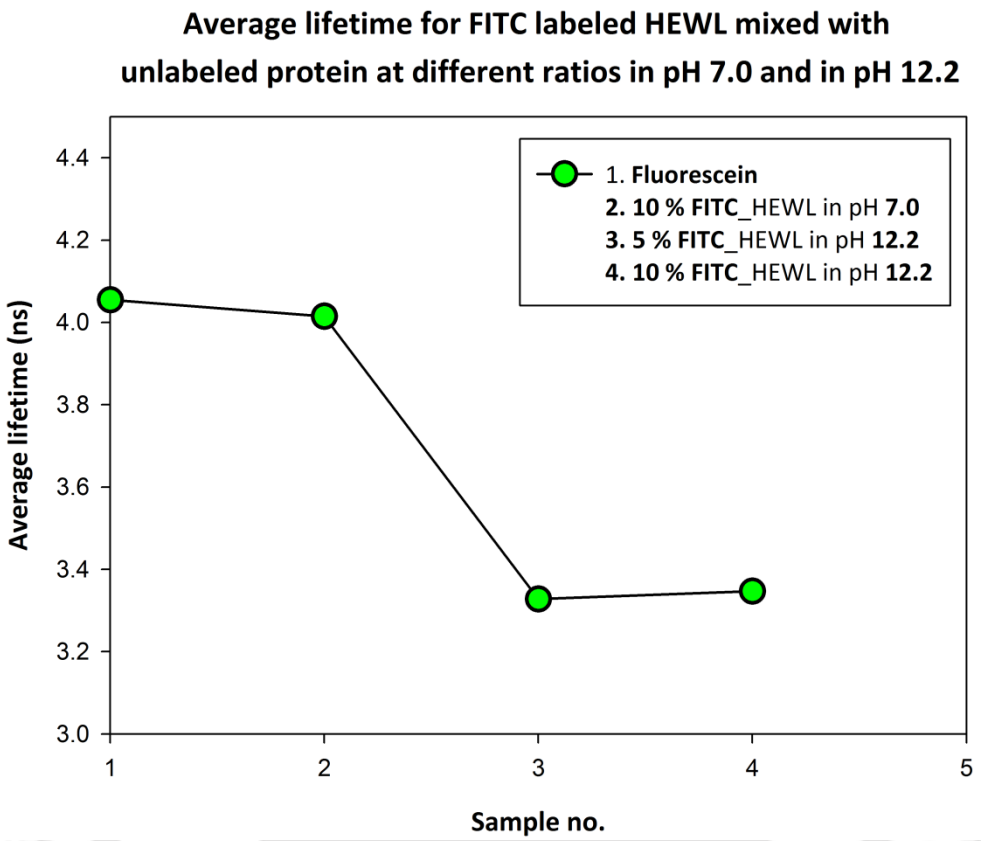

Figure 6.1.3.3 (e): Change in average lifetime for **a)** Fluorescein in 0.1 M $NaHCO_3$ buffer, pH 9.0 **b)** 10 % FITC labeled HEWL mixed with 90 % unlabeled protein incubated in pH 7.0 **c)** 5 % FITC labeled HEWL mixed with 95 % unlabeled protein incubated in pH 12.2 & **d)** 10 % FITC labeled HEWL mixed with 90 % unlabeled protein incubated in pH 12.2.

6.1.4 Conclusion

- Decrease in steady state anisotropy was observed for HEWL samples over labeled with FITC dye molecules i.e. of high molar ratio of dye to protein, incubated in alkaline pH 12.2.
- FITC dye has been used as a tool to elucidate the mechanism of self-quenching when FITC labeled HEWL protein undergoes aggregation in pH 12.2.
- HEWL labeled with FITC and mixed with unlabeled protein when incubated in pH 7.0 (under native conditions), value for average lifetime matched to that of free fluorescein as depicted from time-resolved data. Whereas reduction in average lifetime was evident in case of samples incubated in pH 12.2.

References

1. Wang, L., Shao, Y., Zhang, J. & Anpo, M. Study on the fluorescence properties of fluorescein dye incorporated into SBA-15. *Opt. Mater. (Amst).* **28,** 1232–1234 (2006).

2. Hungerford, G., Benesch, J., Mano, J. F. & Reis, R. L. Effect of the labelling ratio on the photophysics of fluorescein isothiocyanate (FITC) conjugated to bovine serum albumin. *Photochem. Photobiol. Sci.* **6,** 152–158 (2007).

3. Ferrari, L., Rovati, L., Fabbri, P. & Pilati, F. Disposable fluorescence optical pH sensor for near neutral solutions. *Sensors* **13,** 484–499 (2013).

4. Martin, M. M. & Lindqvist, L. The pH Dependence of Fluorescein fluorescence. *J. Lumin.* **10,** 381–390 (1975).

5. Kawski, A. Excitation energy transfer and its manifestation in isotropic media. *Photochem. Photobiol.* **38,** 487–508 (1983).

6. Beechem, J. M. & Brand, L. Time-resolved Fluorescence of Proteins. *Ann. Rev. Biochem.* **54,** 43–71 (1985).

7. Lakowicz, J. R., Malicka, J., Auria, S. D. Õ. & Gryczynski, I. Release of the self-quenching of fluorescence near silver metallic surfaces. *Anal. Biochem.* **320,** 13–20 (2003).

8. Runnels, L. W. & Scarlata, S. F. Theory and Application of Fluorescence Homotransfer to Melittin Oligomerization. *Biophys. J.* **69,** 1569–1583 (1995).

9. Sjoback, R., Nygren, J. & Kubista, M. Absorption and fluorescence properties of fluorescein. *Spectrochim. Acta Part A* **51,** L7–L21 (1995).

10. Kumar, S., Ravi, V. K. & Swaminathan, R. How do surfactants and DTT affect the size, dynamics, activity and growth of soluble lysozyme aggregates? *Biochem. J.* **415,** 275–288 (2008).

6.2 Synthesis of IAF (**Iodoacetamide fluorescein**) modified superfluorescent HEWL nanoparticles

6.2.1 Introduction

The excitation and emission spectra of IAF have considerable overlap thus exhibiting homo-FRET. In other words, this fluorophore with a relatively small Stokes shift will have a greater probability of undergoing homo-FRET.

Presence of free sulfhydryl groups in HEWL aggregates gives us the opportunity to modify it with a thiol reactive probe such as 5-Iodoacetamide fluorescein. This procedure allows sensitive fluorescence detection of aggregates. Iodoacetamides readily react with all thiols to form thioethers. The iodoacetyl group reacts with free sulfhydryl groups by nucleophilic substitution of iodine with thiol to form stable covalent thioether bonds. Iodoacetamides are intrinsically unstable in light; conjugation reactions are therefore carried out under dark conditions. Basically, it is to limit the formation of free iodine which can further react with tyrosine, tryptophan and histidine residues of a protein.

The research question which we have tried to address here: **a) can we modify the available free thiol groups on HEWL aggregates in order to incorporate multiple labels of fluorescein into the aggregates?** The results demonstrated that the aggregates could be successfully labeled with 5-IAF due to the presence of free sulfhydryl groups. After labeling the aggregates with Iodoacetamide, the labeled species were characterized using techniques such as steady state anisotropy, fluorescence intensity, lifetime studies and SDS-PAGE.

The iodoacetamide derivative of fluorescein moiety exhibits maximum reactivity towards –SH groups. Cysteine residues which are oxidized do not show any reactivity towards IAF. Free cysteines are not present in the native protein i.e. HEWL in pH 7.0. However, free thiol groups[10] are abundant in HEWL aggregates incubated in pH 12.2.

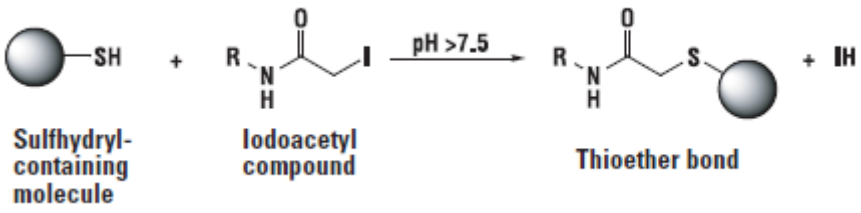

Figure 6.2.1: Reaction mechanism for iodoacetyl group with sulfhydryl group.

6.2.2 Materials and Methods

6.2.2.1 Labeling of HEWL aggregates with 5-IAF

6.2.2.1.1 High molar ratio of dye: protein as 15:1

A stock solution of the dye was prepared freshly by dissolving 1 mg of 5-IAF in 100 µl of DMF (10 mg/ml stock concentration = 19.4 mM). The solution was prepared in an amber coloured tube to protect it from light as Iodoacetamide dyes are very sensitive to light. 92 µl of dye stock solution (10 mg/ml) was added drop wise to 1 ml of protein solution. The protein solution was 120 µM HEWL aggregates incubated in pH 12.2 buffer for 6 days. After addition of dye, the reaction was incubated for 2 hours in dark at room temperature without stirring. The dye labeled protein conjugates were separated from free dye on a gel filtration column (PD-10 column by gravity based separation) pre-equilibrated with sodium phosphate buffer pH 7.0. The fractions were eluted in 50 mM sodium phosphate buffer, pH 7.0. However, for recording the absorbance of the eluted fractions, they were diluted in 0.1 M $NaHCO_3$ buffer, pH 9.2 prior to measurements.

6.2.2.1.2 Low molar ratio of dye: protein as 5:1

Stock solution of Dye was prepared freshly by dissolving 1 mg of 5-IAF in 100 µl of DMF (10 mg/ml stock conc.= 19.4 mM). It was protected from light. 31 µl of dye stock solution (10 mg/ml) was added dropwise to 1 ml protein solution (120 µM HEWL in pH 12.2 was incubated for 5 days at room temperature) with constant stirring. The reaction mixture was incubated for 2 hrs. in dark at room temperature without any stirring. The dye labeled protein conjugates were separated from free dye on a gel filtration column (PD- 10 column). Fraction were eluted in 50 mM sodium phosphate buffer, pH 7.0. Absorbance was measured for the labeled fractions which were diluted 10 times in 0.1 M $NaHCO_3$ buffer, pH 9.2. The fluorescent labeled fractions were then stored at 4 °C for further use. Extinction coefficient of IAF is 80,000 $M^{-1}cm^{-1}$.

6.2.3 Results and Discussion

6.2.3.1 HEWL aggregates labeled with IAF (High molar ratio)

The absorption of the dye shows a significant overlap with the emission spectra which is the property of fluorescein based derivative dyes.

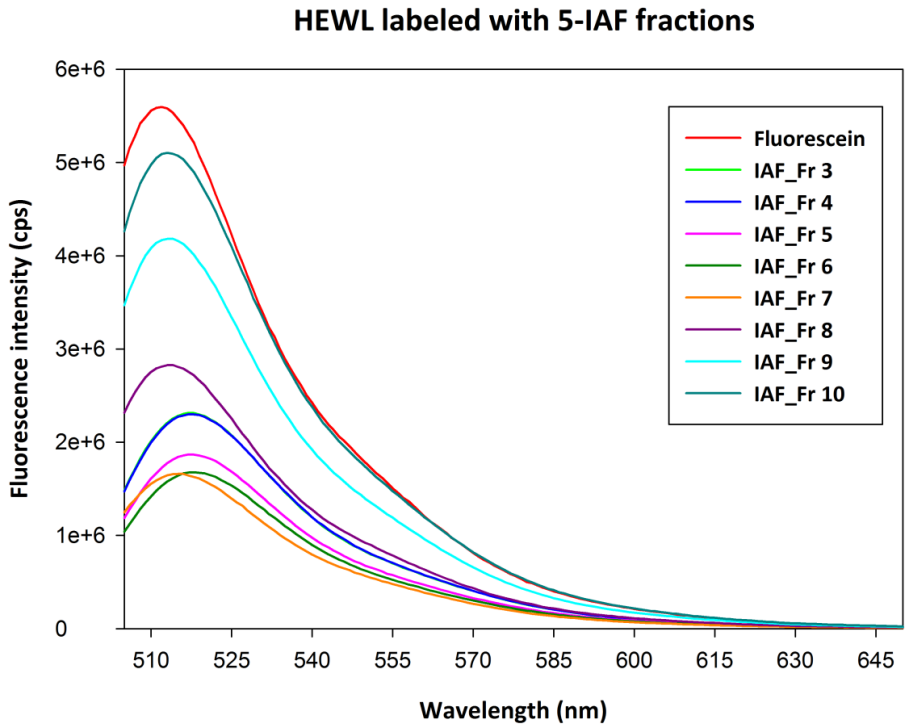

Figure 6.2.3.1 (a): Fluorescence intensity spectra of HEWL aggregates labeled with 5-IAF dye (**high molar ratio of dye: protein which is 15:1**). Excitation was performed at 494 nm with excitation slit as 1 nm and emission slit set as 3 nm. The fractions are numbered in the order they are eluted from PD-10 column after labeling reaction. Concentration of the dye was kept as 0.5 µM in the cuvette for all the fractions as well as for fluorescein also.

The fluorescence for some of the labeled fractions (Fraction no. 3, 4, 5, 6 & 7) is most likely quenched caused by self-quenching effects of the dye. Due to the presence of multiple IAF tags on HEWL aggregates, some of the labeled fractions showed up quenched fluorescence. Thus, more amount of IAF could be incorporated into the aggregates by performing the labeling at high molar ratio of dye to protein as 15:1.

Time resolved measurements for IAF labeled HEWL aggregates (high molar ratio) reveals a significant amount of self-quenching in labeled fractions. It is noteworthy to say that fractions 5 & 6 are the most quenched as depicted from their reduced average lifetime values in comparison to other fractions **[Table 6.2.3.1 (a)]**. A strong correlation can be seen between the steady state integrated fluorescence intensity and average lifetime values for the labeled fractions **[Figure 6.2.3.1 (b)]**. The intensity decay curves for all the labeled fractions were fitted to bi-exponential model, except for fraction 9.

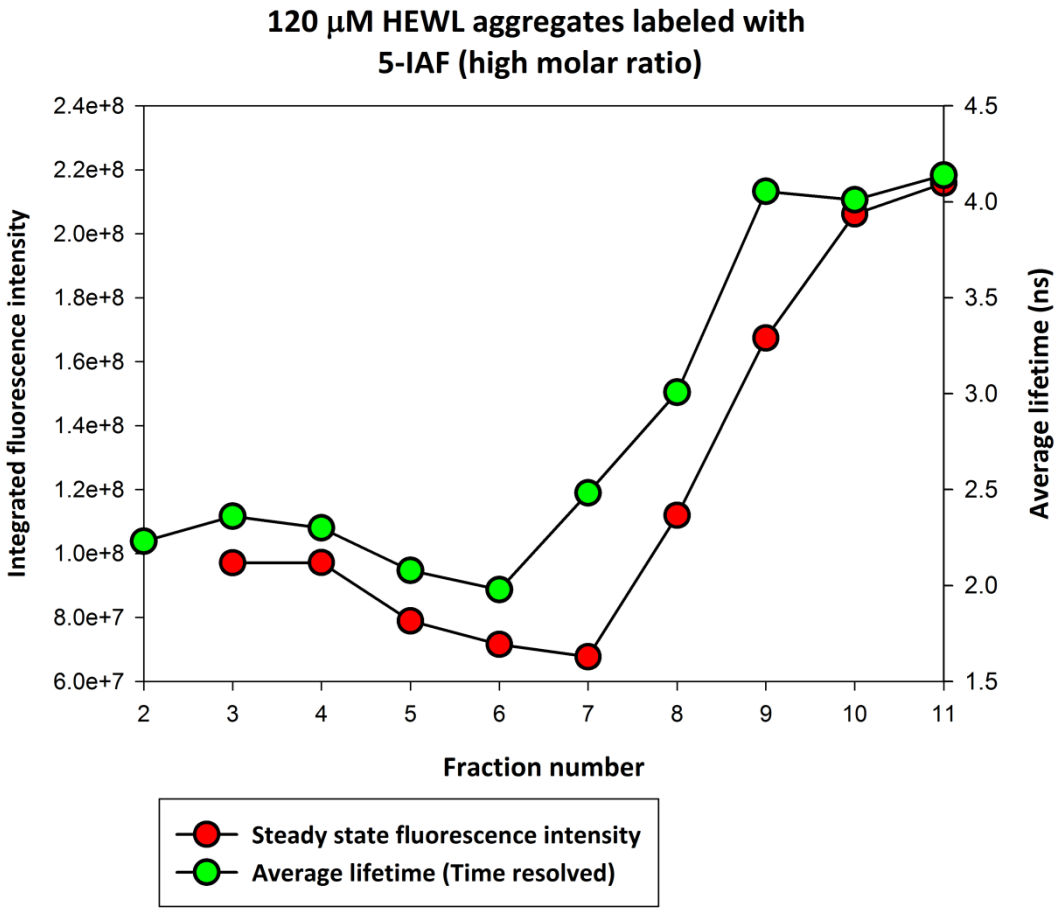

Figure 6.2.3.1 (b): Red circles represent integrated fluorescence intensity for 5-IAF labeled HEWL aggregates (**high molar ratio**). Area under the decay curve was calculated from 505 nm to 650 nm region of the emission intensity spectra. Green circles represent average lifetime for IAF labeled HEWL aggregates. The average lifetime was calculated from lifetime measurements by TCSPC. In the plot, fraction number 11 refers to free fluorescein dye.

IAF fractions	α_1	τ_1 (ns)	α_2	τ_2 (ns)	Average τ (ns)	χ^2
Fraction 2	0.487	0.485	0.513	3.89	2.231	1.166
Fraction 3	0.45	0.52	0.55	3.869	2.361	1.03
Fraction 4	0.463	0.537	0.537	3.821	2.301	1.076
Fraction 5	0.522	0.512	0.478	3.793	2.079	1.26
Fraction 6	0.547	0.52	0.453	3.735	1.978	1.103
Fraction 7	0.414	0.481	0.586	3.896	2.483	1.007
Fraction 8	0.291	0.48	0.709	4.047	3.007	1.017
Fraction 9					4.054	1.057

Table 6.2.3.1 (a): Lifetime data for IAF labeled fractions (**high molar ratio**). Lifetime decay was fitted to bi-exponential model for fractions 2, 3, 4, 5, 6, 7 & 8. However, lifetime decay for fraction number 9 was fitted to single exponential fit.

Standard	τ (ns)	χ^2
Fluorescein	4.138	1.073

Table 6.2.3.1 (b): Lifetime decay of free fluorescein dye was fitted to single exponential fit. Fluorescein was dissolved in 0.1 M $NaHCO_3$ buffer, pH 9.2.

The decay profile for fraction 9 was fitted to single exponential decay model. The reduced χ^2 value obtained from the fit confirms that it was the best fit. The fraction 9, unlike other fractions, displayed a single exponential decay with a lifetime of 4.05 ns which is in good agreement with the lifetime of 4.13 ns for free fluorescein. In addition, fraction 9 also displayed unquenched or higher steady state fluorescence intensity. Thus, fraction 9 represents uncoupled fluorescein dye.

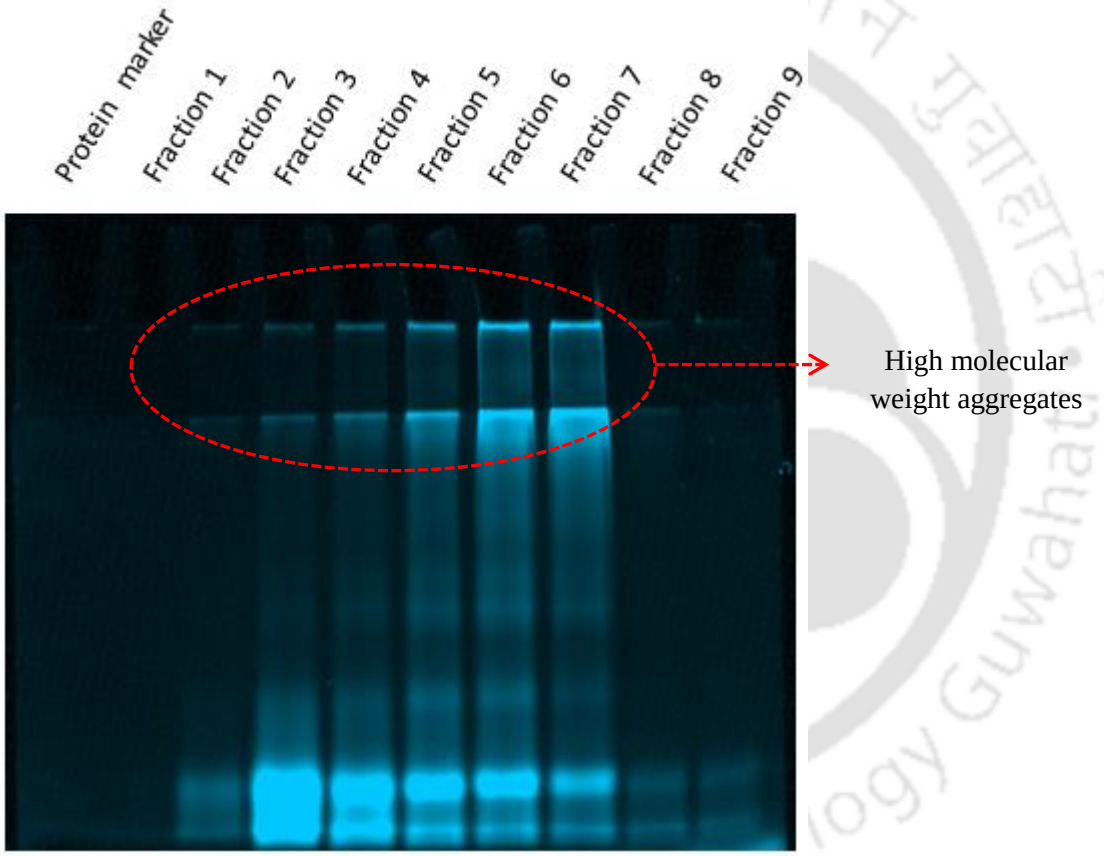

Figure 6.2.3.1 (c): 15 % SDS PAGE of IAF labeled fractions without Coomassie staining. The protein marker consists of hen egg white lysozyme (molecular weight is 14.3 kDa) in water.

Fluorescent IAF labeled HEWL aggregates were visualized on a SDS polyacrylamide gel. The [**Figure 6.2.3.1 (c)**] depicts IAF labeled HEWL aggregates. The gel was imaged under visible light before staining with Coomassie dye to visualize the fluorescent aggregates labeled with fluorescein. The image clearly suggests a high degree of fluorescent labeling of HEWL aggregates which appear as smear on the gel. The high molecular weight aggregates can be seen as bands stuck to the wells of stacking gel. Fluorescein moiety present in the high

molecular weight IAF labeled aggregates is most quenched. The plausible explanation can be the increased proximity of dye molecules in the aggregates resulting in self-quenching.

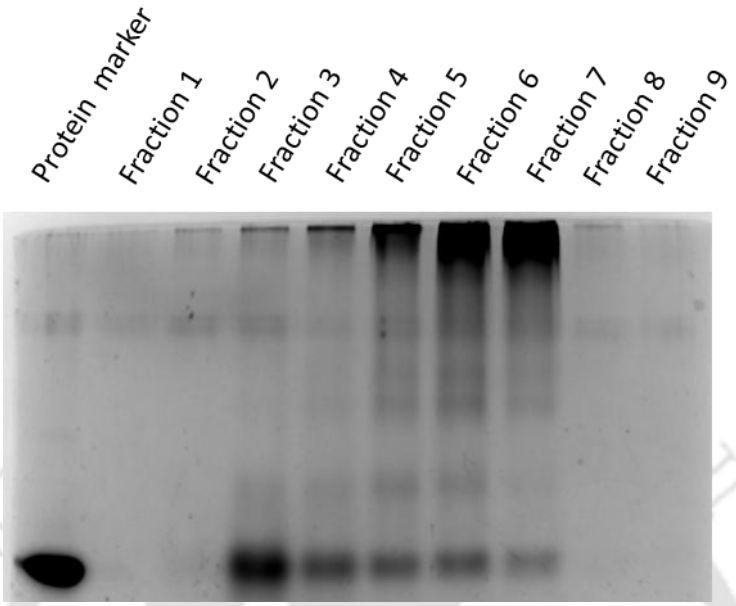

Figure 6.2.3.1 (d): 15 % SDS PAGE of IAF labeled fractions after Coomassie staining. The protein marker consists of hen egg white lysozyme (molecular weight is 14.3 kDa) in water.

6.2.3.2 HEWL aggregates labeled with IAF (Low molar ratio)

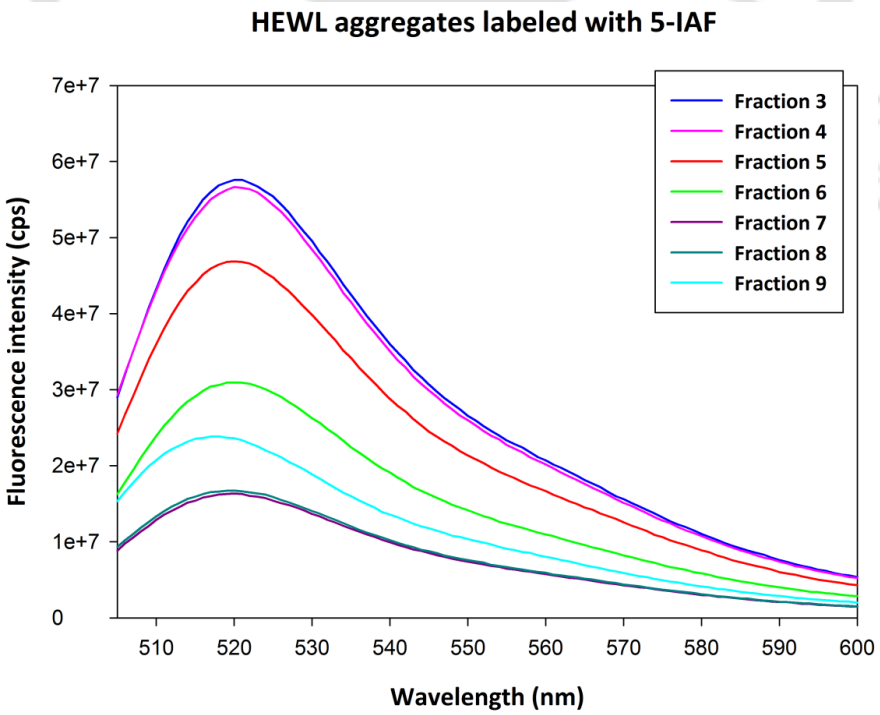

Figure 6.2.3.2 (a): Fluorescence intensity spectra of HEWL aggregates labeled with 5-IAF dye (**low molar ratio of dye: protein which is 5:1**). Excitation was performed at 490 nm with excitation slit as 1 nm and emission slit set as 3 nm. The fractions are numbered in the order they are eluted from PD-10 column after labeling reaction. Concentration of the dye in the cuvette for all the fractions was maintained at 0.5 μM.

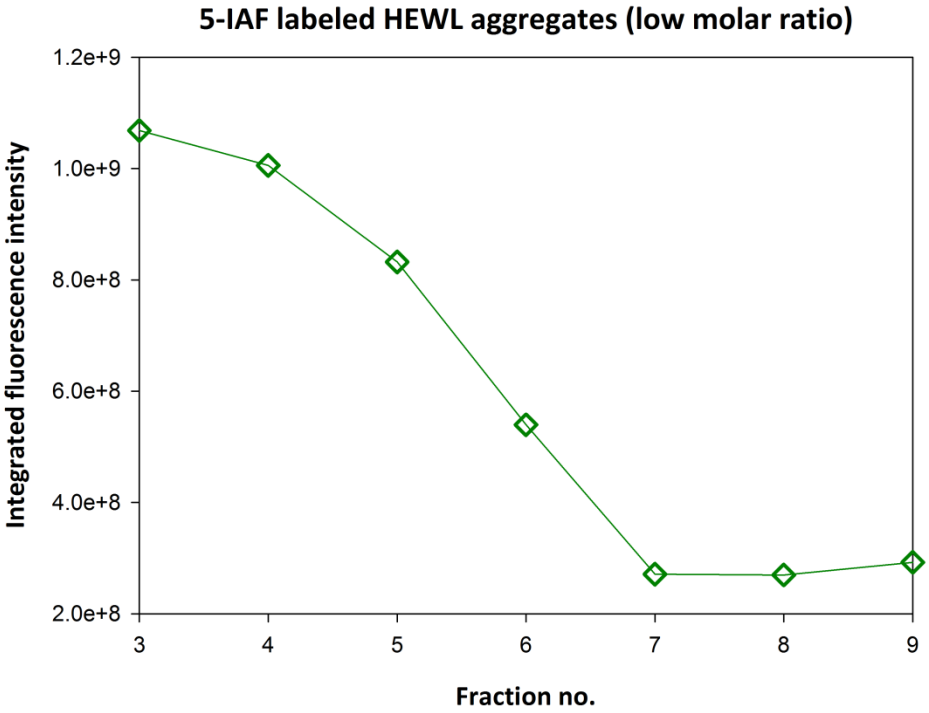

Figure 6.2.3.2 (b): Area under decay curve for 5-IAF labeled HEWL aggregates (120 μM). Area was calculated from 505 nm to 650 nm region of the emission intensity spectra.

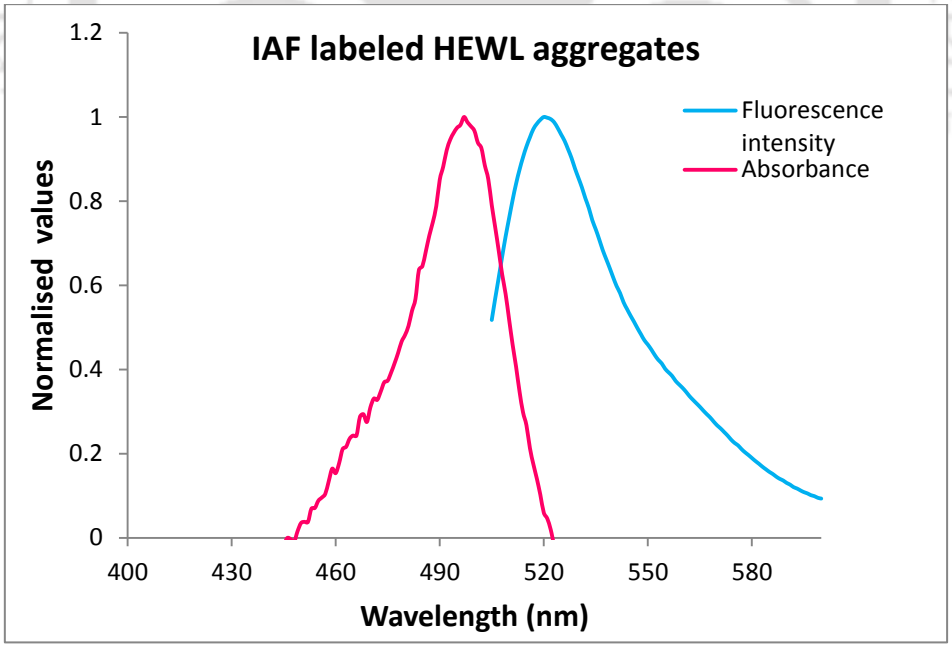

Figure 6.2.3.2 (c): The overlap spectra of absorption and emission for one of the labeled fractions of IAF labeled HEWL aggregates.

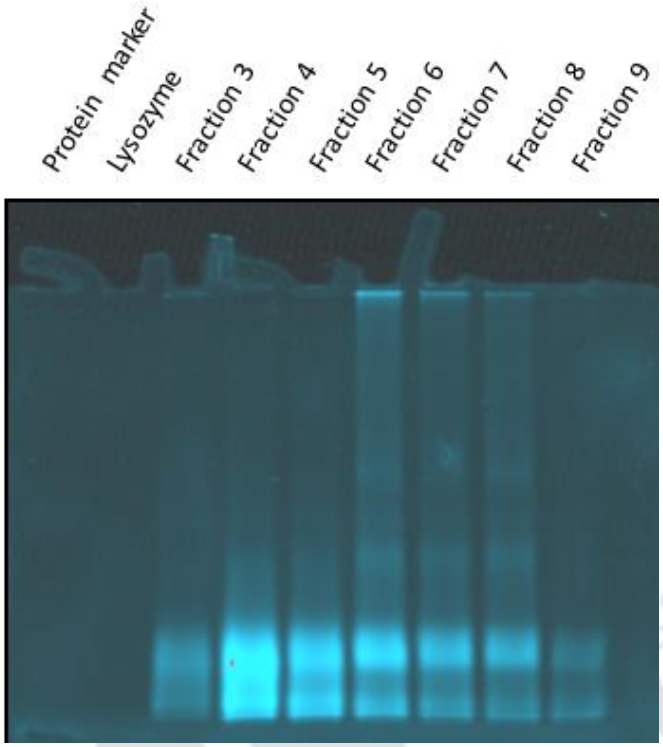

Figure 6.2.3.2 (d): 15 % SDS PAGE of IAF labeled fractions without Coomassie staining.

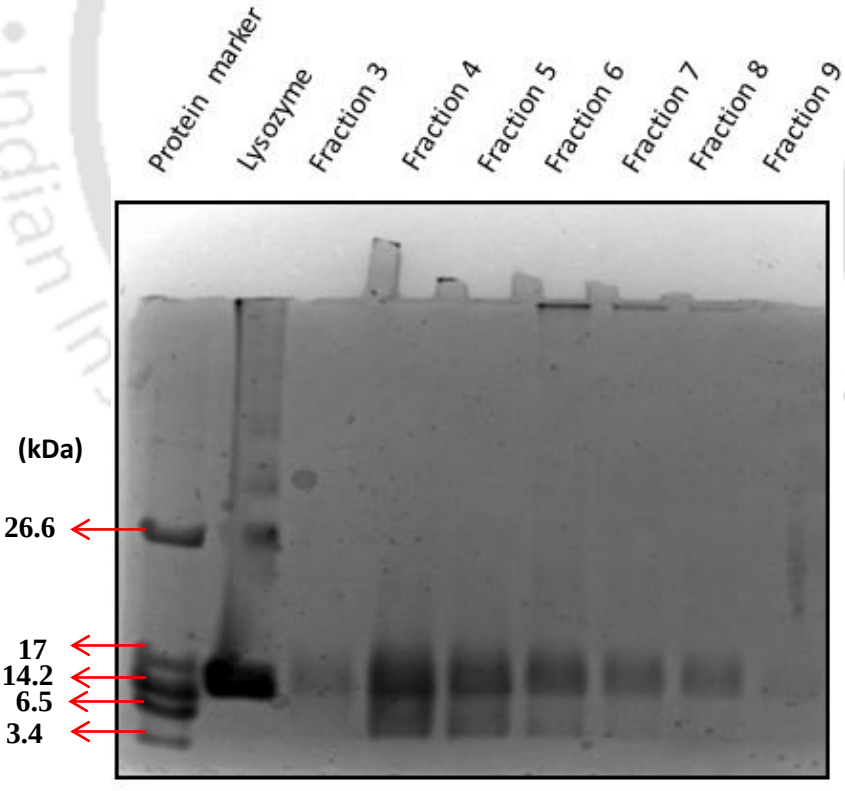

Figure 6.2.3.2 (e): 15 % SDS PAGE of IAF labeled fractions after Coomassie staining.

The IAF labeled fractions (low molar ratio) were subjected to SDS-PAGE. The extent of labeling was less in comparison to labeled fractions with high molar ratio of dye as revealed

from the gel **[Figure 6.2.3.2 (d)]**. Fractions 6, 7 & 8 represent the high molecular weight aggregates as shown in the gel.

TCSPC was used to measure the lifetime of the IAF-labeled HEWL aggregates. Fluorescence emission intensity decay was collected in 4096 channels with a temporal resolution of 0.01221 ns/channel. The peak counts were 10,000 while recording lifetime for the samples. Excitation was performed with pulsed laser diode at 475 nm and emission was collected at 518 nm.

Fluorescein	Lifetime τ(ns)	Chi square
Single fit	4.08	1.22

IAF fractions	α_1	τ_1 (ns)	α_2	τ_2 (ns)	Average τ (ns)	χ^2	Rel % (f_1)	Rel % (f_2)
Fraction 3	0.0136	0.56	0.0297	4	3.79	1.05	6.09	93.91
Fraction 4	0.0127	0.52	0.0282	3.96	3.77	1.13	5.6	94.4
Fraction 5	0.0117	0.84	0.0265	3.99	3.72	1.12	8.5	91.5
Fraction 6	0.0151	0.6	0.0181	3.92	3.54	1.28	11.3	88.7
Fraction 7	0.0175	0.65	0.0244	3.87	3.52	1.07	10.8	89.2
Fraction 8	0.0075	0.67	0.0322	3.84	3.72	1.11	3.9	96.1
Fraction 9	0.0052	0.95	0.0354	3.92	3.82	1.05	3.44	96.56

Table 6.2.3.2: Lifetime data for HEWL aggregates labeled with 5-IAF (low molar ratio). For labeled aggregates, data was fitted with 2-exponential fit (**Reconvolution tail-fit analysis**).

The decay curves for all the labeled fractions show biexponential decay, each displaying a shorter lifetime (τ_1) and a longer component (τ_2). Quenching as revealed by lifetime decay data reveals a small (1-10 %) component with low lifetime. This suggests moderate quenching in case of IAF labeled aggregates (low molar ratio). Fluorescein dye molecules in high molecular weight aggregates apparently seem to be more quenched in comparison to low molecular weight aggregates. In other words, lifetime data show that self-quenching of fluorescein moieties in fractions 6 & 7 is relatively higher as compared to fractions 3, 4 & 5, which are the low molecular weight aggregates.

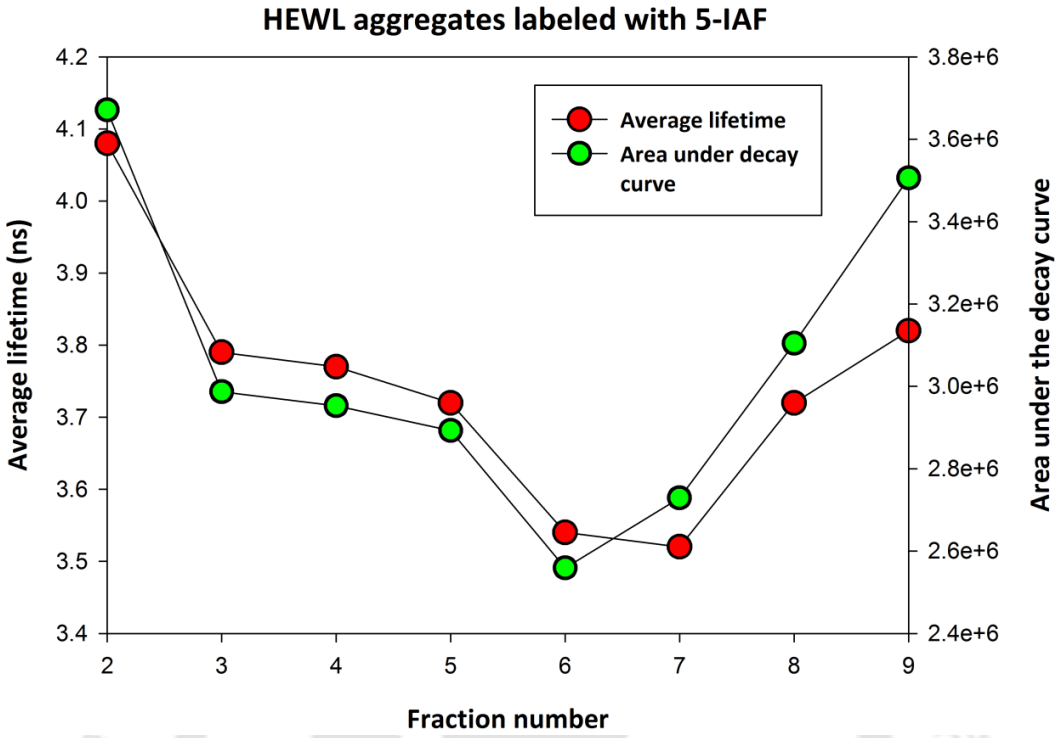

Figure 6.2.3.2 (f): TCSPC data plotted for 5-IAF labeled HEWL aggregates (**low molar ratio**): Area under the intensity decay curve for HEWL labeled with IAF fractions. For the calculation of area, only the fitting range of the curve was selected. Average lifetime is also plotted for all the fractions. Here, Fraction number 2 refers to free fluorescein.

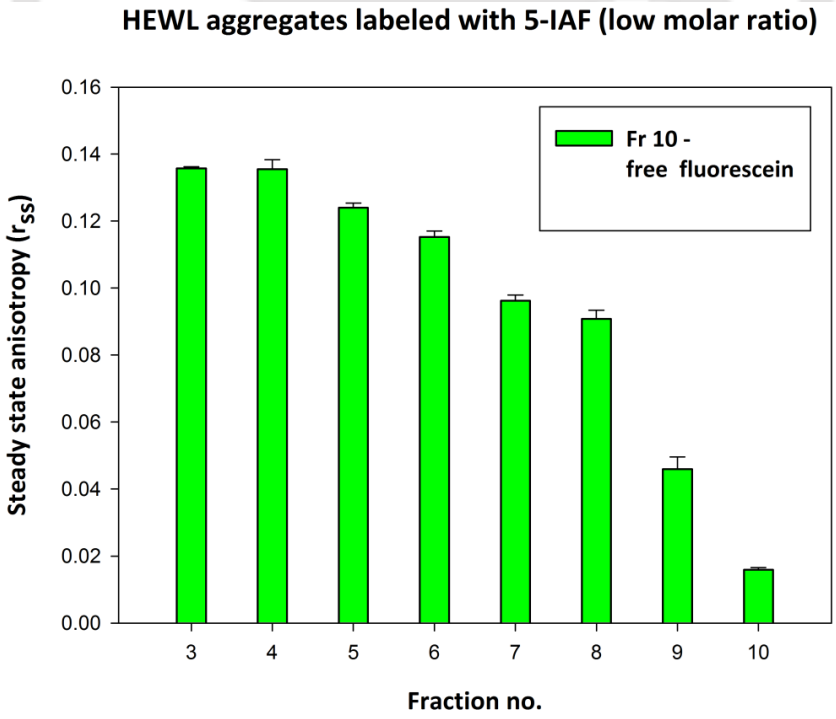

Figure 6.2.3.2 (g): Steady state anisotropy of HEWL aggregates labeled with 5-IAF fractions (low molar ratio).Excitation was performed at 490 nm and emission at 520 nm with Ex/Em slit set as 1 nm and 10 nm respectively. All the fractions were diluted in 0.1 M $NaHCO_3$ buffer, pH 9.2 such that final dye concentration was 0.5 μM in the cuvette.

Detection of homotransfer by steady state anisotropy is the most commonly employed technique. Energy transfer between identical molecules leads to fluorescence depolarization, resulting in decrease of fluorescence anisotropy. For a greater probability of homo energy transfer to occur between fluorescein species, the probes must be within a critical distance of each other when tagged to HEWL oligomers. We have measured the anisotropy of all the fractions of IAF labeled HEWL aggregates (low molar ratio). Free fluorescein in $NaHCO_3$ buffer, pH 9.2 exhibited r_{ss} value of 0.016 which was taken as reference. Fluorescein anisotropy was significantly lower for high molecular weight aggregates i.e. for fractions 6, 7 & 8 in comparison to low molecular weight aggregates (fractions 3, 4 & 5). The decreased anisotropy was due to greater probability of homotransfer in case of high molecular weight IAF labeled aggregates [**Figure 6.2.3.2 (g)**]. Low molecular weight IAF labeled aggregates show high r_{ss} due to reduced homoFRET.

6.2.4 Conclusion

Modification of HEWL aggregates by 5-IAF confirms the availability of cysteine residues for labeling. The IAF modified HEWL aggregates offers unique advantages to use them as imaging agents. The rapid and sensitive detection methods for the labeled products make this method of targeting the thiol groups of the aggregates to label as an attractive approach.

- Time resolved measurements showed that two different lifetime components were obtained for IAF labeled HEWL aggregates. This indicates distinct aggregate population. Labeled fractions corresponding to high molar ratio showed remarkably higher amount of quenching in comparison to that of low molar ratio. This is concluded from the lifetime data.
- The quantum yield for IAF labeled HEWL aggregates is much lowered at high molar ratio (dye: protein = 15:1) than at low molar ratio (dye: protein = 5:1). The effect of self-quenching due to homoFRET between fluorescein molecules was observed in the steady state fluorescence emission spectra of labeled fractions.
- Decrease in fluorescence anisotropy was observed for high molecular weight HEWL aggregates constituting labeled fractions of low molar ratio. Fluorescence depolarization due to homoFRET between labeled fluorescein molecules on HEWL oligomers resulted in low anisotropy.

Chapter 7

F^{19} NMR comparative study on fluorinated HEWL monomer and fluorinated HEWL aggregates

F^{19} NMR comparative study on fluorinated HEWL monomer and fluorinated HEWL aggregates

7.1 Objectives of the experiment

1) To use F^{19} NMR as a spectroscopic tool to characterize the model protein HEWL in its native state and in its oligomeric state.
2) To synthesize fluorine labeled protein aggregates.
3) To get detailed information about protein dynamics in solution from nuclear spin relaxation measurements.

7.2 Introduction

F^{19} NMR has emerged as a powerful tool due to its major attractive properties such as absence of background signal as it doesn't occur naturally in proteins, high resonant frequency, shorter acquisition time; higher sensitivity which is almost 83.4 % to that of H^1, broad chemical shift range which allows detection of structural changes etc.[1] F^{19} nucleus is more favourably used as compared to H^1 and C^{13} nuclei because of its 100 % natural abundance and is most widely preferred to label the biomolecules due to its broad chemical shift range. Lots of reviews have been published in the past where the focus has been given on fluorinated systems.[3] Reported value for gyromagnetic ratio of F^{19} nucleus is 40.0776 MHz/T which is comparable to that of H^1 nucleus (42.5775 MHz/T).[1]

For the past two decades, various researchers have worked on incorporating fluorine labels into different biosystems and F^{19} NMR has received a considerable attention. This chapter describes the use of F^{19} NMR as a tool to characterize the fluorine labeled HEWL nanoparticles. One-dimensional F^{19} spectra and T_1, T_2 relaxation data were acquired for a detailed characterization of fluorine labeled species.

7.2.1 Fluorine as a probe for NMR

Fluorine as exogenous spin label

F^{19} probe continues to be the most favoured spin ½ nuclei to be used for specific labeling of proteins. The chemical shift range spans a broad range of around ~1100 ppm which is mainly due to the lone pair electrons of fluorine resulting in paramagnetic shielding effect.

The chemical shift arising due to covalent bonding is much greater than occurring due to non-covalent interactions in a protein labeled with fluorine probe[3]. Due to the complexity and lack of resolvable signals generated from H^1 NMR data for proteins, fluorine is introduced as an exogenous nuclear spin label into the system of proteins. Moreover, the barrier of unwanted solvent signal doesn't exist in fluorine labeled system, which usually has to be taken care of while recording proton NMR spectra. Even the ease of detection of signals due to its very high sensitivity makes the fluorine spin labeling approach a very efficient method[4].

Steric effects

In order to substitute fluorine in a molecule, various factors have to be taken into consideration. For example, the steric impact of replacing H-atom with fluorine is negligible due to small van der Waals radius of the fluorine atom which can easily replace hydrogen in a molecule. The van der Waals radius for fluorine is 0.14 nm, which is slightly greater (~ 20%) than that of hydrogen which is 0.12 nm.[5] Due to the similarity in size, replacement of C-H bond with C-F bond is also referred to as the mimic effect of fluorine for hydrogen. Several studies have shown that fluorination has a minimal impact on the biological activity of the proteins. In the past, a large no. of reports has addressed the issue of effects of substitution of fluorine in various compounds.[6] Replacement of fluorinated amino acids has been reported to enhance the stability of proteins remarkably. Certain hypotheses proposed that the underlying mechanism behind the increase in stability is due to the increase in the buried hydrophobic surface area within the fluorinated protein[7]. **Benjamin C. Buer** and his co-workers have carried out numerous structural studies on various de-novo designed fluorinated proteins by X-ray crystallography. They have reported that stability imparted by fluorination is neither due to fluorous interactions between the side chain residues nor due to efficient packing of the fluorinated residues into the hydrophobic core. Rather, increase in the hydrophobic surface area and volume is the main contributing factor for protein stability upon incorporation of fluorinated residues.

Effect on polarity

Enhanced lipophilicity in fluorinated compounds has also been linked to the effects of substitution of fluorine-containing groups such as CF_3, OCF_3, and SF_5 etc. It is a general observation that replacement of 'H' by a 'trifluoromethyl' residue in a drug enhances the hydrophobicity and permeability as a result of which the ability of drugs to diffuse across the membranes increases to a great extent[8].

Effect on pK_a of the compounds

Fluorine substitution has a pronounced effect on acidity and basicity of various groups. **Sun W. et al.** have brought to notice the influence of fluorination on well-known fluorescent dyes. The central idea of the paper is based on the synthesis of novel fluorinated fluorescein dyes with novel photophysical properties as compared to the parent dye i.e. unsubstituted fluorescein. The study demonstrates various approaches used for introduction of fluorine into fluorescein which resulted in (a) variation in quantum yield depending upon the substitution position of fluorine; (b) decrease in pKa value; and (c) measurable increase in photostability of the synthesized fluorinated fluorophores. The electronegativity or strong e^- withdrawing nature of fluorine has been reported to be the major contributing factor for the decrease in pK_a values of synthesized fluorinated fluorescein dyes.[9] The decrease in pKa value of the functional groups is mainly due to the electronic effects of fluorine substituent which mainly affects the e^- density of the neighbouring functional groups.

Interactions of fluorine atom with proteins

Incorporation of fluorinated amino acids into the protein do not cause any significant alteration in the structure of the protein which is an advantage of labeling of proteins with fluorine. The changes caused by the placement of a fluorine moiety are reflected as changes in the reactivity, activity, stability or tertiary structure of the protein. The effects of fluorine substitution into proteins have been analyzed by **Gerig et al.** Their analysis focussed on effects of replacement of fluorine in a protein ribonuclease-S. Various van der Waals interactions and other possible interactions such as electrostatic and H-bonding occurring between fluorine and other neighbouring atoms of the structure play an important role in causing a change in chemical shift of the fluorine nucleus. Computational energy minimization methods were employed to investigate the impact of fluorine introduction to the proteins. No appreciable changes were observed on placing a single fluorine atom into the protein and the tertiary structure of the protein also remained unaltered after substitution.[5]

The established methods available for incorporation of fluorine labels into proteins are described as:

Biosynthetic approaches are most widely used methods to incorporate F^{19} labels into biological macromolecules. Researchers have provided a framework for incorporation of 3-fluorotyrosine, a fluorinated analogue of tyrosine into GFP **(Jackson et al., 2006)**.

In this study, protein engineering has been used to substitute the tyrosine residues of GFP into phenylalanine and generate fluorotyrosine labeled GFP mutants containing 10 fluorotyrosine labels. It enabled the use of F^{19} NMR to probe the structural transformations in native and denatured states of GFP. Even to characterize the different intermediate states of folding and solvent exposure of GFP, F^{19} NMR signals proved to be a powerful tool. Chemical shifts in NMR signal and solvent accessibility studies provided a detailed structural characterization of native and denatured states of GFP.[10]

Several methods have also been developed in order to overcome the limitations of biosynthetic approaches i.e. when the incorporation of amino acids to a particular site becomes unachievable. As mentioned above, the methods include selective labeling of side chains of proteins by a covalent modification which is accomplished by the use of amine specific fluorinating agents such as S-ethyl trifluorothioacetate and trifluoroacetamidosuccinic anhydride. As a result, these approaches led to the development of F^{19} labeled biocompatible trifluoroacetylated-albumin derivative as MRI probes.[11] Even the method of chemical modification of the polymer molecules to conjugate to different fluorinated analogues has achieved high success rate in terms of labeling efficiency and yield (%) of the desired conjugate product. This method includes coupling of fluorinated analogues to different classes of polymers by forming linkages with $–NH_2$ (amine) groups in presence of a reducing agent. Incorporation of fluorine by chemical linkage occurs via amine groups or CYS residues of the protein, both the groups are the preferred targets for fluorine labeling.

7.2.2 Previous F^{19} NMR studies on Lysozyme

Lian et al. investigated the effects of incorporation of fluorinated amino acid residues specially Trp and Phe residues into egg white lysozyme from different avian species by F^{19} solution NMR spectroscopic studies[12]. They have performed extensive analysis of F^{19} labeled Trp and F^{19} Phe lysozyme and carried out a series of experiments in order to determine the effect of denaturants on chemical shift of lysozyme, variation of chemical shift as a function of pH, contribution of surface charges of the protein on shielding by acetylation of LYS residues and finally the effect of binding of saccharide inhibitors to F^{19} labeled lysozyme on shielding parameter.

F^{19} NMR data for biosynthetically incorporation of trifluoromethionine (TFM) into bacteriophage lysozyme has been presented by **Duewel et al.**[13] The protein NMR studies reported by the authors mainly centered on the effect of different levels of incorporation of

fluorinated methionine residues on conformational changes in protein structure. Incorporation of TFM into the protein generated distinct resonances in NMR spectra for 3 different methionine residues. Electron spray mass spectra analysis clearly demonstrated the difference between lysozyme labeled with a higher level of TFM and with a lower level of TFM. Increase in hydrophobicity of fluorine incorporated protein due to the introduction of $-CF_3$ group (hydrophobic group) was confirmed by reverse phase HPLC.

7.2.3 Applications of F^{19} NMR

In biological systems, the applications of F^{19} NMR spectroscopy can be extended to various areas.

Conformation changes in a protein

Some studies have clearly demonstrated the applications of fluorine NMR in the investigation of structural changes in proteins. **Xiao et al.** have observed structural changes in the ubiquitin protein induced by the interactions of a fluorinated surfactant with the protein.F^{19} chemical shifts in NMR spectra revealed the formation of aggregates of fluorinated surfactant on binding to ubiquitin.[14]

F^{19} pH sensors in vivo

Another interesting example for an application of F^{19} NMR is the development of fluorine-polymer conjugates as pH sensitive probes. **Mehta et al.** have designed fluorinated pH probes consisting of 6-Fluoropyridoxal covalently attached to carrier polymers such as albumin, polyamino dextran and polylysine. These macromolecular pH sensing agents have been used to assess the changes in pH in the vicinity of the fluorine probe by displaying an altered chemical shift in response to the acidic or basic environment. The study illustrates the excellent characteristics of F^{19} nucleus such as minimal background signal over other nuclei such as P^{31}, H^1 and C^{13} nuclei and a sharp detectable narrow resonance peak as compared to multiple overlapping resonances in the case of other NMR pH indicators. The methodology developed to conjugate the various macromolecules such as protein and polymers with fluorinated molecules is based on their sensitivity of F^{19} chemical shift to pH. This particular work has really facilitated the use of F^{19} pH sensors for in vivo targeting to specific tissues and also for measurement of intra and extracellular pH. These are the unique indicators synthesized for in vivo magnetic resonance imaging purposes.[15]

Fluorinated fluorescent dyes

Owing to many useful properties of fluorescein and its derivatives such as high fluorescence and high quantum yield, they have been used for bioconjugation to different proteins, oligopeptides, nucleotides and various other biomolecules. However, there are certain limitations to their applications in the biological platform as fluorescein has a well-known pH dependence of its fluorescence emission and absorbance spectra. Consequently, difficulties are being faced while using it in a physiological pH range where fluorescein is in a non-fluorescent form. The evolution of fluorinated fluorescent dyes has gained interest because of their lowered range of pKa and broad utilizations in biological systems as reporter molecules. Thus far, studies have confirmed the effectiveness of fluorinated Fluoresceins as conjugates to have apparently higher quantum yield than fluorescein labeled conjugates. Perhaps, the main reason which has been figured out for the enhancement in the fluorescence is due to the increased photostability and resistance to quenching upon introduction of fluorine labels into the dye. Synthesis of various fluoro Fluorescein derivatives made it possible to have bioconjugates with more no. of dyes per protein without compromising the quantum yield or other properties of the dye.[9]

In vivo F^{19} Magnetic Resonance Imaging (MRI)

In the past, several conjugates of fluorinated proteins have been made and evaluated as potential F^{19} MRI agents. The experimental demonstration was carried out for F^{19} labeled albumin in blood samples taken from mice. Extensive applications of fluorine NMR in biological systems has been discussed in detail in the review published in 1994 by **J. T. Gerig.**[4]

7.2.4 Preference for F^{19} NMR

Due to the evolution of new technologies, proton NMR spectroscopy of biological macromolecules is being gradually replaced by fluorine NMR spectroscopy. The complexity of processing and interpretation of H^1 NMR data for proteins makes it a less approachable technique to gather information regarding structure and dynamics. Even the size of a macromolecule is a limiting factor for assigning the resonances in proton NMR spectra. Resolution of the spectra in the case of proteins is also a challenge as the overlapping signals in H^1 NMR spectra dominate the spectra which is overcome in F^{19} NMR spectra as the signals obtained are very sharp and narrow.[4]

The chemical synthesis of fluorinated products is practically possible on a large scale due to the low cost incurred in the preparation of the materials which seems to be very high while considering other labeling reagents such as tagging the proteins with fluorophores or generating N^{15} isotope labeled proteins. In fact, in terms of stability fluorinated products are highly desirable because they have been reported to enhance the stability of the proteins when incorporated as fluorinated amino acids.[7]

The main features which were found to be influencing while considering $-CF_3$ as a probe can be listed as a) excellent sensitivity of chemical shift to its environment, b) 3-fold enhanced signal to noise ratio due to the presence of 3-equivalent fluorine nuclei and c) long transverse relaxation time etc[16].

7.3 Materials and Methods

7.3.1 NMR specifications

1D NMR at 376.59 MHz

NMR measurements were performed on Bruker BioSpin GmbH NMR spectrometer equipped with a 5 mm PABBO BB/19F-1H/D Z-GRD Z114607/0107 fluorine probe for recording 1D spectrum. F^{19} NMR spectra were recorded with 16 scans and spectral widths were set to 83333.3 Hz. A short relaxation delay of 1.00 s was used for measurement of the spectra. All the samples were dissolved in D_2O and then 1D F^{19} NMR spectra were recorded at a temperature of 298.0 K (probe temperature) with a spectrometer frequency of 376.59 MHz. 700 µL of clear solution of each of the sample dissolved in D_2O was taken in NMR tubes. The solvent D_2O is required for the deuterium lock.

Acquisition parameters: Pulse width – 14.1500 µs, Spectral width – 83333.3 Hz, Acquisition time - 0.1966 s (references) and 1.999 s (HEWL samples), Lowest frequency- -81208.9 Hz, Nucleus – 19 F, Probe temperature – 298.0 K, Shim coil temperature – 305 K. The resonances are expressed in terms of ppm. Number of scans and acquisition time varied a little for different samples.

A general sign convention (+ ve or – ve) was followed for ppm scale i.e. high frequency, low field or deshielded values were assigned a positive sign.

MestReNova or Mnova: NMR analysis software package was used to process 1D F^{19} NMR data. Base line corrections and phase corrections were performed with the help of Mnova software for better visualization of the data.

We prepared fluorine labeled HEWL monomer and HEWL aggregates by a method proposed previously by Mehta and Co-workers.[11] The formation of fluorinated products was visibly clear after the reaction with the appearance of white precipitate. However the strategy used to label the aggregates included a little different methodology as compared to monomer in terms of experimental conditions, reaction time, volume of the fluorinating agent, reaction buffer etc.

7.3.2 UV-Vis spectra

UV-VIS spectra measurements were performed on Perkin Elmer UV/Vis spectrometer LAMBDA 25.All the samples were diluted in milliQ water prior to recording of spectra. HEWL in already lyophilized form (nonfluorinated) was taken as a standard to compare with the fluorinated samples. The concentration of the fluorinated samples as well as HEWL control (non-fluorinated) was determined from the UV/Vis spectra using the molar extinction coefficient of 38,400 $M^{-1}cm^{-1}$ at 280 nm.

7.3.3 SDS-PAGE

For performing gel electrophoresis, Bio-Rad apparatus was used. SDS-PAGE was performed under reducing conditions with β-mercaptoethanol added to the sample buffer.15 % resolving gel was run in a vertical gel electrophoresis unit. After conducting the run, gels were stained with Coomassie brilliant blue by placing them in staining solution overnight and then destaining was done with a fresh destain solution of glacial acetic acid/methanol/water.

7.3.4 Reference Standards

Sodium Fluoride (NaF, Sodium fluoride GR, CAS no. 7681-49-4, Merck) – 0.1 M (4.2 mg in 1 mL of D_2O) was prepared to record 1D F^{19} NMR spectra. Molecular weight of NaF is 41.99 g/mol.

Sodium trifluoroacetate (CF_3COONa, 132101-25G, Sigma Aldrich Co.Pvt.Ltd.) – 0.46 M (63 mg in 1 mL of D_2O) was prepared to record 1D F^{19} NMR spectra. Molecular weight of CF_3COONa is 136.01 g/mol.

For F^{19} NMR spectroscopy, sodium trifluoroacetate and sodium fluoride were used as external references in order to assess the chemical shift sensitivity of the fluorinated conjugates.

7.3.5 Reagents

Fluorinating agent: **S-ethyl trifluorothioacetate** (Sigma Aldrich -97 %, Cat no. -177474-10G, Molecular weight- 158.14 g/ mol)

HEWL: Lysozyme from chicken egg white was procured from Sigma-Aldrich Co. Pvt Ltd. in dried powdered form (**Cat no. L6876**) stored at -20 ^{0}C and was used directly without any purification.

7.3.6 Methodology for T_1 measurement

T_1 values were acquired by plotting the decay of integrated intensity between peak regions of the spectra and fitting the curves with standard exponential equation with *Topspin 2.0* software.F^{19} spin–lattice relaxation times were determined by the T_1 inversion recovery method. Relaxation measurements were acquired with proton decoupling. The measurements were repeated several times by varying the delays between the pulses.

T_2 relaxation rates are usually faster than spin–lattice relaxation rates. T_2 relaxation parameter is very effective to carry out studies in case of very large proteins. Evaluation of transverse relaxation time for fluorinated tags attached to protein aggregates of estimated mass range from 1000-2000 kDa (predicted from DLS data) helps us in determining the rotational correlation time of large aggregates

Rotational correlation time (theoretical value) of the macromolecule can be estimated from the ratio of T_1/T_2.

This chapter describes the relevance of F^{19} solution NMR in the investigation of biomolecular systems. The goal of this study was to exploit the useful properties of F^{19} isotope for characterization of synthesized fluorine labeled bioconjugates. Investigation focussed on determining different relaxation parameters in order to predict the mobility of F^{19} labeled species in solution state. A description on emergence of F^{19} as a versatile tool in current scenario and its practical applications in biological system is provided. In addition, basic concepts of NMR and a general definition of T_1 and T_2 relaxation rates are also provided. Hen egg white lysozyme protein was used as a model protein to study the effects of

fluorination on proteins. Chemical incorporation of $-CF_3$ group into Hen egg white lysozyme protein was used as the strategy to develop fluorinated conjugates. A comparative study was carried out in F^{19} labeled HEWL in its native state (monomeric form) and F^{19} labeled HEWL in its aggregated state (oligomeric form). Resonance frequencies were measured for fluorinated proteins along with standard compounds as references. Their relaxation behaviour was also characterized which is discussed in the present study.

7.4 Conjugation reaction mechanism

HEWL protein (monomer) contains 6 LYS residues in total. pKa value for the side chain of LYS residue has been reported to be 10.4 in the literature[17]. Incorporation of fluorine into the side chain of LYS residues in the protein can be assumed to have no major effect on the structure of the protein. Preferential labeling of ε-amino group of lysine residues is achieved by using a reaction pH where the lysine residues are in protonated form which allows the acetylation reaction to proceed. LYS is a basic amino acid with significant hydrophilicity or polarity. The aliphatic amines of LYS ε-amino group are basic in nature and a pH > 8.0 is optimal for modifying the lysine residues. Hence, they are selectively modified at a pH greater than 8.0.

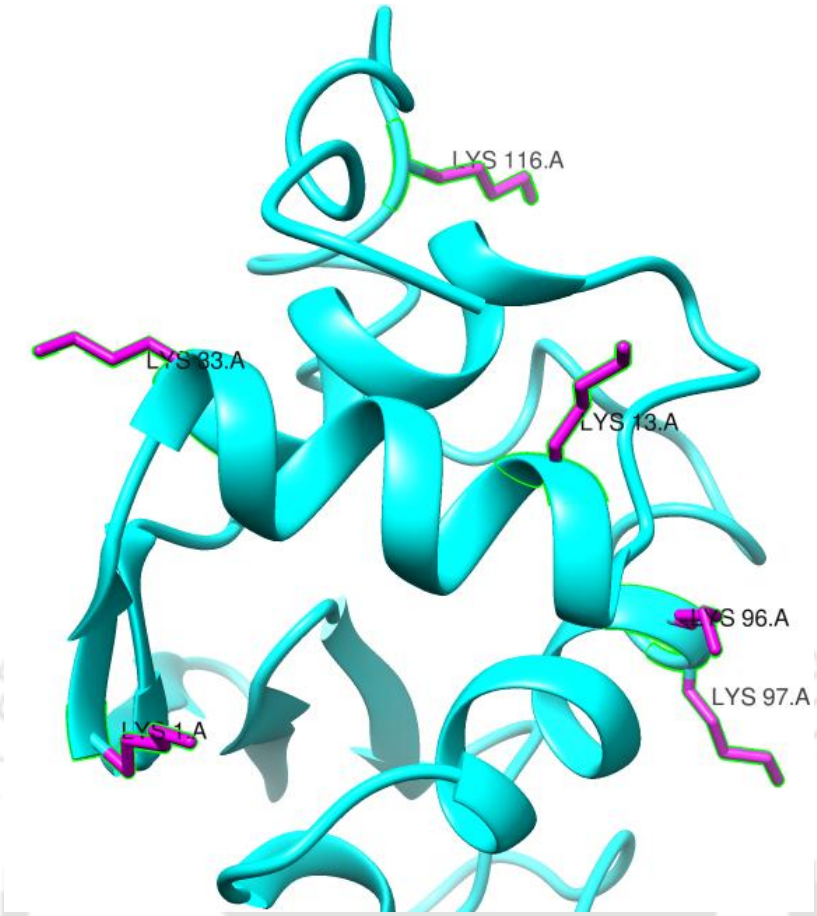

Figure 7.4: Structure of HEWL (PDB Id- 5f14) generated by generated by Chimera 1.11.2rc for visualization of the structure. Lysine residues are shown as side chains (magenta colour).

Herein, LYS residues in oligomeric state of HEWL aggregates are abundant and are targeted site selectively by using the chemical modification strategy of trifluoroacetylation. It is noteworthy that amount of fluorinating agent added to the reaction to proceed was 4 fold less than the amount added for fluorination of monomer and in addition the bioconjugation process in case of aggregates occurred more rapidly most likely due to the presence of large no. of LYS residues in it.

The concentration of the protein used for fluorination of HEWL monomer was 10 mg/mL in aqueous buffer whereas the concentration of HEWL aggregates used for fluorination of nanoparticles was 120 µM (1.7 mg/mL). Fluorine labels or $–CF_3$ groups were introduced into HEWL monomer as well as aggregates by chemical covalent conjugation to amino groups ($-NH_2$) on the protein by trifluoroacetylation with S-ethyl trifluorothioacetate (SETFA).[15]

7.4.1 Fluorinated HEWL monomer

10 mg of HEWL protein was dissolved in 0.1 M $NaHCO_3$ buffer (1 mL), pH 8.0.To the reaction mixture, 2 mL of SETFA (fluorinating solvent) was added and the temperature of the reaction was maintained at 4°C for 1 Hr. Within 2 min of addition of the fluorinating agent, the solution separated into 2 phases, one as aqueous and the other organic phase. The reaction was intermittently shaken manually and gradually the solution turned from transparent to turbid. After 1 hour, the reaction mixture was brought to room temperature and the formation of white precipitate appeared. The precipitate was pelleted down by centrifugation and supernatant was decanted. The fluorinated protein conjugate obtained in the pellet was lyophilized and then stored at room temperature. The lyophilized product was resuspended in 100 % D_2O for recording NMR spectra and the fluorinated conjugate was stable even after 1 month when stored under these conditions. Titration was done by adding different amounts (volume) of fluorinating solvent to the reaction mixture in order to standardize the fluorine labeling procedure.

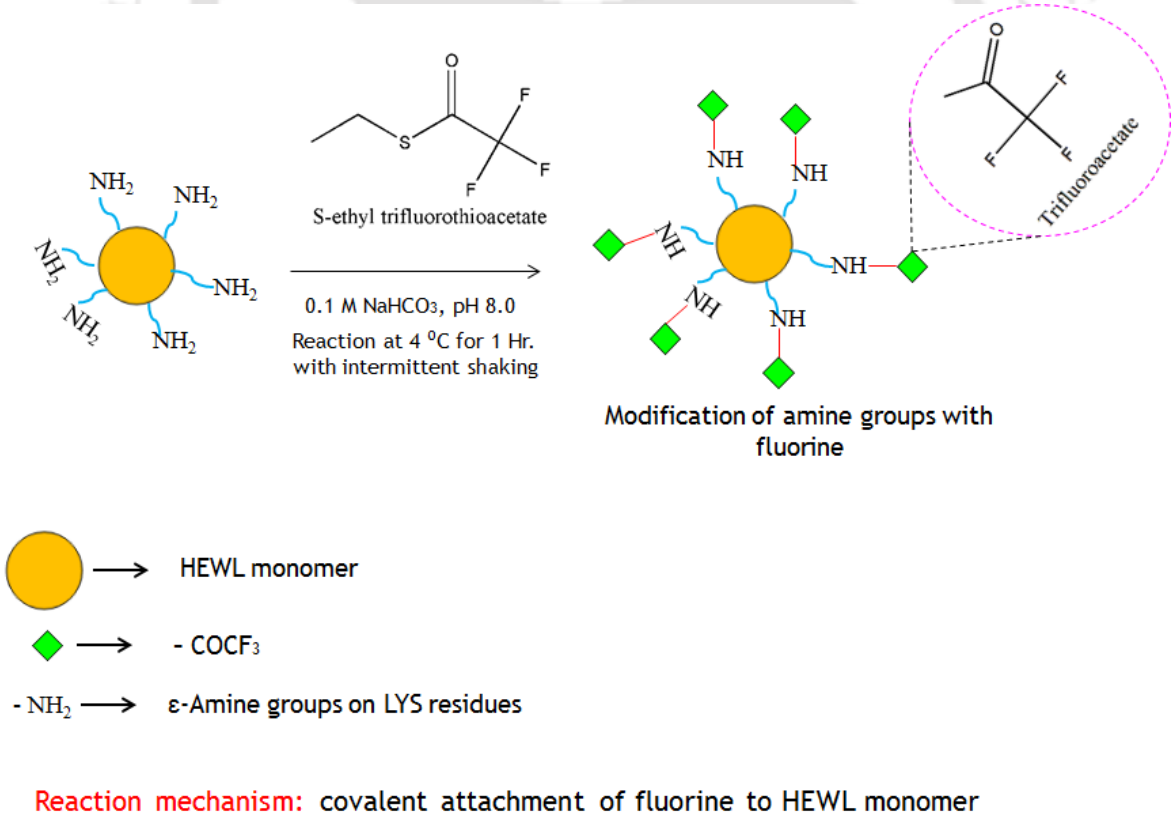

Figure 7.4.1: Synthesis of F^{19} labeled HEWL monomer. Reaction was carried out at 4°C and pH of the reaction was maintained at 8.0.The conjugation between terminal amines of Lysine residues and the trifluoroacetyl group of fluorinating agent results in a stable covalent linkage.

7.4.2 Fluorinated HEWL aggregates 120 µM HEWL aggregates incubated for 4 days in pH 12.2 (6 mL) with 500 µl of 97 % S-ethyl Trifluorothioacetate. No stirring of the solution was required. The tube was shaken for 10 minutes manually, in the first 5 minutes of reaction 2 phases were formed i.e., one aqueous and other organic. After 10 minutes the solution turned turbid and there was formation of white precipitate. Initially for the reaction, 10.2 mg of protein was used. In subsequent steps, the reaction mixture was subjected to centrifugation for 30 minutes which resulted in the separation of fluorinated protein conjugate as precipitate in the pellet and fluorinated organic solvent as well as aqueous buffer as supernatant (*Centrifuge, Sigma®, 2-16 KL, 30 min at 6000 rpm at 25 °C*).The precipitate was lyophilized (*Lyophilizer, Scanvac, CoolSafe™, 100-9 Pro*) to yield the conjugate (TFA-HEWL aggregates). 9.3 mg of fluorinated protein was obtained and thus the recovery product yield % was 91 %. A large amount of fluorinated aggregates made the solution turbid, consequently, a very small amount (~ 1.0 mg) of lyophilized fluorinated aggregates was resuspended in 100 % D_2O so as to obtain a clear transparent solution as they are partially soluble in water.700 µL solution of F^{19}-aggregates in D_2O was used to record 1D NMR spectra.

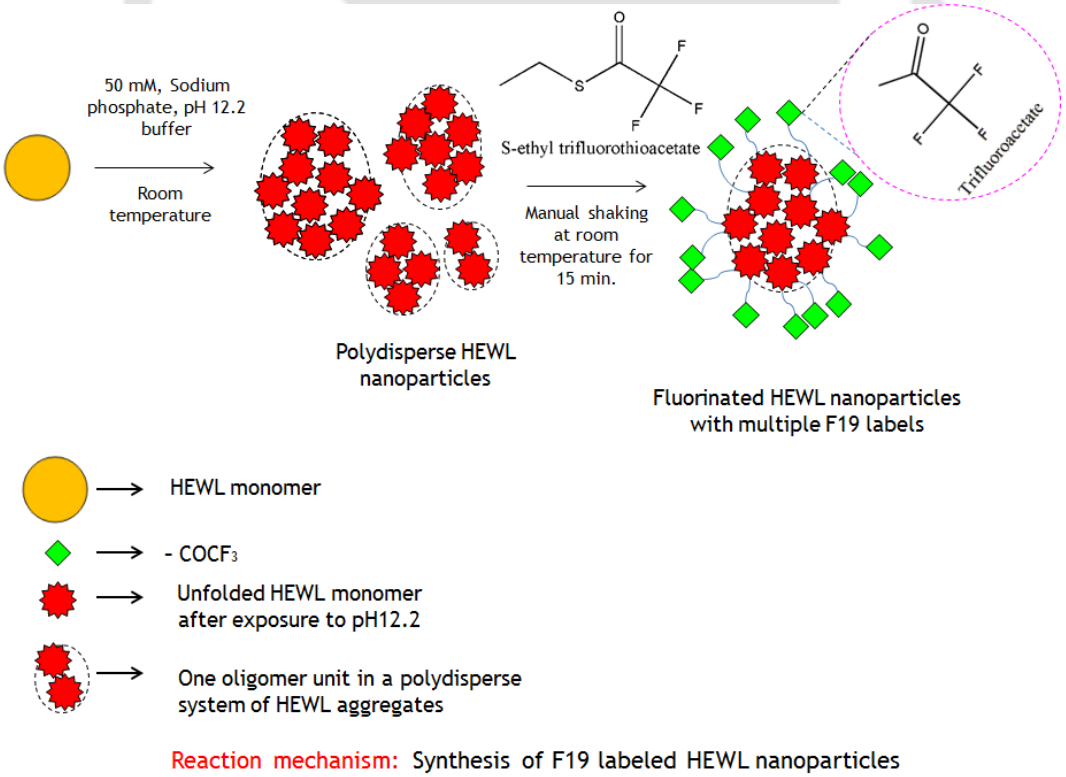

Figure 7.4.2: Reaction methodology employed to tag the fluorine labels onto LYS residues of HEWL aggregates.

[A] Mixing of aqueous and organic phases

[B] The solution turning turbid

[C] Appearance of white precipitate

[D] Settling down of the precipitate to the bottom

Figure 7.4.3: Schematic of the fluorination reaction of 120 µM HEWL aggregates (4 days old) with SETFA

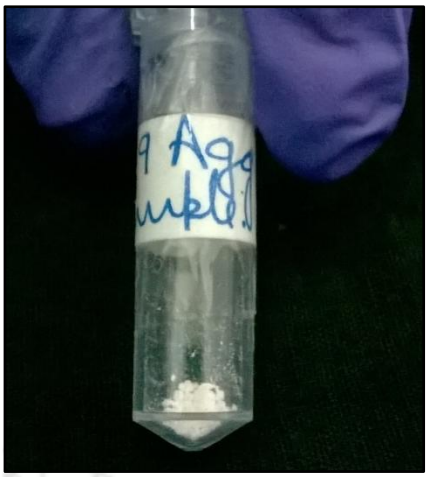

Lyophilized fluorinated monomer Lyophilized fluorinated HEWL aggregates

Figure 7.4.4: F^{19} labeled [a] HEWL monomer [b] HEWL aggregates after freeze drying the labeled product.

[A] Partially soluble F19 aggregates [B] Completely soluble F_{19} monomer

Figure 7.4.5: Assessment of solubility of synthesized fluorinated products [A] fluorinated aggregates show reduced dispersibility in water [B] fluorinated monomer is completely soluble in aqueous solvent.

7.5 Results and Discussion

We have exploited the useful properties of F^{19} labels to develop fluorinated bioconjugates; F^{19} labeled HEWL monomer and F^{19} labeled HEWL protein nanoparticles. The methodology adopted to attach the fluorine labels allowed for selective labeling of the protein. Apparently, LYS residues (side chains) in the protein **[Figure 7.4]** are selectively modified by S-ethyltrifluorothioacetate. The site-specific labeling helped in enhancing the sensitivity and resolution of NMR spectra. The high sensitivity of F^{19} NMR spectroscopy technique eased the characterization of fluorinated monomer and fluorinated aggregates. Even though sensitivity of NMR spectroscopy is relatively less in comparison to fluorescence-based spectroscopy but the approach to use fluorine as a labeling tool rather than the routinely used fluorophores renders the labeled species of interest to be more stable and overcomes the limitation of tagging larger no. of fluorine labels as there is no issue of photobleaching. Moreover, the absence of fluorine in the native protein makes it a very attractive probe to label the proteins and its detectability in the vicinity of macromolecules is easy due to the lack of interference from any background signal.

In this chapter, we have described the methodology used for the development of fluorine labeled protein aggregates. These are the HEWL aggregates or can be referred to as globular protein oligomers, polydisperse in nature of size in the range of 10-20 nm.

Our experimental results agree well with the previous literature reported values for fluorine peak in case of reference standards **[Table 7.5.1]**. Furthermore, the assumption that fluorinated monomer, as well as fluorinated HEWL aggregates, will have peak coinciding with that of CF_3COONa is in complete agreement with the peak values obtained. All the fluorinated conjugates displayed a single sharp F^{19} signal, similar to that of the external reference, CF_3COONa [**Figure 7.5.4 (a) & 7.5.5 (a)**].

The introduction of multiple fluorine labels into HEWL nanoaggregates decreased its solubility in water significantly. In contrast to a reduced or partial solubility of aggregates, the fluorinated monomer was completely soluble in water. Thus, the effect of fluorination on solubility was assessed by dissolving the lyophilized fluorinated aggregates and monomer in water. Surprisingly, even after the formation of precipitate in the case of fluorine derivatized monomer, upon redissolving the whole of the lyophilized product in water (~9 mg of F^{19} monomer in 1 ml of water), it formed a clear transparent solution i.e. hydrophilicity is maintained in HEWL monomer even after fluorination [**Figure 7.4.5 (b)**].

Whereas it appeared different in the case of aggregates i.e. upon dissolving the solid dried powdered form of fluorinated aggregates in water (~2 mg of F^{19} aggregates in 1 ml of water), it formed a turbid solution [**Figure 7.4.5 (a)**]. Hence, it can be inferred that due to the modification of large no. of available polar functional amine groups ($-NH_2$) by the addition of fluorine labels leads to a reduced polarity of F^{19} aggregates. It can also be anticipated that presence of exposed hydrophobic patches in case of aggregates adds to the reduced dispersibility of fluorinated aggregates in an aqueous solvent. Alteration in the solubility properties of fluorinated conjugates can be attributed to increased hydrophobicity of proteins, a manifestation of incorporation of fluorine residues[7].

On the basis of the results obtained from SDS-PAGE [**Figure 7.5.7**], the fluorinated monomeric HEWL seemed to have similar electrophoretic mobility as nonfluorinated monomeric protein. Both the samples showed up in the gel as 14 kDa band which clearly confirms the integrity (in terms of molecular mass, kDa) of the monomeric form after attachment of the fluorine groups. To put it in other words, the purity of the fluorinated monomer and HEWL monomer (unfluorinated) was assessed by SDS-PAGE. In addition, the identity of the different fluorinated species (monomer and aggregates) was confirmed by UV-Vis spectra analysis. SDS gel confirms that the fluorination process didn't integrate the monomers or chemically cross-linked them. It doesn't provide information on functional integrity.

The formation of a white precipitate [**Figure 7.4.3**] after the reaction with the fluorinating agent (SETFA) allowed easy separation of fluorinated protein from any amount of unlabeled protein as well as fluorinating solvent. After the separation of white precipitate by centrifugation which settled down to the bottom of the reaction tube, there was no visible solid product in the supernatant. Labeling efficiency was high (~ 99 %) as no unlabeled monomer or protein was detected in SDS-PAGE from the supernatant fraction containing fluorinated solvent after separation from the precipitated fluorine labeled protein by centrifugation. F^{19} NMR signals from the precipitates confirm that whole of the protein used for fluorination reaction was labeled. There was well resolved band in case of fluorinated HEWL corresponding to that of HEWL monomer without any appearance of additional reaction byproducts in the SDS-PAGE gel. Usually, polydispersity of the aggregates is seen as a broad smear in SDS-PAGE gels. Fluorinated HEWL aggregates appear as broad smear in the gel revealing their polydispersity. This confirms that aggregates didn't disintegrate into monomers or dimers after fluorination.

Our findings suggest that aggregates carrying multiple fluorine labels much higher (depending on the no. of monomer units present in an oligomer) as compared to the monomer show similar resonance peak in NMR and thus no significant difference is found in the F^{19} chemical shift values of the fluorinated monomer and aggregates [**Table 7.5.1**].

Our finding that F^{19} labeled HEWL monomer showed a single clearly resolved peak corresponding to that of CF_3COONa reference peak replicates the findings of experiments conducted by **Mehta et al.** The single peak refers to all the fluorine labels covalently attached to the protein which are present in the chemically equivalent averaged environment. In order to have a detailed structural information, NMR data is further complemented with data from other spectroscopic techniques such as absorption spectroscopy.

Availability of free $–NH_2$ groups (ε $–NH_2$ group of 6 LYS residues) in HEWL monomer was exploited for covalent conjugation to the fluorinating agent by carrying out the reaction in 0.1 M $NaHCO_3$ buffer, pH 8.0.Attempts to label the HEWL nanoaggregates required less amount of fluorinating reagent (500 µl of SETFA: 6 ml of 120 µM HEWL aggregates in pH 12.2) due to the availability of large no. of free $–NH_2$ groups as compared to the monomer. Our previous studies have shown that protein aggregation carried out in pH 12.2 and room temperature led to the formation of HEWL aggregates of nano size which were highly polydisperse or heterogeneous in nature.[18]

UV/Vis absorption spectra for both fluorinated monomer and nonfluorinated HEWL monomer were identical in shape after normalization to the same peak intensity **Figure [7.5.6 (a)]**.Since, the absorption remains unchanged after attachment of fluorine to the protein, it can be concluded from the results that the chemical modification of HEWL with fluorine didn't cause any significant perturbation in the structure of the protein. However, in the overlaid spectra displayed in the **Figure [7.5.6 (b)]**, a huge difference was observed in case of fluorinated HEWL aggregates in comparison to the monomeric form.

The reason to choose SETFA as a fluorinating agent is chiefly due to the presence of trifluoromethyl group in the chemical compound. It has been observed that probes containing $–CF_3$ groups are more commonly employed rather than mono (-CF) or difluorinated ($-CF_2$) species to carry out F^{19} NMR studies[16]. The introduction of $–CF_3$ groups usually generates a very strong NMR signal which is very useful for applications requiring greater sensitivity. The $–CF_3$ moiety present in S-ethyltrifluorothioacetate consists of 3 fluorine atoms which contribute to a relatively strong intense signal in the NMR spectrum.

In case of large proteins, owing to their slow tumbling rate the data from F^{19} NMR studies gets complicated. Even low sample concentration and dominance of chemical shift anisotropy at higher magnetic fields further make the F^{19} relaxation studies of proteins more cumbersome. As a result of which, fluorine tags which tend to amplify the signal to noise ratio are increasingly preferred over other probes. CF_3 moiety has proved to be a suitable probe for us as enhancement of the signal is necessary for low protein concentrations especially while tagging the protein aggregates in which the concentration of protein was in micromolar range (120 µM).

Mehta et al. have successfully labeled various macromolecules such as albumin, IgG etc. with F^{19} fluorinating agents. Attempts to develop fluorinated probes have facilitated the in vivo magnetic resonance imaging in tissues which was not possible in case of other probes. In the paper they have described the synthesis and purification of fluorinated proteins and the yield for the above mentioned lyophilized conjugates varied in a range of 50-70 %. However, our efforts to fluorinate HEWL monomer and nanoparticles resulted in recovery yield of 90 – 99 % of the lyophilized F^{19} labeled bioconjugates. To date, however there has been no experimental evidence on fluorination of protein nanoparticles. No studies have previously been done to fluorinate the protein aggregates or protein nanoparticles. Although researchers have developed various methods in the past to conjugate the polymers with fluorinated compounds for various applications such as imaging agent. Overall, the data presented above demonstrates the comparative analysis of fluorinated HEWL nanoparticles and HEWL monomer. Selective fluorination of amine groups of Lysine residues in HEWL resulted in fluorinated HEWL monomer functionalized with CF_3 groups in reasonably very high yield (~ 90%).

Experimental data regarding consequences of fluorine substitution on HEWL protein have already been shown by the researchers in the past.F^{19} NMR spectra of fluorinated derivatives of lysozyme exhibited up to 6 major resolved resonances.[19] However our data has shown a single narrow line in the F^{19} NMR spectrum for fluorine labeled HEWL monomer which is strikingly in contrast with the results reported earlier by **Adriaensens et al.** The single major resonance peak corresponds to all the lysine residues which are fluorine labeled as all of them are present in chemically equivalent averaged environments in the denatured state of the protein. In case of an unfolded protein, the resonances collapse to give rise to a single peak which is due to the equivalent solvent environment experienced by each of the probes.

Figure [7.5.2 (a-c)] & Figure [7.5.3 (a-c)] illustrate the 1D NMR spectra of the reference standards. 1D NMR spectra for the fluorinated conjugates are represented in **Figure [7.5.4 (a-b)] & [7.5.5 (a-c)]**. Fluorine spectra for multiply labeled HEWL nanoaggregates exhibited a single clear narrow signal in spite of presence of huge number of fluorine labels in the chemically equivalent averaged environment of aggregates. Thus far, it can be said that resonances are overlapped which give rises to a single narrow composite peak.

The signal from fluorinated HEWL monomer appeared ~0.1 ppm downfield of the shift i.e. a very little dispersion of the external reference CF_3COONa whereas it was shifted ~47 ppm downfield to that of another reference NaF. Similarly, spectrum for fluorinated aggregates shows that fluorine resonance signal of trifluoromethyl group attached to the protein has shifted ~0.094 ppm upfield to that of fluorinated HEWL monomer. However, no appreciable line broadening was observed in case of fluorinated aggregates. Herein, oligomeric protein aggregates used here are referred to as soluble aggregates, high molecular weight species. Monomeric mass of HEWL is reported to be 14.3 kDa. Fluorine NMR studies have also been carried out on proteins as large as ~350 kDa.

The acquisition time for recording 1D fluorine NMR spectra is very less i.e. it takes 5-10 min for the complete measurement which is an advantage when the no. of samples for analysis is very large.

Table 7.5.1: F^{19} chemical shift values are summarised below.

Fluorine-19 Environment	Chemical shift (ppm)
Bare nucleus	0 (reported)
CF_3COONa	-75.51
NaF	-122.41
F^{19} - HEWL monomer	-75.41
F^{19} – HEWL aggregates	-75.504

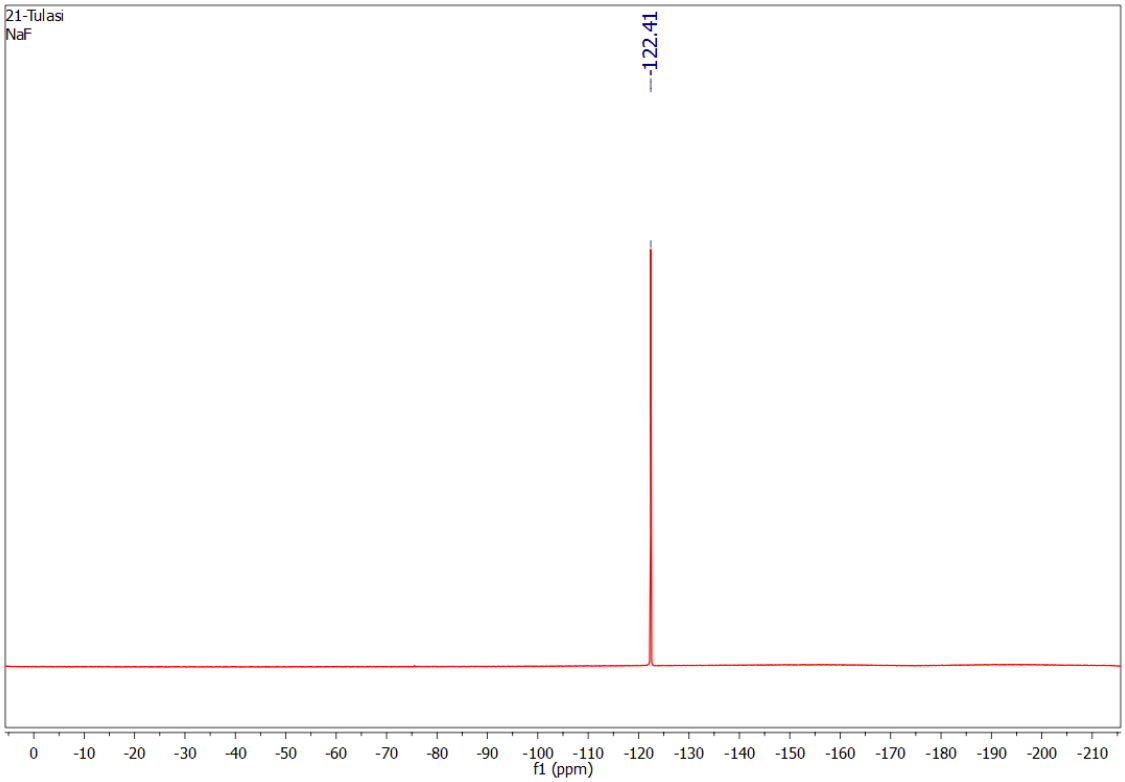

Figure 7.5.2(a): Fluorine NMR spectrum of NaF in D_2O.The signal at -122.41 ppm arises from NaF which is taken as a reference standard.1D spectrum was recorded at 376.59 Hz.

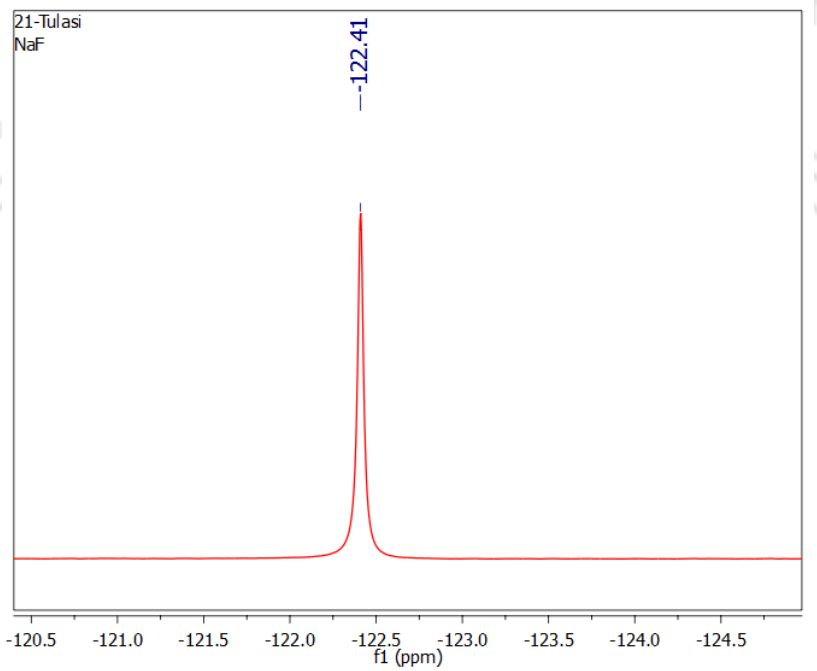

Figure 7.5.2(b): Expanded spectrum of NaF in D_2O.

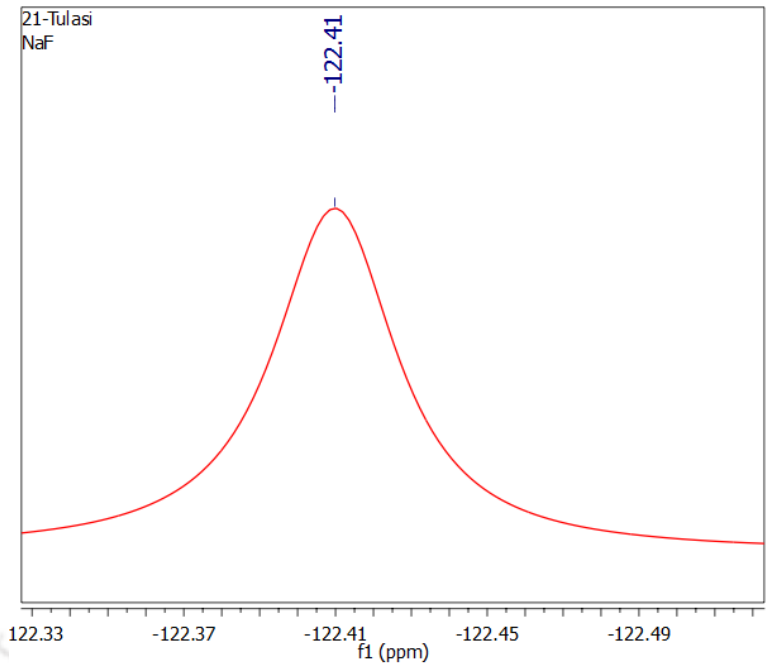

Figure 7.5.2(c): Zoomed spectrum of NaF in D_2O.

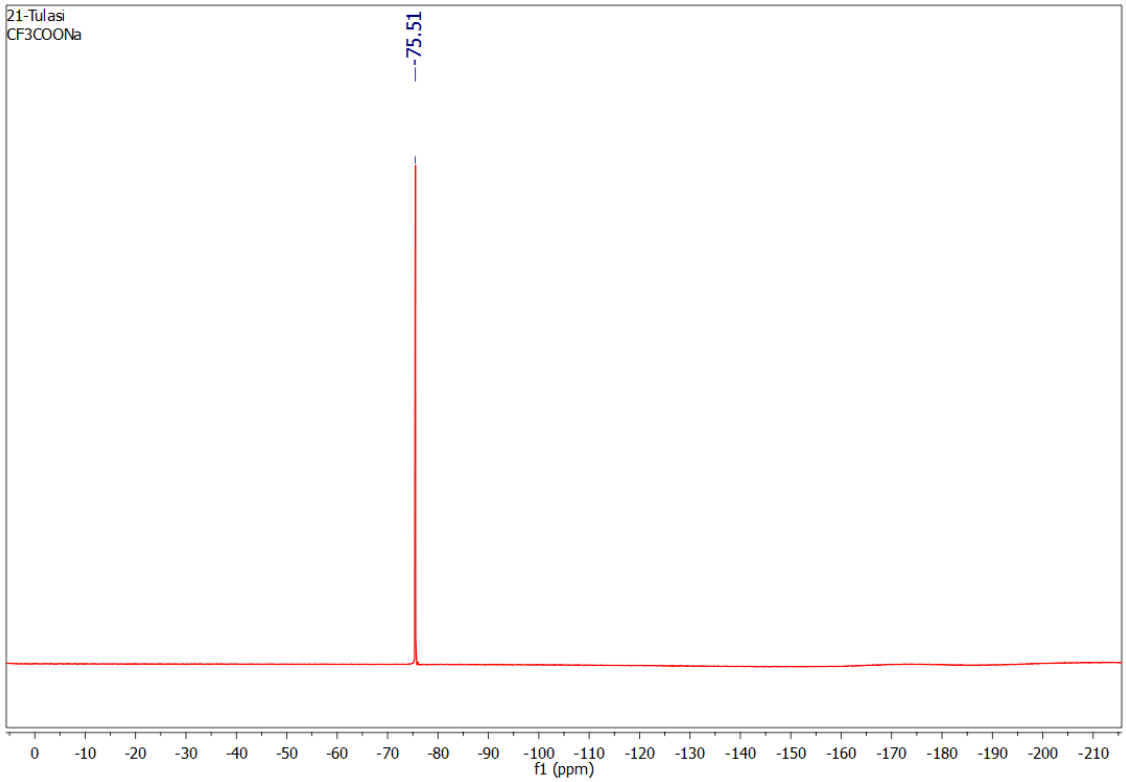

Figure 7.5.3(a): F^{19} NMR spectrum of CF_3COONa, in D_2O, which is taken as an external reference. 1D spectrum was recorded at 376.59 Hz.

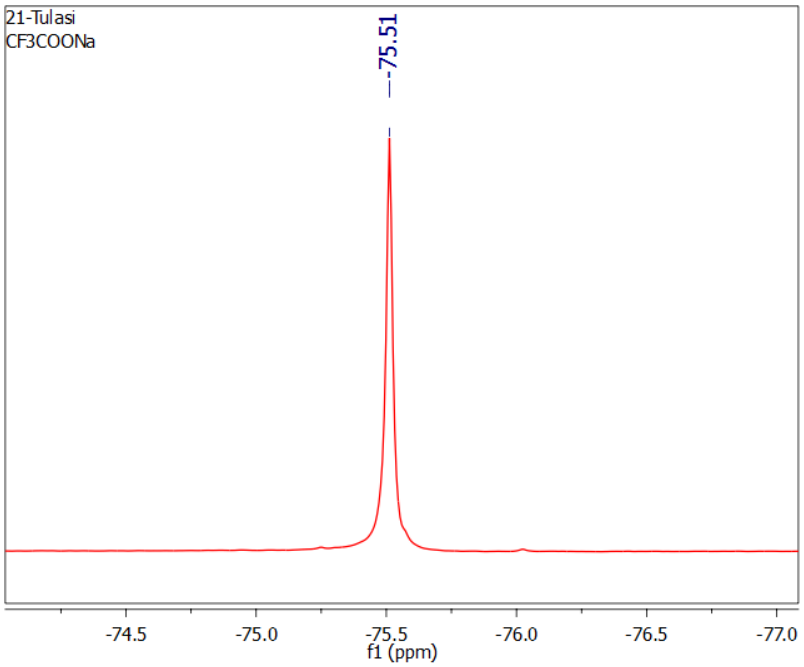

Figure 7.5.3(b): F^{19} spectrum recorded on Bruker BioSpin GmbH spectrometer. (Zoomed spectrum of CF_3COONa)

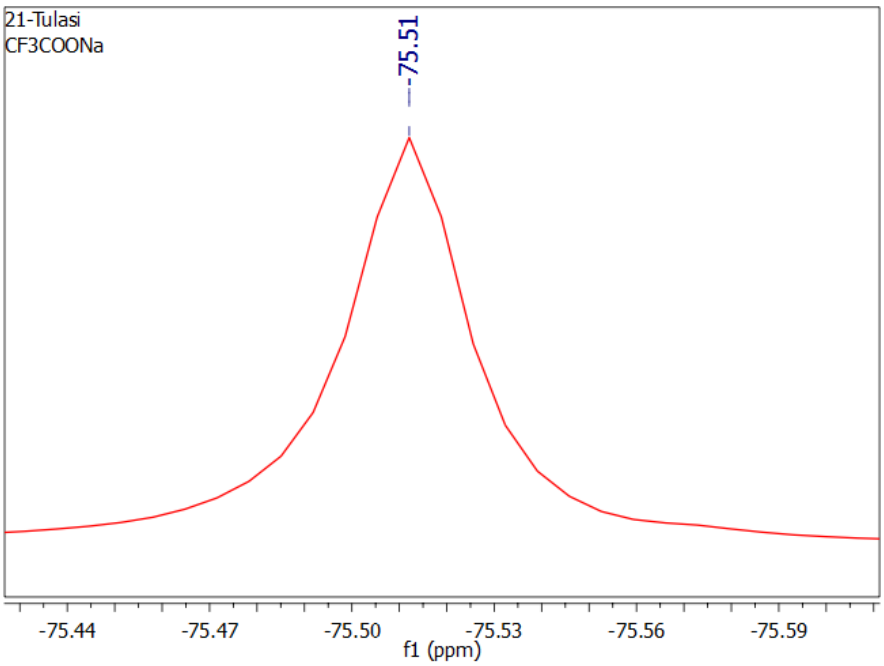

Figure 7.5.3(c): Zoomed spectrum of CF_3COONa, in D_2O.

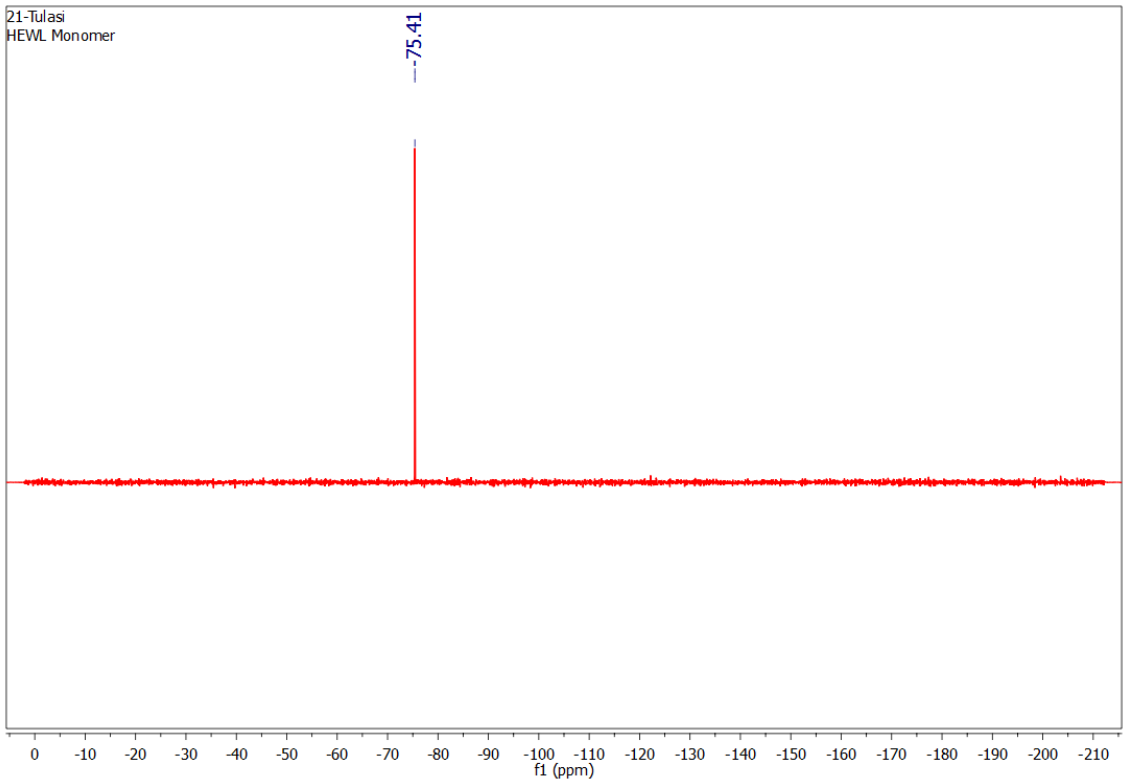

Figure 7.5.4(a): Fluorine NMR spectrum of HEWL monomer labeled with fluorine moiety. The presence of $–CF_3$ group is represented by the strong signal at – 75.41 ppm. The spectrum was recorded at 376.59 Hz.

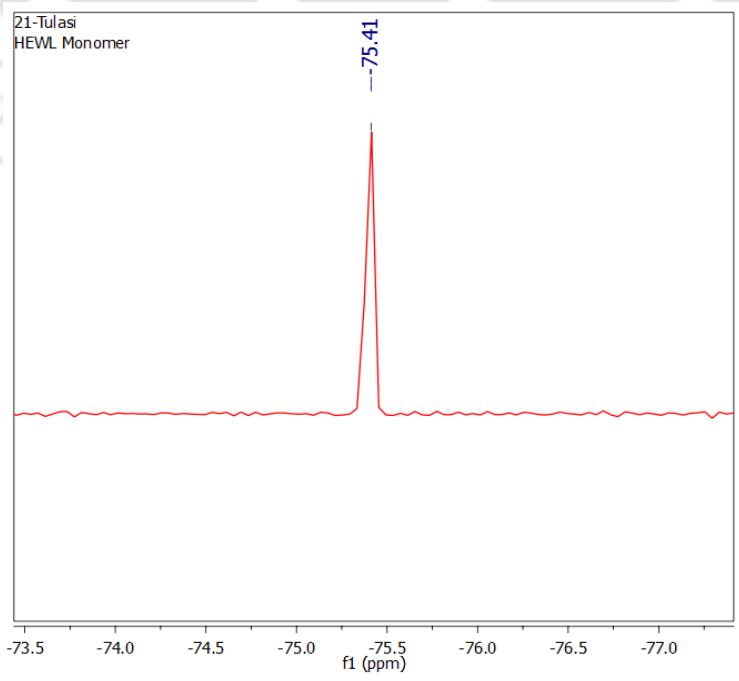

Figure 7.5.4(b): Expanded spectrum of HEWL monomer labeled with fluorine.

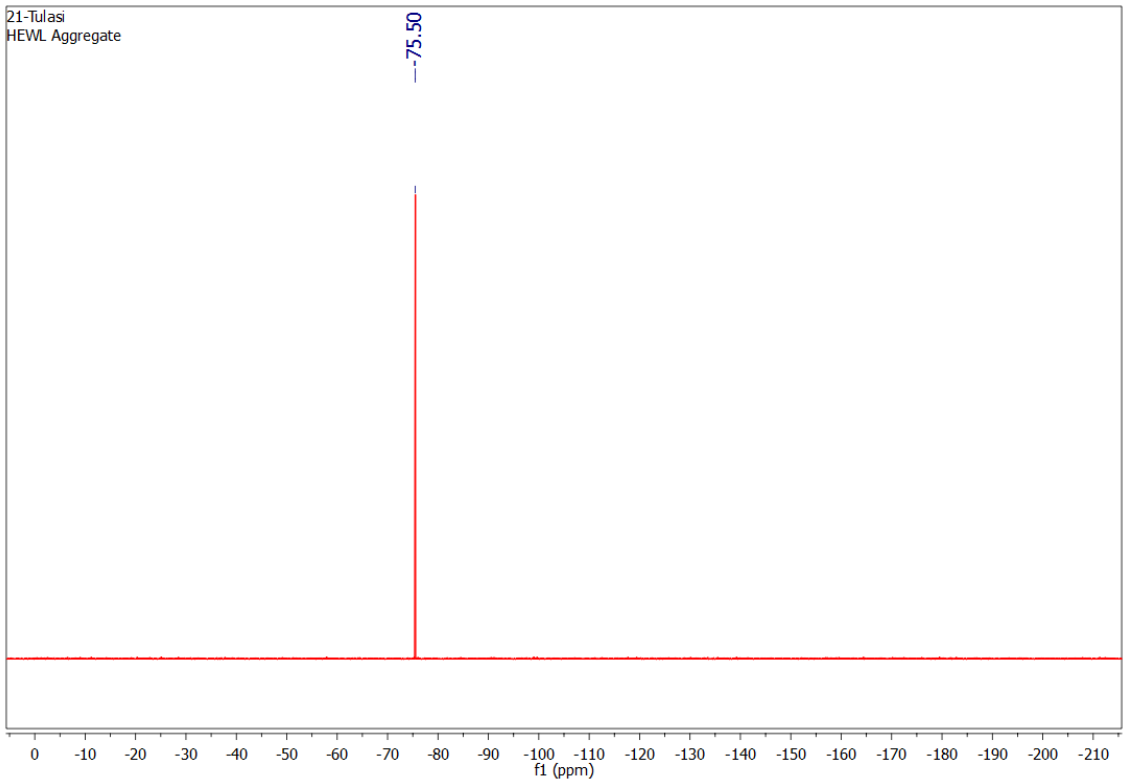

Figure 7.5.5(a): Proton decoupled F^{19} NMR spectrum of HEWL aggregates labeled with fluorine. The sample is dissolved in 100 % D_2O for recording 1 D NMR spectrum. The spectrum was recorded at 376.59 Hz.

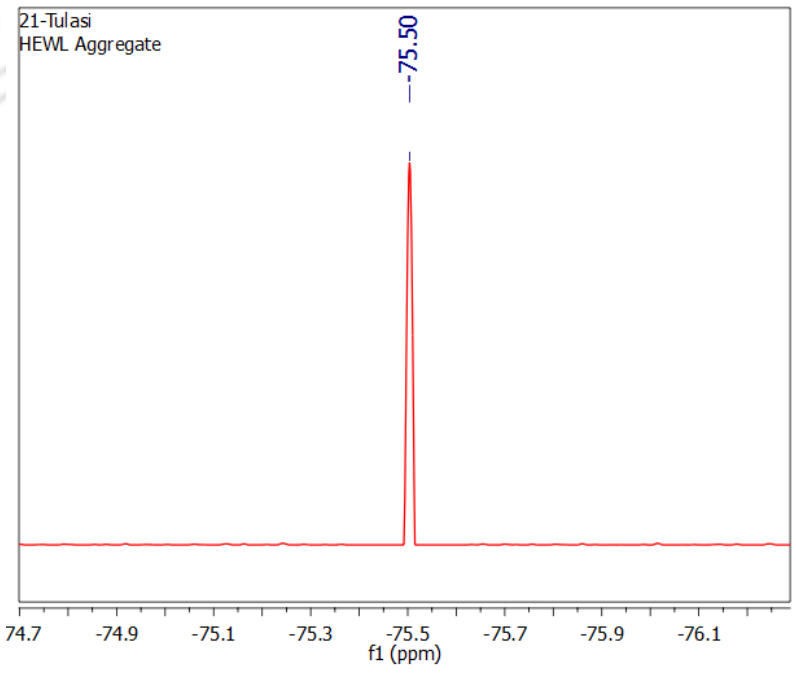

Figure 7.5.5(b): Expanded spectrum of HEWL aggregates labeled with fluorine.

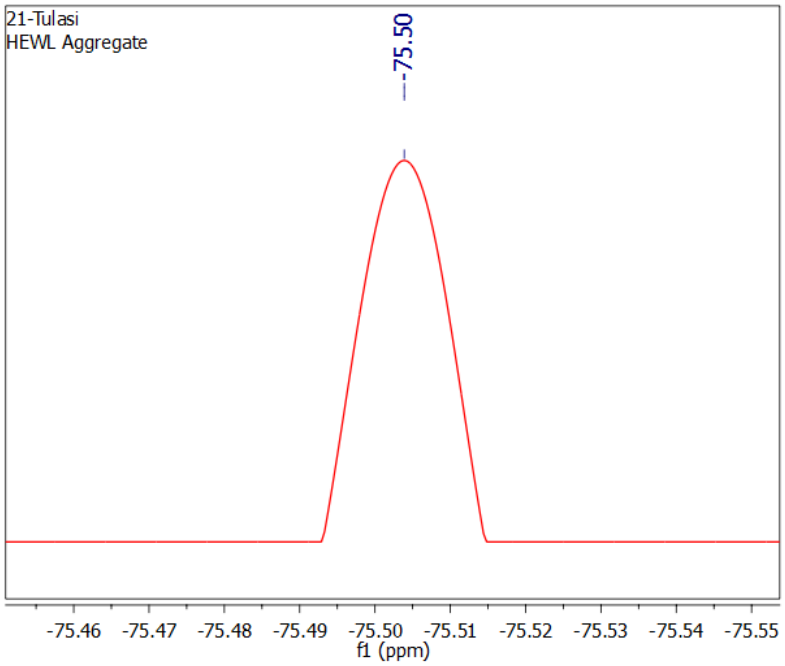

Figure 7.5.5(c): Zoomed spectrum of HEWL aggregates labeled with fluorine.

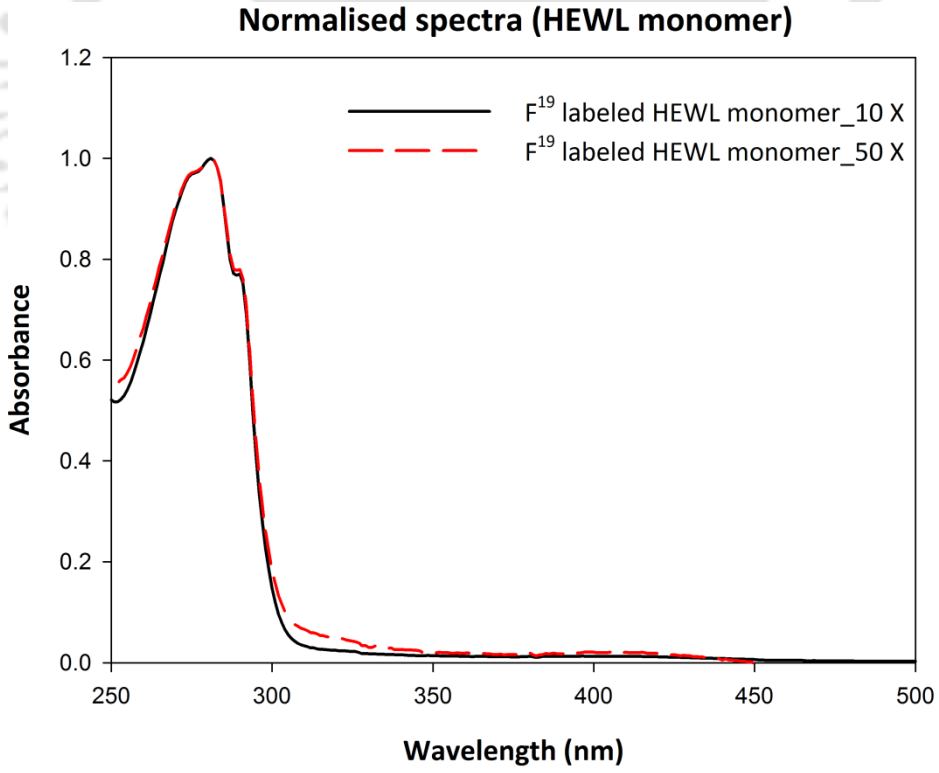

Figure 7.5.6 (a): Normalised absorption spectra for F^{19} labeled HEWL monomer of different dilutions (in milliQ water).

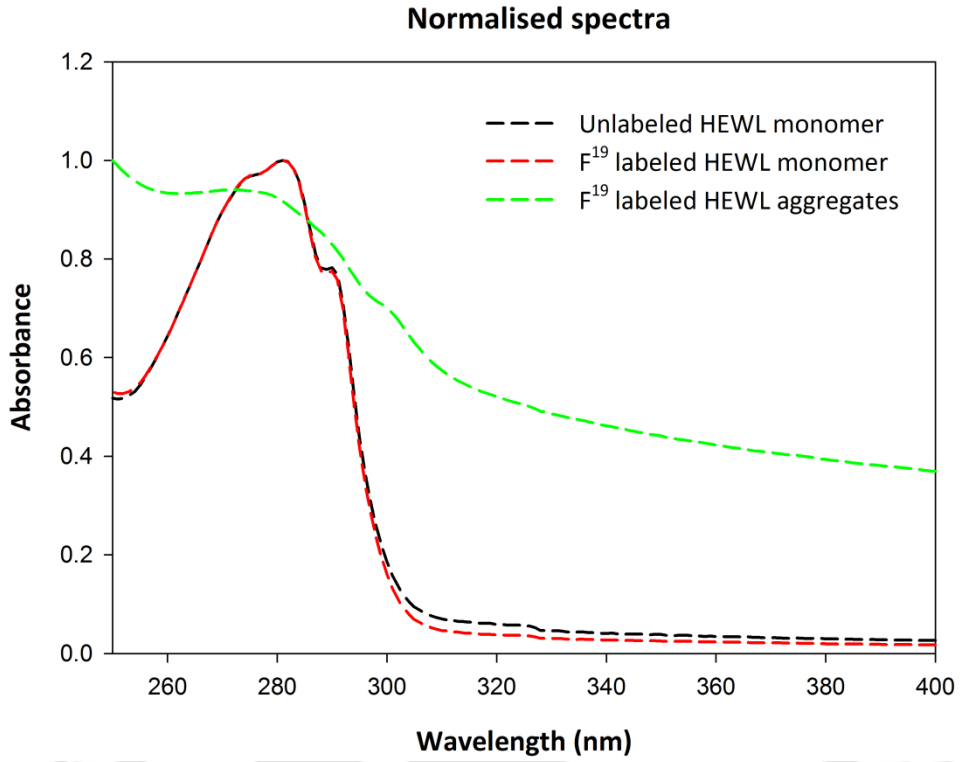

Figure 7.5.6(b): Overlaid normalised spectra for F^{19} labeled HEWL monomer, unlabeled HEWL monomer and F^{19} labeled HEWL aggregates. UV-Vis spectra were recorded in milliQ. Unlabeled HEWL is taken as a control for comparison with fluorinated proteins.

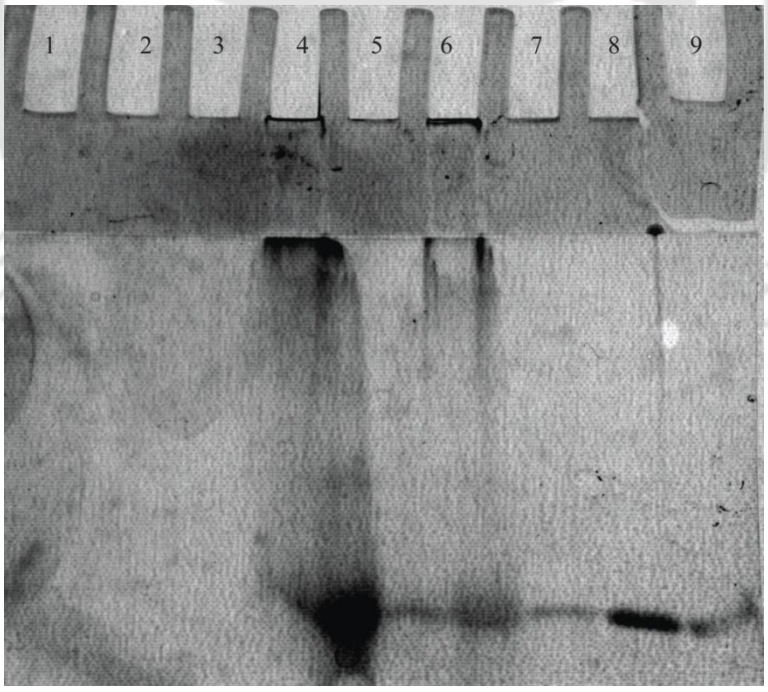

Figure 7.5.7: SDS PAGE run of fluorine labeled samples. Lane 1 – Supernatant; Lane 2- Supernatant; Lane 3 – CF_3COONa in D_2O ; Lane 4 – Aggregate (4 day old, F^{19} labeled low conc.); Lane 6 - Aggregate (4 day old, F^{19} labeled high conc.); Lane 7 – F^{19} labeled HEWL monomer (low conc.); Lane 8- F^{19} labeled HEWL monomer (high conc.); Lane 9 – HEWL in milliQ

Study by SDS-PAGE showed up no evidence of any higher order oligomers or any dimers for the sample containing F^{19} labeled HEWL monomer. Presence of higher order oligomers (high molecular weight) is very prominent in samples of fluorinated aggregates. It is clearly seen as bands stuck in the stacking gel followed by the appearance of a long smear in the resolving gel (**lane 4 & lane 6**). This observation reveals the presence of a significant population of larger oligomeric species copopulated with species of various orders (trimers, dimers, monomers etc.) due to which rather than distinct bands, there is the appearance of smear on SDS-PAGE.

7.6 T_1 relaxation measurement data

Both the parameters longitudinal relaxation rate and transverse relaxation rate are sensitive to the global motion of the macromolecules and thus give an idea regarding protein dynamics.[20] In solution NMR, overall tumbling rate of the proteins affects the T_1 relaxation rate of the spin nuclei under study.

Although it is clear from 1 D NMR spectra data that both HEWL nanoparticles and HEWL monomer are fluorine labeled but very minor changes in the fluorine shift cannot be used to predict the difference in conformation of both the species. In order to elucidate the dynamic motions of polydisperse system of fluorinated nanoparticles and monodisperse fluorinated monomer, a detailed analysis of the relaxation behaviour of the fluorinated species was carried out by measurement of parameters such as T_1 and T_2. Since, the fluorinated nanoparticles are much bulkier than fluorinated monomer; relaxation parameter may provide a basis for differentiating between them. The above mentioned parameters can also give an estimate about the rotational correlation time. The only way to distinguish between fluorinated HEWL monomer and fluorinated HEWL nanoparticles was by means of $1/T_1$ or $1/T_2$, the relaxation rates.

T_1 and T_2 data can give an estimate or idea regarding the mobility of large proteins. Increase in T_1 value indicates a restricted internal motion. Longitudinal and transverse relaxation rates give an idea about the macromolecular environment of fluorine nuclei. The size scale of the macromolecules can be roughly determined by the relaxation times.

T_1 can be defined as spin lattice relaxation time described by the recovery of longitudinal magnetization.T_2 is known as spin-spin relaxation time which is the phenomenon of decay of transverse magnetization.

Studies carried out by **Pan Shi and co-workers** have shown that analysis of the internal motions for extremely large proteins is possible by T_1 and T_2 relaxation values and F^{19} chemical shift studies. They have determined the side chain internal mobility of site specific incorporated fluorinated analog of phenylalanine into proteins. The relaxation measurements were carried out in highly viscous conditions and in micellar systems. Both the conditions mimic large macromolecular environment which is equivalent to large sized globular proteins of molecular weights up to ~7000 kDa.[21] Henceforth, we can say that size limitation which is faced while studying other isotopes (H^1 and C^{13}) is overcome in case of F^{19} NMR.

Rotational correlation time for the macromolecules can be deduced from T_1 and T_2 relaxation parameters and in turn it can give a picture on the oligomeric state of the protein. Hence, in our case for the synthesis of fluorinated aggregates we have used HEWL aggregates (oligomeric form). The goal of our relaxation studies was to determine the correlation times of HEWL in native state and in aggregated state of the protein.

One of the major challenges in solution NMR studies (H^1 NMR) is the difficulty to study internal dynamics of the protein in presence of overall tumbling of the protein.[20]

As per the relaxation data, about a 1.13 fold increase in T_1 was observed for fluorinated monomer and 1.25 fold increase in case of fluorinated aggregates in comparison to CF_3COONa as summarized in **Table [7.6.5]**.Fluorinated aggregates exhibited a larger calculated T_1 value as compared to fluorinated monomer. The T_1 relaxation parameter obtained for the small molecular weight reference compound CF_3COONa was 2.883 s, a similar value of 2.9 s was reported previously in the literature.[11] As the relaxation measurements were carried out in different magnetic field strength even if the values obtained were similar, it would not be ideal to compare both the results because T_1 parameter depends on the magnetic field strength. We have also determined T_1 value for NaF which has only one ‘F’ atom in comparison to 3 ‘F’ atoms of the bulkier compound CF_3COONa. As expected, F_{19} T_1 relaxation value for NaF is 2.202 s which is a substantially reduced value than T_1 of CF_3COONa i.e. a 23.62 % decrease was noticed. In all the cases, relaxation decays obtained were mono-exponential in nature.

It is very important to note that fluorinated aggregates is a polydisperse system unlike the protein in native state i.e. it consists of multiple species such as monomer, dimer, oligomers etc. of varying sizes and different mass.

Hence, T_1 relaxation data may not give a correct picture for the tumbling rate of the above mentioned heterogeneous system. T_1 value of 3.61 s obtained for F^{19} labeled nanoparticles can be assumed to be an underestimated or overestimated value and heterogeneity of the system can be stated as the main reason for this. Interaction between $–CF_3$ groups of different monomeric units present in an oligomer has also to be taken into consideration. The possibility of restrictions in the mobility of $–CF_3$ groups attached to the side chain of the protein aggregates also exists which may affect the relaxation parameter.

Literature data for relaxation measurements at our field strength of 376.59 MHz for F^{19} labeled HEWL is unavailable and thus does not give us the scope for comparison.

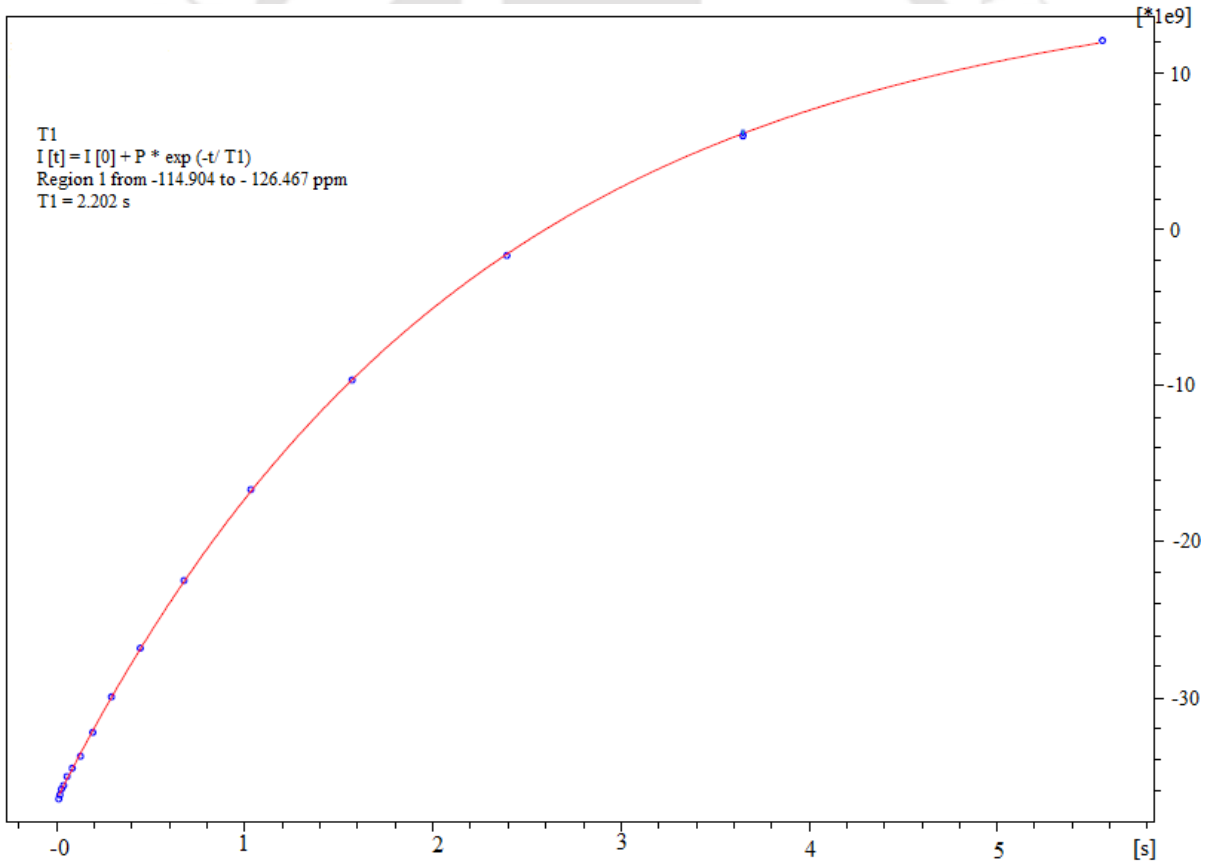

Figure 7.6.1: T_1 relaxation graph for NaF, as an external reference standard. Relaxation measurements were performed at 376.59 Hz.

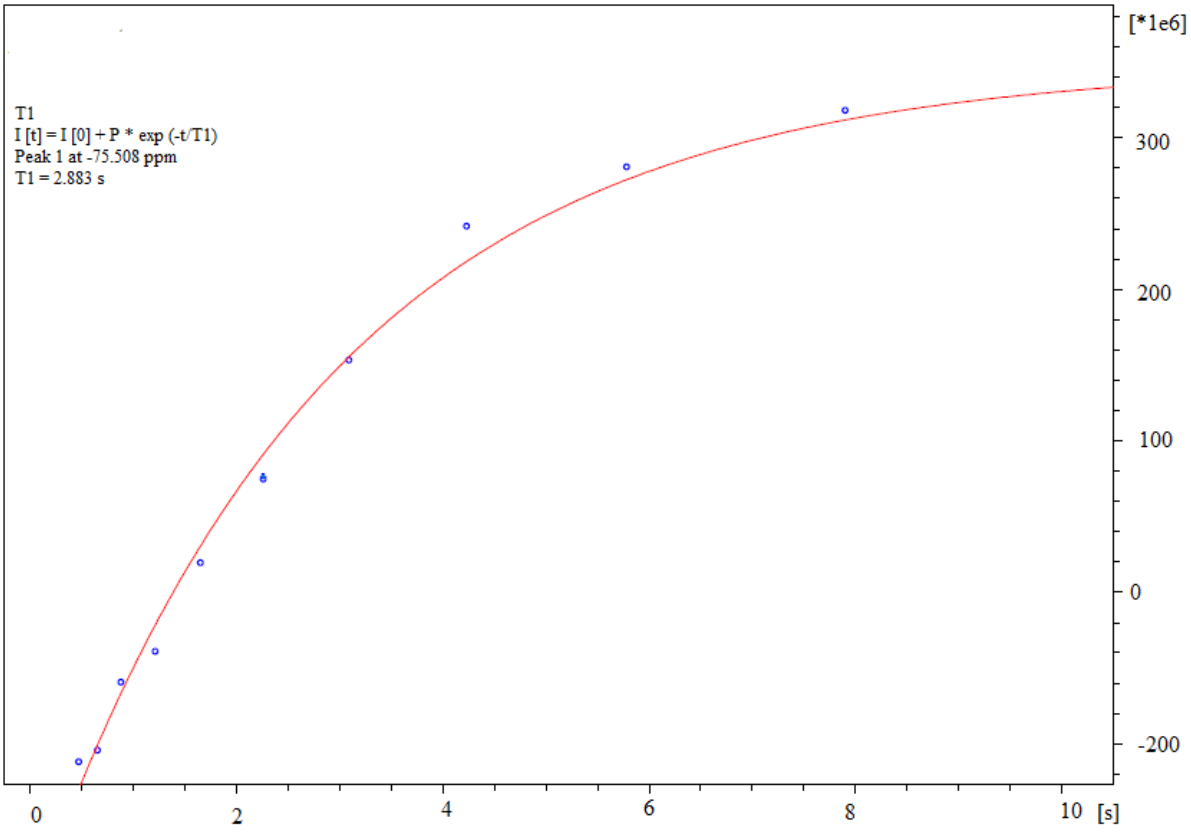

Figure 7.6.2: T_1 Relaxation data for CF_3COONa estimated by inversion recovery method. T_1 relaxation measurements were carried out at 376.59 Hz.

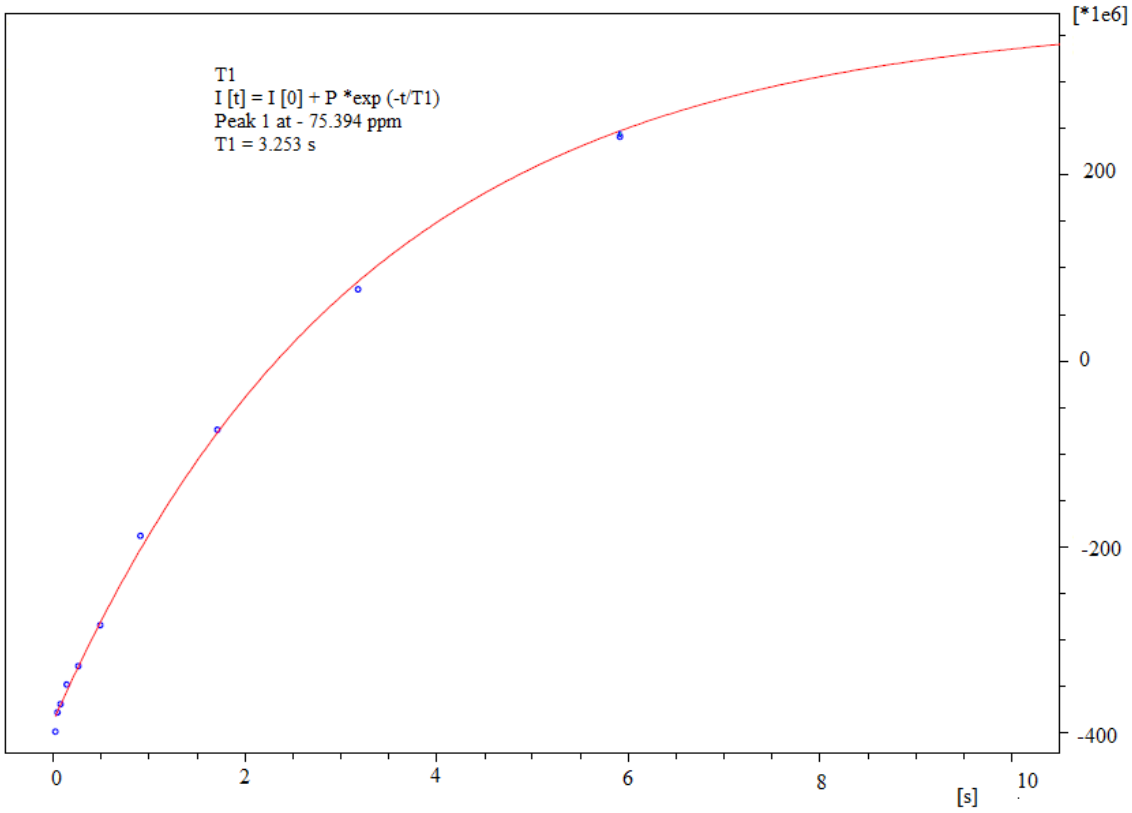

Figure 7.6.3: T_1 relaxation value observed for F^{19} labeled HEWL monomer in D_2O solvent. Spin-lattice relaxation is an exponential growth process. T_1 value was recorded at 376.59 Hz.

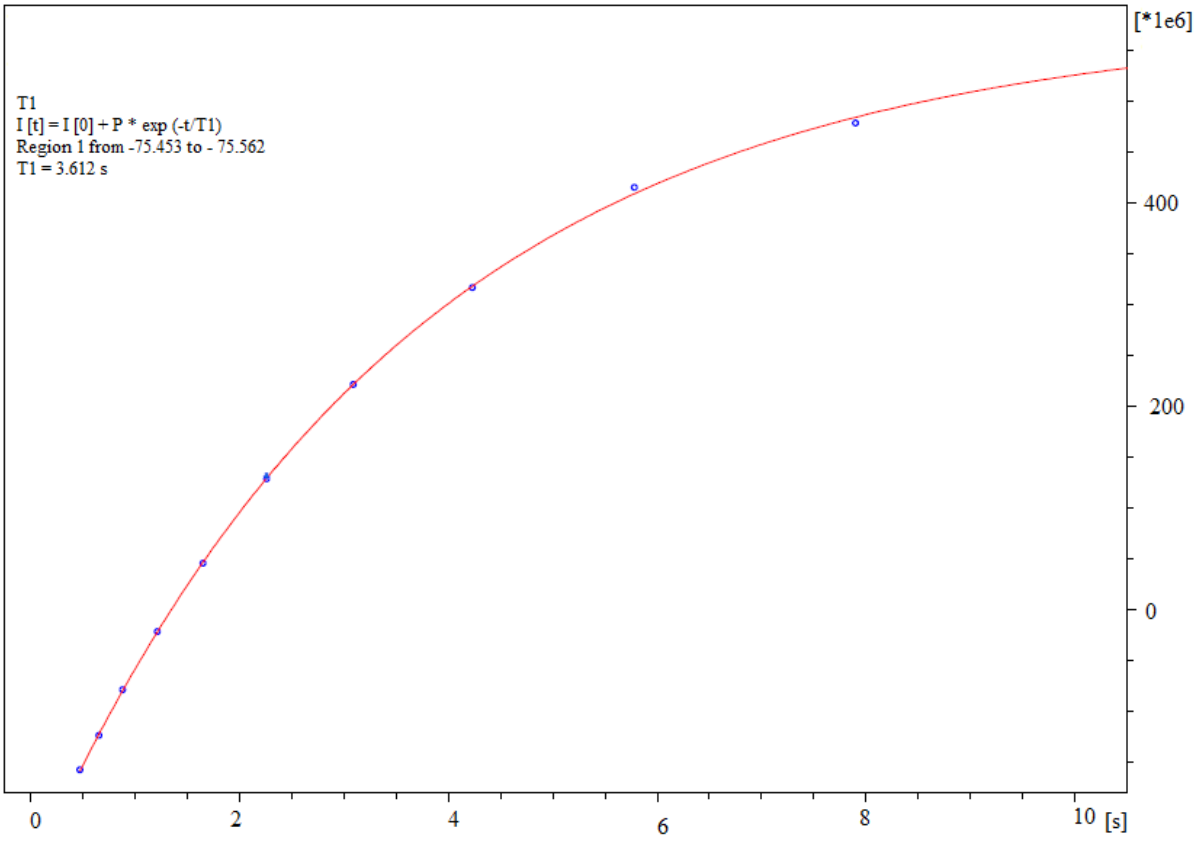

Figure 7.6.4: F^{19} spin-lattice relaxation time (T_1) for HEWL aggregates. T_1 relaxation measurements were performed at NMR frequency of 376.59 Hz.

Samples	T_1 relaxation time (s)
Sodium Fluoride (NaF)	2.202
Sodium trifluoroacetate (CF_3COONa)	2.883
F^{19} labeled HEWL monomer	3.253
F^{19} labeled HEWL nanoparticles	3.612

Table 7.6.5: T_1 relaxation time for external standards (NaF and CF_3COONa) and F^{19} labeled HEWL monomer and F^{19} labeled HEWL aggregates. Measurements were performed at NMR frequency of 376.59 Hz.

7.7 Conclusion

Distinguishable fluorine signals were observed very clearly for all the fluorinated samples. The line widths of the signal observed were much narrow. A single narrow resonance was observed in F^{19} labeled HEWL nanoaggregates at the same chemical shift anticipated for the corresponding trifluoroacetyl groups. We have also reported the quantification of synthesized fluorinated products in terms of weight of the lyophilized product (mg): weight of the protein taken for fluorination reaction (mg). The comparative analysis between the fluorinated and non-fluorinated counterpart gave an insight into the assessment of effect of fluorine attachment to the protein. Fluorinated HEWL monomer can be referred to as '*six spin label*' system as six $–CF_3$ labels are introduced to the ε-amine groups of LYS residues. The direct labeling of LYS amino acid side chains with specific organic fluorinating agent have been successfully used to generate fluorine tagged protein.

Till date, no reports have been published regarding the synthesis of fluorinated protein (HEWL) oligomers. The concentration of HEWL aggregates used here for fluorine tagging was in micro molar range (120 μM) which is much lower in comparison to the concentration of other proteins used for synthesis of fluorinated proteins as previously reported by various authors.[11] In fact, the amount of lyophilized fluorinated aggregates required for obtaining distinguishable F^{19} NMR signal was hardly ~ 1 mg (1 mg dissolved in 1 ml of D_2O).As we know that due to large no. of available labeling sites for fluorine labeling which is dependent on the no. of monomers present in an oligomeric species, we could develop fluorinated HEWL aggregates highly enriched with F^{19} NMR sensitive nuclei. In addition, a dramatic transition was observed from soluble aggregates to partially soluble precipitated aggregates after labeling with F^{19} isotope. F^{19} spin label is directly bonded to the aliphatic amine residues of lysozyme.

Limitation of the study: Our study is limited to characterization of fluorinated products. Further research can be conducted to study the efficiency of synthesized F^{19} labeled HEWL nanoparticles as MRI contrast agents and various comparative studies can be carried out with already available MRI contrast agents. Hence, this area of application remains to be explored. Furthermore; experiments can be performed to attach F^{19} labels to HEWL aggregates under different experimental conditions such as different days incubated aggregates. Up to now, the research has tended to focus on development of fluorinated macromolecule conjugates especially fluorinated proteins.

The non-invasive nature of NMR spectroscopy makes it a powerful technique to study the dynamic of macromolecules in solution. In the context of isotope labelling of target species with multiple fluorine tags, the F^{19} NMR signal doesn't get hindered which is an advantage of labelling the aggregates with F^{19} isotope rather than fluorescence tags where the intensity gets hugely affected in the presence of multiple fluorophores. Information regarding structural and conformational changes cannot be deduced from only F^{19} NMR studies, which is out of the scope for discussions in this chapter.

References

1. Ando, S., Harris, R. K., Scheler, U., Grant, D. M. & Wiley, J. Fluorine-19 NMR of Solids Containing Both Fluorine and Hydrogen Fluorine-19 NMR of Solids Containing Both Fluorine. *Encycl. Nucl. Magn. Reson.* **9,** 531–550 (2002).

2. Thompson, L. E. & Rovnyak, D. Accessible NMR experiments studying the hydrodynamics of 15N-enriched ubiquitin at low fields. *Biochem. Mol. Biol. Educ.* **35,** 49–56 (2007).

3. Danielson, M. A. & Falke, J. J. Use of 19 F Nmr To Probe Protein Structure and Conformational Changes. *Annu Rev Biophs Biomol Struct* **25,** 163–195 (1996).

4. Gerig, J. T. Fluorine NMR of proteins. *Prog. Nucl. Magn. Reson. Spectrosc.* **26,** 293–370 (1994).

5. Gregory, D. H. & Gerig, J. T. Structural effects of fluorine substitution in proteins. *J. Comput. Chem.* **12,** 180–185 (1991).

6. Neil, E. & Marsh, G. Towards the nonstick egg: Designing fluorous proteins. *Chem. Biol.* **7,** 153–157 (2000).

7. Buer, B. C., Meagher, J. L., Stuckey, J. a & Marsh, E. N. G. Structural basis for the enhanced stability of highly fl uorinated proteins. *Proc. Natl. Acad. Sci.* **109,** 4810–4815 (2012).

8. Gerebtzoff, G., Li-Blatter, X., Fischer, H., Frentzel, A. & Seelig, A. Halogenation of drugs enhances membrane binding and permeation. *ChemBioChem* **5,** 676–684 (2004).

9. Sun, W. C., Gee, K. R., Klaubert, D. H. & Haugland, R. P. Synthesis of fluorinated fluoresceins. *J. Org. Chem.* **62,** 6469–6475 (1997).

10. Khan, F., Kuprov, I., Craggs, T. D., Hore, P. J. & Jackson, S. E. 19F NMR studies of the native and denatured states of green fluorescent protein. *J. Am. Chem. Soc.* **128,** 10729–10737 (2006).

11. Mehta, V. D., Kulkarni, P. V, Mason, R. P., Constantinescu, a & Antich, P. P. Fluorinated proteins as potential 19F magnetic resonance imaging and spectroscopy agents. *Bioconjug. Chem.* **5,** 257–261 (2000).

12. Lian, C. *et al.* Fluorine- 19 Nuclear Magnetic Resonance Spectroscopic Study of Fluorophenylalanine- and Fluorotryptophan-Labeled Avian Egg White Lysozymes. *Biochemistry* **33,** 5238–5245 (1994).

13. Duewel, H., Daub, E., Robinson, V. & Honek, J. F. Incorporation of Trifluoromethionine into a Phage Lysozyme: Implications and a New Marker for Use in Protein 19 F NMR. *Biochemistry* **36,** 3404–3416 (1997).

14. Lu, R. C., Guo, X. R., Jin, C. & Xiao, J. X. NMR studies on binding sites and aggregation-disassociation of fluorinated surfactant sodium perfluorooctanoate on protein ubiquitin. *Biochim. Biophys. Acta - Gen. Subj.* **1790,** 134–140 (2009).

15. Mehta, V. D., Sivasubramanian, A., Kulkarni, P. V, Mason, R. P. & Antich, P. P. 6-Fluoropyridoxal Polymer Conjugates : Novel Magnetic Resonance Spectroscopy 19 F pH Indicators for. *Communications* **1802,** 536–540 (1996).

16. Ye, L., Larda, S. T., Frank Li, Y. F., Manglik, A. & Prosser, R. S. A comparison of chemical shift sensitivity of trifluoromethyl tags: optimizing resolution in 19F NMR studies of proteins. *J. Biomol. NMR* 97–103 (2015).

17. Isom, D. G., Castañeda, C. A., Cannon, B. R. & García-Moreno, B. Large shifts in pKa values of lysine residues buried inside a protein. *Proc. Natl. Acad. Sci. U. S. A.* **108,** 5260–5265 (2011).

18. Ravi, V. K., Swain, T., Chandra, N. & Swaminathan, R. On the characterization of intermediates in the isodesmic aggregation pathway of hen lysozyme at alkaline pH. *PLoS One* **9,** 1–12 (2014).

19. Adriaensens, P. *et al.* Investigation of protein structure by means of 19F-NMR. *Eur. J. Biochem.* **177,** 383–394 (1988).

20. Li, C. & Liu, M. Protein dynamics in living cells studied by in-cell NMR spectroscopy. *FEBS Lett* **587,** 1008–1011 (2013).

21. Shi, P. *et al.* Site-specific 19F NMR chemical shift and side chain relaxation analysis of a membrane protein labeled with an unnatural amino acid. *Protein Sci.* **20,** 224–228 (2011).

22. Ahmad, S., Gromiha, M., Fawareh, H. & Sarai, A. ASAView: database and tool for solvent accessibility representation in proteins. *BMC Bioinformatics* **5,** 51 (2004).

7.8 Basics of NMR

1 D (one-dimensional) NMR is used to study the chemical structure. The proton in the nuclei acts as a small magnetic field due to its spin property and causes it to generate a NMR signal. The nuclear spins can be represented as a magnetization vector having both magnitude and direction. The unpaired spins (+1/2 or -1/2) play an important role in NMR. Particles with a spin behave as a tiny magnet and when placed in an external magnetic field, align itself with the magnetic field acting as a magnetic vector. The particle then attains either a low energy configuration or high energy configuration depending upon its alignment.

When the energy difference between two spin states (high energy and low energy states) exactly matches with that of energy of the photon (i.e., the condition of the resonant frequency), absorption of energy occurs. Transition occurs from the lower energy to higher energy state when energy is absorbed and transition from higher energy state to lower energy state results in emission of energy by the spins. NMR signal arises due to this energy difference. NMR signals usually decay exponentially as a function of time. The chemical environment around a nucleus can be determined by the chemical shift.

Gyromagnetic ratio of a particle can be represented as:

$\gamma = \nu/B$…… (1)

Where B is the strength of magnetic field in which the particle is placed and ν is the frequency of the photon which is absorbed by the particle with a net spin. The quantity ν is called the resonant frequency.

The resonant frequency is related to the energy of photon as:

$E = h\nu$ …… (2)

The value for Planck's constant is $h = 6.63 \times 10^{-34}$ Js.

For the nucleus F^{19}, the value of γ is 40.08 MHz/T which has one unpaired proton with a net spin of ½.This isotope of fluorine has a very high natural abundance thus making it suitable for NMR studies[1].

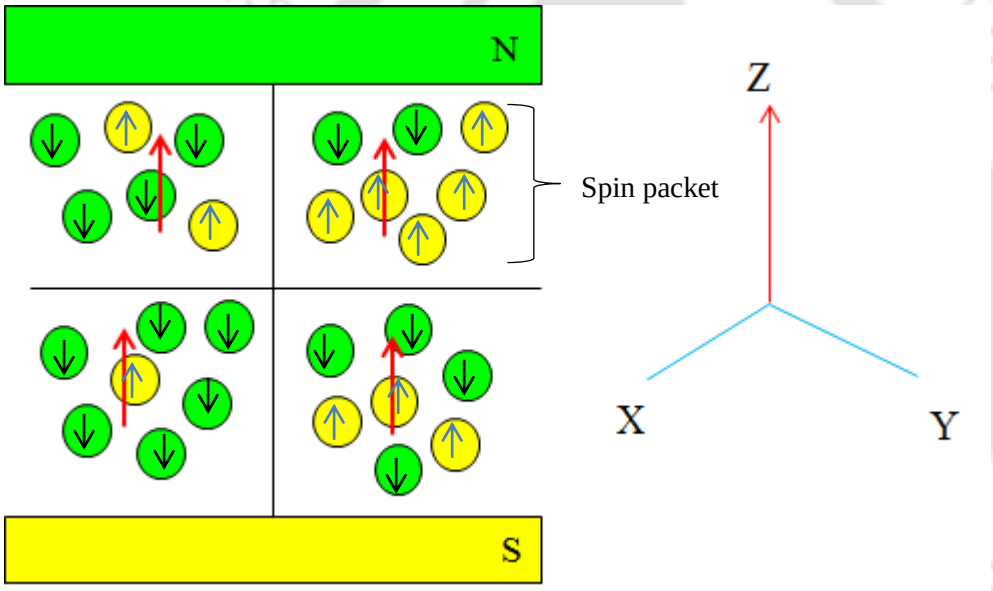

Figure 7.8.1: The spins are represented by yellow or green circles aligned in a particular direction of the external magnetic field. (↑) represents the magnetization vector due to the magnetic fields of spins present in each spin packet.The net magnetization vector is along the Z axis which is the vector sum of the magnetization vectors from the spin packets.

T_1 (Spin-lattice relaxation time): It is also known as longitudinal relaxation or relaxation in z-direction. T_1 relaxation rates are used to determine the internal motions of macromolecules. T_1 is the measure of time required for the net magnetization vector to recover its equilibrium value in the direction of B_o. The equation which describes the behaviour of T_1 relaxation process:

$M_z = M_o (1-e^{-t/T1})$…… (3)

Longitudinal magnetization is changed to its equilibrium value by a factor of e. When the net magnetization vector is along - Z axis then it attains its equilibrium position at a rate of T1 along + Z axis described as:

$M_z = M_o (1\text{-}e^{-t/2T1})$..... (4)

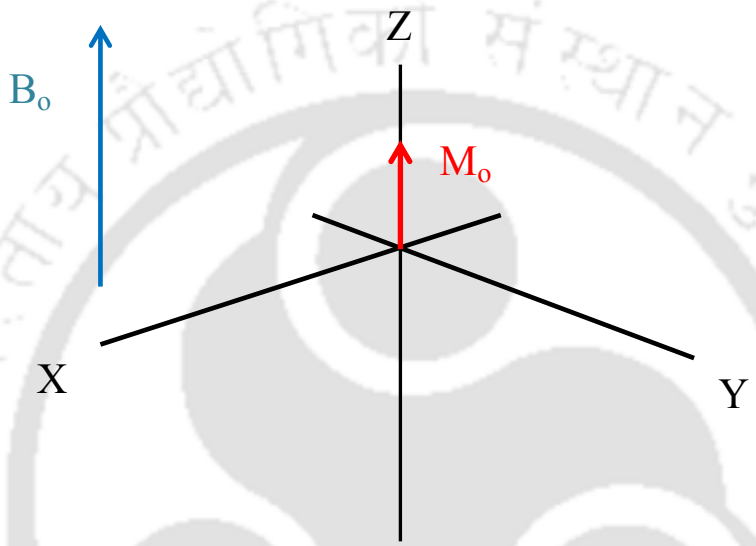

Figure 7.8.2: Magnetization vector at equilibrium. M_o is referred to as equilibrium magnetization. M_z is the z component of magnetization, otherwise known as longitudinal magnetization. Here the net magnetization vector (M_z) lies along the direction of applied magnetic field B_o.

Chemical shift: This parameter can be defined as the difference in resonance frequency of the nuclei under study and a standard which is taken as reference standard. This term is represented as δ (delta) and the values are reported in terms of ppm. The chemical shift is also an indicator of chemical environment surrounding a nucleus. Henceforth, any change in chemical environment experienced by a nucleus will be reflected as variation in the values of chemical shift.

$\delta = (\nu - \nu_{ref}) \times 10^6 / \nu_{ref}$ ..... (5)

Representation of nuclear spin relaxation

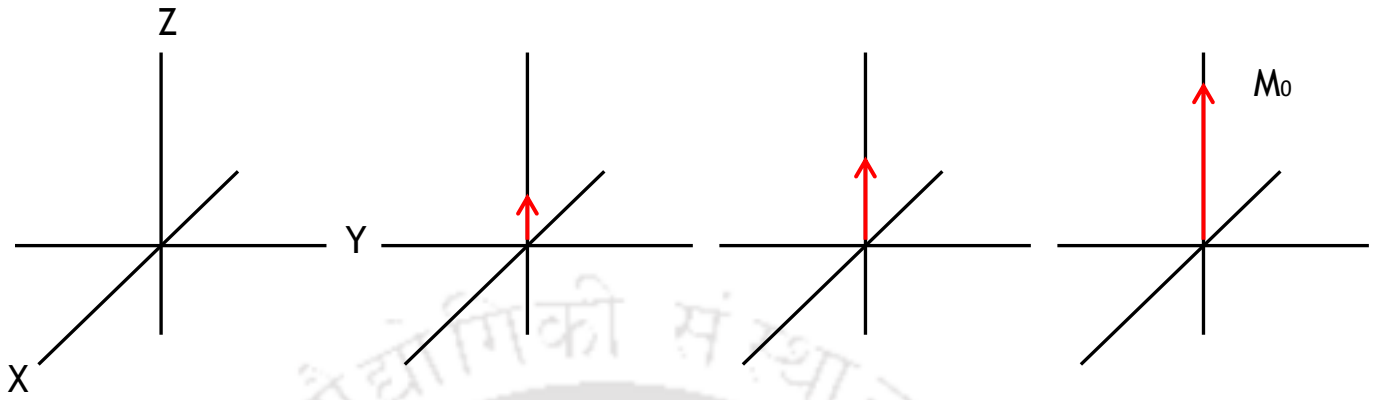

Figure 7.8.3: Spin-lattice relaxation (T_1 relaxation)[2]

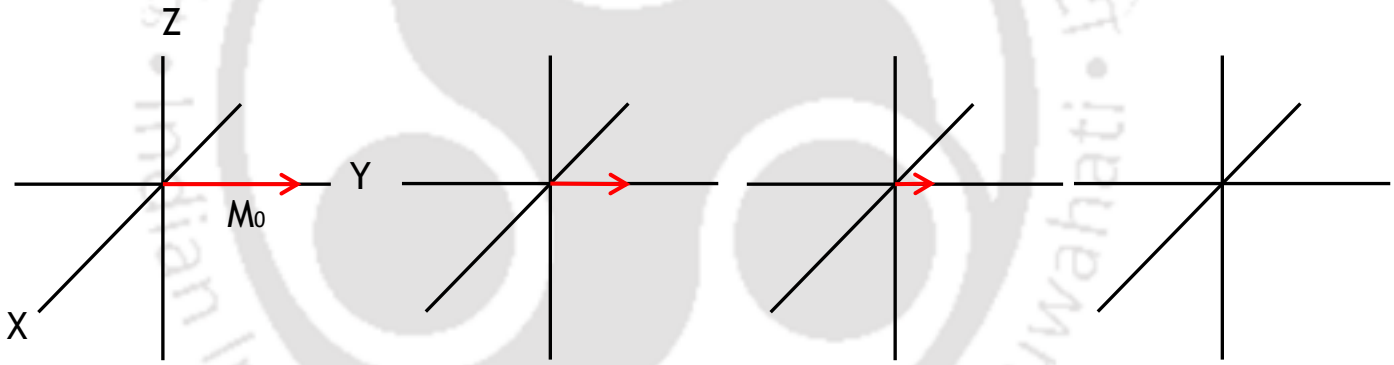

Figure 7.8.4: Spin-spin relaxation (T_2 relaxation)[2]

7.9 ASAView

Freely available online server was used for graphical representation of solvent accessibility of amino acid residues in proteins[22]. PDB file of Hen egg white lysozyme with PDB Id as 5F14 (structure of native hen egg white lysozyme) was given as an input.

Accessible surface area (ASA) or solvent accessibility of amino acids in Lysozyme protein was computed and the output was generated in form of a spiral plot as shown above in the figure. The spiral plot is a method for representing the surface residues in a protein.

This plot is generated by ASAView tool which displays the amino acid residues according to their relative solvent accessibility (**Ahmad et al., 2004**). Amino acids are shown in the form of spheres and radius of each of the spheres is proportional to the accessible surface area of that residue. More accessible residues are shown visually in the form of large spheres. The residues are arranged in a spiral plot such that more exposed or solvent accessible are arranged in the outer ring of the spiral and the most buried residues are present in the innermost region of the spiral plot. This 2D spiral plot provides a graphical view of exposed surface areas of the residues.

Relative ASA values are computed for each amino acid for the corresponding PDB file. Relative values are normalized to the scale of 1.0 such that amino acid having the maximum exposed surface is assigned a value of 1.0.A residue number and residue name is assigned to circle representing amino acids. Buried residues with smallest relative ASA value is placed at the origin of the spiral and subsequently residues with increasing values of ASA are placed successively on the outer ring of the spiral.

Lysine residues in HEWL	ASAView
K1	0.369
K13	0.408
K33	0.296
K96	0.209
K97	0.457
K116	0.496

Table 7.9.1: Relative % Solvent exposure for the Lysine residues in HEWL based on PDB structure: 5F14 computed using the online server *ASAView*. Values were normalized to 1 for the residue exhibiting maximum solvent exposure (Glycine as 1.0). The information provided helps us in estimating the solvent accessibility of LYS residues.

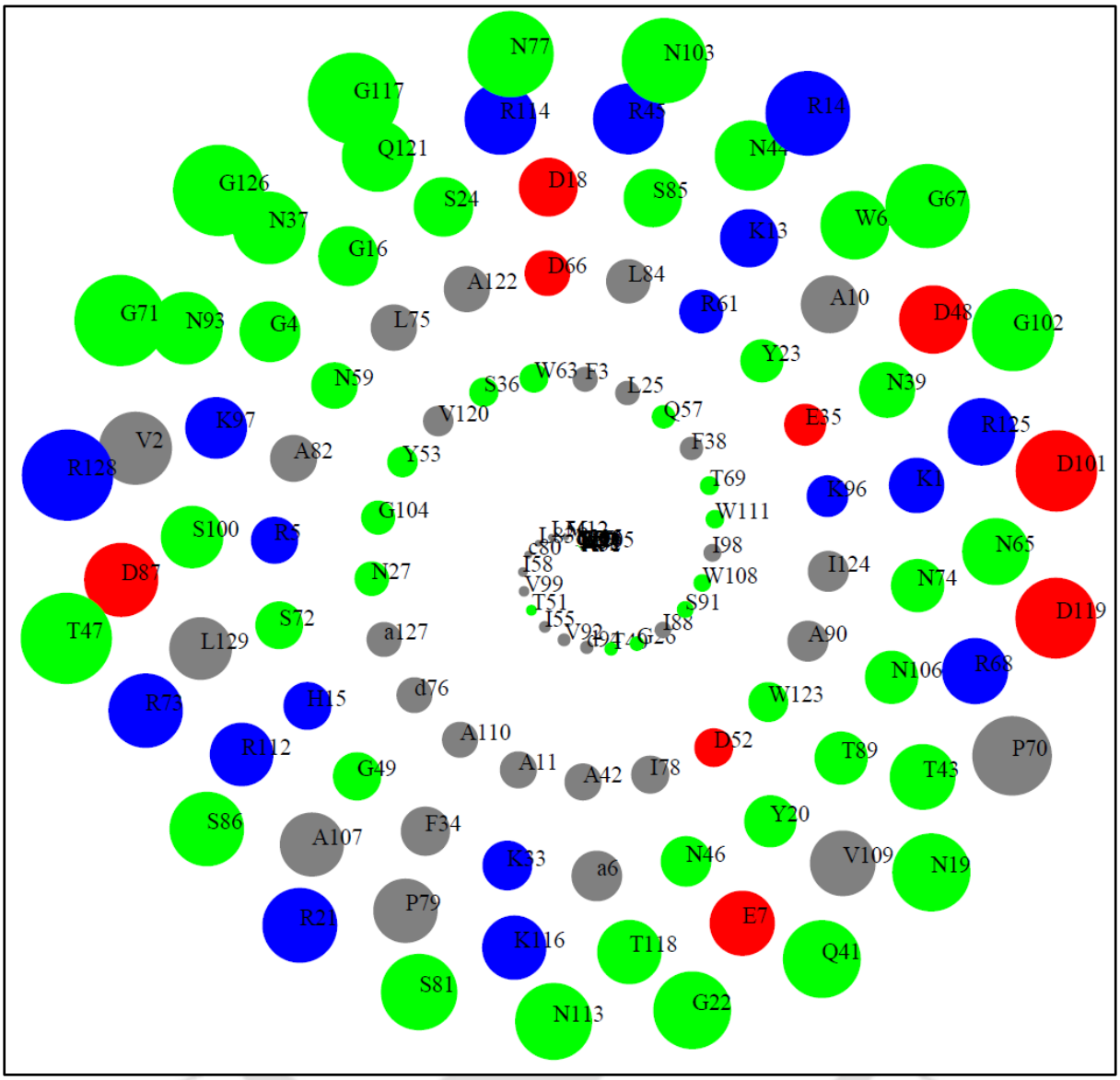

Figure 7.9.2: Spiral plot representing solvent accessibility of amino acid residues of Hen egg white lysozyme (5F14 – PDB file) generated by ASAView.

Colour notations for different amino acids

a) Blue denotes positively charged residues (Arginine –R, Lysine – K, Histidine – H)

b) Red denotes negatively charged residues (Aspartic acid – D, Glutamic acid – E)

c) Green denotes polar uncharged residues (Glycine – G, Asparagine – N, Tyrosine – Y, Glutamine – Q, Serine – S, Threonine – T, Tryptophan – W)

d) Gray represents hydrophobic residues.

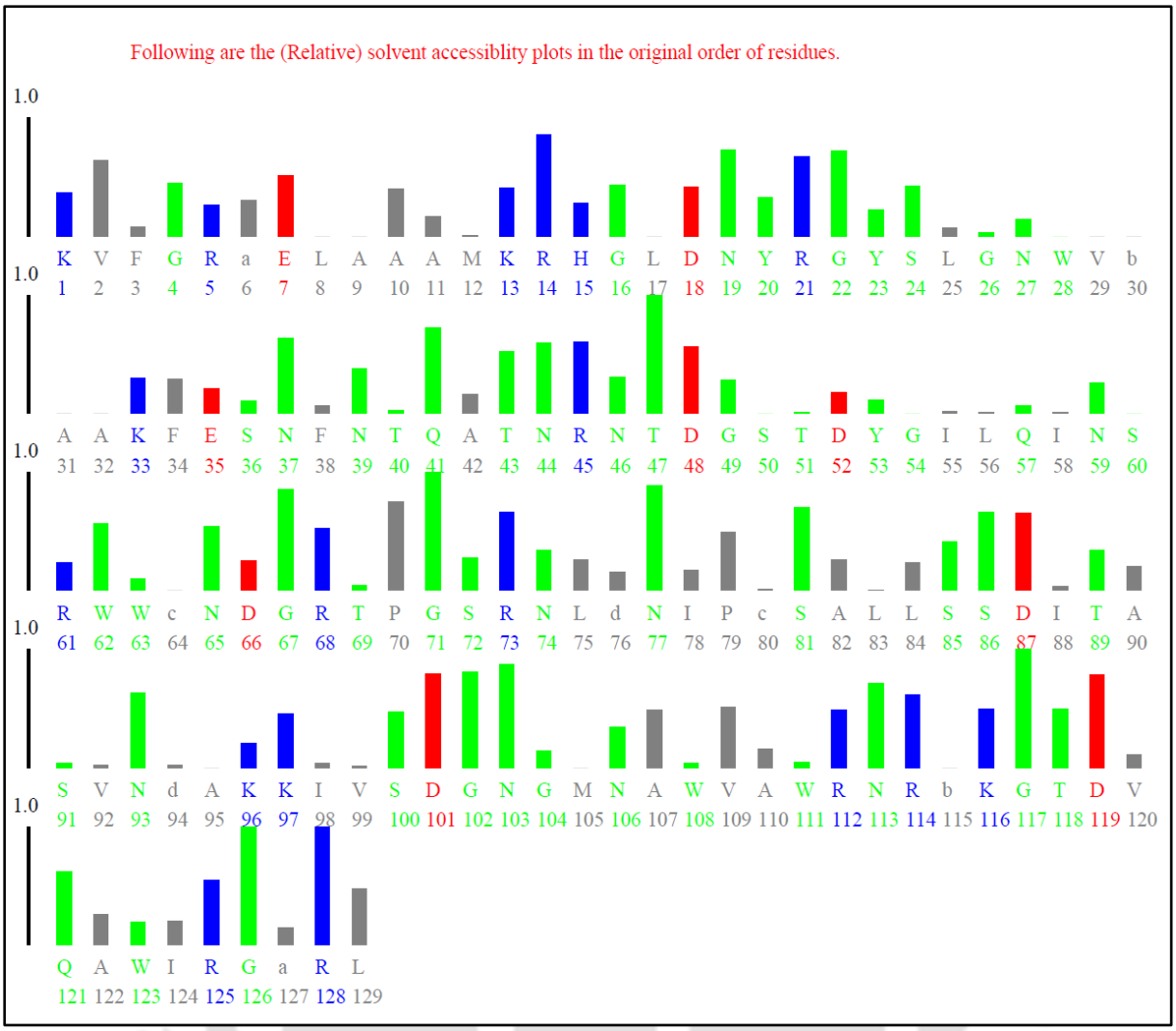

Figure 7.9.3: Relative solvent accessibility plots of amino acid residues in the original order in the protein Hen egg white lysozyme (PDB ID – 5F14).

Bar plots display the relative solvent accessibility of amino acid residues within lysozyme protein. Residues are shown in the sequence in which they appear in the original protein sequence. Length of the bar represents relative ASA of the amino acid residue.

Concluding remarks

A novel strategy for the synthesis of HEWL nanoparticles, by alkaline pH induced aggregation at room temperature, with subsequent stabilization by intermolecular disulfide bonds has been reported. The self-assembled HEWL nanoparticles have been shown have improved stability in physiological pH, 7.0 after 5 days of transfer from alkaline pH 12.2.

Self-assembled nanoaggregates of lysozyme have been studied in detail and characterized extensively. The detailed characterization of these protein nanoparticles helped us to understand the unique features displayed by the HEWL aggregates. A range of techniques such as steady state anisotropy, ANS assay, DLS, TEM, size exclusion chromatography, SAXS and fluorescence spectroscopy have been used to study HEWL aggregation at alkaline pH 12.2 and for HEWL aggregates transferred to pH 7.0.

Control of size and shape of nanoparticles have remained a formidable challenge. As a result there is a large demand on development of novel strategies for synthesis of nanoparticles. We have demonstrated that it is possible to synthesize polycationic HEWL nanostructures in a size controlled way by manipulating the monomer concentration in the aggregation pathway of HEWL. Based on r_{ss} of dansyl probe and ANS binding data for HEWL aggregates transferred to pH 7.0, we have concluded that the nanoparticles remain stable for a week in pH 7.0 when transferred after 134 hours of incubation in alkaline pH. These nanoparticles get interlinked by interdisulfide bonds which strengthen them against any kind of repulsive forces. This gives an edge over other reported protein nanoparticles as there is no requirement of any cross linkers to improve the particle stability.

Their interesting features made it possible to use them for different innovative applications. Unique properties that make them attractive and which could be exploited for different applications include: a) Surface accessible thiol groups which can be covalently linked to various fluorescent thiol reactive dyes b) Polycationic supercharged nanoparticles makes them favourable to interact with negatively charged domains of biological membranes for uptake into cells.

Future perspectives

The development of protein nanoparticles with novel physical, chemical and biological properties have really proven to be a remarkable tool in this new era of nanotechnology. As modulation of properties is relatively easy in case of protein nanoparticles, their functionalities can be modified to impart useful properties to them. In fact, the various methodologies and techniques which have been used for characterization of HEWL nanosystem have contributed hugely to our existing knowledge of protein aggregation.

We propose here that the synthesized HEWL nanoparticles would be favourable for drug delivery. The results obtained, for hydrophobic studies on the nanoparticles, from ANS binding assay & pyrene probe, encourage us to do that. The relatively smaller hydrodynamic diameter of these nanoparticles makes it to be considered for injectable drug delivery system.

Most important advantage of these nanoparticles is the presence of numerous positive charges on their surface. HEWL nanoparticles are polycationic at pH 7.0 due to which they can bind to negatively charged cargoes such as DNA and act as a nano delivery vehicle.

The question of how the self-assembled HEWL oligomeric system would behave in vivo still remains unexplored.

Publication

- *Ravi, V. K., **T. Swain**, N. Chandra and R. Swaminathan **(2014)** - On* the characterization of intermediates in the isodesmic aggregation pathway of hen lysozyme at alkaline pH. ***PLoS ONE*** 9(1): e87256 doi 10.1371/journal.pone.0087256

Conferences and poster presentation

- 2015, October 25-30 - Biophysical Society thematic meeting (Polymers and Self-Assembly: From Biology to Nanomaterials). *Rio de Janeiro, Brazil*.

  Poster: Synthesis, Characterization and Applications of Size Restricted Polycationic Hen Egg White Lysozyme Nanoparticles.

- 2015, December 08-15 - ICANN (International Conference on Advanced Nanomaterials and Nanotechnology). *Indian Institute Of Technology, Guwahati, India.*

  Poster: Synthesis, Characterization and Applications of Size Restricted Polycationic Hen Egg White Lysozyme Nanoparticles.

- 2013, December 01-03 - ICANN (International Conference on Advanced Nanomaterials and Nanotechnology). *Indian Institute Of Technology, Guwahati, India.*

  Poster: Synthesis, Characterization and Applications of Polycationic Hen Lysozyme Nanostructures.

- 2012, December 03-07 - FCS (National Fluorescence workshop on Fluorescence methods in Single molecule Spectroscopy). *Saha Institute of Nuclear Physics and Indian Institute of Chemical Biology, Kolkata, India.*

  Poster: Engineering Size controlled polycationic Lysozyme nanostructures.

- 2011, December 08-10 - ICANN (International Conference on Advanced Nanomaterials and Nanotechnology). *Indian Institute Of Technology, Guwahati, India.*

  Poster: Manipulating the size of hen lysozyme protein nanoparticles created by self-assembly.